Characterization of Influenza A Viruses-Methicillin-Resistant *Staphylococcus aureus* Co-infections at the Alveolar-Capillary Barrier

By

Michaela Nickol

A Thesis Submitted to the Faculty of Graduate Studies of

The University of Manitoba

In Partial Fulfillment of the Requirements for the Degree of

Master of Science

Department of Medical Microbiology and Infectious Diseases

University of Manitoba

Winnipeg, Manitoba

Canada

Abstract

Influenza viruses have posed a threat to public health in the form of seasonal epidemics and sporadic pandemics for centuries, despite an intensive vaccine program and the existence of antivirals. Moreover, it is widely known that secondary bacterial co-infections are able to complicate influenza infections, resulting in increased morbidity and mortality. Secondary bacterial pathogens include *Streptococcus pneumoniae*, *Streptococcus pyogenes*, and *Haemophilus influenzae*. However, *Staphylococcus aureus*, specifically methicillin-resistant *S. aureus* (MRSA) remains one of the most commonly seen secondary bacterial pathogens in influenza infections. In the case of influenza-bacterial co-infections, these pathogens are able to colonize the alveolar-capillary barrier, where the respiratory epithelial cells of the alveoli are in close proximity to the pulmonary endothelial cells of the capillary, allowing for gas exchange in the lungs. The breakdown of the alveolar-capillary barrier results in severe disease, hypoxemia, and fluid leakage. It is believed that this severe disease is the result of a combination of host-, viral-, and bacterial-mediated responses. However, there is a paucity of information regarding the mechanisms underlying influenza-bacterial co-infection pathogenesis. To further our understanding of severe disease pathogenesis, a co-culture model of the alveolar-capillary barrier was created using primary alveolar respiratory epithelial cells and pulmonary microvascular endothelial cells. This model was used to study modulation of MRSA's replication kinetics and bacterial virulence factors in the presence of IAV. Additionally, the host response to influenza-MRSA co-infection was studied by measuring alveolar-capillary barrier integrity, the host kinome, and cytokine expression. We found that alveolar-capillary barrier disruption during co-infection is mediated primarily through host response dysregulation, resulting in the loss of alveolar-capillary barrier integrity.

Acknowledgements

First to my advisor, Jason Kindrachuk, thank you for your advice, patience, and unwavering support over the past two years. I'm especially grateful for your contagious passion for virology, and for believing in me when I found it hard to. Thank you for allowing me the opportunity to grow in confidence and independence as a scientist, and yet always allowing me to come to you with any questions.

To my committee members, Michael Drebot, Yoav Keynan, and Adrian West, thank you for your guidance, advice, and support over the past two years.

To my students, Justine Ciric, Brendan Dennehy, and Sarah Lyle, thank you for all your help with this project, and for going along with all my ideas, no matter how crazy they sounded. To all the other graduate students in the Kindrachuk lab, thank you for the laughs and for the support throughout this degree.

Dedication

To Tanner, for never making me feel like I was doing this alone.

Table of Contents

Tables

Figures

Abbreviations

A549	adenocarcinomic human alveolar basal epithelial cells
AJ	adherens junctions
ALI	acute lung injury
ARDS	acute respiratory distress syndrome
ATI	alveolar type I
ATII	alveolar type II
ATP	adenosine triphosphate
CA-MRSA	community-acquired methicillin-resistant *Staphylococcal aureus*
Coa	coagulase
ClfB	clumping factor B
CT	computed tomography
DMEM	Dulbecco's modified Eagle medium
DNA	deoxyribonucleic acid
DPBS	Dulbecco's phosphate buffered saline without Calcium and Magnesium
DPI	day(s) post-infection
EbpS	elastin binding protein of *Staphylococcus aureus*
ECIS	electric cell-substrate impedance sensing
ECM	extracellular matrix
Efb	extracellular fibrinogen binding protein
EGF	epidermal growth factor
Eno	enolase

FBS	fetal bovine serum
FGF	fibroblast growth factor
Fnb	fibronectin binding protein
GRO	growth-related oncogene
h	hours
H; HA	haemagglutinin
HA-MRSA	health-care/ hospital-acquired methicillin-resistant *Staphylococcus aureus*
HBEC3-KT	normal human bronchial epithelial cells infected with human telomerase and CDK4-expressing retrovirus
Hla	α-hemolysin
HlgA	γ-hemolysin component A
HPAEpiC	human pulmonary alveolar epithelial cells
HPAI	highly pathogenic avian influenza
HPMEC	human pulmonary microvascular endothelial cells
IAV	influenza A virus
ica	intracellular adhesion
ICU	intensive care unit
IFN	interferon
IgG	immunoglobulin G
IL	interleukin
IP-10/CXCL10	interferon-γ induced protein 10
IRF	interferon regulatory factor

JAK/STAT	Janus Kinase/Signal Transducer and Activator of Transcription
LPAI	low pathogenic avian influenza
M1	matrix protein 1
M2	matrix protein 2
MAPK	mitogen-activated protein kinase
MCP-1/CCL2	monocyte chemoattractant protein -1
MDA5	melanoma differentiation-associated protein 5
MDCK	Madin-Darby canine kidney cells
MDP	muramyl dipeptide
min	minute
MOI	multiplicity of infection
mRNA	messenger ribonucleic acid
MRSA	methicillin-resistant *Staphylococcus aureus*; MRSA USA300
N; NA	neuraminidase
nm	nanometer
NEP	nuclear export protein
NFκB	nuclear factor kappa-light-chain-enhancer of activated B cells
NHP	nonhuman primates
NLR	nucleotide-binding oligomerization domain-like receptors
NLRP3	nucleotide-binding oligomerization domain-like receptors family pyrin domain containing 3
NOD	nucleotide-binding oligomerization domain

NP	nucleoprotein
NS1	nonstructural protein 1
NSE	neuron-specific enolase
p75(NTR)	p75 neurotrophin receptor
PA	polymerase acidic protein
PAMP	pathogen-associated molecular patterns
pH1N1	pandemic H1N1; Influenza A/Mexico/4108/09
pH3N2	pandemic H3N2; Influenza A/Hong Kong/8/68
PB1	RNA-directed RNA polymerase catalytic subunit
PB2	polymerase basic protein 2
PBST	phosphate buffered saline with Tween-20
PBP	penicillin binding protein
pH1N1+MRSA	complexed pandemic H1N1 and methicillin-resistant *Staphylococcus aureus*
PIIKA 2	Platform for Integrated, Intelligent Kinome Analysis
PKR	protein kinase R
PNAG	poly-N-acetylglucosamine
PVL	Panton-Valentine leukocidin
RIG-1	retinoic acid-inducible gene I
RNA	ribonucleic acid
rpm	revolutions per minute
RT-qPCR	reverse transcription quantitative polymerase chain reaction

SAB	*Staphylococcus aureus* bacteremia
Sbi	staphylococcal binder of immunoglobulin
SCC*mec*	staphylococcal cassette chromosome *mec*
sH1N1	seasonal H1N1; Influenza A/New Jersey/8/76
sH3N2	seasonal H3N2; Influenza A/Brisbane/10/2007
SpA	protein A
SE	staphylococcal enterotoxin
TBST	Tris buffered saline with Tween-20
TEER	transepithelial/transendothelial electrical resistance
TGF-β	transforming growth factor β
TJ	tight junctions
TLR	Toll-like receptor
TNF	tumor necrosis factor
TRAF6	tumor necrosis factor receptor-associated factor 6
TRIM 25	tripartite motif-containing protein 25
TS	test statistic
TSA	tryptic soy agar
TSB	tryptic soy broth
TSP-1	thrombospondin-1
μm	micrometer
US	United States
VEGF	vascular endothelial growth factor

vRNP	viral ribonucleoprotein
WHO	World Health Organization
ZO	zonula occludens

Introduction

1 – Influenza Viruses

1.1 – Taxonomy

Influenza viruses belong to the family *Orthomyxoviridae*, which is composed of six genera which diverged thousands of years ago: *Influenzavirus A*, *Influenzavirus B*, *Influenzavirus C*, *Influenzavirus D*, *Thogotovirus*, and *Isavirus* [1-3]. Each genus differs in terms of its genome, host range, and pathogenicity [1, 3, 4]. Viruses belonging to the *Influenzavirus A*, *Influenzavirus B*, and *Influenzavirus C* genera each contain eight RNA segments, while viruses belonging to the *Influenzavirus C* and *Influenzavirus D* genera only contain seven RNA segments [3]. Viruses belonging to the *Influenzavirus A*, *Influenzavirus B*, and *Influenzavirus C* genera are able to infect humans, although only those belonging to the *Influenzavirus A* genus are able to cause pandemics in humans [3]. *Influenzavirus B* and *Influenzavirus C* viruses are predominantly human adapted viruses, with humans acting as their primary host; however, limited spillover has been observed in seals and pigs, respectively [3, 5]. Despite being predominantly human adapted, *Influenzavirus C* viruses are only known to cause mild illness, specifically in children [1, 3]. Lastly, the *Influenzavirus D* genus was only recently discovered, and is known to infect swine, cattle, and small ruminants [5]. Only influenza A viruses (IAV), belonging to the *Influenzavirus A* genus, will be discussed here.

1.2 – Structure and Genome

IAVs are enveloped, negative-sense, single-stranded RNA viruses with a segmented genome [1, 3]. The viral envelope can range from 80-120 nm, with three different surface glycoproteins: haemagglutinin (H; HA), which is involved in entry, neuraminidase (N; NA),

which is involved in viral release, and matrix protein 2 (M2), a proton ion channel (Figure 1) [3, 6].

The IAV genome is made up of eight gene segments, which code for 10 proteins [2, 3]. The first, second, and third genome segments code for polymerase basic protein 2 (PB2), RNA-directed RNA polymerase catalytic subunit (PB1), and polymerase acidic protein (PA), respectively, which make up the viral polymerase complex [3]. The fourth gene segment codes for HA, while the sixth segment codes for NA [3]. The fifth gene segment codes for nucleoprotein (NP) which encases each of the eight gene segments [3]. The seventh gene segment, known as M, codes for both matrix protein 1 (M1), the matrix protein which provides a scaffold for the virion structure, and M2 [3]. The eighth, and final, segment also codes for two proteins: nonstructural protein 1 (NS1), and nuclear export protein (NEP) [3]. Certain IAV proteins are known to have immunomodulatory functions, specifically NS1, which suppresses key components of the host antiviral response, including suppression of RIG-1/TRIM25-mediated sensing of viral RNA and PKR-activated antiviral activity [7, 8].

1.3 – Subtypes

IAVs are subtyped based on the antigenic variation of HA and NA glycoproteins found on the surface of the virion [1-4, 9]. There are currently 18 different HA subtypes and 11 different NA subtypes, which theoretically allows for 198 strain variations [1-3, 10]. Of these, two evolutionarily distinct IAV subtypes, H17N10 and H18N11, have only been observed in bats, which may act as an important reservoir for human IAV infections [10]. While various

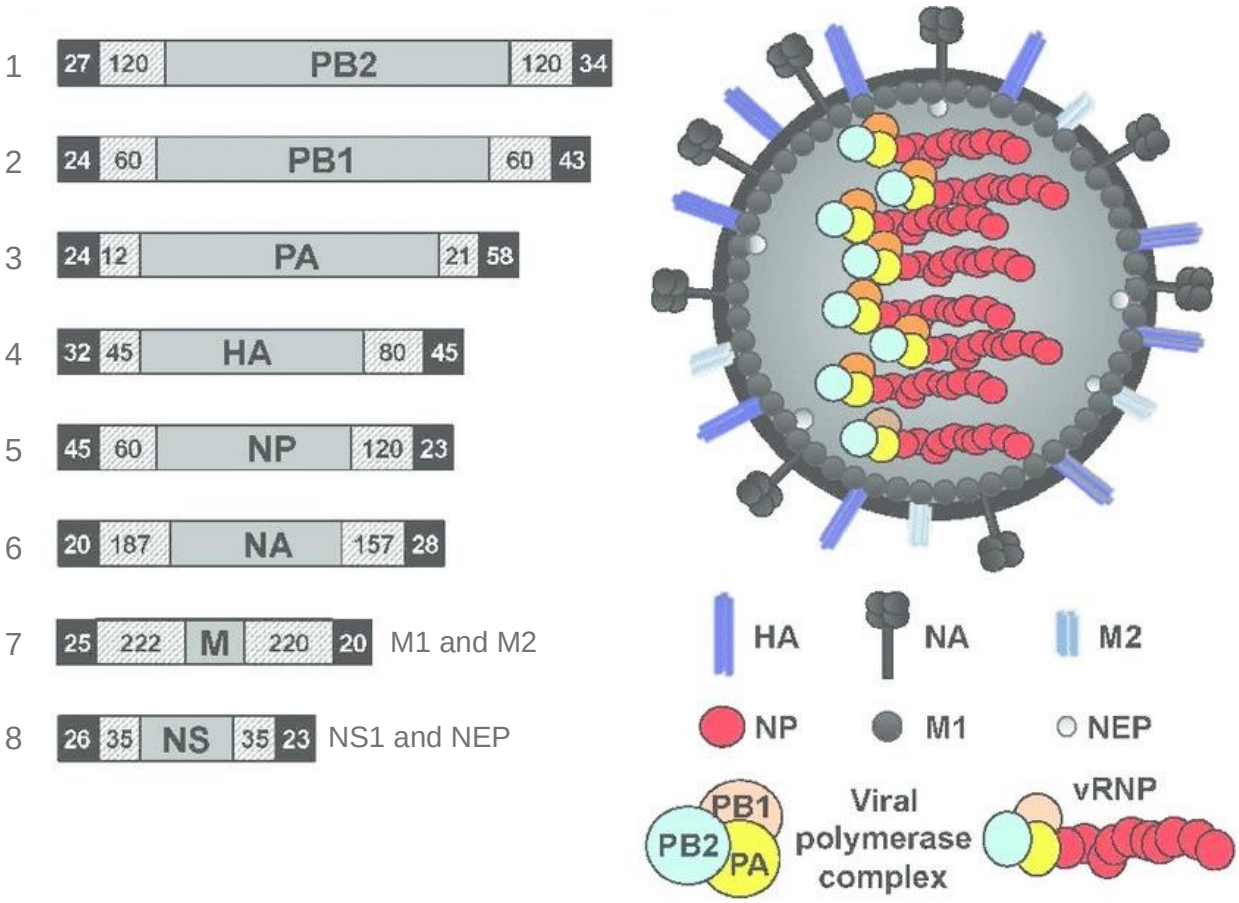

Figure 1: Influenza A Virus Structure and Genome.

Figure 1: Influenza A Virus Structure and Genome.

The IAV genome is made up of eight gene segments, coding for 10 proteins. The first, second, and third segments code for the three proteins which make up the viral polymerase complex (PB1, PB2, and PA). The fourth and sixth gene segments code for the surface proteins HA and NA. The fifth segment codes for NP, which encases each of the eight gene segments. The seventh and eight segments each code for two proteins. The seventh segment codes for M1 and M2, while the eight segment codes for NS1 and NEP.

From Breen *et al.* [6].

combinations of the HA and NA glycoproteins are consistently found within avian hosts, only H1, H2, and H3 are currently known to be capable of human-to-human transmission [1, 2].

1.4 – Antigenic Shift and Drift

The segmented genome of IAV allows for reassortment between viruses, also known as antigenic shift (Figure 2A). In short, when two IAVs infect the same cell, the viruses are able to exchange genome segments, resulting in the introduction of entirely new surface proteins to IAV strains [3]. As such, antigenic shift allows for an increase in virus diversity and, occasionally, in the creation of a pandemic IAV strain [3]. Alternatively, antigenic drift can also occur in IAVs (Figure 2B). Antigenic drift occurs constantly, and is the accumulation of point mutations within the HA and NA glycoproteins, due to the lack of proofreading ability of the viral RNA polymerase complex [3, 9]. Antigenic drift allows for selective mutation in the antigenic domains of HA and NA, and may allow IAVs to evade pre-existing immunity; it is also the reason why influenza vaccines must be updated yearly [1].

1.5 – Life Cycle

IAV invasion and replication, summarized in Figure 3, can occur in both non-immune and immune cell types, but generally targets either respiratory or intestinal tract epithelial cells, depending on the host [3, 11, 12]. First, HA, which is involved in both receptor binding and fusion, binds sialic acids present on the host cell glycoproteins [1, 3]. Binding affinity can be for either α2,3-linked or α2,6-linked sialic acids. Following binding of HA to sialic acid, the virus is internalized into the host cell via an endosome [1, 3]. The acidic pH of the endosomal compartment results in a conformational change in HA, facilitating fusion of the endosomal and viral membranes [1, 3]. The eight gene segments of the virus, known as viral ribonucleoproteins

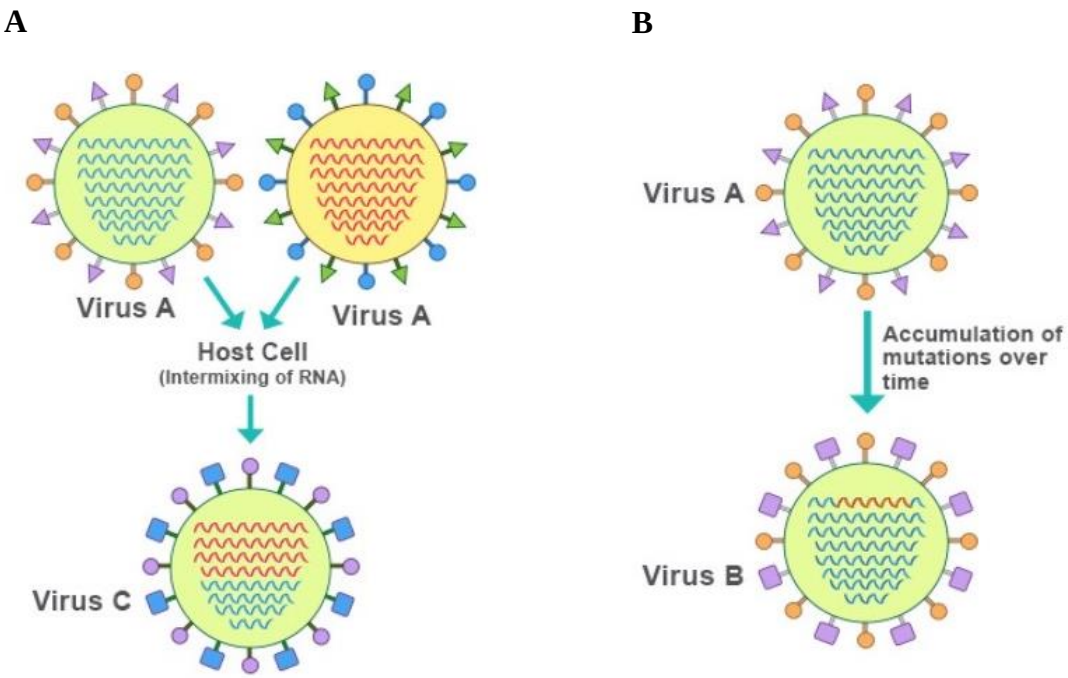

Figure 2: Antigenic Shift vs Antigenic Drift.

Figure 2: Antigenic Shift vs Antigenic Drift.

A) Antigenic shift occurs when two IAVs (Virus A + Virus A) infect the same host cell and exchange gene segments. This results in the creation of an entirely new IAV strain (Virus C).

B) Antigenic drift occurs when selective mutations in the antigenic domains of HA and NA of a virus (Virus A) accumulate over time, resulting in a virus able to evade pre-existing immunity (Virus B).

From https://healthhearty.com/antigenic-drift-vs-antigenic-shift

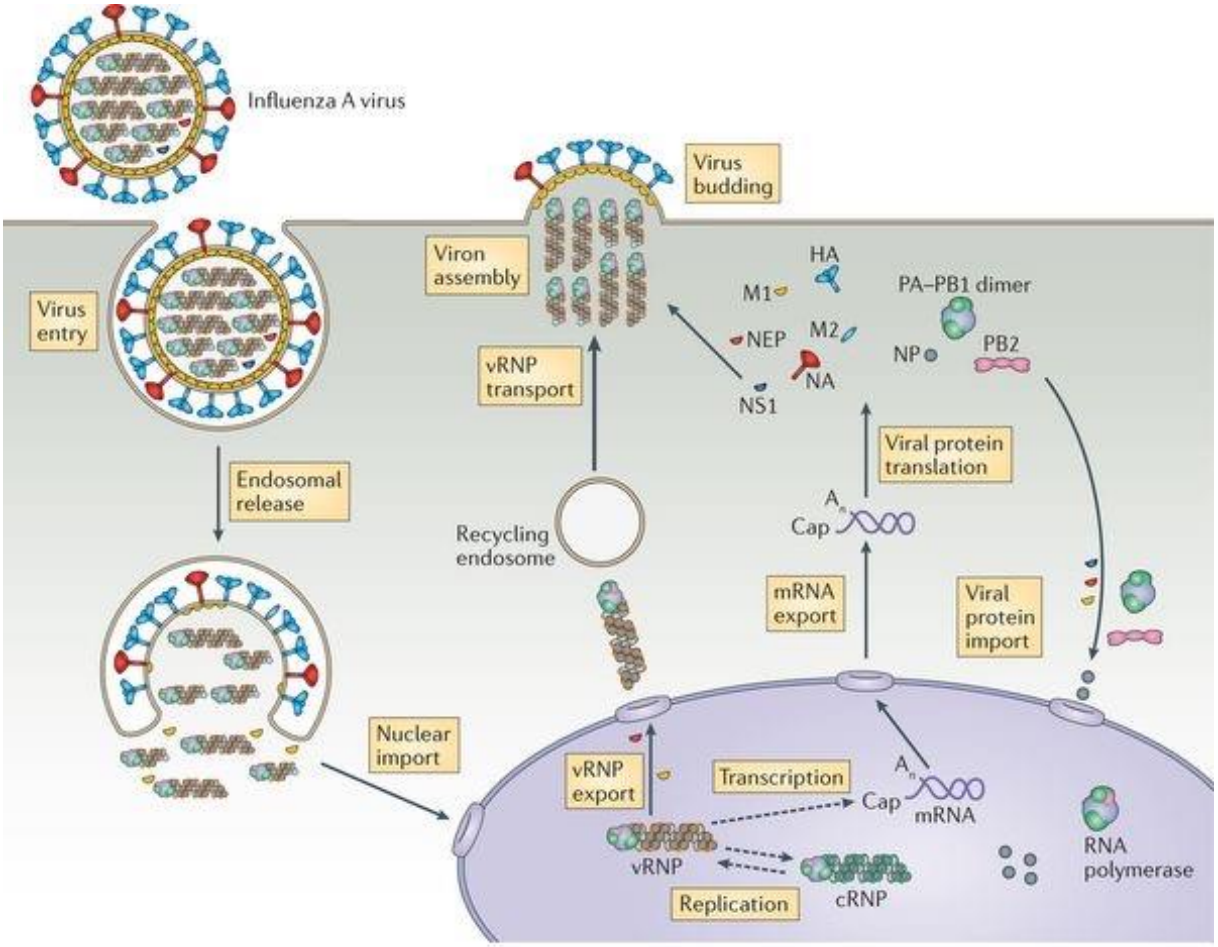

Figure 3: Influenza A Virus Life Cycle.

Figure 3: Influenza A Virus Life Cycle.

IAV replication begins by HA binding to sialic acid present on the host cell, followed by internalization via an endosome. A conformational change in HA due to the acidic pH of the endosomal compartment results in fusion of the endosomal and viral membranes, releasing the eight gene segments into the cytoplasm. The gene segments are immediately transported to the nucleus where transcription and replication occurs, mediated by the viral polymerase complex. Positive-stranded viral mRNA is transcribed, capped, polyadenylated, and transported to the cytoplasm. HA, NA, and M2 are inserted into the cell membrane. M1 and NEP localize to the nucleus, bind vRNPS, and mediate their transport to the cytoplasm. The vRNPs migrate to the plasma membrane and are bundled into the eight vRNPs necessary for the creation of a successful virion. NA cleaves host cell sialic acids, mitigating viral release. From te Velthuis and Fodor [12].

(vRNPs), are released into the cytoplasm and immediately transported to the nucleus, where transcription and replication occurs [1, 3]. Transcription and replication are mediated by the viral polymerase complex, which is made up of PA, PB1, and PB2 [3]. Transcription results in positive-stranded viral mRNA, which are capped and polyadenylated prior to being transported to the cytoplasm for translation [3]. Newly synthesized viral polymerase complexes and nucleoproteins are transported back to the nucleus, to increase the rate of transcription of viral RNA [3]. Alternatively, HA, NA, and M2 are transported to and inserted into the cell membrane upon synthesis [3]. In late stages of infection, M1 and NEP localize to the nucleus, where they bind vRNPs in order to mediate their transport to the cytoplasm [3]. The vRNPs then migrate to the plasma membrane, where they are bundled into the eight vRNPs necessary for the creation of a successful virion prior to budding [3]. Lastly, NA mitigates viral release, by cleaving host cell sialic acids [1, 3].

1.6 – Hosts

Swine, avian, and mammalian species each act as reservoirs for IAVs, with wild aquatic birds being the primary host reservoir [1, 2, 4]. Infection with IAV causes subclinical to minimal disease in their primary host, and as such is called low pathogenic avian influenza (LPAI) [13]. Host traits which affect exposure, such as foraging behaviour, migration, or reproduction, and which affect susceptibility to infection, such as age, body condition, or pre-existing immunity, are thought to influence the efficiency of LPAIs [13].

Highly pathogenic avian influenza (HPAI) viruses can evolve directly from LPAI progenitors [14-17]. This emergence is a result of antigenic drift via insertion/substitution of amino acids at the HA cleavage site or of antigenic shift via nonhomologous recombination resulting in the insertion of a foreign nucleotide sequence [18-23]. The emergence of novel

HPAI viruses, including H5 and H7 subtypes, are of particular concern due to their pandemic potential. Circulating HPAI viruses are of potential concern to global public health, as HPAI viruses can arise from previously known low-pathogenicity viruses with only minor mutations [14, 24, 25]. For example, Asian lineage avian H5N1 IAV, which circulates in fowl, is rarely found in humans but has resulted in life-threatening cases when able to establish stable lineages and H7N9 IAV has resulted in sporadic human infections in China resulting in >1500 infections with an estimated 39% case fatality rate since 2013 [24, 26].

As shown in Figure 4, IAVs are also able to naturally infect a multitude of other warm-blooded animals, including domestic animals, pigs, horses, and poultry [1, 3, 9, 27]. Host specificity is determined by the affinity of the surface glycoprotein HA for certain sialic acid linkages. For example, IAVs which are specific to birds have an affinity for α2,3-linked sialic acids, whereas IAVs adapted to humans have an affinity for α2,6-linked sialic acids [1].

1.7 – Human Infections

Human IAV infection occurs via aerosols, respiratory droplets, or direct contact with respiratory secretions of an infected individual [28-30]. Infections can range from asymptomatic to deadly [28, 29]. IAVs infect people of all ages and backgrounds; however, disease severity is greatest in infants <2 years of age, the elderly, and individuals with co-morbidities, including cardiac disease, diabetes, or obesity [1, 9, 31]. These individuals are at a high risk of developing severe complications, including hemorrhagic bronchitis and pneumonia [9].

It is estimated that annual influenza epidemics infect 10-20% of the worldwide population, resulting in ~1 billion infections, 3-5 million cases of severe illness, and 300,000-500,000 deaths each year [3, 29, 32]. Severe cases of influenza in humans are a leading cause of global morbidity and mortality [32].

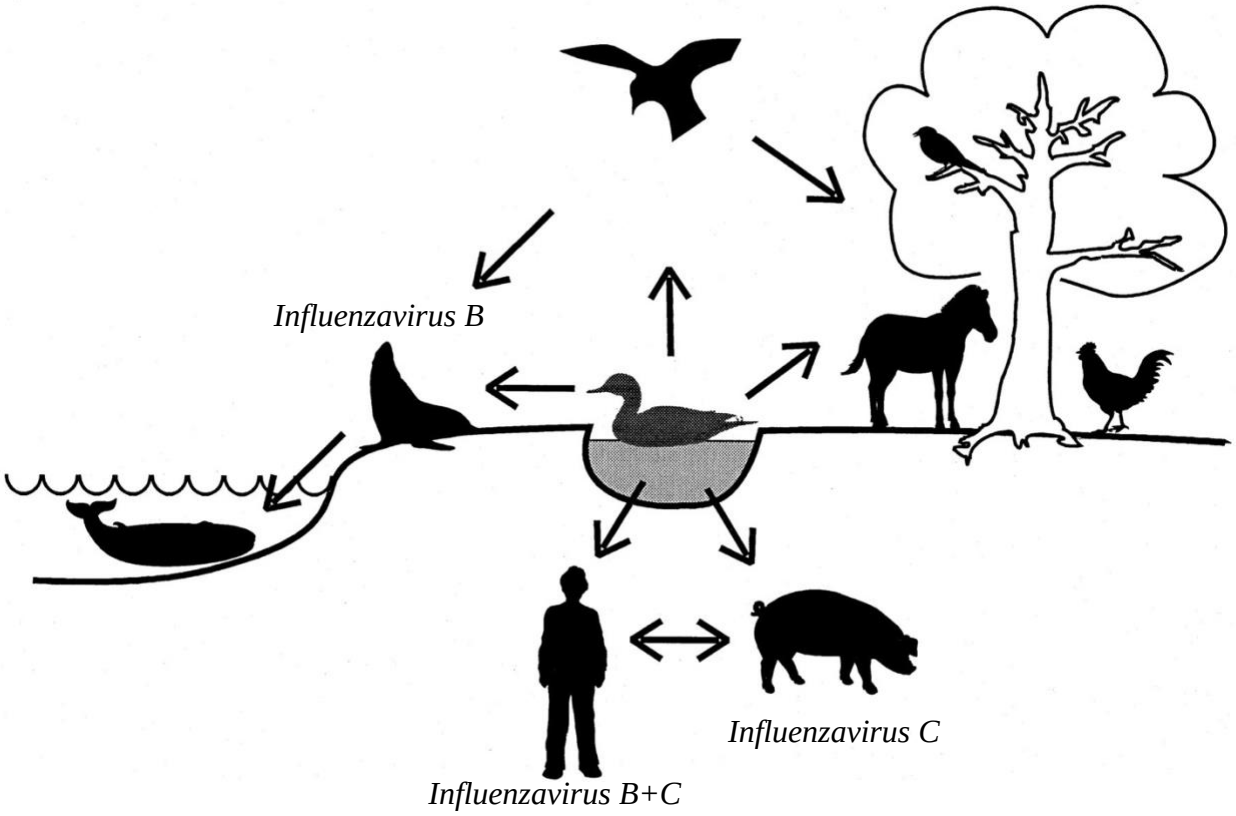

Figure 4: Influenza A Virus Hosts.

Figure 4: Influenza A Virus Hosts.

Swine, avian, and mammalian species each act as reservoirs for IAVs, allowing for a unique relationship between the three. Wild aquatic birds act as the primary host reservoir, but IAVs are also able to naturally infect a multitude of other warm-blooded animals, such as domestic animals, pigs, horses, and poultry. Other influenza viruses, such as *influenzavirus B* viruses are able to infect humans, as well as seals. *Influenzavirus C* viruses are able to infect both swine and humans, similar to IAVs.

From Horimoto and Kawaoka [27].

1.7.1 – Signs and Symptoms

Influenza virus infections generally manifest as an acute, self-limiting infection in both the upper and lower respiratory tract [1, 9]. Clinical symptoms include the sudden onset of a high fever, coryza, cough, headache, myalgia, and general malaise [1, 9, 31]. Some gastrointestinal symptoms, such as nausea, vomiting, and diarrhea are also common [33]. In healthy adults, symptoms generally peak around 3-5 days post-infection, and persist for 7 to 10 days [1, 9, 31]. Replication peaks around 48-72 hours post-infection, with virus shedding occurring for ~6 days [1, 9, 31].

Certain host factors, such as age, genetic predisposition, and the presence of co-morbidities as described above, often result in severe disease complications [9, 28, 32]. These complications often include hemorrhagic bronchitis and pneumonia [9]. However, severe cases of influenza infection can also result in a wide range of non-respiratory complications, such as cardiovascular, neurological, musculoskeletal, renal, hepatic, and hematologic complications [32]. The most commonly described complications include viral myocarditis and viral encephalitis [32].

1.7.2 – Pathogenesis

In humans, IAVs replicate in the respiratory epithelium, ultimately inducing an inflammatory response [34, 35]. IAV pathogenesis is the result of a combination of both viral and host factors [34]. Following viral entry into the cell, IAV is recognized by pattern recognition receptors, such as endosomal Toll-like receptor (TLR)-7 or cytosolic RIG-I, which recognize the single-stranded RNA of influenza [34]. Recognition induces anti-viral host responses via a series of signaling cascades, resulting in the production of type I interferon (IFN) which limits viral replication [34]. Transcription factors such as interferon regulatory factor

(IRF)-3 and IRF-7 are virus induced and play essential roles in the expression of type-I IFN [34]. Activated pattern recognition receptors are also able to induce the production of pro-inflammatory mediators including interleukin (IL)-1, IL-6, IL-12, IL-18, tumor necrosis factor (TNF)-α, and chemokines such as CCL5, CXCL8, CXCL10, and CCL2 [34, 36, 37]. These chemokines are able to recruit macrophages which can induce apoptosis in infected alveolar epithelial cells, leading to lung inflammation [34].

1.7.3 – Acute Lung Injury and Acute Respiratory Distress Syndrome

In severe cases of disease, IAV infection can result in acute lung injury (ALI) or acute respiratory distress syndrome (ARDS) [38]. Both ALI and ARDS are manifestations of an inflammatory response in the lung, characterized by severe hypoxemia, hypercapnia, and diffuse infiltration present in chest x-rays [38]. ALI is diagnosed by the presence of bilateral pulmonary infiltrates consistent with edema in chest radiographs [38]. ARDS is the more severe form of the disease, resulting in potentially fatal respiratory complications with a high mortality rate of ~52% [37, 38]. A major contributor of ARDS is progressive hypoxemia induced by diffuse damage to the alveolar-capillary barrier, thus impairing gas exchange [37-39]. This damage occurs in three different phases: inflammation, fluid exudation, and cellular proliferation leading to pulmonary fibrosis [37]. ALI and ARDS pathogenesis likely involves both pathogen- and host-mediated mechanisms, including IAV virulence and diffuse lung damage [37].

1.8 – Prevention

1.8.1 – Influenza Vaccines

Current influenza vaccines provide protection against circulating IAVs and influenza viruses belonging to the *influenzavirus B* genera [40]. These vaccines are reformulated seasonally, based on recommendations by the World Health Organization (WHO), who conduct

worldwide surveillance studies throughout the year on currently circulating influenza strains [40]. Within Canada there are several vaccine options available, each of which fall into two general categories: inactivated influenza vaccines and live attenuated influenza vaccines [41]. The most commonly administered is a quadrivalent inactivated influenza vaccine, which is formulated with an IAV H1N1 strain, an IAV H3N2 strain, and two *influenzavirus* B strains, one from each of the commonly circulating lineages [41]. Despite the existence of the seasonal influenza vaccine, it is only ~60% effective [40]. Efficacy is dependent on the characteristics of the individual being vaccinated, such as the age and overall health as well as the match between the strains included in the vaccine formulation and currently circulating strains [40]. In Canada, only ~35% of all adults aged 18 and over received the influenza vaccine each year from 2015-2018 [42].

1.8.2 – Antivirals

Two major classes of antivirals exist for therapeutic treatment of severe influenza virus infections: adamantane antivirals and NA inhibitors. Adamantane antivirals were the first licensed influenza antivirals and target the M2 surface protein, blocking the ion channel protein from properly functioning, thus effectively blocking membrane fusion [43, 44]. However, adamantane antivirals are only able to target IAVs [43]. Moreover, more than 90% of IAVs are resistant to adamantane compounds, due to the high mutation rate of the virus [43, 45]. Instead, NA inhibitors are recommended [45]. NA inhibitors block the NA surface protein, thus preventing the release of progeny virus and infection of additional cells [45]. NA inhibitors are highly effective in the majority of patients; however, resistance has been observed in some influenza virus strains [45].

1.9 – History of Pandemics

Influenza pandemics occur approximately every 10-50 years, and can infect up to 50% of the worldwide population [3, 9]. It is thought that influenza pandemics have been occurring since as early as 412 BC, when Hippocrates described an influenza-like illness which peaked around the winter solstice and manifested as pharyngitis, coryza, and myalgia [2, 46]. However, it was not until 1580 that the first unanimously agreed-upon influenza pandemic occurred. While influenza pandemics occurred throughout the 16th -19th centuries, the largest, and final, pandemic of the 19th century began in November 1889 [47]. Known as the Russian flu, it spread across Europe and the rest of the world within just 4 months, with a case fatality rate of 0.1% to 0.28%, comparable to pandemics of the 20th century [2, 48]. Most of the current information concerning IAV pandemics has been garnered through the four pandemics which have occurred over the past century: the Spanish flu in 1918, the Asian flu in 1957, the Hong Kong flu in 1968, and the swine flu pandemic in 2009 (Figure 5). Interestingly, pandemic strains are known to become seasonal epidemic strains in subsequent years [3, 29].

1.9.1 – The Spanish Flu

The Spanish flu pandemic took place from 1918-1919, when an H1N1 strain believed to have originated in swine ravaged countries worldwide, resulting in an estimated 500 million infections and 50 million deaths [2, 46, 49]. The 1918 H1N1 influenza strain was the worst influenza pandemic in history [9, 46]. In fact, the virus lowered the average life expectancy in the United States by 10 years, thanks to its propensity for young adults aged 15-34 years [2, 50]. Additionally, each of the three pandemics in 1957, 1968, and 2009 were caused by descendants of the 1918 strain, lending it the nickname ‘The Mother of all Pandemics’ [51]. The 1918 pandemic began early in the final year of the First World War, which enabled greater viral

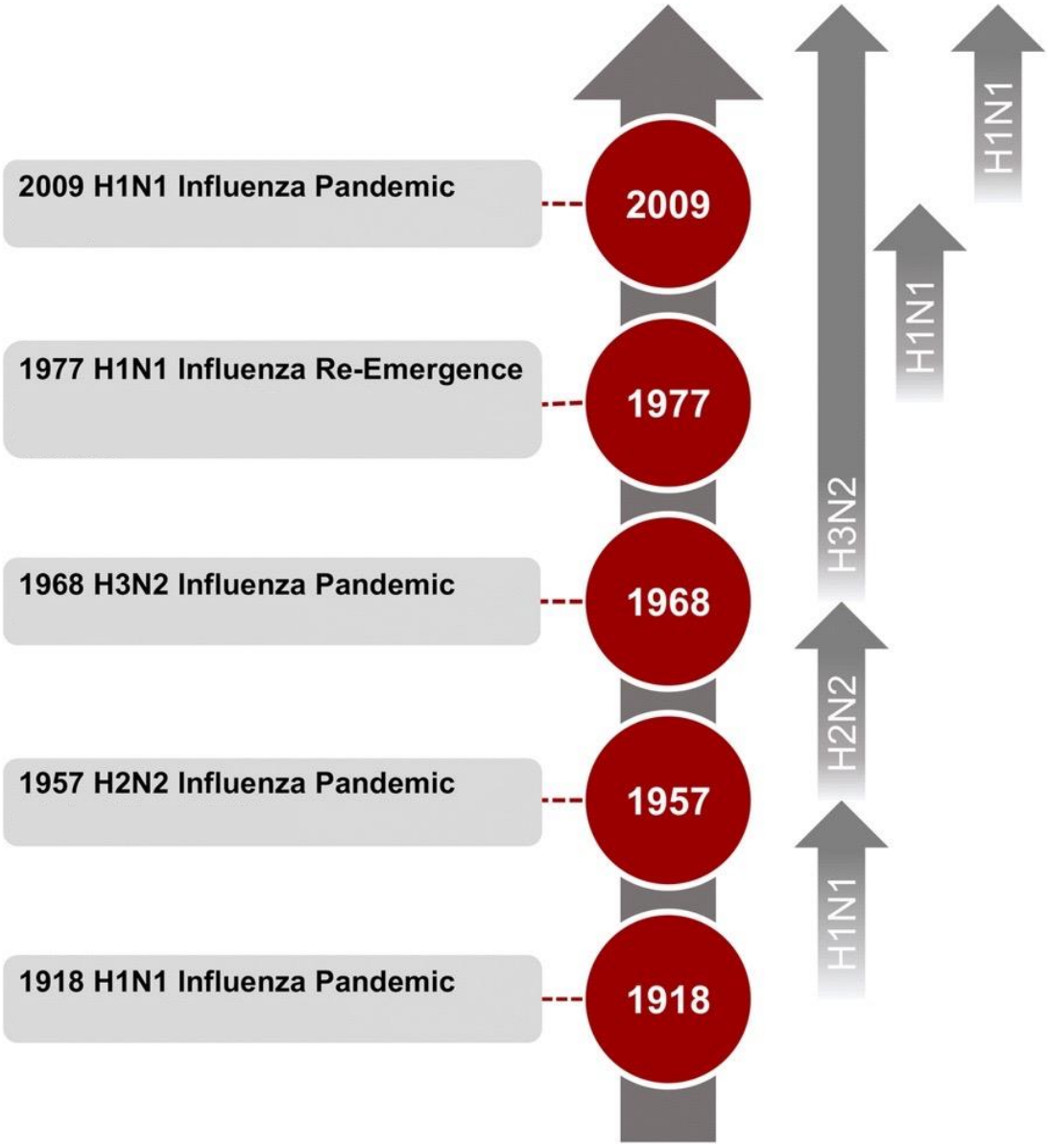

Figure 5: Emergence of Pandemics and Circulating Influenza A Strains over the Past Century.

Figure 5: Emergence of Pandemics and Circulating Influenza A Strains over the Past Century.

Four pandemics have taken place since 1918: the H1N1 Spanish flu in 1918, the H2N2 Asian flu in 1957, the H3N2 Hong Kong flu in 1968, and the H1N1 swine flu in 2009. In each case, the pandemic strains continued circulating, becoming a seasonal epidemic strain in subsequent years. Additionally, a suspicious re-emergence of a H1N1 strain occurred in 1977, which is believed to have been the cause of an accidental laboratory introduction to the general public. As such, H1N1 began circulating seasonally along with the H3N2 strain from 1968.

From Nickol and Kindrachuk [46].

spread facilitated by the mass mobilization of military personnel and civilians [2, 46, 52]. This was further augmented by the poor health and sanitation conditions found within trenches along the frontlines of the war, facilitating disease transmission [46, 53]. Investigations concerning the origins of the first wave of the pandemic, beginning in March 1918, have primarily focused on the US and China, but is ultimately still unknown [46, 54]. Throughout the second, and most fatal, wave of the 1918 pandemic, the case fatality rate was >2.5%, more than 25 times higher than any other pandemic [51, 55]. Ultimately, the pandemic would result in an estimated 500 million infections worldwide, ~1/3 of the world's population at the time [51, 55].

1.9.2 – The Asian Flu

The Asian flu pandemic, subtype H2N2, emerged in China in February 1957, replacing H1N1 as the circulating strain [2, 46, 56]. The virus spread to eastern Asia and the Middle East throughout April, May, and June before afflicting South American and African countries in July and August [56]. By September, North America and Europe were also experiencing widespread epidemics [56]. The Asian flu lasted into 1959, resulting in an estimated 1 million deaths and a case fatality rate of 0.67% [2, 46, 57, 58]. From 1957 to 1968, H2N2 was the only known IAV strain circulating in humans [3].

1.9.3 – The Hong Kong Flu

In July 1968, an H3N2 influenza strain emerged in Hong Kong [2, 46]. The virus spread throughout Europe, North America, and Australia by January 1969, and is believed to have been driven by the return of Vietnam War veterans to their home countries [46]. This pandemic resulted in a low mortality rate, which is thought to have been due to previous immunity to the N2 neuraminidase antigen, which had circulated widely throughout the 1957 Asian Flu pandemic [2]. However, it still resulted in an estimated 500,000 to 2,000,000 deaths worldwide [2, 46].

Generally, influenza pandemics result in the extinction of previously circulating IAVs, and as such this H3N2 strain was the only circulating strain in humans until 1977 [46]. However, in 1977 there was a suspicious re-emergence of a descendant of the 1918 Spanish flu, postulated to have been the result of a man-made event, which established itself as a co-circulating H1N1 strain, along with the reassortant H3N2 virus following the 1968-1970 Hong Kong flu pandemic [46].

1.9.4 – The 2009 Swine Flu

Two simultaneous outbreaks of the H1N1 swine flu occurred in Mexico and the US in April 2009 [2]. By June 2009, the WHO had declared a global influenza pandemic, as the virus had spread to more than 30 countries worldwide, thanks to the globalization of travel and trade [2]. The pandemic was not officially declared over by the WHO until August 2010 [2]. Interestingly, the 2009 swine flu pandemic showed a propensity for young adults, as seen throughout the 1918 Spanish Flu pandemic [2]. Despite its high virulence, the total number of fatalities was estimated at only 575,400 which has been attributed to worldwide emergency pandemic preparedness [2].

1.10 – Seasonal Outbreaks

Seasonal IAV epidemics generally occur throughout the winter months, when low humidity and temperatures are thought to encourage human-to-human transmission [3]. It is estimated that 3-5 million severe infections and 291,243-645,832 deaths occur each year due to seasonal IAV strains, making influenza epidemics a major burden of disease [3]. Currently, only H1N1 and H3N2 strains are circulating in humans [3].

2 – Methicillin-Resistant *Staphylococcus aureus*

2.1 – *Staphylococcus aureus*

Staphylococcus aureus belongs to the *Staphylococcaceae* family, within the order Bacillales, and was first described in 1884 [59, 60]. *S. aureus* acquired its name from the Greek *staphylos* (“grape”) and *kokkos* (“berry”), and the Latin *aurum* (“gold”) [59]. *S. aureus* are Gram-positive, catalase-positive, coagulase-positive, bacitracin-resistant, non-spore forming bacterium which are resistant to a variety of harsh environments and disinfectants [60]. It is one of the most common human pathogens and has resulted in millions of infections and mortalities thanks to its adaptability and tenacity [59-63]. *S. aureus* is also able to infect domestic cats and dogs, horses, goats, sheep, cattle, rabbit, pigs, and poultry [64].

2.2 – *Staphylococcus aureus* Structure

As with all Gram-positive bacteria, the cell wall of *S. aureus* consists of a 20-40 nm thick peptidoglycan structure composed of a series of cross-linked glycan chains (Figure 6) [65]. The peptidoglycans are crosslinked, which is catalyzed by transpeptidases, known as the penicillin-binding proteins (PBPs) [66]. In the case of *S. aureus*, cross-linking is catalyzed by four PBPs in *S. aureus*: PBP1, PBP2, PBP3, PBP4 [65, 67]. The cell wall is also composed of teichoic acids [68, 69]. Cell wall teichoic acids are covalently linked to peptidoglycan and are known to play a role in adhesion, colonization, cell division, and biofilm formation [69]. Additionally, overexpression of cell wall teichoic acids is known to increase the virulence of *S. aureus* [69-73]. Lastly, the composition of the cell includes wall-associated surface proteins, which are anchored to peptidoglycan [69, 74, 75]. These surface proteins are involved in many important roles, such as in cell division or *S. aureus* virulence [76].

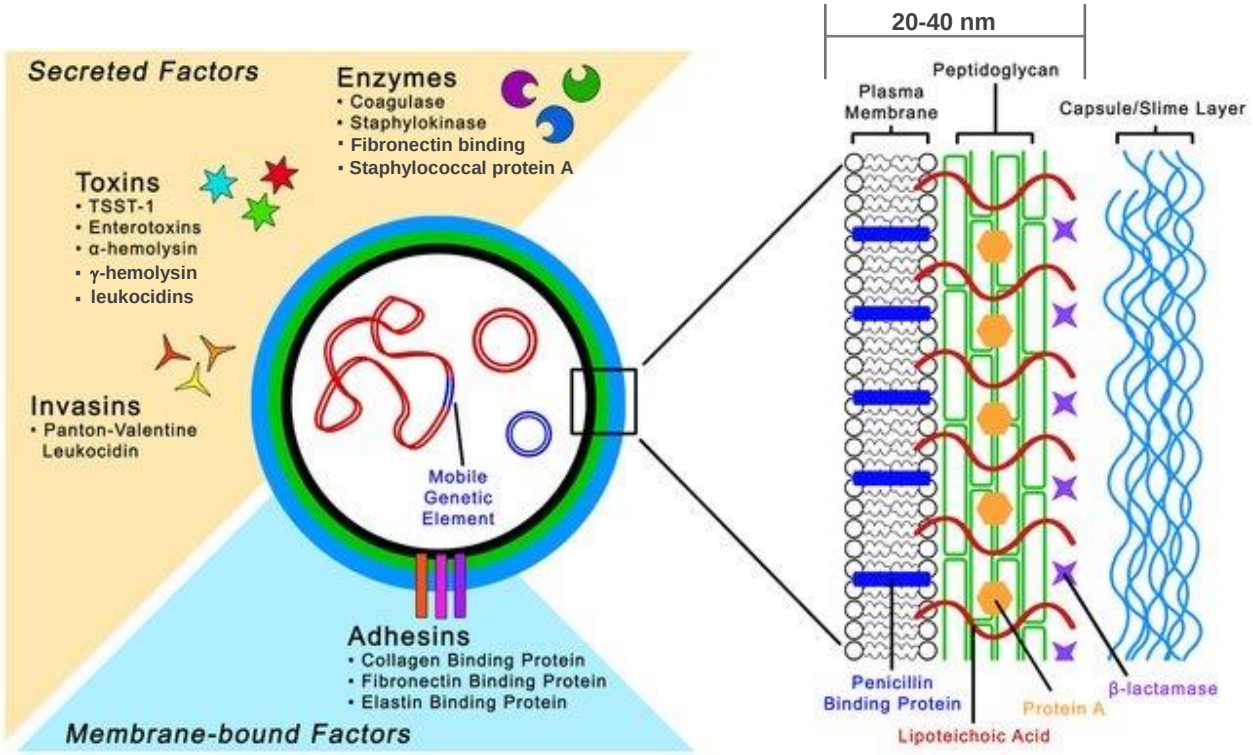

Figure 6: Schematic of the Cell Structure and Virulence Factors of *Staphylococcus aureus*.

Figure 6: Schematic of the Cell Structure and Virulence Factors of *Staphylococcus aureus*.

The cell wall of *S. aureus* is composed of a thick peptidoglycan layer, teichoic acids, and wall-associated surface proteins. Penicillin-binding proteins are responsible for cross-linking of the peptidoglycans. The capsule consists of repeating units of polysaccharides dependent on the serotype, but expression can be highly variable. *S. aureus* is able to encode a large number of virulence factors, all of which are largely related to its ability to target and damage the host cell membrane. Importantly, the Panton-Valentine Leukocidin invasin is specific to community-acquired methicillin-resistant *S. aureus* strains.

From Kong *et al.* [62].

S. aureus clearance is often facilitated by the innate immune system, specifically phagocytic neutrophils which are able to phagocytose and intracellularly kill bacteria [77, 78]. To combat this, *S. aureus* is able to express a polysaccharide capsule attached to the cell wall, which masks the bacterial surface and surface-associated proteins from phagocytic recognition [77, 78]. The polysaccharides which make up the capsule consist of repeating units which vary between serotypes [79]. Currently, 13 *S. aureus* serotypes have been identified [80, 81]. It is important to note however that capsule expression can be highly variable, is dependent on environmental factors, and may be subject to the location of bacterium in the body [77].

2.3 – *Staphylococcus aureus* Virulence Factors

S. aureus is able to encode a large number of virulence factors which enable it to infect different tissues within its host. The virulence of *S. aureus* is largely related to its ability to target and damage the host cell membrane [82-84]. These membrane-damaging toxins and peptides can be split into three groups: hemolysins, bi-component leukocidins, and cytolytic peptides [84]. The most studied of these virulence factors is α-hemolysin (hla), which plays an important role in *S. aureus* pathogenesis by killing phagocytes, disrupting epithelial and endothelial barriers, and lysing erythrocytes to provide nutrients necessary for bacterial growth [85]. Furthermore, upregulation of hla has been shown to play a role in the development of *S. aureus* moving from a commensal pathogen to an invasive pathogen [86, 87]. Another well-studied Staphylococcal toxin are γ-hemolysins, bi-component leukocidins capable of damaging the host cell plasma membrane [84, 88, 89]. HlgA is one part of a bicomponent leukotoxin which is primarily known for its lytic activity towards phagocytes and hemolytic activity [85, 90, 91]. It is able to specifically target the CXCR1, CXCR2, and CCR2 chemokine receptors abundantly present on phagocytes, allowing *S. aureus* to differentially target phagocytes [88]. However, the most

notable of these toxins are the superantigen exotoxins known as Staphylococcal entertoxins (SEs), of which *S. aureus* produces at least 20 serologically distinct exotoxins [92]. SEs are able to stimulate a robust T cell activation resulting in the production of a strong cytokine response [93, 94].

Another important factor in *S. aureus* virulence is the formation of biofilms, which facilitates colonization of the host while providing resistance to both antibiotics and the host immune system [95]. Biofilm accumulation requires mechanisms for intercellular aggregation of bacteria, primarily mediated by the intercellular adhesion (ica) locus [95]. The major constituents of staphylococcal biofilms are polysaccharides, which are synthesized by the four products of the *ica* operon: icaA, icaB, icaC, and icaD [95, 96]. To further underline the importance of these four proteins, *ica* knockout mutants are not able to form a biofilm as compared with wild-type *S. aureus* [97]. Other virulence factors, such as fibronectin-binding proteins A and B (FnbA and FnbB, respectively) and Staphylococcal protein A (SpA), also all contribute to biofilm formation, though to a lesser effect [98, 99].

While FnbA and FnbB are involved in biofilm formation, their primary function is to mediate bacterial invasion of cells [100-103]. Both FnbA and FnbB play an important role in the adhesion to and invasion of non-professional phagocytic cells, such as epithelial and endothelial cells [104]. Other factors are also specifically involved in *S. aureus* adhesion. For example, elastin binding protein (EbpS) is able to explicitly interact with elastin thus promoting bacterial colonization, while clumping factor B (ClfB) has been proposed to play a role in colonization both *in vitro* and *in vivo* [105-108]. Additionally, the binding of cell wall-associated enolase (eno) with plasminogen and laminin facilitates bacterial adhesion and invasion, and has been

shown to enhance bacterial invasiveness and metastasis to secondary sites of infection [92, 109-112].

S. aureus has also developed several strategies to protect itself against neutrophil phagocytosis. *S. aureus* secretes an extracellular fibrinogen-binding protein (Efb) which attracts fibrinogen to the bacterial surface, thus covering the bacteria with a layer of fibrinogen which prevents surface recognition by phagocytic cells [78, 113]. Coagulase (Coa), another secreted protein, colocalizes with fibrin and fibrinogen to form a protective structure, preventing phagocytes from accessing and clearing *S. aureus* [114]. The binding motif of Coa is structurally and functionally related to the binding sites of Efb [115]. Secreted IgG-binding proteins, such as SpA and *S. aureus* binder of IgG (Sbi), are able to prevent neutrophil-mediated opsonophagocytosis, thus promoting bacterial survival [78, 116]. SpA is a cell wall-anchored protein and one of the most prominent IgG-binding proteins [78]. Sbi exhibits IgG-binding domains similar to SpA [117, 118]. Binding of IgG is thought to help *S. aureus* escape from phagocytic killing, though the exact mechanism is still unclear [78, 119].

2.4 – Antimicrobial Resistance of *Staphylococcus aureus*

Strains of *S. aureus* have acquired resistance to a number of antimicrobials, including penicillin, erythromycin, streptomycin, tetracyclines, and methicillin [59, 63]. This resistance is acquired through a number of different mechanisms, including limiting the uptake of the drug, modifying the drug target, enzymatically inactivating the drug, active efflux of the drug, or a combination of these mechanisms [63, 120-123].

2.5 – The Rise of Methicillin-Resistant *Staphylococcus aureus*

Methicillin-resistant *S. aureus* (MRSA) colonies were first observed in 1960, only one year after methicillin was first introduced [124-127]. However, it was not until the late 1970's

that MRSA became epidemic across Europe, Australia, and the United States [59]. Interestingly, only a handful of MRSA lineages are responsible for the majority of MRSA infections [59]. While the origin of MRSA is unknown, the existence of distantly related MRSA lineages indicates that MRSA likely did not arise from a single common ancestor [59].

While methicillin is no longer used clinically, the term methicillin resistance is used to refer to resistance to virtually all β-lactams, other than the latest generation of cephalosporin β-lactams [64]. β-lactams, such as penicillins, interfere with PBP enzymes which are involved in the synthesis of peptidoglycan, the major cell wall component of *S. aureus* [128-130]. β-lactams are able to inhibit the transpeptidase domain of PBPs, thus stopping cross-linking, resulting in a weak cell well, the release of cytoplasmic contents, and cell death [67, 128]. The acquirement of PBP2a, a transpeptide separate from PBP2, from a secondary species resulted in methicillin resistance [65, 67]. PBP2a is able to usurp the role of peptidoglycan cross-linking of *S. aureus* host PBPs in the presence of methicillin, while providing cross-resistance to most available β-lactams. It is able to remain active in the presence of therapeutic methicillin levels due to its much lower affinity for β-lactams as compared with other PBPs [65].

Methicillin resistance was acquired when the foreign staphylococcal cassette chromosome *mec* (SCC*mec*) of *Staphylococcus sciuri* was incorporated into the chromosome of *S. aureus* [65, 131]. PBP2a, the protein responsible for methicillin resistance, is encoded by the *mecA* gene present on the foreign *mec* DNA [65]. Two genes also present on the *mec* element, *ccrA* and *ccrB*, are believed to have played a role in the acquisition and integration of the *mec* element into the chromosome [132]. Synthesis of PBP2a is regulated by the products of the *mecI* and *mecRI* genes, also present on the *mec* element [65].

MRSA is also able to acquire resistance to multiple other antimicrobials, such as vancomycin, linezolid, and daptomycin, further complicating treatment [133-136]. In some cases, native *S. aureus* proteins may contribute to this resistance. For example, teichoic acids support antimicrobial resistance to glycopeptides, such as vancomycin, which are generally able to bind to peptidoglycan precursors with high affinity and specificity thus preventing their incorporation into the bacterial cell wall [69]. Additionally, the expression of *eno* is directly related to bacterial resistance to penicillin-induced autolysis [137].

2.5.1 – Methicillin-Resistant *Staphylococcus aureus* USA300

MRSA clones are named in reference to a specific pulse field gel electrophoresis pattern [59]. Some MRSA clones, such as USA300, are commonly seen in both hospital- and community-acquired infections [59]. MRSA USA300 was first isolated in several states in the US in 2000, and became the predominantly circulating MRSA strain by 2011 [138-141]. It is the most common cause of skin and soft tissue infections in the United States and predominates in both community and health-care settings [142-144]. While other MRSA strains have considerable heterogeneity, USA300 isolates are remarkably similar [145].

The USA300 strain differs from other MRSA strains in several ways. First, the USA300 strain nearly always carries the Panton-Valentine leukocidin (PVL) toxin genes [138, 144, 145]. PVL is a pore-forming exotoxin encoded by the lukSF-PV genes which reside in the genomes of temperate bacteriophages [146, 147]. Following the infection of MRSA, the phages lysogenize into the bacterial chromosome [146]. While there are a number of different PVL phages, the genes which encode PVL are relatively conserved [146]. While the presence of *pvl* genes suggests that PVL could be an important virulence factor in MRSA USA300, the role of PVL is still controversial as results from *in vitro* and *in vivo* models differ [145, 148]. *In vitro,* PVL has

been reported to form lytic pores, destroying human neutrophils, monocytes, and macrophages [149-151]. While Labanderia-Rey *et al.* reported that *in vivo*, PVL is a key virulence factor in pulmonary infections, Voyich *et al.* reported that while PVL may be a marker for community-associated MRSA, it is not an important virulence determinant and may even be protective [82, 141, 152].

The MRSA USA300 strain also harbours broader susceptibility to antimicrobial classes as compared with other MRSA strains [144, 145]. While most MRSA strains are susceptible to vancomycin, linezolid, and daptomycin, MRSA USA300 is also susceptible to trimethoprim-sulfamethoxazole, doxycycline, rifampin, and clindamycin, though increasing resistance has been reported [145]. Many USA300 isolates are developing reduced susceptibility; this resistance is associated with plasmid-carriage [153, 154]. Lastly, as described previously, MRSA carries other methicillin resistance elements through SCC*mec*, of which there are 12 types described so far [155, 156]. MRSA USA300 specifically carries SCC*mec* type IV [138, 144, 145].

2.5.2 – Community-acquired MRSA and Healthcare-acquired MRSA

Patients who develop staphylococcal pneumonia while in nursing homes, extended-care facilities, or hospitals are generally infected with healthcare- or hospital-acquired MRSA (HA-MRSA) [157]. In general, these patients are elderly and have significant underlying diseases [157, 158]. These pneumonia cases are associated with a mortality rate of 55.5%, despite early and appropriate therapy [157, 158]. HA-MRSA carries SCC*mec* types I, II, and III, with the most common subtype being MRSA USA100 [159-162].

Alternatively, MRSA can also be spread in the community, known as community-acquired MRSA (CA-MRSA), by contact with infected people or objects carrying the bacteria,

which can survive for days to months on surfaces [163, 164]. However, the primary mode of CA-MRSA transmission is human-to-human contact [145]. CA-MRSA is often associated with young, previously healthy adults and generally results in an acute illness with numerous complications and a high mortality rate [157, 165-169]. CA-MRSA infections are frequently described in prisoners, athletes, children, and injection drug users [139, 170-172]. Interestingly, CA-MRSA has been found to be composed of more-diverse clonal groups than HA-MRSA, and show higher drug susceptibility [173, 174]. CA-MRSA carry SCC*mec* types IV and V, with the most common subtypes being MRSA USA300 and USA400 [159-162, 175]

Unfortunately, there is an imprecise distinction between CA-MRSA and HA-MRSA as it is difficult to accurately identify the exact location of transmission [176]. Moreover, CA-MRSA strains have begun moving into hospital settings, while HA-MRSA strains have been moving into the community [176].

2.3 – Human Infections

S. aureus is both a commensal bacterium and a human pathogen; ~30% of the human population is colonized with *S. aureus* at mucosal sites of the body, including the nostrils, throat, and other dedicated, moist areas of the skin surface (e.g. the axilla, groin, and perineum) [60, 177, 178]. The most commonly affected sites by *S. aureus* infection are skin and soft tissue [64, 173]. Other serious infections manifest as bacteremia, pneumonia, endocarditis, bone and joint infections, and toxic shock syndrome [64, 177, 179].

2.3.1 – Risk Factors

Risk-factors commonly associated with HA-MRSA include recent hospitalization, surgery, exposure to antibiotics or other medications, dialysis, nursing-home residence, and other co-morbid conditions such as diabetes, chronic renal failure, and chronic pulmonary diseases

[160, 173, 175, 180, 181]. Breaches in natural defence due to an invasive device, such as a central line, endotracheal intubation, or mechanical ventilation is also often observed in HA-MRSA [160, 180, 182].

Risk factors commonly associated with CA-MRSA are intimately associated with social determinants of health [150, 183]. As the primary mode of transmission is skin-to-skin contact, crowded living environments such as military barracks, homeless shelters, subsidized housing, and prisons are associated with increased risk of CA-MRSA infection [184-187]. Additionally, limited access to clean water has significantly higher rates of MRSA infection [188].

2.3.2 – Indigenous Populations

In Canada, CA-MRSA is 6 times more likely to be isolated from the Indigenous population as compared with the non-Indigenous population [184]. The epidemiology and clinical characteristics of MRSA infection in the Indigenous population is distinct from the general population in Canadian hospitals [184]. Incidence of CA-MRSA has been increasing in small Indigenous communities in northern Canada and the prairie provinces [189-191]. In the Northwest Territories, a study of CA-MRSA cases revealed that 83% of cases were Indigenous, who comprise about 50.6% of the population [192]. These observations may be explained in part by the socioeconomic and demographic factors described above; however, they do not fully explain the disparity [177, 184, 193].

2.4 – Pulmonary Infections

Though primarily a cause of skin and soft tissue infection, MRSA USA300 is also a substantial cause of pneumonia [157, 194]. *S. aureus* was first documented throughout the 1918 Spanish flu epidemic as a devastating secondary co-infection [46, 195]. MRSA has remained an important factor in hospitalized patients with respiratory infections, playing a role in all major

subsets of pneumonia (HA-MRSA, CA-MRSA, and ventilator-associated MRSA) [165, 177, 196-199].

2.4.1 – Clinical Signs and Symptoms

In the first 24-48 hours, isolated tachypnoea may be observed usually with no other signs of severe illness and normal chest radiography appearance [195]. Minimal bilateral infiltrates may occasionally be observed but, unfortunately, no radiological features are highly specific for MRSA pneumonia [168, 195]. Influenza-like symptoms are most commonly seen in MRSA pneumonia such as high fever and cough. Other severe respiratory symptoms including shortness of breath, cough with sputum production, and chest pain may also be present [157, 200-202]. Other reported symptoms of MRSA pneumonia include leukopenia, hypotension, hemoptysis, hypoxemia, rash, and altered mental status [157, 200-203]. At day 4-5, clinical signs of bronchopneumonia often develop [204, 205]. Chest radiographies reveal infiltrates, pleural effusion, empyema, and pyopneumothoraces [157, 200-202, 204, 205]. These infiltrates may cavitate as seen on serial chest radiographies or CT scans [168, 195].

2.4.2 – Pathogenesis

It is likely a combination of many factors which results in enhanced virulence of MRSA in pulmonary infections, including host, bacterial, and environmental [195]. MRSA elicits a robust host immune response in both *in vivo* and *in vitro* models [206]. First, neutrophils are recruited to the site of infection in response to chemotactic factors, such as IL-8 [206-208]. Secreted bacterial virulence factors (e.g. enterotoxins) are able to elicit IL-8 production by epithelial, endothelial, and monocytic cells, thus promoting transmigration of neutrophils to the site of infection [206-208]. Other cell surface components, such as the capsular polysaccharide

and peptidoglycan, are able to stimulate CD4+ T-cells, resulting in the production of potent chemotactic molecules [209-211].

Following neutrophil attraction to the site of infection, MRSA is phagocytosed in an attempt to remove the bacterium [206]. While neutrophils are generally able to efficiently kill most ingested MRSA bacteria, host tissues may be damaged by the inadvertent release of cytotoxic components [206]. In some cases, certain MRSA strains such as USA300, may alter the progression of bacteria-induced apoptosis, resulting in neutrophil lysis and thus pathogen release [152, 212]. In other cases, MRSA is able to interact with Toll-like receptors expressed on the neutrophil cell surface prior to phagocytosis, activating signaling pathways which promote cell survival, phagocytosis, and cytokine release [213-215].

As previously described MRSA has a number of bacterial virulence factors, some of which are known to play an important role in the development of staphylococcal pleuropulmonary infections [177]. In various mouse pneumonia models, SpA, α-hemolysin, and PVL have each been shown to play an important role in the pathogenesis of pneumonia [195]. Labandeira-Rey *et al.* showed that PVL-positive MRSA strains, such as USA300, cause necrotizing pneumonia similar to that seen in humans, while PVL-negative strains did not [82, 195]. It is believed to cause extensive tissue necrosis by destroying leukocytes, thus contributing to the pathogenesis of MRSA pneumonia [82, 151, 166]. While the precise role of PVL in pulmonary infections has yet to be uncovered, it is evidently significant. The pore-forming toxin α-hemolysin, is essential for the pathogenesis of clinical pneumonia [216]. It is believed that α-hemolysin promotes inflammasome activation and platelet-neutrophil aggregates, both of which dysregulate inflammatory responses leading to necrotic lung injury [177, 217, 218]. Wardenburg *et al.* reported that MRSA mutants which inhibited SpA were unable to cause lethal lung

infections, suggesting that SpA is important for lung parenchymal damage [216]. Interestingly, immunization against α-hemolysin has been shown to be protective against lethal pneumonia in mice [219, 220].

2.5 - Treatment

Prior to the current antibiotic era, an *S. aureus* infection was considered a death sentence, with blood stream infections having a case fatality rate of 80% [59, 60, 177, 221]. While this case fatality rate immediately lowered following the introduction of penicillin in 1942, antibiotic efficacy has plateaued in recent years, with case fatality rates of 15-50% still being observed [177, 222, 223]. In general, treatment with intravenous drugs for >2 weeks is recommended for MRSA pneumonia [61, 157]. Importantly, the delay of effective therapy is associated with increased mortality [224].

Currently, vancomycin and linezolid are both recommended for treatment of MRSA pneumonia [145, 165, 225]. Vancomycin, a tricyclic glycopeptide derived from *Streptococcus orientalis*, is the primary treatment of choice [226-228]. Vancomycin is used to treat Gram-positive bacterial infections, by inhibiting biosynthesis of the peptidoglycan layer [226, 227, 229-231]. This inhibition weakens bacterial cell walls, resulting in leakage of intracellular components and bacterial cell death [229, 230]. In cases of vancomycin failures, linezolid is used [145]. Linezolid is an oxazolidinone antibiotic which binds to the 50S ribosomal subunit of MRSA, inhibiting protein synthesis [141, 232]. It has proven efficacious in hospital-acquired pneumonia, as it shows superior penetration into lung parenchyma, better availability at the tissue level, and inhibition of toxin production [136, 141, 145, 232, 233]. In the case of CA-MRSA, linezolid appears to have activity against the PVL toxin, as well as α-hemolysin [141, 157].

In cases of both vancomycin and linezolid failure, other antibiotics such as trimethoprim-sulfamethoxazole, fluoroquinolones, doxycycline, rifampin, tetracyclines, and clindamycin may be used [145, 234]. However, MRSA USA300 is becoming more resistant to tetracycline and clindamycin [145, 173]. Additionally, while daptomycin is generally effective in MRSA treatment, it should not be used in cases of pneumonia due to poor lung penetration [145].

3 – The Lungs

To maintain metabolism and life, vertebrates require a continuous supply of oxygen [235]. This constant supply of oxygen is supplied by the lungs, a major organ of the respiratory system whose main function is to facilitate the exchange of oxygen and carbon dioxide with air from the atmosphere [235, 236]. Gas exchange within the lungs faces several fundamental challenges, such as keeping air and blood from mixing while transferring inspired oxygen into circulating hemoglobin, and maintaining the integrity of the air-tissue-blood interface while maximizing transfer efficiency [235]. This is primarily circumvented by exchanging respiratory gases across a very large epithelial surface area within the lungs, which is highly permeable to gases [235].

3.1 – Anatomy of the Lungs

The lungs are a paired organ connected to the trachea by the right and left bronchi (Figure 7) [236, 237]. Each lung is composed of smaller units called lobes, which are separated by fissures. The right lung is composed of three lobes, known as the superior, middle, and inferior lobes, while the left lung is composed of only the superior and inferior lobes. Each lobe is further divided into multiple bronchopulmonary segments, each of which receives air from its

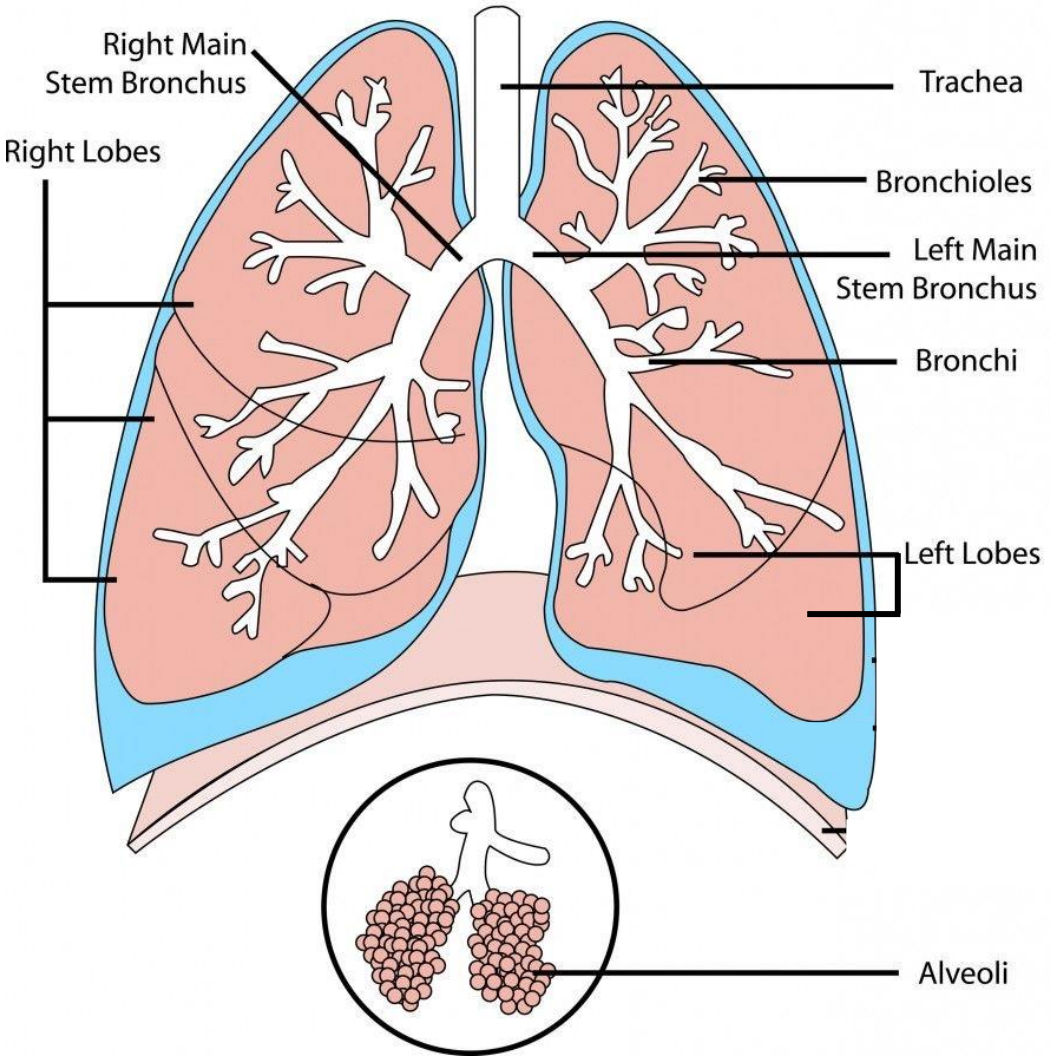

Figure 7: Diagram of the Lungs.

Figure 7: Diagram of the Lungs.

The lungs are connected to the trachea by the right main stem and left main stem bronchi. The right lung is composed of three lobes, while the left is composed of two lobes. Each lobe receives air from tertiary bronchi, which further branch into bronchioles. At the end of each bronchiole are alveoli, which is where gas exchange occurs.

From Hashim *et al.* [237].

own tertiary bronchus and is supplied with blood by its own artery. As the bronchi branch into bronchioles, they form subdivisions known as pulmonary lobules, which are separated by walls of connective tissue known as an interlobular septum. At the end of the bronchioles are alveoli [236].

3.2 – Blood Supply to the Lungs

Gas exchange within the lungs requires blood from the pulmonary circulation to transport oxygen from the lungs to other tissues in the body [236]. Deoxygenated blood is transported to the lungs by the pulmonary circulation, where red blood cells pick up oxygen to be transported to tissues throughout the body. Transportation of deoxygenated blood occurs by the pulmonary artery, an artery which arises from the pulmonary trunk. The pulmonary artery branches as it follows the bronchi, with each branch becoming smaller in diameter. These are known as arterioles and supply deoxygenated blood to one pulmonary lobule [236]. As the pulmonary arterioles near the alveoli, they become the pulmonary capillary network which consists of tiny vessels with very thin walls. The capillary network branches, following the bronchioles and structure of the alveoli until eventually the capillary wall meets the alveolar wall, creating the alveolar-capillary barrier. Following oxygenation of the blood, it is drained from the alveoli by the pulmonary veins [236].

3.3 - Structure of the Alveolar-Capillary Barrier

The alveolar-capillary barrier within the lungs is the site of gas exchange in mammals [86]. It is composed of epithelial cells facing the alveolar lumen, endothelial cells facing the capillary lumen, and an extracellular matrix (ECM) composed of the epithelial and endothelial basement membranes (Figure 8) [238-240]. While incredibly thin, the alveolar-capillary barrier is also incredibly strong, in order to tolerate tension [241]. The continuity and tightness of both the

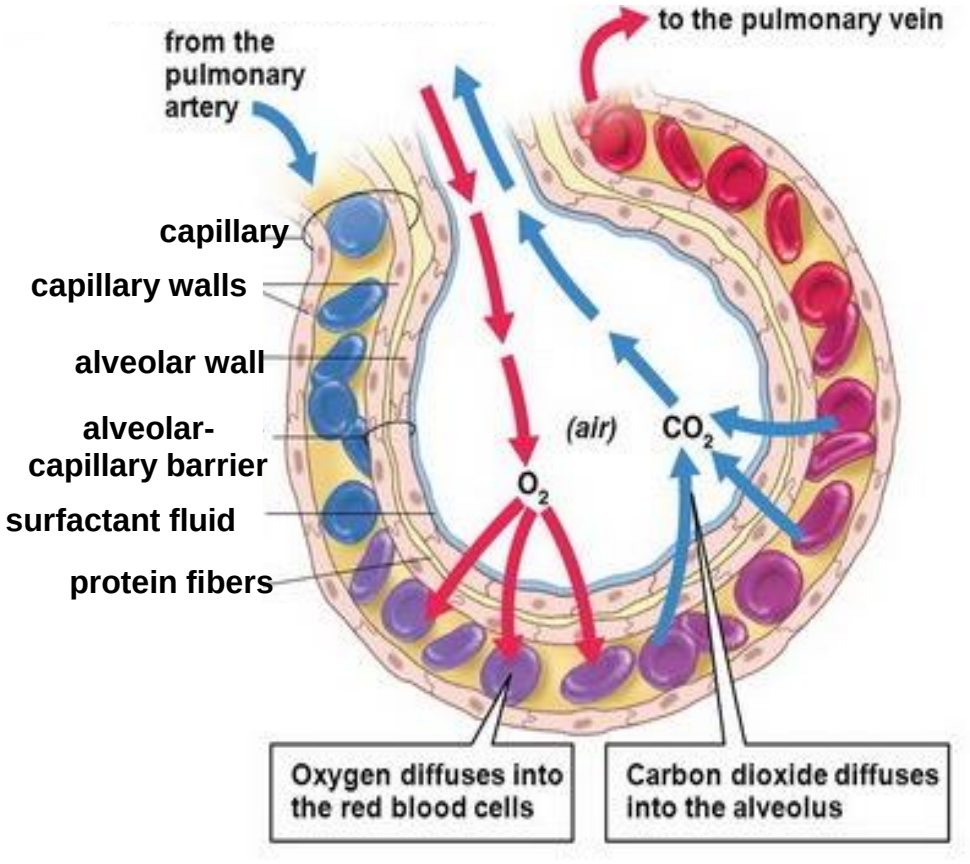

Figure 8: Structure and Function of the Alveolar-Capillary Barrier.

Figure 8: Structure and Function of the Alveolar-Capillary Barrier.

The primary function of alveoli is the exchange of oxygen and carbon dioxide to and from the bloodstream. To accomplish this, the basement membranes of alveolar epithelial cells are in close proximity to endothelial cells of the capillary. Between the basement membranes of each cell type is an amalgamation of proteinaceous fibers. This membrane ensures that air does not enter the bloodstream, while simultaneously ensuring that blood does not enter the alveoli; it is formally known as the alveolar-capillary barrier.

From Biology: Life on Earth (8th edition) [240].

alveolar epithelium and capillary endothelium are essential for fluid balance as they work to separate and regulate extracellular fluid compartments, such as blood plasma, interstitial fluid, and surfactant [238].

3.4 – Function of the Alveolar Epithelial Barrier

The alveolar epithelial barrier acts as a physical barrier between the internal environment and the external environment. Previous studies have shown that it is the alveolar epithelial cells which control permeability of the alveolar-capillary barrier [242]. There are two main transport pathways across the epithelium: transcellular and paracellular [243]. Transcellular transport is dependent on the polarised distribution of ion channels and transports across the alveolar epithelium [243]. Paracellular transport is dependent on diffusion processes driven by chemical and electrochemical gradients, with transport occurring through the extracellular compartment between the lateral membranes of neighbouring epithelial cells [243]. Paracellular transport is controlled by tight junctions of the alveolar epithelium [243]. Respiratory epithelial cells also operate as a critical barrier preventing pathogenic infections from spreading beyond the respiratory system [244]. Clinical studies have shown that barrier dysfunction (i.e. due to severe pneumonia or ARDS) is often fatal [245].

3.4.1 – Structure of the Alveolar Epithelial Barrier

The alveolar epithelial barrier is composed of alveolar type I (ATI) cells and alveolar type II (ATII) cells [239, 246]. ATI cells are thin, squamous cells which make up 95% of the alveolar epithelium [235, 238, 239]. The cuboidal ATII cells, which make up the remaining 5% of the alveolar epithelium, act as the progenitors of ATI cells and are recognizable by their characteristic secretory organelles [238, 239]. These secretory organelles are responsible for the synthesis, storage, and secretion of all surfactant components, which stabilizes the alveoli and

prevents collapse [238]. Surfactant constitutes the surface film at the air-liquid interface, and is composed of 90% lipids and 10% proteins [238, 247]. While surfactant works to stabilize alveoli and prevents collapse, it also has immunomodulatory functions [238]. Surfactant proteins-A and -D play a role in the innate immune system and are able to regulate the functions of other innate immune cells, such as macrophages [248]. Additionally, surfactant has been shown to modulate the function of adaptive immune cells as well, such as dendritic cells and T cells [248].

3.4.2 – Tight Junctions of the Alveolar Epithelial Barrier

ATI and ATII cells form a barrier that, when healthy, is largely impermeable to proteins and solutes, thanks to the expression and regulation of apical junction complexes, which are composed of TJs, AJs, desmosomes, and gap junctions [246, 249]. TJs specifically are able to control the permeability of the epithelial barrier, protecting against the entry of pathogens to the airway lumen [249]. For example, zonula occludens (ZO; i.e. ZO-1, ZO-2, ZO-3) run across the apical surface of ATI cells, as well as between ATI and ATII cells [242, 250]. ZO-1 specifically forms band-like structures in ATI and ATII cells [245]. The claudin family, which are highly expressed in both ATI and ATII cells, are also involved in regulation of the permeability of the alveolar epithelial barrier [246]. The claudin family is also thought to be associated with fluid clearance at the alveolar epithelium [246]. Lastly, occludin is believed to contribute to the formation of cell-cell junctions in the epithelial barrier [245].

Unfortunately, very little is known about the composition and regulation of TJs within the alveolar barrier [245]. It is generally accepted that the presence of viruses or bacteria results in the disruption of these tight junctions [250]. Moreover, certain host factors which are expressed upon barrier infection may result in tight junction disruption even after the infection has been resolved [250]. For example, the paracellular permeability of claudin-3, which is expressed

abundantly in the alveolar epithelium, is known to increase upon exposure to TNF-α [251]. Moreover, activation of NFκB by TNF-α, is known to attenuate claudin-5 expression in the alveolar epithelium, even in the absence of inflammation [252]. The maintenance of this complex network of intercellular junctions linking individual epithelial cell cytoskeletons keeps respiratory infections from transitioning to pulmonary edema or excess infiltration of immune cells [244].

3.5 – The Extracellular Matrix

The ECM acts as the scaffold for both the alveolar epithelium and capillary endothelium, and provides the structural basis for gas exchange [238, 239, 241]. Importantly, it forms a self-stabilizing tension and integrity structure in the lung [253]. It plays many roles involved in cell survival, proliferation, migration, and differentiation, as well as tissue morphogenesis and repair [239]. Additionally, the ECM plays an important role in alveolar-capillary barrier function, as it regulates cell-cell interaction and controls the trafficking of fluid and molecules [239].

The ECM is composed of the epithelial basement membrane, the endothelial basement membrane, and interstitial connective tissue whose composition and thickness varies [235, 238, 254]. This interstitium is associated with connective tissue fibers, such as bundles of type I and II collagen, elastin, and proteoglycans [235, 238, 239]. In some places, this interstitial space between the alveolar epithelium and capillary endothelium does not exist, as the basement membranes of the respiratory epithelial cells and the capillary endothelial cells are fused instead; on average, there is only 0.5 - 2 μm separating the alveoli from the capillaries [235, 238, 254]. This, in combination with its large surface area of ~140 m_2 in humans, allow for efficient diffusion of oxygen and carbon dioxide across the alveolar-capillary barrier [255]. The elastic and collagen fibers of the extracellular matrix are able to stretch, helping to balance the force

generated by surface tension at the alveolar air-liquid interface during gas exchange [252]. This, in concert with the surfactant covering the alveolar epithelium, work to stabilize alveoli during gas exchange, to ensure that alveolar epithelial cells are not subjected to undue mechanical stress [252].

3.6 – Function and Structure of The Endothelial Capillary Barrier

The capillary endothelium, similar to the alveolar epithelium, forms a semipermeable barrier which regulates fluid and nutrient exchange [239, 256]. The endothelium is composed of a thin, singular layer of cells, which separates the vascular lumen from the alveoli [256]. The close proximity of the endothelial cells of the capillaries to the alveolar epithelia strongly suggests that direct crosstalk exists between the two membranes [257]. It is thought that when the alveolar epithelium encounters pathogens, such as inhaled bacteria, it likely results in the activation of crosstalk from the alveolar epithelia to the capillary endothelium [257]. These signaling mechanisms are thought to sequentially move through the apical and basolateral aspects of the epithelial membrane, before moving to the underlying endothelium, resulting in inflammation at the capillaries [257]. Interestingly, immune cell recruitment initiated by endothelial cells is thought to play an essential role in barrier loss during inflammation, though the mechanism is yet unknown [258].

3.6.1 – Tight Junctions of the Endothelial Capillary Barrier

The endothelial capillary barrier, similar to the epithelial alveolar barrier, maintains its integrity via apical junction complexes, including AJs, TJs, and gap junctional channels [246, 249]. ZO-1 is known to play a similar role in the endothelial capillaries as in the alveolar epithelia, forming band-like structures across cells [242, 245, 250]. Occludin also plays an important role in tight junctions of the endothelial barrier, by contributing to cell-cell junctions

[245]. Within the human lung endothelium, AJs are primarily formed by VE-cadherin, a transmembrane cadherin which connects neighbouring endothelial cells [246, 256]. Preserving the function of VE-cadherin is known to improve the outcome of inflammatory diseases; studies in which AJs were inhibited resulted in a drastic increase in endothelial permeability, revealing the incredible importance of AJs within the endothelial barrier [256].

4 – Current Knowledge on Influenza-Bacterial Co-infections

There is an increasing appreciation that a large percentage of severe or fatal influenza infections are associated with secondary bacterial infections [49]. Typically, an IAV infection alone is not sufficiently virulent to result in death in healthy adults [259]. Instead, hospitalization and mortalities are most frequently due to either exacerbation of an underlying condition or to secondary bacterial pneumonia [259].

4.1 – Secondary Bacterial Infections Throughout History

The contribution of bacterial infection to influenza morbidity and mortality has been well documented throughout each of the pandemics over the past century. Modern analyses of lung tissue and review of historical autopsy data from fatal 1918 Spanish IAV infections demonstrated that 95% of lethal cases were complicated by bacterial co-infection due to *Streptococcus pneumoniae*, *Streptococcus pyogenes*, *Haemophilus influenzae*, and *S. aureus* [49, 260, 261]. During the 1957 and 1968 influenza pandemics, secondary bacterial pneumonia also caused significant morbidity and mortality, with *S. aureus* and *S. pneumoniae* being the predominant bacterial pathogens [49]. Most recently, during the 2009 influenza pandemic, up to 34% of severe influenza infections managed in intensive care units and up to 55% of fatal cases were complicated by bacterial co-infections [262]. Additionally, during seasonal epidemics, bacterial co-infections complicate 0.5% of all influenza cases in healthy adults, and 2.5% of all

cases in the elderly and individuals with co-morbidities[262]. In the U.S., it is estimated that approximately 65,000 influenza- and pneumonia-related deaths occur each year [261, 262].

4.2 – Animal Models

A number of animal models have been used to study co-infections, including nonhuman primates (NHP), ferrets, and mice. Both NHPs and ferrets can be naturally infected with human IAVs, with similar symptoms and disease severity as humans [263, 264]. Mice are also often used to study IAV infection; however, they are not natural hosts of IAVs, and isolates must first be adapted [263].

4.2.1 –Nonhuman Primates

Five NHP studies using intratracheal influenza infection followed by bacterial infection have been carried out since 1954, with four showing that co-infection resulted in more severe bronchopneumonia than viral infection alone [264-268]. A nonhuman primate model of influenza and bacterial co-infection which mimics severe disease in humans was developed by Chertow *et al.* [264]. Rhesus macaques were inoculated with IAV, followed by MRSA four days post-influenza infection. High-resolution CT scans were used to quantitatively assess the course of illness and severity over a two week period (Figure 9). No evidence of pneumonia was seen in mock-infected animals; however, Chertow *et al.* reported evidence of pneumonia in all animals infected with MRSA, influenza, or co-infected with influenza and MRSA. At 6, 10, and 14 days post-influenza infection, the hyper-intensity of infiltrates in the animals co-infected with influenza and MRSA was significantly increased compared with the other animals. Overall, Chertow *et al.* found that a more severe lung histopathology was seen in co-infected animals, compared with animals infected with influenza alone or with MRSA alone [264].

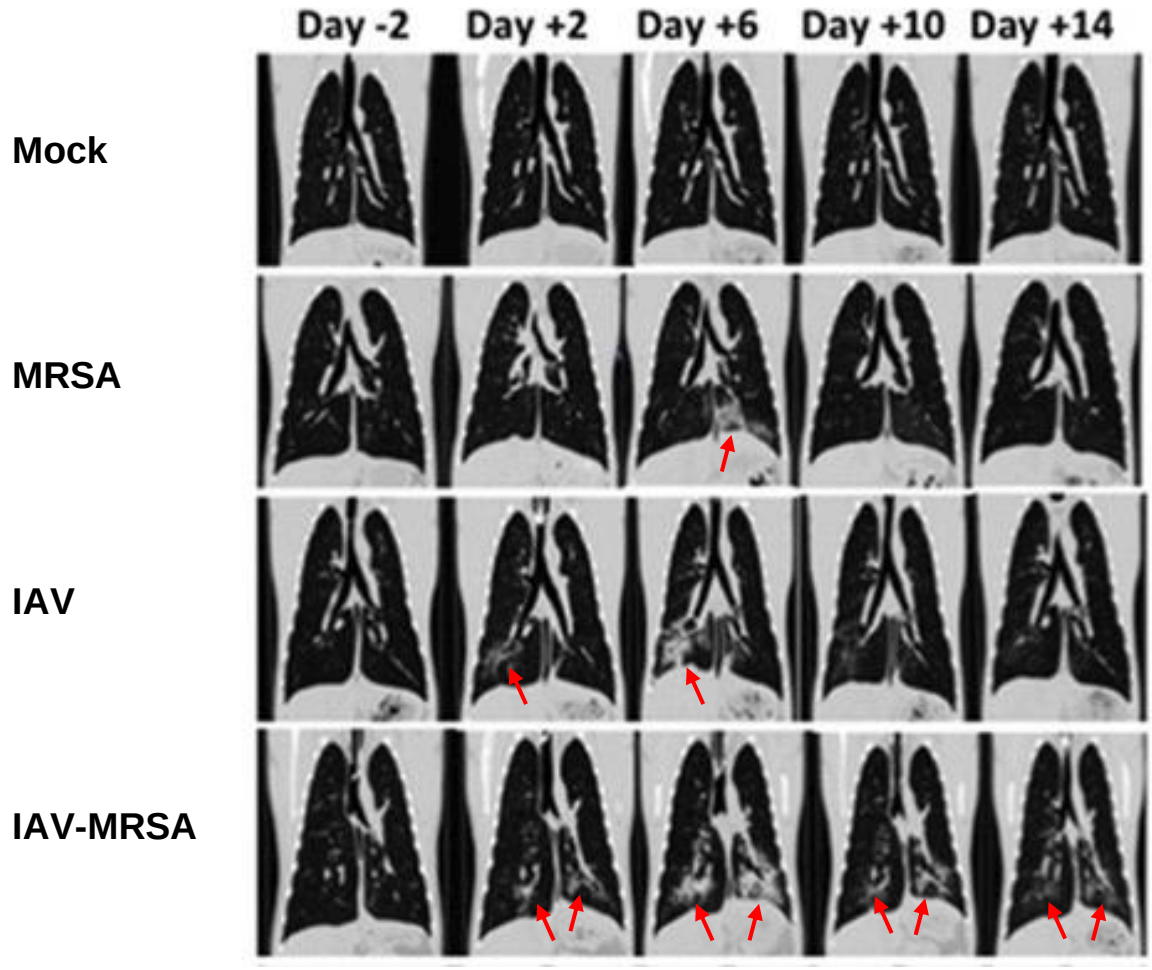

Figure 9: Computed Tomography Scans Showing Diffuse Bilateral Infiltrates in Rhesus Macaques.

Figure 9: Computed Tomography Scans Showing Diffuse Bilateral Infiltrates in Rhesus Macaques.

Rhesus macaques were infected with IAV on Day 0, followed by MRSA on Day +4. Red arrows show evidence of pneumonia as seen by CT scan. Evidence of pneumonia was observed in animals infected with MRSA, IAV, and IAV-MRSA at Day +6. The hyperintensity of infiltrates in IAV-MRSA co-infected animals was significantly increased at Days +6, +10, and +14 as compared with other animals.

From Chertow *et al.* [264].

4.2.2 - Ferrets

In ferrets inoculated with 2009 pandemic H1N1 IAV, significant upregulation of TNF-α, IL-6, and IL-8 was observed in the lungs at 1 day post-infection (dpi) [269]. *In situ* hybridization revealed that TNF-α was primarily produced by alveolar and bronchial epithelial cells, as well as macrophage-like cells [269]. IL-6 production was primarily mediated by epithelial cells of the bronchus, bronchioles, and alveoli; IL-8 was predominantly expressed by neutrophils [269]. Exposure of capillary endothelial cells to TNF-α alone, or TNF-α followed by IFN-γ, resulted in impaired barrier function, and specifically, local disruption of ZO-1 [270].

4.2.3 - Mice

A study by Walters *et al.* showed that secondary bacterial infections in mice enhanced lung pathology, damaged endothelial cells, and activated coagulation [271]. In short, mice were infected with 1918 pandemic H1N1 IAV, prior to *S. pneumoniae* infection. The co-infected mice had a shortened survival time, increased bacterial replication, and an altered host response to infection [271]. Global transcriptional profiling revealed that co-infection resulted in enrichment of genes related to inflammatory response, immune cell trafficking, haematological systems, and tissue injury [271]. Immune response-related genes involved in neutrophil recruitment, neutrophil activation, platelet aggregation, platelet activation, and coagulation were all either highly expressed or uniquely expressed in co-infected mice [271].

4.2 – IAV-Bacterial Co-Infections in Humans

Various studies have been done on patients suffering from IAV-bacterial infections over the past century. In general, severe influenza-bacterial co-infections present similarly to severe influenza infections; however, co-infections present an increased mortality risk [260]. Autopsies done on patients from the 1918, 1957, and 2009 IAV pandemics, as well as decedents of

seasonal influenza, reveal no significant differences in pulmonary pathologies [9, 272-275]. As such, only studies involving patients infected with 2009 pandemic IAV are discussed here. Throughout the 2009 H1N1 pandemic, critical illness often occurred in young adults rapidly after hospital admission, and was associated with severe hypoxemia and multisystem organ failure [276].

A case of IAV-MRSA co-infection was reported by Memoli and Chertow [262]. A patient was admitted to hospital with fever, cough, myalgia, and shortness of breath, consistent with severe IAV infection [262]. Further evaluation revealed findings consistent with severe hypoxia and sepsis; a chest radiography showed diffuse bilateral infiltrates (Figure 10) [262]. A nasopharyngeal wash specimen tested positive for 2009 H1N1 pandemic IAV, while sputum and blood cultures tested positive for MRSA [262]. Despite being treated with both antivirals and antibiotics, the patient suffered from respiratory failure complicated by hemoptysis and died within 24 hours of hospital admission [262]. Studies have shown that many IAV-bacterial co-infections mirror the one described above. Infected individuals often present with fever, cough, dyspnea, and myalgia, with a median of 7 days from the onset of symptoms to death [272, 277].

A study by Gill *et al.* described the clinicopathologic characteristics of patients who died following confirmed 2009 H1N1 IAV infection. Gill *et al.* used chest radiographs to study the lungs of four patients, revealing pathological differences in patients infected with IAV alone, or with an IAV-bacterial co-infection [272]. Computed tomography (CT) scans revealed patchy "ground-glass" opacities in each of the patients; the underlying parenchymal architecture remained visible with discernible bronchovascular margins consistent with diffuse alveolar damage (Figure 11A) [272]. In one case, areas of denser consolidation were seen, which obscured the underlying parenchymal architecture and bronchovascular margins (Figure 11B)

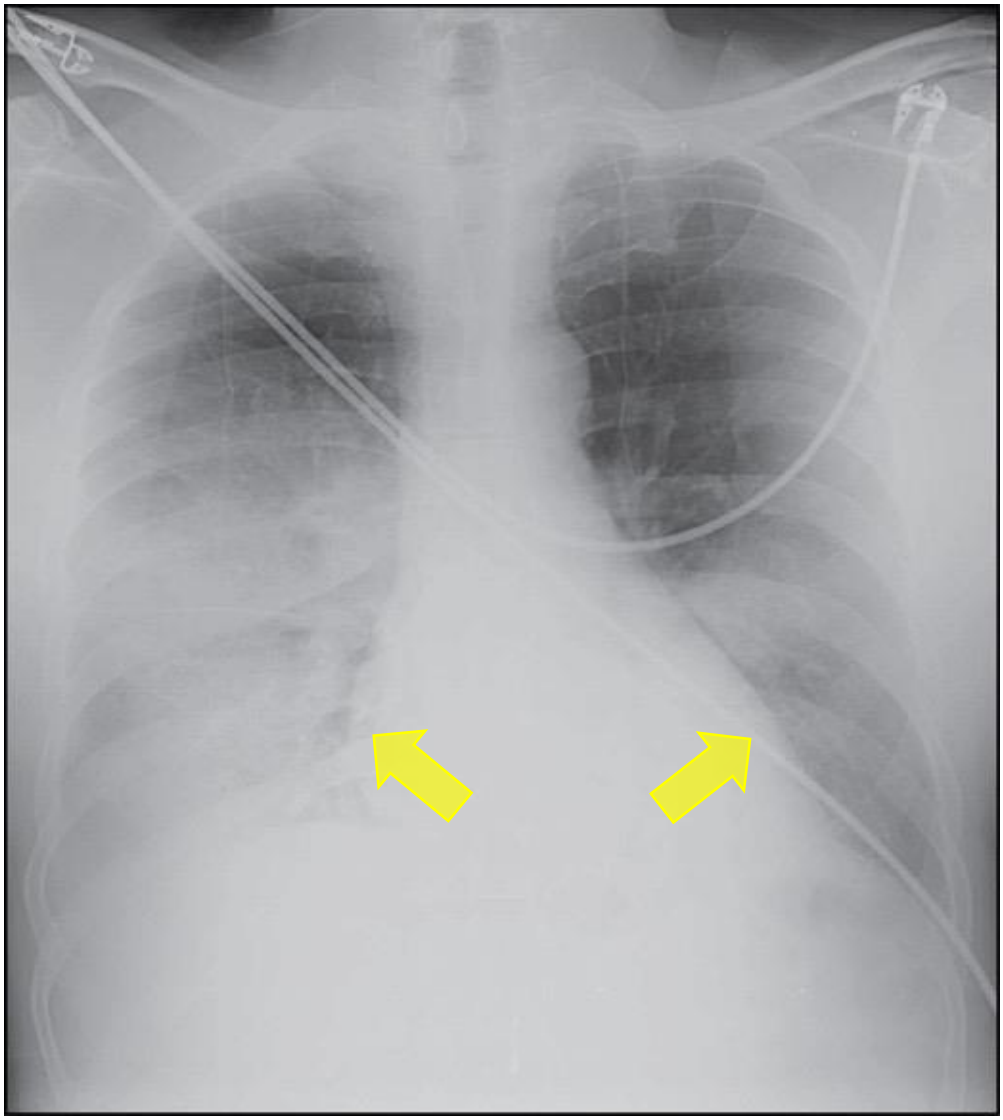

Figure 10: Chest Radiography of a Fatal Case of Influenza-Bacterial Co-infection.

Figure 10: Chest Radiography of A Fatal Case of Influenza-Bacterial Co-infection.

Chest radiography of a patient co-infected with 2009 H1N1 pandemic IAV and MRSA. Yellow arrows indicate diffuse bilateral infiltrates, a characteristic of ALI and ARDS. From Memoli and Chertow [262].

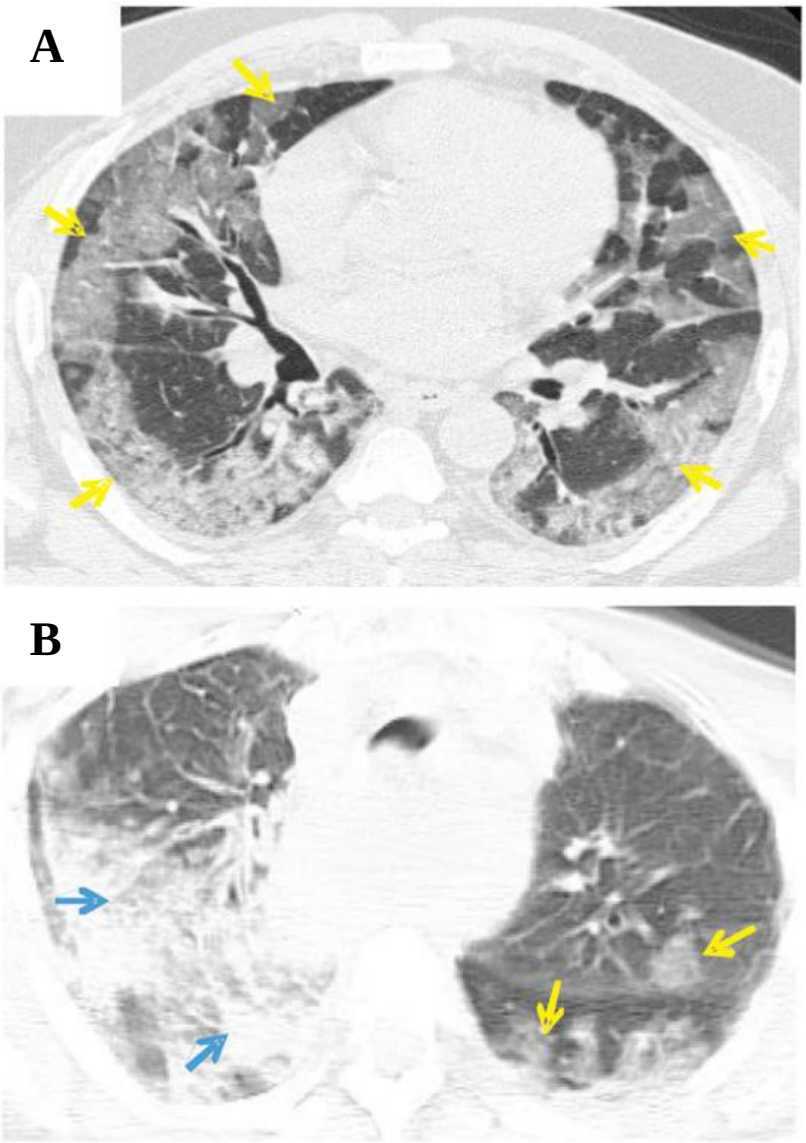

Figure 11: Computed Tomography Scans of Fatal Influenza-Bacterial Co-infections.

Figure 11: Computed tomography scans of two fatal cases of influenza-bacterial co-infections.

A) Yellow arrows indicate diffuse alveolar damage where the underlying parenchymal architecture remained visible.

B) Yellow arrows indicate diffuse alveolar damage where the underlying parenchymal architecture remained visible. Blue arrows indicate denser consolidation which obscured the underlying parenchymal architecture.

From Gill *et al*. [272].

[272]. These findings were consistent with secondary bacterial pneumonia, which was identified at autopsy [272]. Bacterial pneumonia was observed in 55% of the cases studied by Gill *et al.*, who underlined the necessity of diagnosing and treating bacterial pneumonias in patients infected with influenza virus [272].

Autopsy findings of patients with IAV-bacterial co-infections manifesting as ALI showed an increase in capillary endothelial permeability, injury to the alveolar epithelium and loss of the tight permeability barrier [270]. Additionally, pro-inflammatory cytokines, such as TNF-α and IFN-γ, are elevated in ALI patients [270]. Autopsies of patients diagnosed with ARDS due to the presence of bilateral pulmonary infiltrates, reveal diffuse alveolar damage, diffusely edematous lungs, and variable degrees of hemorrhage [277].

4.4 – Mechanisms of Bacterial Co-Infections at the Alveolar-Capillary Barrier

While it is generally accepted that influenza-bacterial coinfections result in more severe disease, the molecular mechanisms have not yet been elucidated [260]. It is known that IAV infection can cause changes to the lung which may facilitate secondary bacterial invasion [49]. Increased bacterial and/or viral loads during co-infection have been associated with enhanced disease severity; however, how this occurs is still unknown [49, 271].

4.4.1 – Molecular Mechanisms of Co-infection

Several changes occur at the alveolar epithelium upon IAV infection, including damage to the epithelial airway and disruption of surfactant released by ATII cells [49]. Damage to alveolar epithelial cells is the primary driver of alveolar-capillary barrier dysfunction [262, 278]. This damage occurs via several different mechanisms: physical damage to the alveolar epithelial barrier, damage to TJs, and the production of cytokines which can damage the alveolar-capillary barrier [279].

Physical damage to the airway occurs in several steps during IAV-bacterial co-infection (Figure 12). First, IAV infection along the airway epithelium results in the cleavage of cell-surface sialic acids and in epithelial sloughing, which is thought to expose sites for bacterial attachment [262]. As such, when patients with prior IAV exposure breathe in pathogenic bacteria through the nasopharynx, it is able to bind to these newly cleaved and exposed sialic acid sites [262]. Second, the presence of IAV along the airway epithelium leads to mucociliary dysfunction, resulting in an increase in mucus production in the lower respiratory tract [262]. This excess mucus is meant to facilitate viral clearance; however, it is thought to impede bacterial clearance [260, 261]. Finally, the pathogens are able to reach the alveoli, resulting in cellular dysfunction, aberrant immune responses, and cell death [262].

It is thought that the endothelial cells of the capillary may be exposed to viral particles produced by alveoli cells during viral infection, due to their close proximity to alveolar epithelial cells [254]. However, infection is generally only seen during infection with highly pathogenic H5N1 IAVs; in most animal models and human autopsies, IAV infection of the endothelial barrier is not observed [254]. Regardless of their infection status, endothelial cells continue to play a key role in severe disease pathogenesis, as they induce an inflammatory response through the production of cytokines [254, 280].

4.5 – The Innate Immune Response to Influenza-Bacterial Co-infections

In the case of influenza-bacterial coinfections at the alveolar-capillary barrier, priming of the immune response by initial influenza infection results in a massive over-recruitment of immune cells due to the cytokine storm generated by alveolar epithelial cells which are primed and actively secreting cytokines to respond to the primary infection [281]. Cytokines and growth factors produced by the innate immune response in response to IAV infection play a crucial role

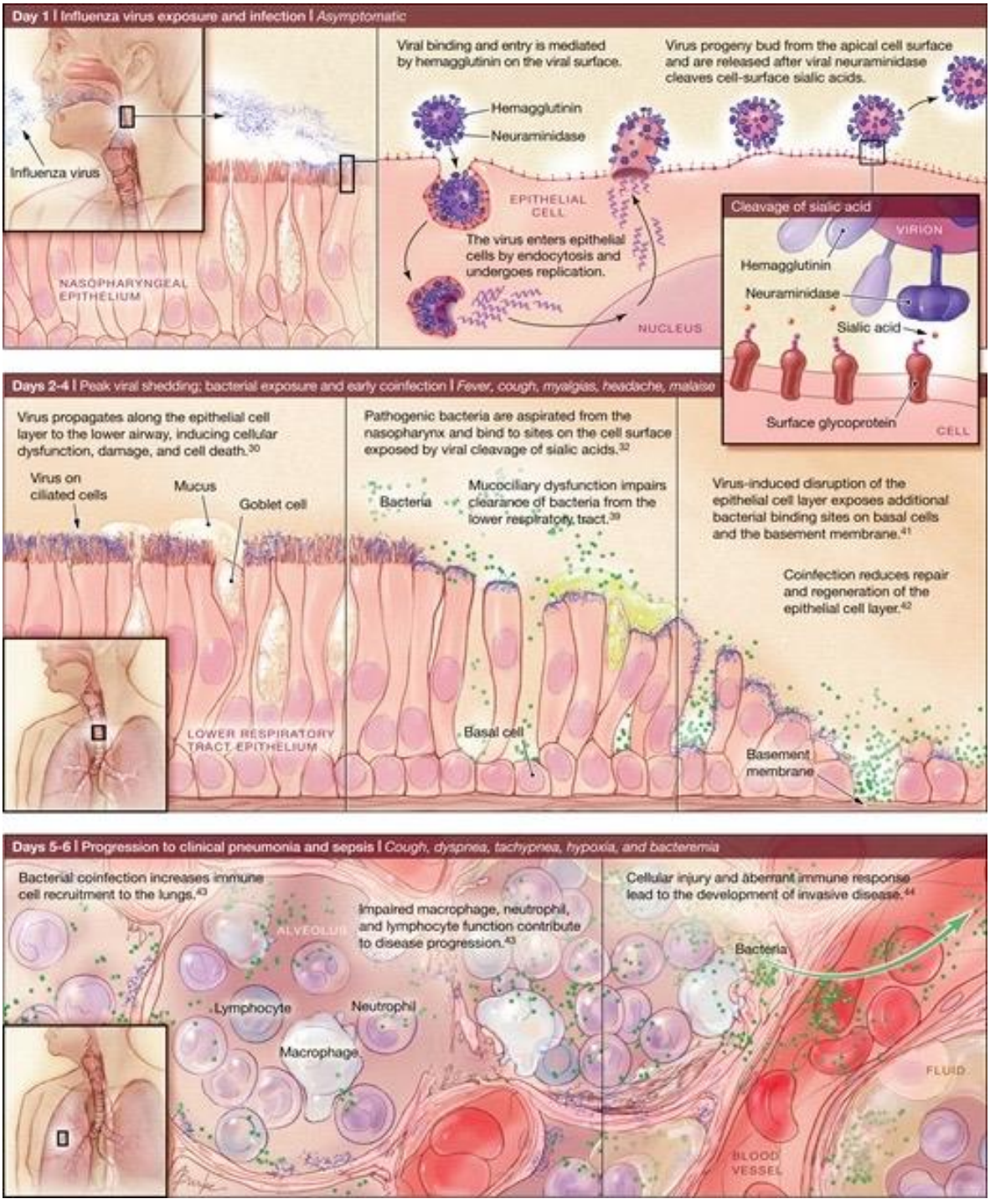

Figure 12: Proposed Mechanism of Influenza-Bacteria Co-infection at the Airway Epithelium.

Figure 12: Proposed Mechanism of Influenza-Bacterial Co-infection at the Airway Epithelium.

Physical damage to the airway occurs in several steps during IAV-bacterial co-infection. First, IAV infection and replication occurs along the airway epithelium. This replication results in the cleavage of sialic acids during viral release from the host cells (top panel). IAV continues to replicate along the epithelial airway towards the lower respiratory tract resulting in cellular damage and dysfunction, including mucociliary dysfunction. As the host aspirates pathogenic bacteria, the previously cleaved sialic acids act as binding sites while mucociliary dysfunction impairs bacterial clearance (middle panel). Finally, co-infection leads to the recruitment of immune cells and subsequent impaired function leading to damage to the alveolar-capillary barrier and invasive disease (bottom panel).

From Chertow & Memoli [262].

in host tolerance by suppressing inflammation, initiating tissue repair, and returning the pulmonary system to a state of homeostasis after the resolution of infection [244]. Further, cytokines are able to act on the epithelium to induce proliferation and growth, making it vital in mediating repair following infection [244]. In their absence, virally infected hosts become more susceptible to secondary bacterial infections [282].

The innate immune response is rapidly triggered after IAV infection, resulting in the production of massive amounts of type I IFN and ILs which strongly participate in virus clearance [283-286]. Upregulation of type I IFN expression in respiratory epithelial cells correlates with a significant upregulation of TLRs, which is thought to contribute to the upregulation of cytokine secretion and the initiation of a cytokine storm [287-290]. Additionally, IAV infection has been shown to result in a cytokine storm by inducing the expression of other pro-inflammatory cytokines beyond IFN and ILs, such as TNF [291-293]. Limiting the magnitude of a cytokine storm has been shown to improve survival, as well as augment host tolerance to secondary bacterial infection, as it is incredibly detrimental to the host during pulmonary infections [287, 288, 291, 292]. Further, activation of inflammasomes and NF-κB further promote the release of pro-inflammatory cytokines and chemokines [286]. Interestingly, while inflammasome activation is generally crucial for the clearance of many lung pathogens, delaying activation during IAV infection decreases inflammation and bacterial burden during a secondary infection [294]. The secretion of these cytokines by the respiratory epithelium results in the subsequent recruitment and activation of numerous immune cells, such as macrophages, and neutrophils [286].

Inflammatory macrophages infiltrate the lung following pathogen infection, playing an important role in mediating early defense mechanisms and facilitating the return to homeostasis

during the resolution of infection [244]. While they are important mediators of the inflammatory response, they also contribute to an excessive inflammatory response and damage [244]. However, depletion of alveolar macrophages during IAV infection further exacerbates inflammation and contributes to decreased epithelial barrier function and vascular leakage [295, 296]. Seemingly in contrast, failure to induce programmed cell death of macrophages results in unregulated, prolonged inflammation decreasing tolerance to infection, underlining the importance of proper regulation of macrophages during co-infection [297-299]. Macrophages can also act as phagocytes, helping to control the pathogen burden while removing dead cells and debris that accumulate during infection [244]. Alveolar macrophages are also known to produce proteases and miRNA directly involved in degradation of tight junctions such as ZO-1, pulmonary inflammation, and tissue damage [300, 301].

Neutrophils act as potent mediators of the immune response early in co-infection by unleashing powerful antimicrobial defenses [244]. However, this generally results in extreme tissue damage and dampening their effect has actually been shown to be beneficial for improving pulmonary inflammation during infection [244, 302]. In a rat model, depletion of neutrophils resulted in increased mortality due to delayed viral clearance, but was associated with decreased inflammation and breakdown of the epithelium [303]. Further, proteases present on the surface of neutrophils are able to cleave VE-cadherin, an adherens junction which plays an important role in endothelial barrier integrity [304].

4.2.1 - Current Treatment of IAV-Bacterial Co-infections

It is recommended that early antiviral and antibiotic treatment be initiated in all patients with a suspected IAV-bacterial co-infection [262]. Observational studies have found a correlation between oseltamivir administration and reductions in ICU admission and deaths

[262]. Additionally, a correlation between administration of antibiotic treatment within 8 hours of hospital admission and reduced mortality has been revealed by large observational studies [262]. As such, vancomycin or linezolid should be administered to hospitalized patients with severe or necrotizing community-associated pneumonia, even if the presence or absence of influenza cannot be distinguished [262]. Despite these recommendations, management of severe co-infections is largely supportive [262].

Hypothesis and Objectives

Despite our current knowledge and understanding of IAV infections, MRSA infections, and the alveolar-capillary barrier, the molecular mechanisms surrounding barrier dysfunction upon IAV-MRSA co-infections is still unknown. *We hypothesize that secondary bacterial co-infections result in severe dysfunction of the alveolar-capillary barrier due to the modulation of bacterial virulence factor expression in the presence of IAV, thus leading to dysregulated host cell signaling responses.* In order to test this hypothesis, our primary objectives will be as follows:

i) Characterization of pathogen replication kinetics and bacterial virulence factor modulation in an alveolar monolayer during IAV-MRSA co-infection. The role of prior IAV infection on subsequent MRSA replication and abundance of genes related to adhesion/ attachment will be studied in an alveolar monolayer, allowing synergism between different strains of IAV and MRSA to be investigated.

ii) Determination of cell barrier dysfunction and dysregulation of host cell kinome response during IAV-MRSA co-infection in an alveolar monolayer. Investigations of the effect of bacterial replication and virulence factors from objective (i) on the host cell kinome response and subsequent cell barrier dysfunction when MRSA co-infection occurs with different strains of IAV will allow for a direct characterization of the inter-relation between MRSA and the host cell.

iii) Establishment of a co-culture model of the human alveolar-capillary barrier using primary alveolar epithelial and pulmonary microvascular endothelial cells. Co-culturing of primary alveolar epithelial and endothelial cells derived from the lower respiratory tract on the membrane of a transwell insert will provide a

physiologically-relevant model for investigations concerning the role of distal lung barrier function in IAV and IAV-bacterial pathogenesis.

iv) Characterization of pathogen replication kinetics and route of invasion in a co-culture model of the alveolar-capillary barrier. A thorough analysis of viral and bacterial replication kinetics, pathogen transmigration to the underlying endothelium, and potential relation of enhanced route of invasion to IAV-MRSA co-infections will help rectify current knowledge gaps in the role of pathogen replication and transmigration in severe co-infections.

v) Determination of bacterial virulence factor responses during IAV-MRSA co-infection in a co-culture model of the alveolar-capillary barrier. Investigations of the temporal expression patterns of bacterial virulence factors during co-infection with IAV will provide a detailed characterization of the potential roles for bacterial virulence factors in alveolar-capillary barrier permeability.

vi) Assess barrier dysfunction during IAV-MRSA co-infection in a co-culture model of the alveolar-capillary barrier. Analysis of the direct effects of IAV-MRSA co-infection on the permeability of the alveolar-capillary epithelial-endothelial co-culture system will provide greater biological context as permeability modulation will reflect changes in both cell types.

vii) Investigation of epithelial and endothelial host cell signaling responses. Characterization of host cell signaling responses related to maintenance of cell-cell contacts, cell damage and apoptosis, wound healing, and inflammatory responses will provide valuable information regarding potential host-centric contributions to alveolar-capillary barrier dysfunction.

Materials and Methods

Virus, Bacteria, and Cell Conditions

The 2009 pandemic H1N1 Influenza A/Mexico/4108/09 (pandemic H1N1; pH1N1) was kindly provided by Dr. Kevin Coombs (University of Manitoba, Canada). The following reagents were obtained through BEI Resources, NIAID, NIH (Bethesda, MD, USA): Influenza A/Hong Kong/8/68 (pandemic H3N2; pH3N2); Influenza A/Brisbane/10/2007 (seasonal H3N2; sH3N2); Influenza A/New Jersey/8/76 (seasonal H1N1; sH1N1). All virus stocks were grown in Madin-Darby canine kidney cells (MDCK; ATCC, Manassas, VA, USA) maintained in Dulbecco's modified Eagle medium (DMEM; Gibco, Grand Island, NY, USA), concentrated following ultracentrifugation on a 35% sucrose cushion, and kept at -80 °C . Viral titres for pH1N1, pH3N2, sH1N1, and sH3N2 are summarized in Table 1 and were determined via plaque assay [305]. MRSA USA300 (herein referred to as MRSA) was kindly provided by Dr. George Zhanel (University of Manitoba, Canada). MRSA inocula were generated following growth to mid-log phase in tryptic soy broth at 37°C with shaking (TSB; Hardy Diagnostics, Santa Maria, CA, USA). Bacterial titres are summarized in Table 1 and were determined via standard plate count [306]. Adenocarcinomic human alveolar basal epithelial cells (A549) were obtained from ATCC (Manassas, VA, USA). Cells were grown in DMEM supplemented with 10% fetal bovine serum (FBS; Gibco, Grand Island, NY, USA) and 1% penicillin-streptomycin (HyClone Laboratories, South Logan, UT, USA) at 37°C and 5% CO_2. Normal human bronchial epithelial cells containing SV40 promoter sequences and immortalized by CDK4-expressing retrovirus and human telomerase reverse transcriptase (HBEC3-KT) were kindly provided by Dr. Neeloffer Mookherjee (University of Manitoba, Canada). Cells were grown in Airway Epithelial

Basal Cell Medium (ATCC, Manassas, VA, USA) fully supplemented with the Bronchial Epithelial Cells

Table 1: Pathogen Titres.

Viral titres of pH1N1, sH1N1, pH3N2, and sH3N2 were determined via plaque assay, as previously described by Qi *et al.* [305]. Bacterial titres of MRSA USA300 was determined via standard plate count as previously described by Sanders [306].

Pathogen	**Titre**
Influenza A/Mexico/4108/09 (pH1N1)	1.04×10^6 PFU/mL
Influenza A/New Jersey/8/76 (sH1N1)	7.20×10^6 PFU/mL
Influenza A/Hong Kong/8/68 (pH3N2)	3.04×10^6 PFU/mL
Influenza A/Brisbane/10/2007 (sH3N2)	2.04×10^6 PFU/mL
MRSA USA300	1.5×10^8 CFU/mL

Growth Kit (ATCC, Manassas, VA, USA) at 37°C and 5% CO_2. Human pulmonary alveolar epithelial cells (HPAEpiC) were obtained from ScienCell Research Laboratories (Carlsbad, CA, USA). Cells were grown in Airway Epithelial Basal Cell Medium fully supplemented with the Bronchial Epithelial Cells Growth Kit (ATCC, Manassas, VA, USA) at 37°C and 5% CO_2. Human pulmonary microvascular endothelial cells (HPMEC) were obtained from ScienCell Research Laboratories (Carlsbad, CA, USA). Cells were grown in Basal Endothelial Cell Medium complete kit (ScienceCell Research Laboratories, Carlsbad, CA, USA).

Co-sedimentation of pH1N1 and MRSA

Co-sedimentation of pH1N1 and MRSA (herein referred to as pH1N1+MRSA) was performed as previously described [307]. Mid-log MRSA and pH1N1 were both added to DMEM supplemented with 2% FBS at a multiplicity of infection (MOI) of 0.1. Bacterial MOIs of 0.1 were achieved by serial dilution of mid-log phase culture in DMEM supplemented with 2% FBS. The pH1N1+MRSA inocula was incubated at 37°C and 5% CO_2 with rocking for 30 min. Samples were centrifuged at 5,000 g for 25 min to pellet bacteria and adherent virus. The supernatant was removed, pellets washed with Dulbecco's phosphate buffered saline without Calcium and Magnesium (DPBS; Gibco, Grand Island, NY, USA), and resuspended in DMEM supplemented with 2% FBS.

Viral and Bacterial Infection of Respiratory Epithelial Cells

A549 cells were seeded at 5E5 cells/ mL (1.3e5 cells/ cm_2) in DMEM supplemented with 2% FBS 1 day prior to viral infection. Cells were either mock-infected with DMEM supplemented with 2% FBS or infected with IAV (pH1N1, sH1N1, pH3N2, sH3N2, or pH1N1+MRSA) at a MOI of 0.1 with gentle rocking every 15 min to ensure equal distribution of virus. After 1 h, viral inocula were aspirated from alveolar epithelial cells and replenished with

DMEM supplemented with 2% FBS. Cells were rested for 24 h post-influenza infection, followed by infection with mid-log phase MRSA at a MOI of 0.1 or mock-infected with DMEM supplemented with 2% FBS. Bacterial infection continued for 1 h at 37°C with 5% CO_2 and gentle rocking every 15 min. Bacterial inocula were aspirated from cells and refreshed with DMEM supplemented with 2% FBS. Cells were harvested at 1, 4, 8, 12, 16, 20, and 24 h post-bacterial infection for further investigation of bacterial replication kinetics, bacterial virulence factors' expression, and kinome analysis.

Creation of a Co-culture Model of the Alveolar-Capillary Barrier

The basal side of 0.4 μm transwell inserts (Corning Life Sciences, Montreal, QC) were coated with GelTrex LDEV-Free Reduced Growth Factor Basement Membrane Matrix (ThermoFisher Scientific, Mississauga, ON) and rested basal side up for 1 h at 37°C and 5% CO_2. Transwell inserts were turned apical side up, the apical side coated with GelTrex, and rested for 1 h at 37°C and 5% CO_2. Transwell inserts were turned basal side up, the basal side of the transwell inserts seeded with HPMEC at a concentration of 1.5E5 cells/ mL (4.5E4 cells/ cm_2) in a 1:1 mix of HPAEpiC and HPMEC media, and rested for 3 h at 37°C and 5% CO_2. Transwell inserts were turned apical side up and HPAEpiC were seeded on the apical side at a concentration of 3E5 cells/ mL (9E4 cells/ cm_2) in a 1:1 mix of HPAEpiC and HPMEC media. After 24 h, media was removed from the upper compartment of the transwell insert, to allow primary epithelial cells to grow at the air-liquid interface. Media in the lower compartment was refreshed with a 1:1 mix of HPAEpiC and HPMEC media. Cells were allowed to grow to confluency for 14 days, with media in the lower compartment being refreshed every second day. A schematic of the model can be seen in Figure 13 [280]. Cells were imaged prior to infection to ensure confluency, as described below.

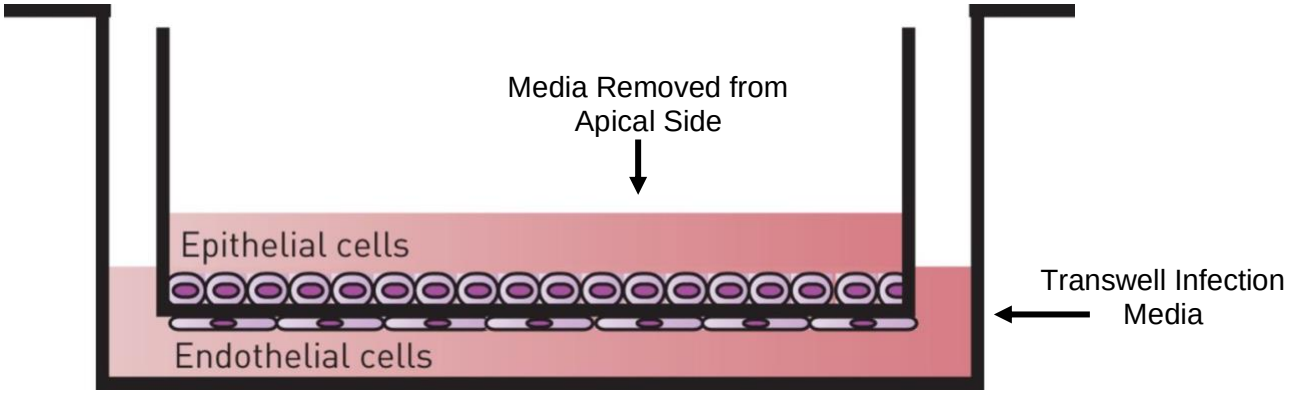

Figure 13: Depiction of the Co-culture Model of the Alveolar-Capillary Barrier.

Error! Reference source not found.**: Depiction of the Co-culture Model of the Alveolar-Capillary Barrier.**

To most closely mimic the human alveolar-capillary barrier, primary alveolar epithelial cells are plated on the apical side of the membrane of a transwell insert, while microvascular endothelial cells are plated on the basal side. This enables both cell types to grow in close proximity, allowing for cell-cell communication between epithelial and endothelial cells. Growth media in our model will be removed from the apical side of the membrane, allowing the alveolar epithelial cells to grow at the air-liquid interface.

From Short *et al.* [280].

Imaging and Histology

Imaging of fixed cells was performed on a Zeiss AxioObserver.Z1 with a x10 lens and images captured using LSM 7 Elyra Software (Release Version 7.0). Prior to fixation, cells were washed 3 times for 15 min with warm DPBS. Cells were fixed with 3.7% formaldehyde (ThermoFisher Scientific, Mississauga, Ontario, Canada) at room temperature for 30 min, followed by washing 3 times for 15 min with PBST. Cells were permeabilized with 0.5% TritonX-100 for 5 min, washed 3 times with PBST for 15 min, and incubated with Image IT Fx Signal Enhancer (ThermoFisher Scientific, Mississauga, Ontario, Canada) for 30 min, followed by a final wash with PBST 3 times for 15 min. Cells were incubated with blocking buffer (5% BSA) for 1 h. Cells were stained with DAPI (Abcam, Toronto, Ontario, Canada; ab228549; 1:500) for 5 min and washed 3 times for 15 min with PBST. Cells were stained with phalloidin (Abcam, Toronto, Ontario, Canada; ab176759; 1:200) for 1 h, washed with PBST 3 times for 15 min with PBST. Cells were mounted with ProLong Diamond Antifade Mountant (ThermoFisher Scientific, Mississauga, Ontario, Canada). Confocal images showing HPAEpiC and HPMEC at 95% confluency can be seen in Figures 14 and 15, respectively.

Viral and Bacterial Infection of Tissue Culture Model

Epithelial and endothelial cells were washed 2X with warm DPBS. Transwell infection media (a 1:1 mix of unsupplemented Airway Epithelial Basal Cell Medium and Basal Endothelial Cell Medium) was added to the lower compartment, and epithelial cells were infected by adding viral inocula to the upper compartment of the transwell insert. Cells were infected with pH1N1 at a MOI of 0.1 or mock-infected with transwell infection media for 1 h at 37°C and 5% CO_2. Following infection, viral inocula were aspirated from cells. Cells were rested for 24 h post-viral infection. Cells were infected with mid-log phase MRSA or mock-infected 24

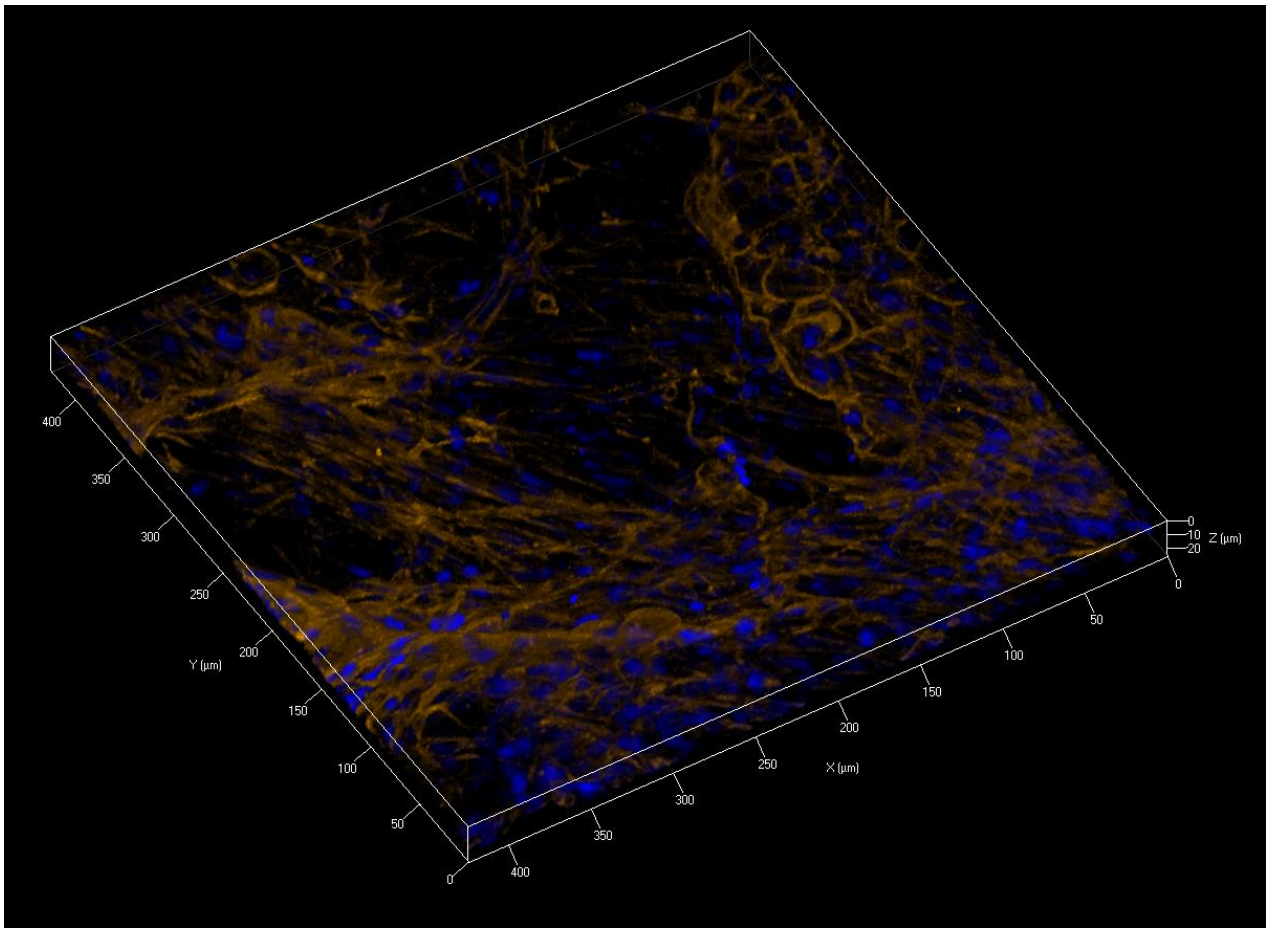

Figure 14: Confocal Image of Human Primary Alveolar Epithelial Cells.

Figure 14: Confocal Image of Human Primary Alveolar Epithelial Cells.

HPAEpiCs were seeded on the apical side of a 0.4 μm transwell insert at a concentration of 3E5 cells/ mL (9E4 cells/cm^2). Cells were allowed to grow for 14 days at the air-liquid interface, followed by fixation with 3.7% formaldehyde and staining with DAPI and phalloidin. Imaging of fixed cells was performed on a Zeiss AxioObserver.Z1 with a x10 lens and images captured using LSM 7 Elyra Software (Release Version 7.0).

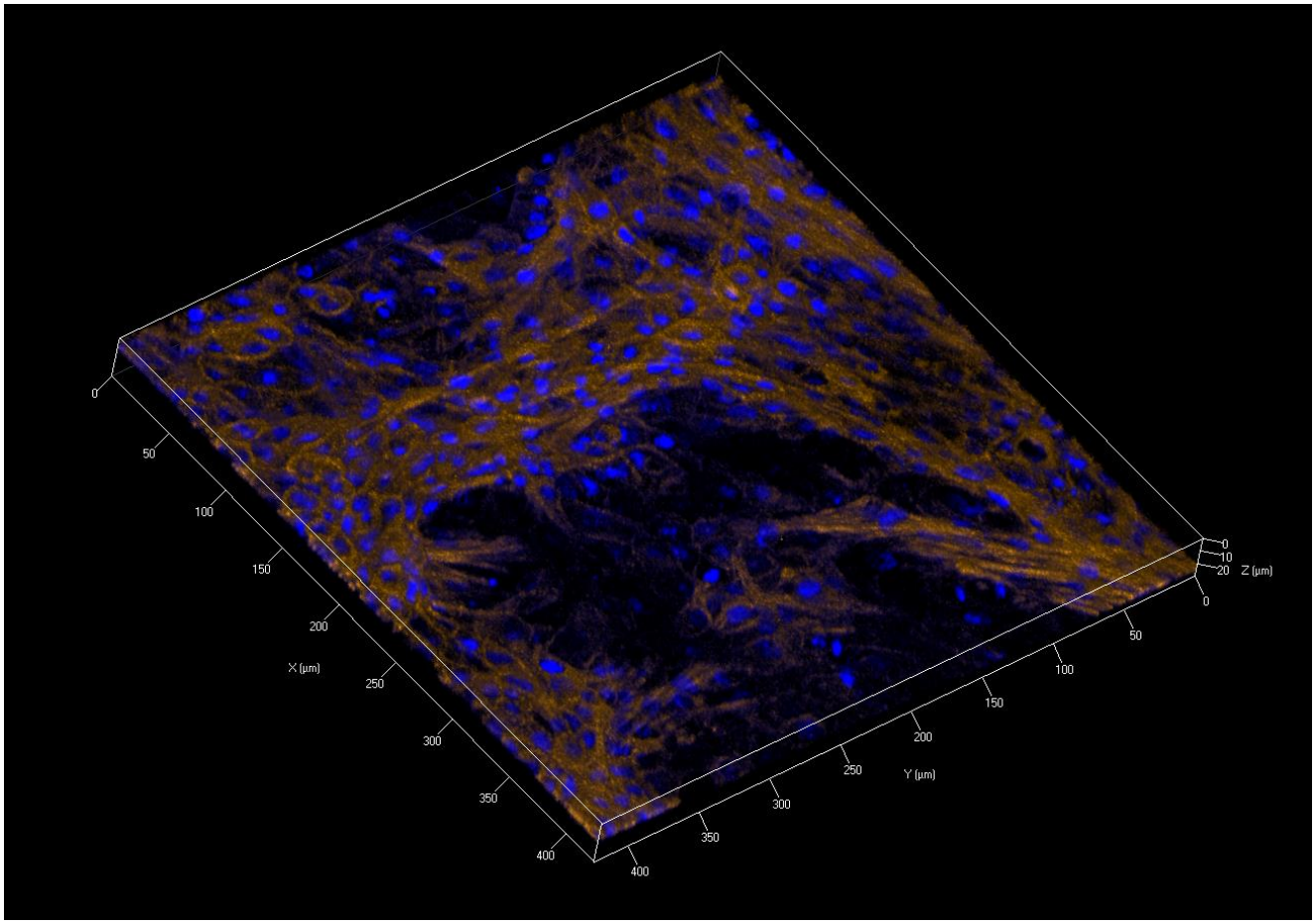

Figure 15: Confocal Image of Human Primary Microvascular Endothelial Cells.

Figure 15: Confocal Image of Human Primary Microvascular Endothelial Cells.

HPMECs were seeded on the apical side of a 0.4 μm transwell insert at a concentration of 1.5E5 cells/ mL (4.5E4 cells/ cm^2). Cells were allowed to grow for 14 days, followed by fixation with 3.7% formaldehyde and staining with DAPI and phalloidin. Imaging of fixed cells was performed on a Zeiss AxioObserver.Z1 with a x10 lens and images captured using LSM 7 Elyra Software (Release Version 7.0).

h post-influenza addition with transwell infection media for 1 h. Bacterial MOIs of 0.1 were used and were achieved by serial dilution of mid-log phase culture in transwell infection media. Bacterial inocula were aspirated from cells and both HPAEpiC and HPMEC cells were harvested by gentle scraping for further investigation of bacterial replication kinetics, bacterial virulence factors' modulation, and kinome analysis.

Quantification of Bacterial and Viral Replication Kinetics

Quantification of the total number of adherent and internalized bacteria was determined at 1, 4, 8, 12, 16, 20, and 24 h post-bacterial infection. Respiratory epithelial A549 cells were harvested for bacterial enumeration by aspirating media and washing 2x with DPBS. Cells were lysed with 0.025% Triton X-100 (VWR Life Science, Solon, OH, USA) and lysates (including intact bacteria) collected by gentle scraping. Respiratory epithelial HPAEpiCs were harvested for bacterial enumeration by washing 2X with DPBS followed by gentle scraping. Cells were pelleted by centrifugation at 5,000 rpm for 10 min, supernatant removed, and cells resuspended in 0.025% Triton X-100. Colony forming units (CFU) were quantified by standard bacterial plating on tryptic soy agar (TSA; MP Biomedicals, LLC, Solon, OH, USA). RT-qPCR was used to quantify viral replication by collecting supernatant samples from IAV-MRSA infected alveolar epithelial cells. Total RNA was extracted from the supernatant using the PureLink Viral RNA/DNA Mini Kit (Life Technologies, Burlington, ON) according to the manufacturer's instructions. Reverse transcription of total RNA was performed using the Superscript IV first-strand cDNA synthesis kit (Life Technologies, Burlington, ON) using primers specific for the viral H1N1 HA sequence. Viral copy number was quantified by comparing RT-qPCR results to an established external standard of viral copy number.

RNA Extraction, cDNA Synthesis, and Quantitative PCR

Three biological replicates with two technical replicates were collected at 1, 4, 8, 12, 16, 20, and 24 h post-bacterial infection to determine the modification of bacterial virulence factors in the presence of influenza. Following aspiration of media, both A549 cells and HPAEpiCs were collected by gentle scraping, pelleted by centrifugation at 1200 rpm for 10 min, and stored at -80°C until RNA extraction. Standard TRIzol-chloroform extraction (Ambion, Calrsbad, CA, USA) was performed to extract bacterial RNA, before concentration and purity of the RNA were assessed by A_{260}:A_{280} spectrophotometry. Total bacterial RNA was normalized to 35 ng and complementary DNA (cDNA) synthesized using random primers and the QuantiNova reverse transcription kit (Qiagen, Hilden, Germany). 10 ng of cDNA was amplified in triplicate by RT-qPCR performed on the Applied Biosystems QuantStudio 6 Flex Real-Time PCR system (Life Technologies, Burlingtion, ON) using PowerUp SYBR Green Master Mix (Applied Biosystems, Austin, TX, USA) as a detection method and 8 μM of the appropriate primers (Table 2 and Table 3). Primers were designed and selected using PrimerQuest (https://www.idtdna.com/primerquest). Cycling conditions involved an initial 2 min incubation at 50°C and a 2 min incubation at 95°C for SYBR Green activation and polymerase activation, respectively. This was followed by 40 cycles of 15 sec at 95°C for denaturation and 1 min at 60°C for annealing and extension. Bacterial gene expression was quantified through comparison to the MRSA housekeeping gene 16S, and relative fold change in expression was calculated using the $2^{-\Delta\Delta CT}$ method [308]. Relative fold change values represent IAV-MRSA (normalized to 16S)/MRSA-alone (normalized to 16S).

Table 2: MRSA Virulence Factor Primers

Virulence factors were chosen according to previous research and reviews concerning MRSA virulence [82-84]. Primers were designed and selected using PrimerQuest (https://www.idtdna.com/primerquest).

Gene Name (Code)	**Primers**	**Accession No. (Amplicon Location)**
16S ribosomal RNA (16S)	F: 5'-CATGCTGATCTACGATTACT-3' R: 5'-CCATAAAGTTGTTCTCAGTT-3'	L37597.1 (801-894)
Coagulase (coa)	F: 5'-TTCCACAGGGCACAATTACA-3' R: 5-CGGGACCTTGAACGATTTC-3'	AJ306908.1 (1206-1331)
Elastin-binding protein (EbpS)	F: 5'-GGTGAACCTGAACCGTAGTATT-3' R; 5'-CAGCAACAACAACGTCAAGG-3'	MH920607.1 (183-281)
Enolase (Eno)	F: 5'-TGGTTACAAACCAGGTGAAGAA-3' R: 5'-CGCCTTCGAACTTACTGTAGTC-3'	AF065394.1 (1215-1317)
Fibronectin-binding protein A (FnbA)	F: 5'-CCCATTTCCGTTCGCTTTATTAC-3' R: 5'-GTAGGACATCCAGAGCAACTTTA-3'	KP096552.1 (1531-1636)
Fibronectin-binding protein B (FnbB)	F: 5'-TGTCGCGCTGTATGATTGT-3' R: 5'-GTAGAGGAAAGTGGGAGTTCAG-3'	KY024703.1 (2587-2692)
Intercellular adhesion A (IcaA)	F: 5'-GCAGTAGTTCTTGTCGCATTTC-3' R: 5'-GTTGGGTATTCCCTCTGTCTG-3'	AF500262.1 (1144-1234)
Intercellular adhesion B (IcaB)	F: 5'- AGCCTATCCTTATGGCTTGATG-3' R: 5'-GAGTTCGGAGTGACTGCTTT-3'	MF630927.1 (378-533)
Immunoglobulin-binding protein Sbi (Sbi)	F: 5'-AGCCAACAAGTTTGGGTAGAA-3' R: 5'-CGTGTGGTGCTTTGTTATCTTG-3'	AF027155.1 (493-515)
Protein A (SpA)	F: 5'-GCTGCACCTAAGGCTAATGATA-3' R: 5'-GATAAGAAGCAACCAGCAAACC-3'	X61307.1 (692-790)

Table 3: MRSA Exotoxin Primers.

Exotoxins were chosen according to previous research and reviews concerning MRSA virulence [82-84]. Primers were designed and selected using PrimerQuest (https://www.idtdna.com/primerquest).

Gene Name (Code)	**Primer Sequences**	**Accession No. (Amplicon Location)**
α-hemolysin (Hla)	5'- CTGTAGCGAAGTCTGGTGAAA-3' 5'- AGATTCTTGGAACCCGGTATATG-3'	KM019672.1 (388-501)
γ-hemolysin A (HlgA)	5'- CCAGCAGCACGAGACTATTT-3'- CACCTTTACCTCTTTCGTGTGA-3'	KT284333.1 (618-716)
Staphylococcal enterotoxin K (Sek)	5'- ATCGACATCCAAATGGAATTTCTC-3' 5'- CTACACAGGAGATGATGGGTTAC-3'	GQ358928.1 (525-619)
Staphylococcal enterotoxin Q (Seq)	5'-GTAGAAACCTCGTCTGTAGATATAGTG-3' 5'- GGAATTACGTTGGCGAATCAAA-3'	MF417550.1 (314-418)

Respiratory Epithelial A549 Cell Barrier Integrity Determination

Changes in barrier integrity of A549 cells during IAV-MRSA co-infection was quantified using the electric cell-substrate impedance sensing (ECIS) Z, 96W Array Station, and 96W20idf PET plates (Applied BioPhysics, Troy, NY, USA). Cells were seeded at 5E5 cells/ mL (1.3E5 cells/ cm_2) in 96W20idf PET plates and rested for 24 h at 37°C and 5% CO_2 in the 96W Array Station (Applied BioPhysics, Troy, NY, USA). Cells were mock-infected with DMEM supplemented with 2% FBS or infected with IAV at a MOI of 0.1. Followed by resting for 24 h, cells were either mock-infected with DMEM supplemented with 2% FBS or infected with mid-log phase MRSA at a MOI of 0.1. Resistance measurements were acquired at 4000 Hz during the entirety of the entire experiment (72 h). Control conditions included: (i) cells infected with influenza-alone (MOI 0.1); (ii) cells infected with MRSA-alone (MOI 0.1); (iii) mock-infected cells (background barrier resistance); and (iv) cells treated with 1% Triton X-100 (positive control for barrier dysfunction).

Determination of Barrier Integrity in a Co-culture Model

The ECIS TEER 24, 24-well TEER 24 microplates, and Common Electrode Array (Applied Biophysics, Troy, NY, USA) were employed to quantify barrier integrity in a co-culture model during pH1N1-MRSA co-infection. Epithelial cells were infected with influenza (MOI 0.1) or mock-infected with transwell infection media (denoted as Time 0) for 1 h followed by resting for 24 h. Viral and mock-infected cells were subsequently infected with mid-log phase MRSA (MOI 0.1) or mock-infected with transwell infection media for 1 h. Resistance measurements were acquired at 4000 Hz every 4 h for 48 h. At each time point, the upper compartment of each transwell insert was filled with 600 μL of transwell infection media and resistance measured for 1 min. Transwell infection media was removed from each transwell

insert and the cells allowed to rest until the next time point. Control conditions included: (i) cells infected with influenza-alone (MOI 0.1); and (ii) cells infected with MRSA-alone (MOI 0.1).

Western Blot Analysis

The expression of tight junctions in primary pulmonary microvascular endothelial cells were detected by Western blotting, using the Tight Junction Antibody Sampler Kit (Cell Signal, Danvers, MA, USA) according to the manufacturer's protocol. Equal amount of total protein (20μg) were heated to 95°C for 10 min, followed by cooling on ice. Samples were centrifuged for 30 seconds at maximum rpm and resolved by 8% SDS-gel electrophoresis with subsequent transfer to PVDF membranes using the iBLOT II gel transfer system (ThermoFisher Scientific, Mississauga, ON). The membrane was blocked by incubating with 5% skim milk for 1 h at room temperature, followed by incubation with 1:1000 anti-ZO-1 and anti-ZO-2 antibodies with gentle agitation at 4°C overnight. The following day, the membrane was washed three times with TBST (ThermoFisher Scientific, Mississauga, ON) for 5 min each. To detect biotinylated protein markers, the membrane was incubated with anti-rabbit IgG, HRP-linked antibody and anti-biotin, HRP-linked antibody for 1 h with gentle agitation at room temperature. To detect proteins, membrane-bound HRP was washed with TBST 3X for 5 min. Blots were developed with SuperSignal™ Western Blot Enhancer (ThermoFisher Scientific, Mississauga, ON) according to the manufacturer's protocol.

Kinome Peptide Array Analysis

Kinome peptide array analysis was performed as previously described [309, 310]. For A549 cells, IAV-, MRSA-, IAV-MRSA, and mock-infected cells were collected at 4, 8, 12, 16, 20, and 24 h post-bacterial infection by gentle scraping. For both HPAEpiCs and HPMECs, IAV-, MRSA-, IAV-MRSA-, and mock-infected cells were collected at 4, 8, 12, and 24 h post-

bacterial infection by gentle scraping. Cells were pelleted by centrifugation at 14,000 rpm for 10 min, treated with kinome lysis buffer (20 mM Tris-HCl pH 7.5, 150 mM NaCl, 1mM EDTA, 1 mM EGTA, 1% Triton X-100, 2.5 mM sodium pyrophosphate, 1 mM Na3V04, 1 mM NaF, 1 ug/mL leupeptin, 1 ug/mL apropotinin, 1 mM phenylmethylsulfonyl fluoride) incubated on ice for 10 min, and transferred to fresh microcentrifuge tubes. The Pierce BCA Protein Assay Kit (ThermoFisher Scientific, Mississauga, ON) was used to quantify total protein concentration. Activation mix (50% glycerol, 50 uM ATP, 60 mM $MgCl_2$, 0.05% Brij 35, 0.25 mg/mL bovine serum albumin) was added to the equivalent amounts of total protein (100 μg) for each sample, and total sample volumes were matched by the addition of kinome lysis buffer. Kinome peptide arrays (JPT Peptide Technologies GmnbH, Berlin, Germany) were spotted with samples and incubated for 2 h at 37°C and 5% CO_2. After incubation, arrays were rinsed once with 1% Triton X-100 and once with deionized H_2O. Arrays were stained using PRO-Q Diamond phosphoprotein stain (Invitrogen, Carlsbad, CA, USA) for 1 h with gentle agitation. Following staining, arrays were washed 3X with kinome destain (20% acetonitrile, 50 mM sodium acetate pH 4.0) for 10 min. Arrays were washed a final time with deionized water for 10 min and dried by centrifugation. A PowerScanner microarray scanner (Tecan, Morrisville, NC, USA) with a 580-nm filter was used to image arrays and Array-Pro Analyzer version 6.3 software (Media Cybernetics, Rockville, MD, USA) was used to collect signal intensity values. Intensity values for spots and background were collected for each array.

Kinome Data Preprocessing

The Platform for Integrated, Intelligent Kinome Analysis (PIIKA 2) software (available online: https://saphire.usask.ca/saphire/piika) was used to analyze kinome data as previously described [311]. To calculate specific responses of each peptide, background intensity

was subtracted from foreground intensity and the resulting data transformed using the variance stabilization model, as previously described [312, 313]. In short, each microarray data set is treated as a rectangular table y_{ki} where *k* corresponds to the rows of gene probes on the array and *i* represents the columns which correlate to each sample and *d* represents the number of columns. The number of probes is denoted by *n*. The values y_{ki} , where $k = 1,\ldots n$ and $i = 1,\ldots d$ are the intensity data as produced by the Array-Pro Analyzer software. In order to directly compare the y_{ki} values, background subtraction is calculated by:

$$y_{ki} \rightarrow \widetilde{y_{kı}} = o_i + s_i\, y_{ki}$$

where $i = 1,\ldots d$, $o_1 = 0$, and $s_1 = 1$. The variance stabilization model has been previously trained by a larger MAP kinome data set to bring all transformed data onto the same scale while alleviating variance-mean-dependence. Additionally, intensities from the mock-infected control samples were subtracted from the intensities induced by the time-matched infection condition for each of the peptides in question, and test statistics calculated, as previously described [313]. The average intensities of three replicate intensities were taken and these values were subjected to hierarchical clustering analysis.

Kinome Test Statistics Calculations

Paired t-tests were used to compare the signal intensities of peptide phosphorylations during each infection condition with the time-matched mock-infection condition. The *P* value cutoff was 0.20. The test statistic (TS) was calculated as:

$$TS = \frac{D}{S_D\sqrt{n}}$$

Where D is the mean of differences between responses induced by two different infection conditions for the same peptides, S_D is the standard deviation of the differences, and n is the

number of replicates for that peptide in each infection condition (n = 3 for our datasets). The P values for phosphorylation events was calculated using one-sided t tests:

$$P\left[TS > t^{(n-1)}\right]$$

Similarly, the p value for dephosphorylation events were calculated as:

$$P\left[TS < t^{(n-1)}\right]$$

Peptides with significant changes in phosphorylation (P<0.20) were selected.

Hierarchical Clustering Analysis

Hierarchical clustering and principle component analysis was used to cluster the preprocessed data for each infection condition at each time point based on their kinome profiles. For hierarchical clustering, McQuitty + (1 – Pearson Correlation) was used, as previously described [313]. In short, each infection condition at each time point was considered a singleton, or a cluster with a single element. The (1 – Pearson Correlation) was used to calculate the distance between any two singletons. For example, if X and Y are singletons, the Pearson correlation is:

$$V_{xy} = \frac{\frac{300}{i=1^{x_i}} - x(y_i - y)}{\frac{300}{i=1}(x_i - x)\frac{300}{j=1}(y_i - y)}$$

and

$$dist(X, Y) = 1 - V_{xy}$$

The McQuitty method is then able to update the distance between clusters that upon merging two clusters into a new cluster (i.e. X and Y have merged to form C_{xy}), the distance between this new cluster and the remaining clusters is calculated in concern with the sizes of X

and Y. For example, let C_R be the remaining cluster and the size of X and Y be n_x and n_y, respectively. Then:

$$D(C_{xy}, C_R) = \frac{nX \times DC_x, C_R + nY \times D(C_y, C_R)}{nX + nY}$$

Heatmaps were derived using the Heatmapper software suite [314]. In short, hierarchical clustering was augmented by a heatmap using the *R* function heatmap.2 to convert intensity values to statistical z-scores. Z-scores were then depicted as green/red intensities, where green indicates a value lower than the mean and red indicates a value higher than the mean. Phosphorylation fold changes were validated using the Proteome Profiler Human Phospho-Kinase Array Kit according to the manufacturer's instructions (R&D Systems, MN, USA).

Pathway Overrepresentation and Gene Ontology Analysis

Pathway overrepresentation and gene ontology analyses of differentially-phosphorylated proteins were performed using InnateDB software (www.innatedb.com) as described previously [309, 310, 315]. InnateDB, a publicly available resource, predicts biological pathways based on experiment fold change datasets, dependent on differential expression or phosphorylation. Pathways are assigned a *P* value based on the number of proteins present for a particular pathway as well as the degree to which they are differentially expressed or modified relative to a control condition. Input data were limited to peptides that demonstrated statistically-significant changes in expression as compared with their respective time-matched mock-infected controls ($P < 0.10$), as described previously [316]. Multiple comparisons were automatically corrected and controlled for by InnateDB. Protein identifiers, phosphorylation fold changes (>1), and *P*-values (<0.05) were uploaded to InnateDB.

Chemokine and Cytokine Measurement

Chemokine levels were determined using the microbead array assay Milliplex MAP multiplex kit (Human Cytokine/Chemokine Magnetic Bead Panel 96 Well Plate Assay; Millipore, Billerica, MA, USA) and analyzed on the BioPlex-200 (Biorad, Mississauga, ON). Supernatants were collected at 4, 8, 12, and 24 h for mock-, pH1N1-, MRSA-, and pH1N1-MRSA-infected samples and stored at -80°C until use. Supernatants were analyzed according to the manufacturer's overnight protocol. Lower detection limit was 2.09 pg/mL for EGF, 24.84 pg/mL for FGF-2, 1.73 pg/mL for IFN-α2, 2.02 pg/mL for IFN-γ, 1.84 pg/mL for GRO, 1.66 pg/mL for IL-1β, 1.61 pg/mL for IL-3, 2.47 pg/mL for IL-6, 2.26 pg/mL for IL-8, 1.72 pg/mL for IP-10, 1.95 pg/mL for MCP-1, 1.59 pg/mL for RANTES, 1.55 pg/mL for TNF-α, and 1.53 pg/mL for VEGF.

Statistical Analyses

All numerical data are presented as mean ± SEM. Statistical analyses were performed using ANOVA for comparisons of groups means using Prism 8 for macOS (version 8.2.1), unless otherwise stated. This includes pathogen replication kinetics, RT-qPCR, ECIS, and Milliplex MAP multiplex kit, as previously described [317, 318]. A P value of ≤ 0.05 was considered statistically significant for all analyses. P values less than 0.05 are summarized by a single asterisk (*), less than 0.01 are summarized by two asterisks (**), less than 0.001 are summarized by three asterisks (***), and less than 0.0001 are summarized by four asterisks (****).

Results

MRSA Replication Kinetics in A549 Cells are Similar during Bacterial Infection-Alone and IAV-MRSA Infection

We first sought to characterize bacterial replication kinetics in A549 human lung epithelial cells during IAV-MRSA co-infection. While it is widely accepted that IAV-bacterial co-infections can result in increased lung pathology in both humans and animal models, there is a paucity of information available regarding the relation of bacterial replication kinetics to increased disease severity [264, 268, 319]. To address this, we assessed the temporal replication kinetics of MRSA in a monolayer of A549 alveolar epithelial cells during MRSA and IAV-MRSA infections. Observational data during the 2009 H1N1 pandemic revealed that bacterial co-infection commonly occurred during the peak of viral infection [262]. To mimic this *in vitro*, MRSA was added to mock-infected or IAV-infected cells 24 h post-infection (n = 3 for each IAV strain studied, with two technical replicates per biological replicate). To confirm that cells were productively infected by influenza, supernatants were harvested from pH1N1-MRSA-infected cells at the same time points as those used for CFU determination (n = 3), and RT-qPCR used to determine the vRNA abundance. Influenza virus was confirmed within the infected cells and gradually decreased throughout the course of co-infection (Figure 16). Standard bacterial plating was used to enumerate the total number of adherent and internalized bacteria in alveolar epithelial cells at each time point. Cells infected with MRSA-alone entered the early phase of exponential growth at 1 h post-infection and the stationary phase by 16 h post-infection. This was largely mirrored in IAV-MRSA co-infected cells, regardless of the IAV strain, as seen in Figure 17. While statistically significant MRSA replication was observed over time (P =

0.0145), no statistically significant differences in replication were observed between any infection condition (P = 0.8349), or between any

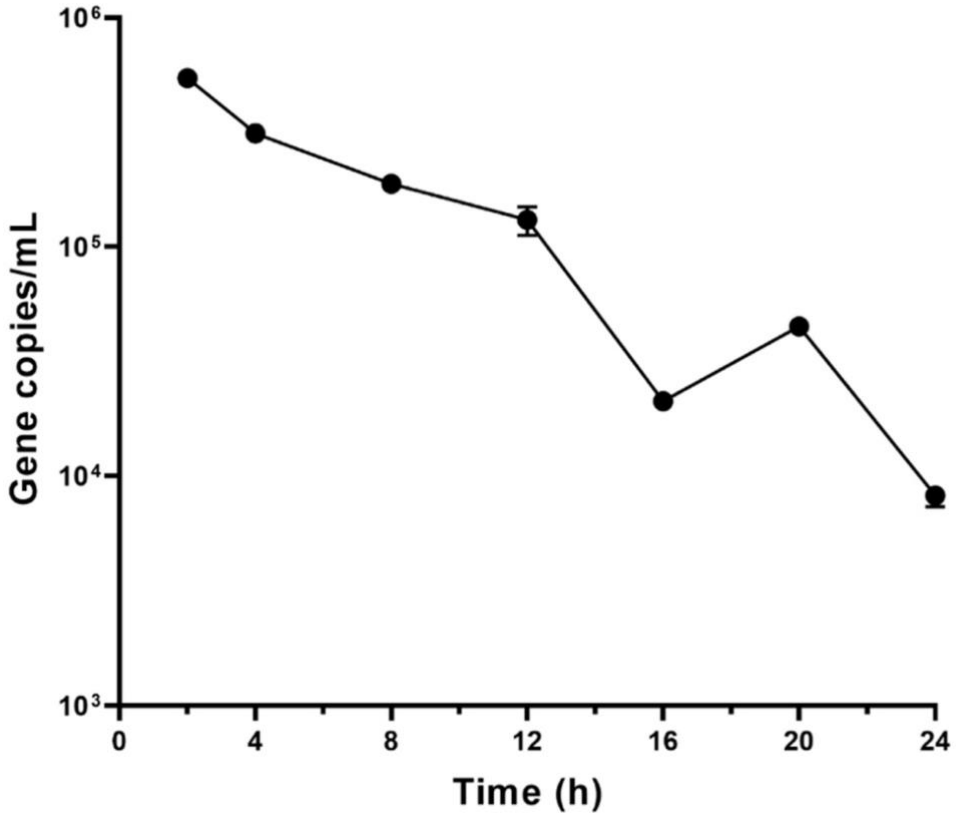

Figure 16: IAV Replication Kinetics during IAV-MRSA Co-infection.

Figure 16: IAV Replication Kinetics during IAV-MRSA Co-infection.

To confirm productive infection of host cells by IAV, supernatants were collected at each time point and gene copies/mL determined using RT-qPCR with primers specific for the viral H1N1 HA sequence. IAV gradually decreased over the course of the experiment. Error bars represent SEM calculated from three biological replicates. Error bars for some of the time points are not visible due to the y-axis scale.

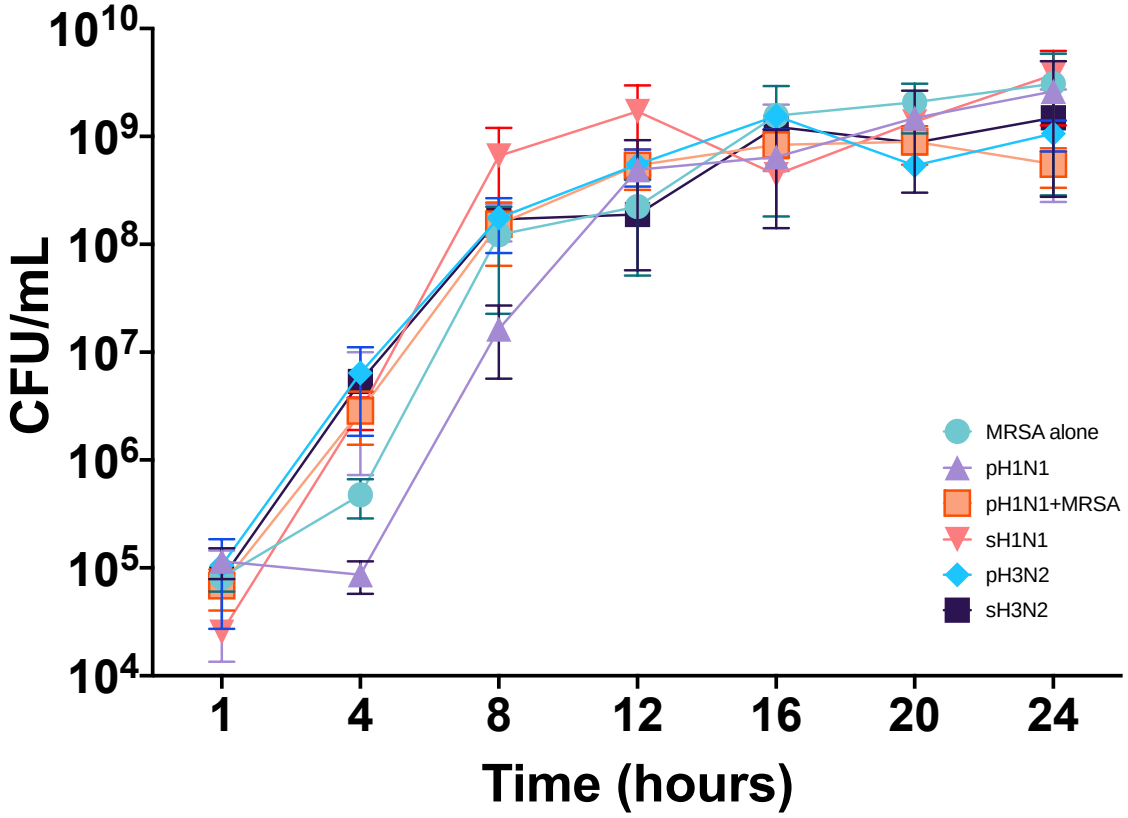

Figure 17: MRSA Replication Kinetics during MRSA Infection and IAV-MRSA Infection.

Figure 17: MRSA Replication Kinetics during MRSA Infection and IAV-MRSA Infection.

MRSA replication kinetics were determined in alveolar epithelial A549 cells in the presence of pH1N1, sH1N1, pH3N2, and sH3N2. Cells were infected with an IAV strain at a MOI of 0.1 followed by resting for 24 h. At T0, cells were infected with MRSA at a MOI of 0.1. Standard bacterial plating was used to determine CFU/mL at each time point. Error bars represent SEM calculated from three biological replicates (n = 3). Error bars for some of the time points are not visible due to the y-axis scale. Statistically significant MRSA replication was observed over time (P = 0.0145). However, no statistically significant differences in replication were observed between any infection condition (P = 0.8349), or between any infection condition at any time point (P = 0.9672).

infection condition at any time point ($P = 0.9672$). To allow further clarity of the effect of each IAV strain on the replication kinetics of MRSA, Figure 17 has been split into four further figures (Figure 18A, B and Figure 19A, B).

As seen in Figure 18A, bacterial colony counts in pH1N1-MRSA infected cells began increasing exponentially at 4 h post-infection and entered the stationary phase by 12 h post-infection. This is in contrast to cells infected alone, where MRSA entered the exponential phase at 1 h and the stationary phase at 16 h. Compared with MRSA in the presence of pH1N1, MRSA-alone trended towards faster bacterial replication at 4 and 8 h post-infection.

When pH1N1 and MRSA were pre-complexed by co-sedimentation (pH1N1+MRSA) leading to simultaneous IAV and bacterial infection as recently described by Rowe *et al.*, a trend towards faster MRSA growth was seen at 1 h post-infection compared with MRSA-alone (Figure 18A) [307]. Cells infected with pH1N1+MRSA entered the exponential phase at 1 h post-infection and the stationary phase at 12 h post-MRSA infection. When compared with cells infected with pH1N1 24 h prior to MRSA-infection, pH1N1+MRSA infection trended towards faster bacterial replication at 4 and 8 h post infection. Near identical bacterial numbers were observed at 12 and 16 h post-MRSA infection in both pH1N1-MRSA and pH1N1+MRSA infected cells. This data suggests that whether bacterial co-infection occurs simultaneously with pH1N1 or at peak viremia bears no effect on MRSA growth kinetics.

When respiratory epithelial cells were infected with sH1N1 prior to MRSA infection, there was a trend towards faster bacterial replication at 4, 8, and 12 h post-MRSA co-infection as compared with cells infected with MRSA-alone (Figure 18B). Cells infected with MRSA-alone and cells infected with sH1N1-MRSA both resulted in MRSA entering the exponential phase at 1 h post MRSA-infection. However, MRSA entered the

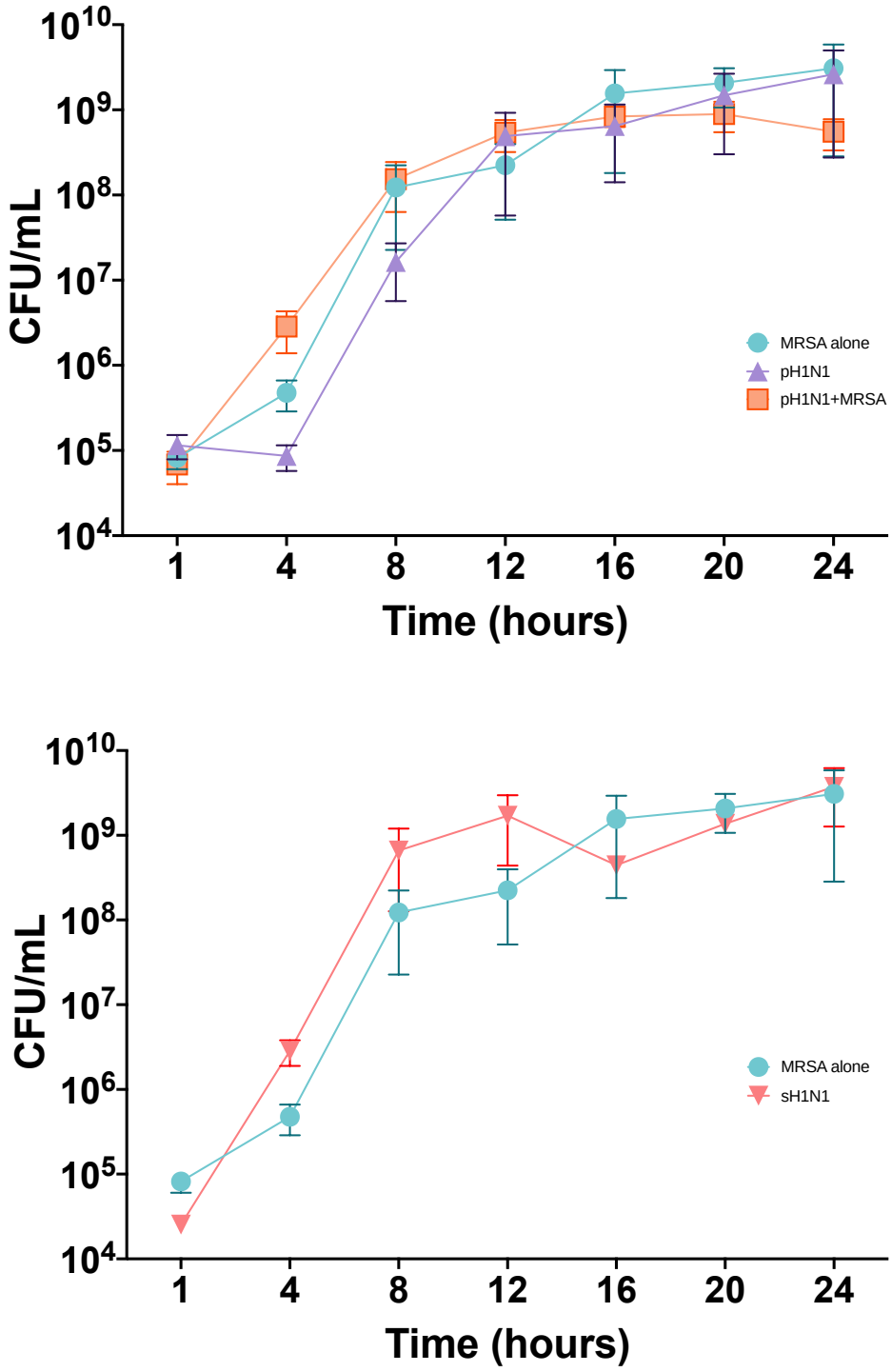

Figure 18: MRSA Replication Kinetics during MRSA Infection and H1N1-MRSA Infection.

Figure 18: MRSA Replication Kinetics during MRSA Infection and H1N1-MRSA Infection.

MRSA replication kinetics were determined in alveolar epithelial A549 cells in the presence of pH1N1 and sH1N1.

A) Cells were infected with pH1N1(MOI 0.1) or mock-infected followed by resting for 24 h. At T0, cells were infected with MRSA (MOI 0.1), pH1N1+MRSA (MOI 0.1), or mock-infected.
B) Cells were infected with sH1N1 at a MOI of 0.1 or mock-infected followed by resting for 24 h. At T0, cells were infected with MRSA at a MOI of 0.1.

Standard bacterial plating was used to determine CFU/mL at each time point. Error bars represent SEM calculated from three biological replicates (n = 3). Error bars for some of the time points are not visible due to the y-axis scale. Visual summary only. Statistical comparisons and analyses are made in the direct experimental comparisons (see Figure 17).

stationary phase by 12 h post-infection when cells were infected with sH1N1 prior to bacterial infection, while MRSA-alone did not enter the stationary phase until 16 h post-infection. Compared with cells infected with pH1N1, bacteria in the presence of sH1N1 showed a trend towards faster bacterial replication at 4, 8, and 12 h post-MRSA infection. MRSA replication kinetics were nearly identical at 16, 20, and 24 h post addition regardless of whether prior IAV infection had occurred with pH1N1 or sH1N1. This suggests that MRSA fitness is not altered by the presence of H1N1 IAVs, regardless of whether the IAV is a pandemic or seasonal strain.

As seen in Figure 19A, when A549 cells were infected with pH3N2 24 h prior to bacterial addition, MRSA entered both the exponential and stationary phases simultaneous to MRSA-alone, at 1 h and 16 h, respectively. Faster bacterial replication was observed at 4 h post-MRSA infection compared with MRSA-alone. In contrast, the number of bacterial colonies seen at 8 and 20 h in pH3N2-MRSA infection was virtually identical to MRSA-alone infection. When comparing the fitness of MRSA in the presence of pH3N2 to pH1N1, faster replication was observed in pH3N2-MRSA co-infections at 4, 8, 12, and 16 h. This suggests that the presence of pandemic IAV strains does not alter MRSA fitness in alveolar epithelial cells.

In the case of respiratory epithelial cells co-infected with sH3N2-MRSA, MRSA entered the exponential and stationary phases at 1 h and 16 h, respectively, which mimicked growth seen in MRSA-alone (Figure 19B). Nearly identical growth was seen at 1, 8, 12, and 16 h between MRSA-alone and MRSA in the presence of sH3N2; however, faster replication was observed at 4 h post-bacterial addition in sH3N2-MRSA co-infection. Regardless of whether co-infection occurred with sH3N2 or pH3N2, MRSA entered the exponential phase at 1 h and the stationary phase at 16 h. Interestingly, nearly identical growth was observed at 1, 4, 8, 16, and 24

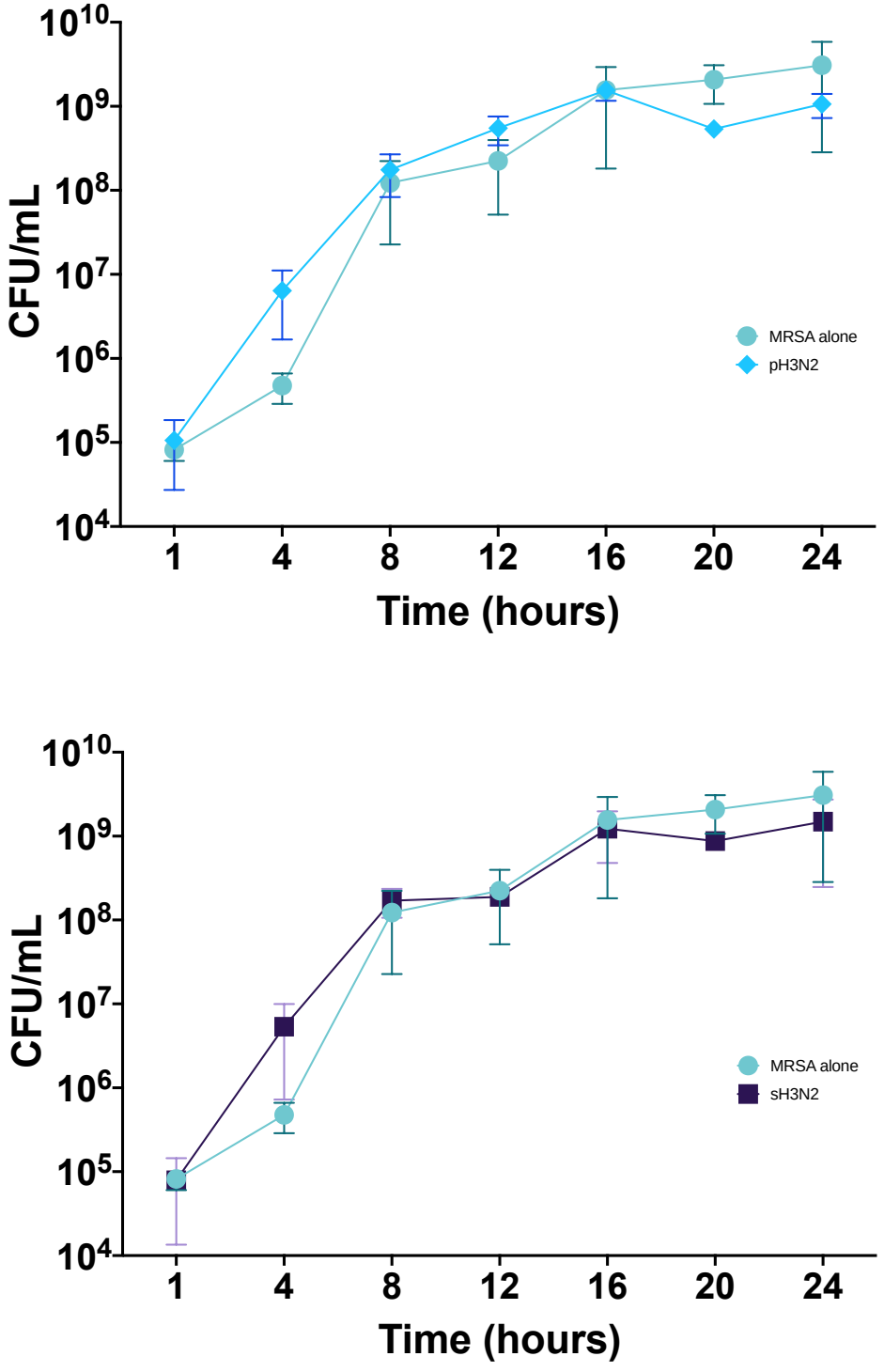

Figure 19: MRSA Replication Kinetics during MRSA Infection and H3N2-MRSA Infection.

Figure 19: MRSA Replication Kinetics during MRSA Infection and H3N2-MRSA Infection.

MRSA replication kinetics were determined in alveolar epithelial A549 cells in the presence of pH3N2 and sH3N2.

A) Cells were infected with pH3N2 at a MOI 0.1 or mock-infected followed by resting for 24 h. At T0, cells were mock-infected or infected with MRSA at a MOI of 0.1.
B) Cells were infected with sH3N2 at a MOI of 0.1 or mock-infected followed by resting for 24 h. At T0, cells were infected with MRSA at a MOI of 0.1.

Standard bacterial plating was used to determine CFU/mL at each time point. Error bars represent SEM calculated from three biological replicates (n = 3). Error bars for some of the time points are not visible due to the y-axis scale. Visual summary only. Statistical comparisons and analyses are made in the direct experimental comparisons (see Figure 17).

h in the presence of either H3N2 IAV. These data suggest that H3N2 strains do not affect MRSA fitness. When comparing bacterial growth kinetics in the presence of sH3N2 or sH1N1, MRSA entered the exponential phase at 1 h in both cases. However, in the case of sH1N1-MRSA, MRSA entered the stationary phase at 12 h post-infection, 4 h sooner than sH3N2-MRSA. These data suggest that seasonal IAV strains, whether H1N1 or H3N2, do not alter the replication kinetics of MRSA.

As mentioned previously, no statistically significant differences were observed between any infection condition at any time point ($P = 0.9672$), suggesting that IAV infection does not play a role in the replication kinetics of MRSA in alveolar epithelial cells.

To further confirm that bacterial replication kinetics are not impacted during influenza co-infection, MRSA replication was studied in the presence of pH1N1 in HBEC3-KT cells ($n = 3$), an immortalized human bronchial cell line. Similar bacterial replication trends were observed in HBEC3-KT cells as in A549 cells (Figure 20). While MRSA growth over time was statistically significant ($P = 0.0393$), no statistically significant differences were found between either infection condition ($P = 0.4902$), or between either infection condition at any time point ($P = 0.8795$). MRSA entered the exponential phase at 1 h and the stationary phase at 16 h, independently of whether prior pH1N1 infection had occurred. The lack of statistically significant differences observed at any of the measured time points between either condition suggests that bacterial replication kinetics are not impacted during influenza co-infection in anatomically- and physiologically-distinct regions of the lungs.

Taken together, these data suggest that despite the more severe disease progression observed in IAV-MRSA infections in both humans and animals, this is not due to an increased

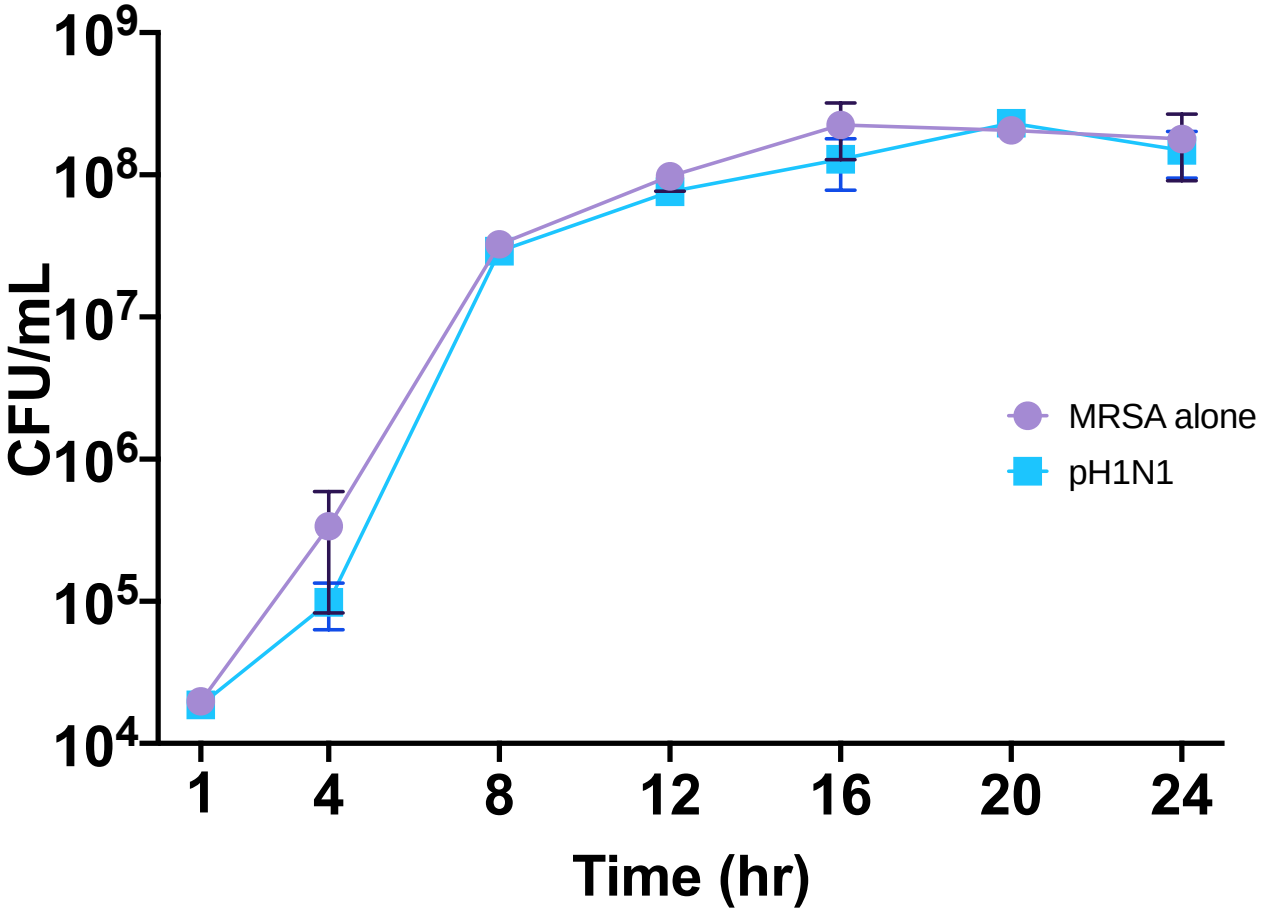

Figure 20: Growth Kinetics of MRSA in HBEC3-KT Cells Infected with pH1N1.

Figure 20: Growth Kinetics of MRSA in HBEC3-KT Cells Infected with pH1N1. MRSA replication kinetics were determined in normal human bronchial epithelial HBEC3-KT cells in the presence of pH1N1. Cells were infected with pH1N1 at a MOI of 0.1 followed by resting for 24 h. At T0, cells were infected with MRSA at a MOI of 0.1. At each time point, standard bacterial plating was used to determine CFU/mL. No statistically significant differences were observed between either infection condition at any time point. Error bars represent SEM calculated from three biological replicates (n = 3). Error bars for some of the time points are not visible due to the y-axis scale. While MRSA growth over time was statistically significant (P = 0.0393), no statistically significant differences were found between either infection condition (P = 0.4902), or between either infection condition at any time point (P = 0.8795).

bacterial load within the respiratory epithelium owing to prior IAV infection, as previously postulated [262, 264, 269, 271].

Bacterial Invasion- and Attachment-Related Virulence Factor Expression Patterns Are Modulated Early During IAV-MRSA Infection

We next employed RT-qPCR to examine the potential role of selective modulation of bacterial virulence factors on IAV-MRSA co-infection pathogenesis. For this, MRSA was added to mock-infected or IAV-infected cells 24 h post-infection, and cells harvested at each time point (n = 3 for each IAV strain). RT-qPCR was then utilized to study the expression of 13 MRSA virulence factor genes related to host cell adhesion and invasion in the presence of IAV, including: *coa*, *ebpS*, *eno*, *fnbA*, *fnbB*, *hla*, *hlgA*, *icaA*, *icaB*, *sbi*, *sek*, *seq*, and *spA*. Our primary data using pH1N1 revealed that the time point, the virulence factor, and the interaction were each statistically significant ($P < 0.0001$, $P = 0.0002$, and $P < 0.0001$, respectively). At 1 h post-MRSA infection, *hla*, *spA*, and *fnbB* were each upregulated; *hla* was significantly upregulated ($P = 0.0006$). From 8 h onwards, the expression of virulence factors was largely repressed (<1) in alveolar epithelial cells co-infected with pH1N1-MRSA, compared with MRSA-alone (Figure 21). Thus, we focused only on the modulation of bacterial virulence factors at 1 and 4 h post-MRSA infection.

When alveolar epithelial cells were infected with pH1N1-MRSA, the infection condition, the virulence factor studied, and the interaction between the two were each statistically significant ($P < 0.0001$ for all three). At 1 h post-MRSA addition, the expression patterns of *coa*, *eno*, *fnbB*, *hla*, *hlgA*, *icaB*, *sbi*, *sek*, and *spA* were differentially upregulated relative to infection with MRSA-alone; however, only *hla* and *hlgA* were significantly upregulated ($P = 0.0006$, $P <$

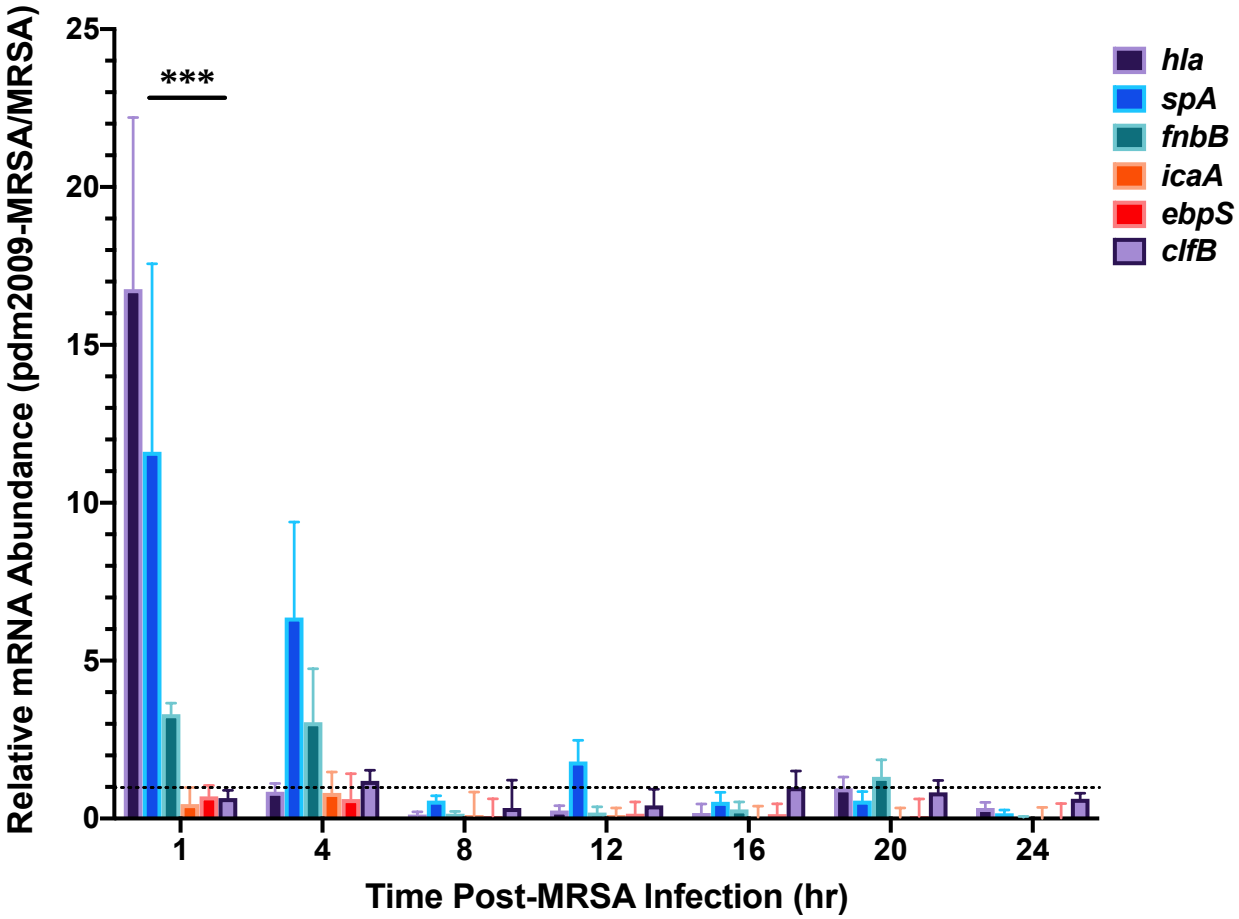

Figure 21: pH1N1-MRSA Co-infection Alters Bacterial Virulence Factor Expression Early in Infection in Alveolar Epithelial Cells as Compared with MRSA Infection Alone.

Figure 21: pH1N1-MRSA Co-infection Alters Bacterial Virulence Factor Expression Early in Infection in Alveolar Epithelial Cells as Compared with MRSA Infection Alone.

RT-qPCR was employed to examine differential modulation of MRSA virulence factor mRNA abundance in the presence or absence of pre-existing pH1N1 infection in alveolar epithelial cells. Relative mRNA abundance fold changes represent pH1N1-MRSA vs MRSA infection alone and were calculated by the $2^{-\Delta\Delta CT}$ method. Error bars represent SEM calculated from three biological replicates ($n = 3$). The time point, the virulence factor, and the interaction were each statistically significant ($P < 0.0001$, $P = 0.0002$, and $P < 0.0001$, respectively). At 1 h post-MRSA infection, *hla*, *spA*, and *fnbB* were each upregulated; *hla* was significantly upregulated ($P = 0.0006$).

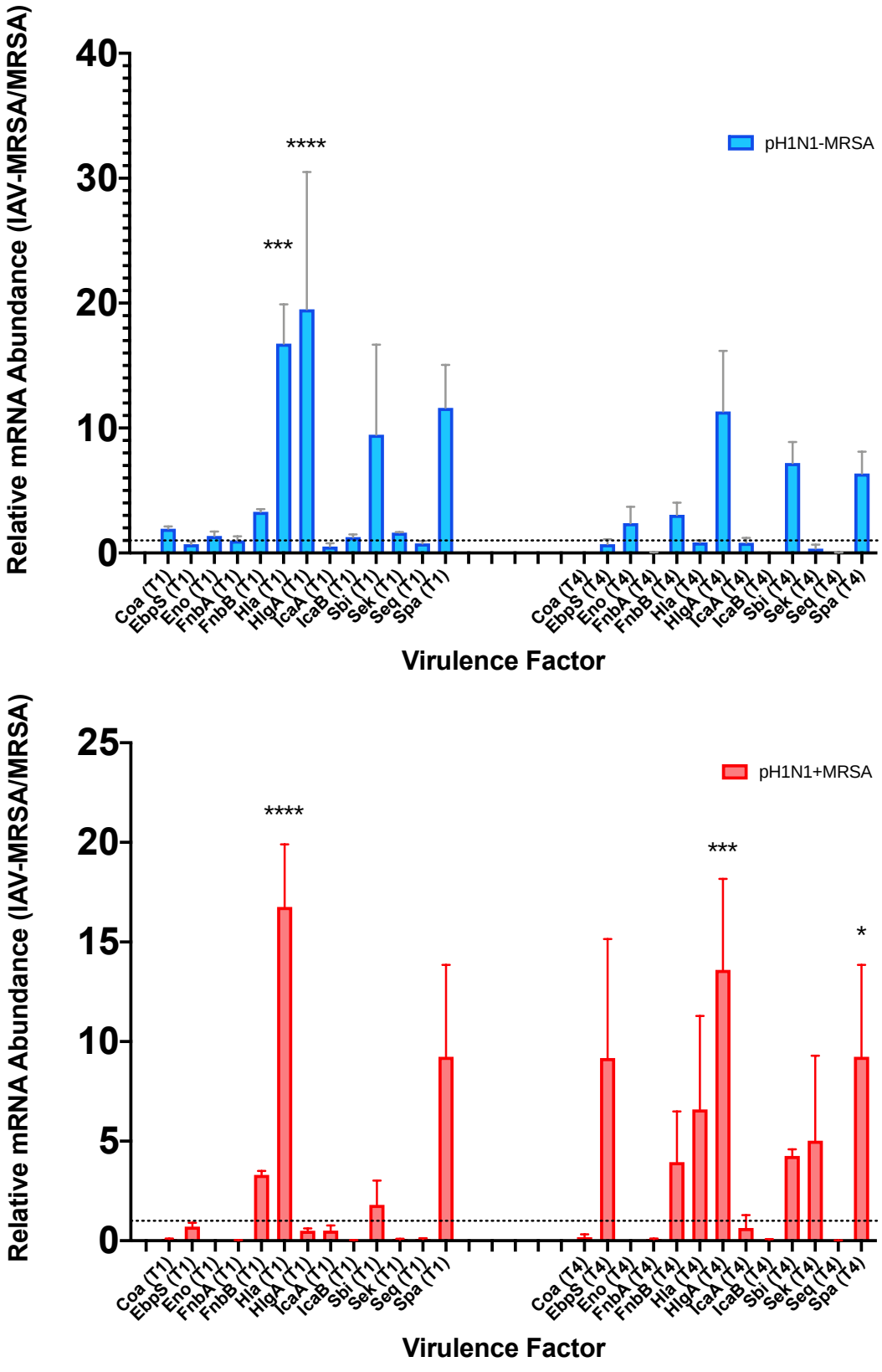

Figure 22: pH1N1 Alters MRSA Virulence Factor Expression at 1 and 4h.

Figure 22: pH1N1 Alters MRSA Virulence Factor Expression at 1 and 4 h.

RT-qPCR was employed to examine differential modulation of relative MRSA virulence factor mRNA abundance in the presence or absence of pre-existing pH1N1 infection in alveolar epithelial cells. Relative mRNA abundance fold changes represent pH1N1-MRSA vs MRSA infection alone and were calculated by the $2^{-\Delta\Delta CT}$ method. Error bars represent SEM calculated from three biological replicates ($n = 3$).

A) When alveolar epithelial cells were infected with pH1N1-MRSA, the infection condition, the virulence factor, and the interaction between the two were each statistically significant ($P < 0.0001$ for all three). At 1 h, *hla* and *hlgA* were significantly upregulated ($P = 0.0006$, $P < 0.0001$, respectively).

B) When alveolar epithelial cells were infected with pre-complexed pH1N1+MRSA, the infection condition, the virulence factor, and the interaction between the two were each significantly upregulated (P 0.0002, $P < 0.0001$, $P < 0.0001$, respectively). At 1 h post-infection, *hla* was significantly upregulated ($P < 0.0001$). At 4 h, both *hlgA* ($P = 0.0005$) and *spA* ($P = 0.0223$) were significantly upregulated.

0.0001, respectively) (Figure 22A). At 4 h post-infection, the expression of *eno*, *fnbB*, *hlgA*, *sbi* and *spA* remained upregulated in the co-infected cells, while the expression of *coa*, *hla*, *icaB*, and *sek* was downregulated. The remaining five virulence factor genes examined were largely repressed (<1) at both 1 and 4 h post-MRSA addition in pH1N1-MRSA infection. These data suggest that the modulation of specific virulence factors may be important in the early phase of bacterial attachment which coincides with 1 and 4 h in the presence of pH1N1.

When A549 cells were infected with pre-complexed pH1N1+MRSA, the infection condition (pH1N1+MRSA vs MRSA alone) showed statistical significance ($P = 0.0002$), as well as the virulence factor studied ($P < 0.0001$) and the interaction between the infection condition and virulence factor ($P < 0.0001$). At 1 h post-infection, the expression of *fnbB*, *hla*, *sbi*, and *spA* was upregulated in pH1N1+MRSA infected cells as compared with MRSA-alone (Figure 22B). However, only *hla* was significantly upregulated ($P < 0.0001$). At 4 h post-infection, *ebpS*, *fnbB*, *hla*, *sbi*, and *spA* all remained upregulated. Upregulation of *hlgA* and *sek* was also seen at 4 h post-infection. Upregulation of both *hlgA* and *spA* was statistically significant at 4 h ($P = 0.0005$ and $P = 0.0223$, respectively). The expression of each of the other virulence factors studied were largely repressed during the early exponential phase of MRSA replication in pH1N1+MRSA infected cells, as compared with MRSA-alone.

Interestingly, relative expression of *fnbB* and *hla* was almost identical at 1 h post-MRSA infection in cells co-infected with pH1N1-MRSA and pH1N1+MRSA. However, this phenomenon was not observed at 4 h post-infection. Each of the four genes upregulated at 1 h post-pH1N1+MRSA infection were also upregulated at 1 h post-MRSA addition in pH1N1-MRSA co-infection, suggesting these virulence factors are particularly important early in pH1N1 co-infection pathogenesis, regardless of when infection with MRSA occurs.

When alveolar epithelial cells were infected with sH1N1-MRSA, the infection condition, the virulence factor, and the interaction between the two were each statistically significant ($P < 0.0001$, $P = 0.0051$, $P < 0.0001$, respectively; Figure 23). The expression of *coa*, *fnbB*, *hla*, and *spA* was upregulated in sH1N1-infected cells relative to MRSA-alone infection at 1 h. Upregulated expression of *fnbB*, *hla*, and *spA* was also observed at 4 h post-MRSA infection. While upregulation of *coa* was no longer observed at 4 h post-infection, expression of *ebpS*, *eno*, and *sbi* was upregulated in sH1N1-MRSA co-infected cells. At 4 h, *sbi* was significantly upregulated ($P = 0.0372$). Each of the four genes upregulated at 1 h in sH1N1-MRSA infected cells were also upregulated in the presence of pH1N1, suggesting that *coa*, *fnbB*, *hla*, and *spA* may each play an important role in H1N1-MRSA pathogenesis early on in co-infection.

When A549 cells were infected with pH3N2-MRSA, the expression of virulence factors at 1 and 4 h post-infection was largely repressed (<1) in the case of each of the investigated 13 bacterial virulence factors (Figure 24A). Neither the infection condition, the virulence factor, or the interaction between the two were statistically significant ($P = 0.9001$, $P = 0.9037$, $P = 0.9046$). To further confirm that MRSA virulence factor expression was repressed in epithelial alveolar cells when co-infected with pH3N2, later time points were also studied (data not shown), revealing that each of the bacterial virulence factors were largely repressed (<1) at each of the examined of the time points. This suggests that modulation of MRSA virulence factor expression does not occur in the presence of pH3N2.

In contrast, when alveolar epithelial cells were co-infected with sH3N2-MRSA, the infection condition, the virulence factor, and the interaction between the two were each statistically significant ($P = 0.0035$, $P = 0.0007$, $P = 0.0007$, respectively). The expression of *fnbB*, *hla*, and *spA* was upregulated at 1 h post-infection (Figure 24B). While this upregulation of

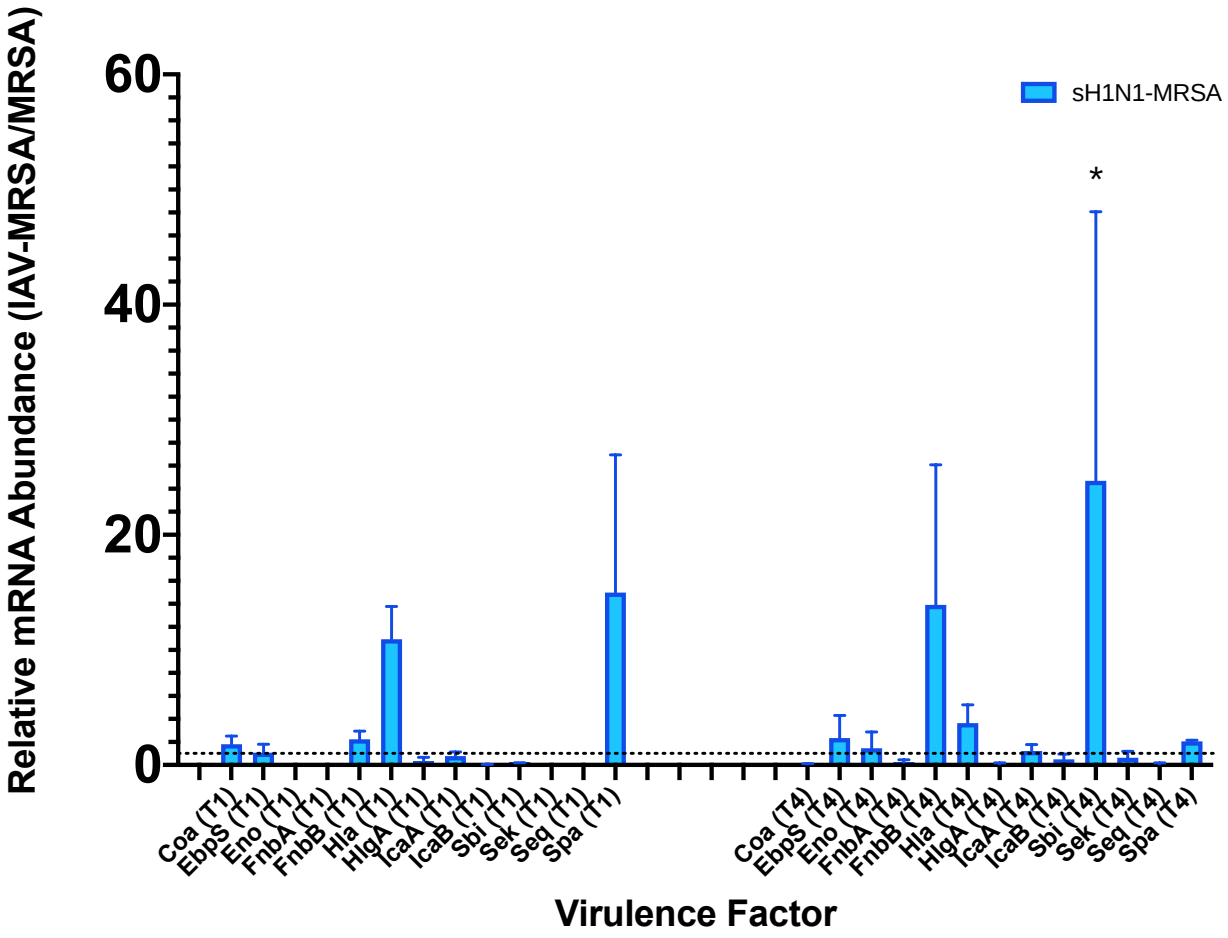

Figure 23: sH1N1 Alters MRSA Virulence Factor Expression at 1 and 4 h.

Figure 23: sH1N1 Alters MRSA Virulence Factor Expression at 1 and 4 h.

RT-qPCR was employed to examine differential modulation of relative MRSA virulence factor mRNA abundance in the presence or absence of pre-existing sH1N1 infection in alveolar epithelial cells. Relative mRNA abundance fold changes represent sH1N1-MRSA vs MRSA infection alone and were calculated by the $2^{-\Delta\Delta CT}$ method. Error bars represent SEM calculated from three biological replicates ($n = 3$). The infection condition, the virulence factor, and the interaction between the two were each statistically significant ($P < 0.0001$, $P = 0.0051$, $P < 0.0001$, respectively). At 4 h, *sbi* was significantly upregulated ($P = 0.0372$).

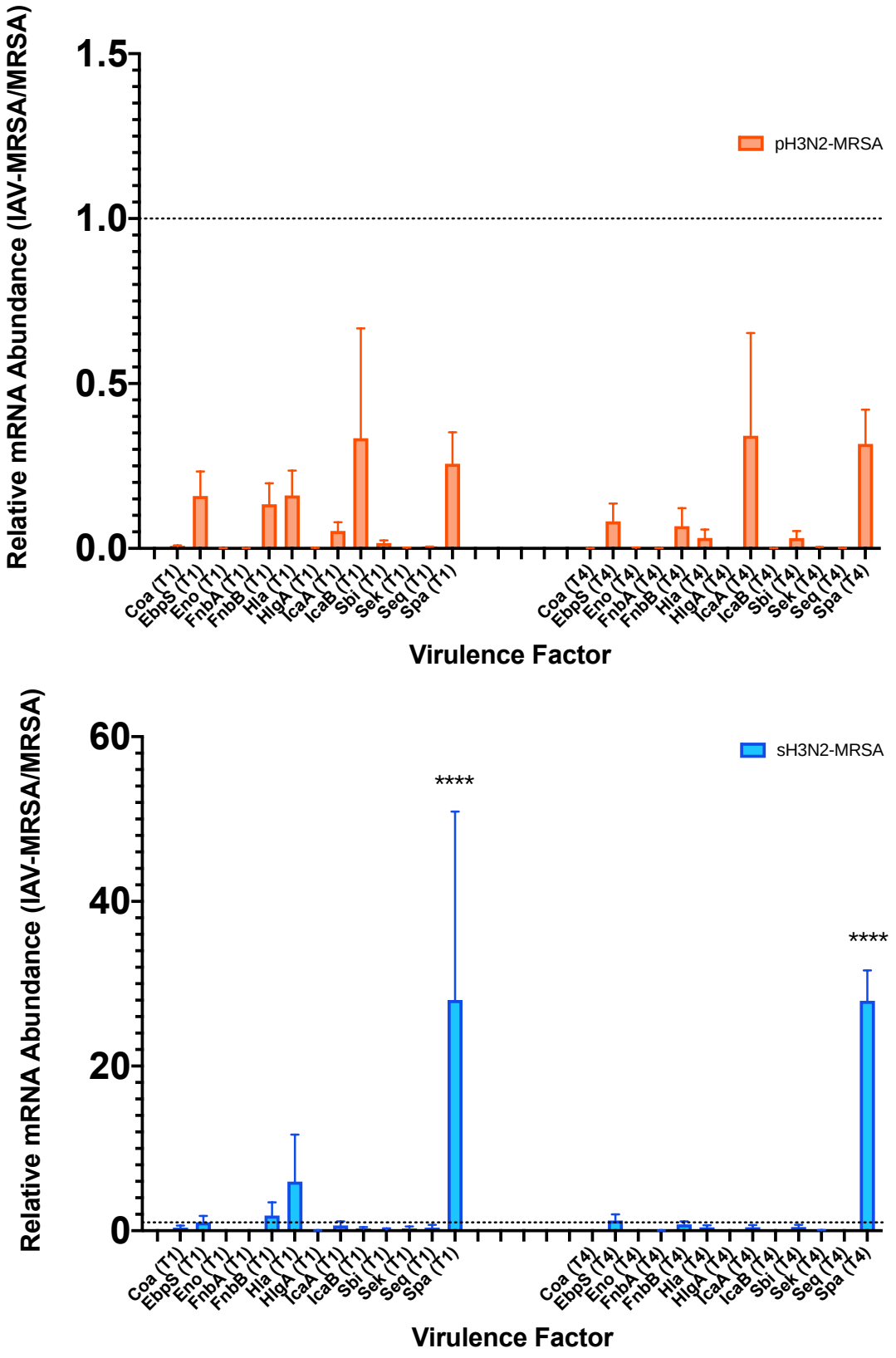

Figure 24: H3N2 Modulates MRSA Virulence Factor Expression at 1 and 4 h.

Figure 24: H3N2 Modulates MRSA Virulence Factor Expression at 1 and 4 h.

RT-qPCR was employed to examine differential modulation of relative MRSA virulence factor mRNA abundance in the presence or absence of pre-existing H3N2 infection in alveolar epithelial cells. Relative mRNA abundance fold changes represent H3N2-MRSA vs MRSA infection alone and were calculated by the $2^{-\Delta\Delta CT}$ method. Error bars represent SEM calculated from three biological replicates ($n = 3$).

A) When alveolar epithelial cells were infected with pH3N2-MRSA, neither the infection condition, the virulence factor, or the interaction between the two were statistically significant ($P = 0.9001$, $P = 0.9037$, $P = 0.9046$).

B) When alveolar epithelial cells were infected sH3N2-MRSA, the infection condition, the virulence factor, and the interaction between the two were each significantly upregulated ($P = 0.0035$, $P = 0.0007$, $P = 0.0007$, respectively). At 1 and 4 h post-infection, *spA* was significantly upregulated ($P < 0.0001$ at each time point).

fnbB and *hla* quickly fell at 4 h post-MRSA infection, *spA* remained highly upregulated. Upregulation of *ebpS* was also observed at 4 h post-MRSA addition. The only virulence factor significantly upregulated was *spA* at both 1 and 4 h ($P < 0.0001$ at both 1 and 4 h). The expression of the remaining virulence factors at 1 and 4 h relative to A549 cells infected with MRSA-alone was largely repressed (<1). Each of the three genes upregulated at 1 h in sH3N2-MRSA co-infected cells were also upregulated at 1 h in sH1N1-MRSA co-infected cells, suggesting that *fnbB*, *hla*, and *spA* may play an important role in the pathogenesis of seasonal IAVs early in infection.

Of the 13 virulence factors examined, only *sek* was not modulated at any time point or any condition, suggesting that it may not play a role in IAV-MRSA co-infection pathogenesis. Taken together, our data suggest that specific MRSA virulence factors may contribute to co-infection pathogenesis in the case of pH1N1, sH1N1, sH3N2, and pH1N1+MRSA co-infection during the early phase of bacterial attachment and invasion in alveolar epithelial cells. However, MRSA virulence factors do not seem to play a role in pH3N2-MRSA pathogenesis.

MRSA-alone and IAV-MRSA Infection Result in Alveolar Epithelial Cell Barrier Dysfunction

As bacterial replication kinetics were virtually identical in the presence of IAV, and the modulation of virulence factor genes did not appear to alter MRSA fitness, we next sought to characterize the potential role of dysregulated host responses in IAV-MRSA-mediated cytopathology. We employed ECIS to characterize alveolar-epithelial cell barrier function in response to IAV-MRSA infection by measuring temporal changes in resistance [320]. In short, alveolar epithelial cells were plated 24 h prior to IAV infection (0 h). Cells were then infected with IAV or mock-infected (denoted by the first arrow). IAV- and mock-infected cells were

subsequently infected with mid-log phase MRSA or mock-infected with media alone (denoted by the second arrow) (Figure 25). Resistance was continually monitored throughout the duration of the experiment. Subtraction of the baseline values of blank wells was automatically performed by the ECIS software provided by Applied Biophysics. Time, the infection condition, and the interaction between the two were each statistically significant ($P < 0.0001$ for all three).To allow further clarity of the effect of each IAV strain on the barrier integrity of alveolar epithelial cells, Figure 25 has been split into Figure 26A, B and Figure 27A, B. Statistical analyses are seen on Figures 26 and 27 for visual clarity but were obtained from analyses performed on Figure 25.

Infection of alveolar epithelial cells with pH1N1-alone (MOI 0.1) resulted in no changes to resistance during the first 24 h of infection (Figure 26A). The addition of MRSA at a MOI of 0.1 (second arrow) to mock-infected alveolar epithelial cells at 44 h resulted in a loss of resistance in the alveolar epithelial monolayer beginning at 56 h. Infection with MRSA at a MOI of 0.1 in cells previously infected with pH1N1 resulted in a nearly identical loss in resistance across the alveolar epithelial cells as that seen in cells infected with MRSA-alone. This trend was also observed when cells were infected with pH1N1+MRSA. Cells infected with 1% triton, MRSA-alone, pH1N1-MRSA, and pH1N1+MRSA were all significantly downregulated at 90 h compared with mock-infected cells ($P < 0.0001$ for all). This suggests that infection of alveolar epithelial cells with pH1N1 does not result in a detrimental host response.

When cells were infected with sH1N1 at a MOI of 0.1, resistance measurements remained largely unchanged over the course of infection (Figure 26B). When cells previously infected with sH1N1 were mock-infected at 44 h (second arrow), a small loss in resistance was seen, similar to that observed in mock-infected cells. Upon the addition of MRSA (MOI 0.1) to

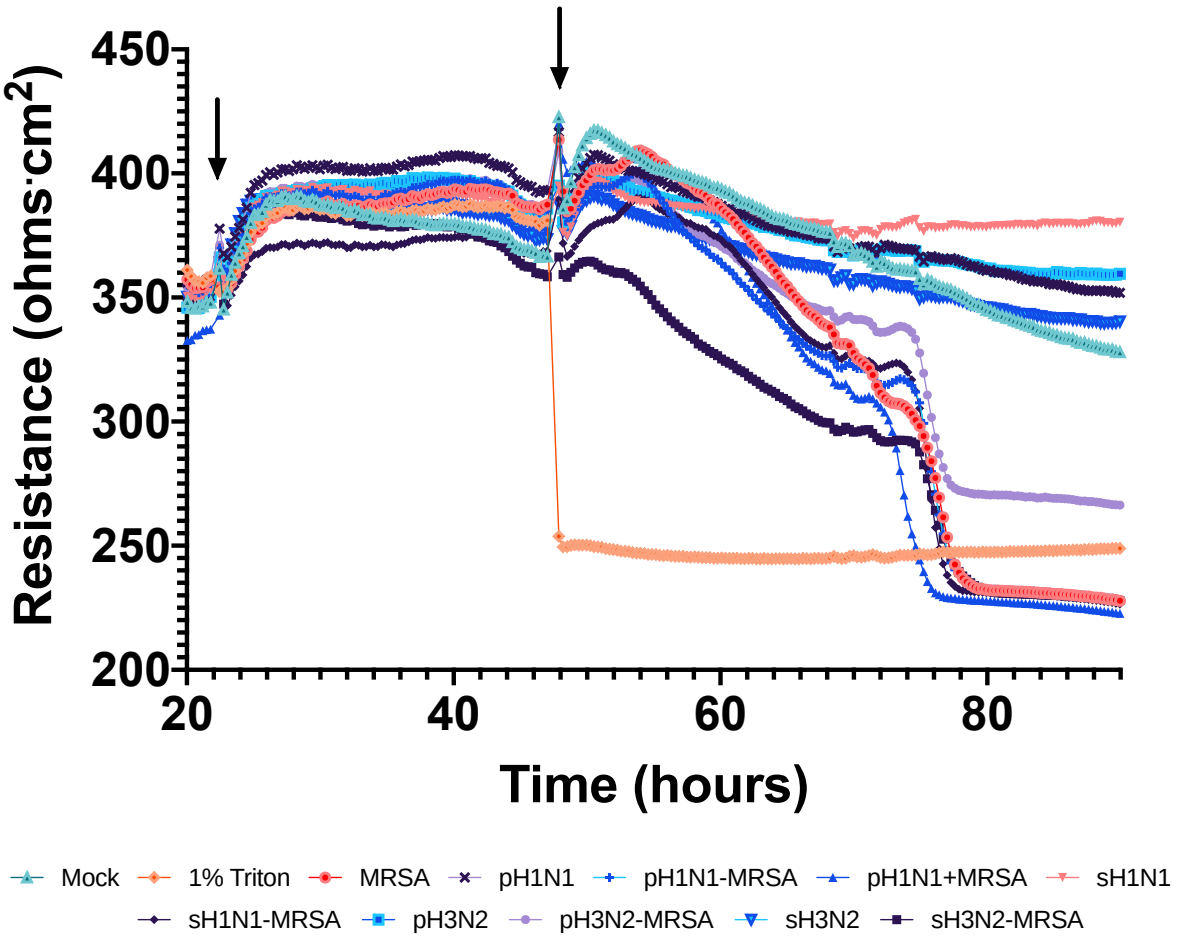

Figure 25: IAV-MRSA Co-infection Decreases Barrier Function in Alveolar Epithelial Cells.

Figure 25: IAV-MRSA Co-infection Decreases Barrier Function in Alveolar Epithelial Cells.

Median resistance values have been plotted for all data points obtained during the experiment. Alveolar epithelial A549 cells were plated 24 h prior to initial infection with IAV at a MOI of 0.1. Cells were infected or mock-infected with IAV and MRSA (MOI 0.1) was added 24 h later. Controls included cells infected with MRSA-alone, IAV-alone, 1% triton, and mock-infection. Arrows designate the addition of IAV (first arrow) and MRSA or 1% triton (second arrow) to the cells. Resistance data represent the median of three biological replicates with eight technical replicates per biological replicate ($n = 3$). Error bars have been removed to allow for clear visualization of all datasets, but were consistent across all biological replicates. Time, the infection condition, and the interaction between the two were each statistically significant ($P < 0.0001$ for all three). At 20 h and 44 h (just prior to IAV infection and MRSA infection, respectively), no statistically significant differences were seen between any infection condition as compared with mock-infected cells. At 90 h, MRSA -alone ($P < 0.0001$), pH1N1-MRSA ($P < 0.0001$), pH1N1+MRSA ($P < 0.0001$), sH1N1-MRSA ($P < 0.0001$), pH3N2-MRSA ($P = 0.0004$), sH3N2-MRSA ($P < 0.0001$), and 1% triton ($P < 0.0001$) were each significantly downregulated as compared with mock-infected. For clarity, statistical significance is indicated on the individual graphs.

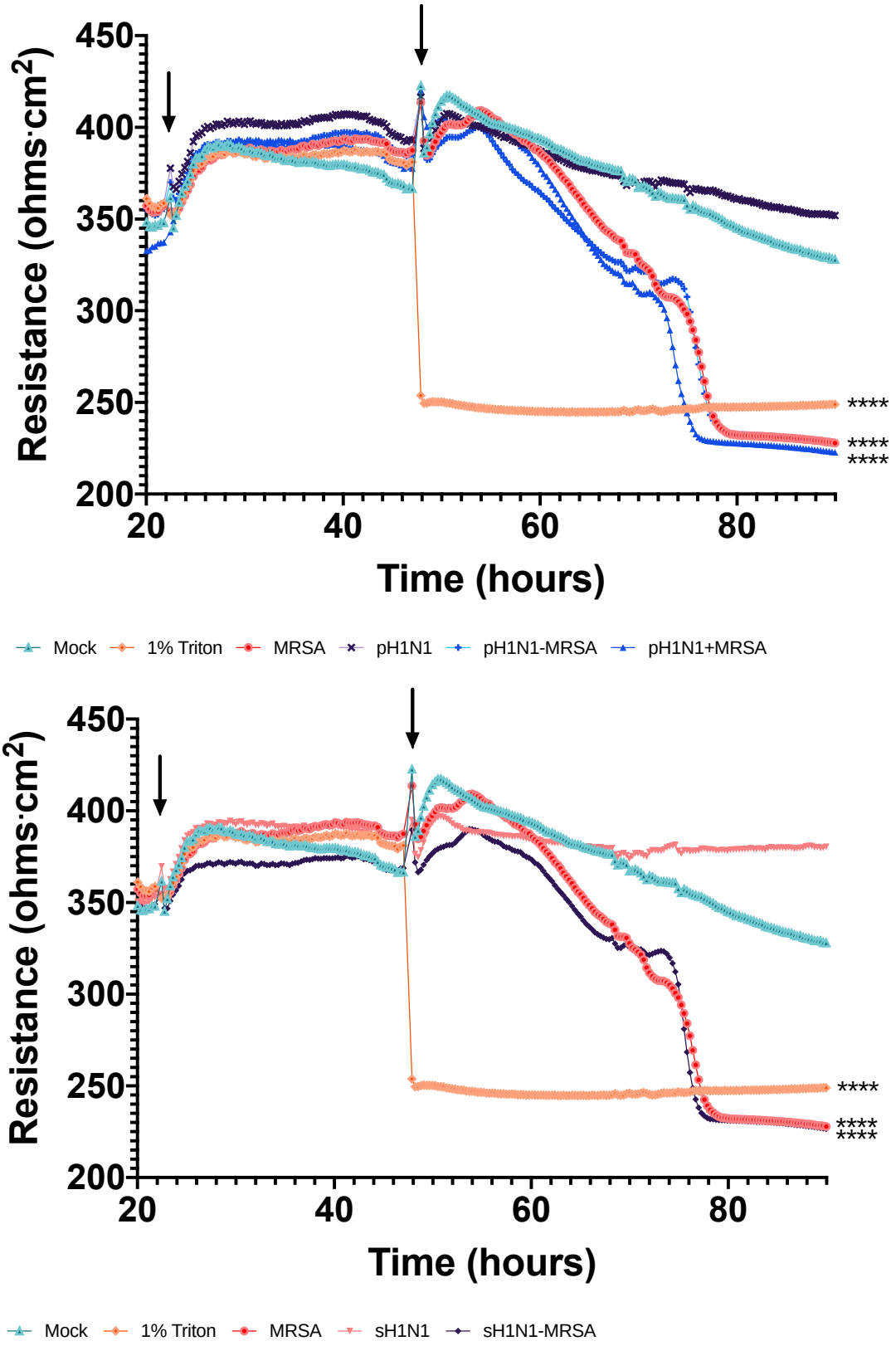

Figure 26: H1N1-MRSA Co-infection Decreases Barrier Function in Alveolar Epithelial Cells.

Figure 26: H1N1-MRSA Co-infection Decreases Barrier Function in Alveolar Epithelial Cells.

Resistance values have been plotted for all data points obtained during the experiment. Resistance data represent the median of three biological replicates with eight technical replicates per biological replicate (n = 3). Error bars have been removed to allow for clear visualization of all datasets, but were consistent across all biological replicates.

Visual summary only. Statistical comparisons and analyses were derived from the direct experimental comparisons (see Figure 25).

A) Alveolar epithelial A549 cells were plated 24 h prior to mock-infection or infection with pH1N1 at a MOI of 0.1. Cells were infected with pH1N1+MRSA (MOI 0.1), MRSA (MOI 0.1), or mock-infected 24 h later. Controls included cells infected with MRSA-alone, pH1N1-alone, 1% triton, and mock-infection. Arrows designate the addition of pH1N1 (first arrow) and MRSA or 1% triton (second arrow) to the cells. Cells infected with 1% triton, MRSA-alone, pH1N1-MRSA, and pH1N1+MRSA were all significantly downregulated at 90 h compared with mock-infected cells ($P < 0.0001$ for all).

B) Alveolar epithelial A549 cells were plated 24 h prior to mock-infection or infection with sH1N1 at a MOI of 0.1. Cells were infected with MRSA (MOI 0.1) or mock-infected 24 h later. Controls included cells infected with MRSA-alone, sH1N1-alone, 1% triton, and mock-infection. Arrows designate the addition of pH1N1 (first arrow) and MRSA or 1% triton (second arrow) to the cells. Cells infected with 1% triton, MRSA-alone, and sH1N1-MRSA were all significantly downregulated at 90 h compared with mock-infected cells ($P < 0.0001$ for all).

sH1N1-infected cells, a complete loss of resistance occurred at 56 h, only 12 hours post-MRSA infection. Cells infected with 1% triton, MRSA-alone, and sH1N1-MRSA were all significantly downregulated at 90 h compared with mock-infected cells ($P < 0.0001$ for all). The addition of MRSA to both pH1N1- and sH1N1-infected cells resulted in a near identical loss of resistance. While the addition of pH1N1- or sH1N1-alone did not result in a complete loss of resistance, the addition of pH1N1 to cells resulted in a small loss in resistance as compared with sH1N1-infected cells, indicating that pH1N1 may result in greater perturbations to epithelial cell barrier function than sH1N1.

Similar to infection with pH1N1- and sH1N1-alone, infection with pH3N2-alone (MOI 0.1) resulted in no changes to resistance during the first 24 h of infection, while the addition of mock-infected inoculum at 44 h (second arrow) resulted in a small loss of resistance at the alveolar epithelial monolayer (Figure 27A). When alveolar epithelial cells were co-infected with pH3N2-MRSA at a MOI of 0.1, a loss in resistance which mimicked that observed when alveolar epithelial cells were infected with MRSA-alone (MOI 0.1) was seen. Cells infected with 1% triton, MRSA-alone, and pH3N2-MRSA were all significantly downregulated at 90 h compared with mock-infected cells ($P < 0.0001$, $P < 0.0001$, $P = 0.0004$). Perhaps unsurprisingly, the loss in resistance observed in both pH1N1-MRSA and sH1N1-MRSA co-infected cells was more severe than the loss in pH3N2-MRSA co-infected cells. This may suggest that pH3N2 does not have the same effect on the loss of barrier integrity as other IAVs, specifically H1N1 IAV strains.

Lastly, infection with sH3N2 at a MOI of 0.1 resulted in only a minor loss in resistance over the course of 48 h, while cells co-infected with sH3N2-MRSA (MOI 0.1) showed a loss in resistance similar to when alveolar epithelial cells were infected with MRSA-alone (Figure

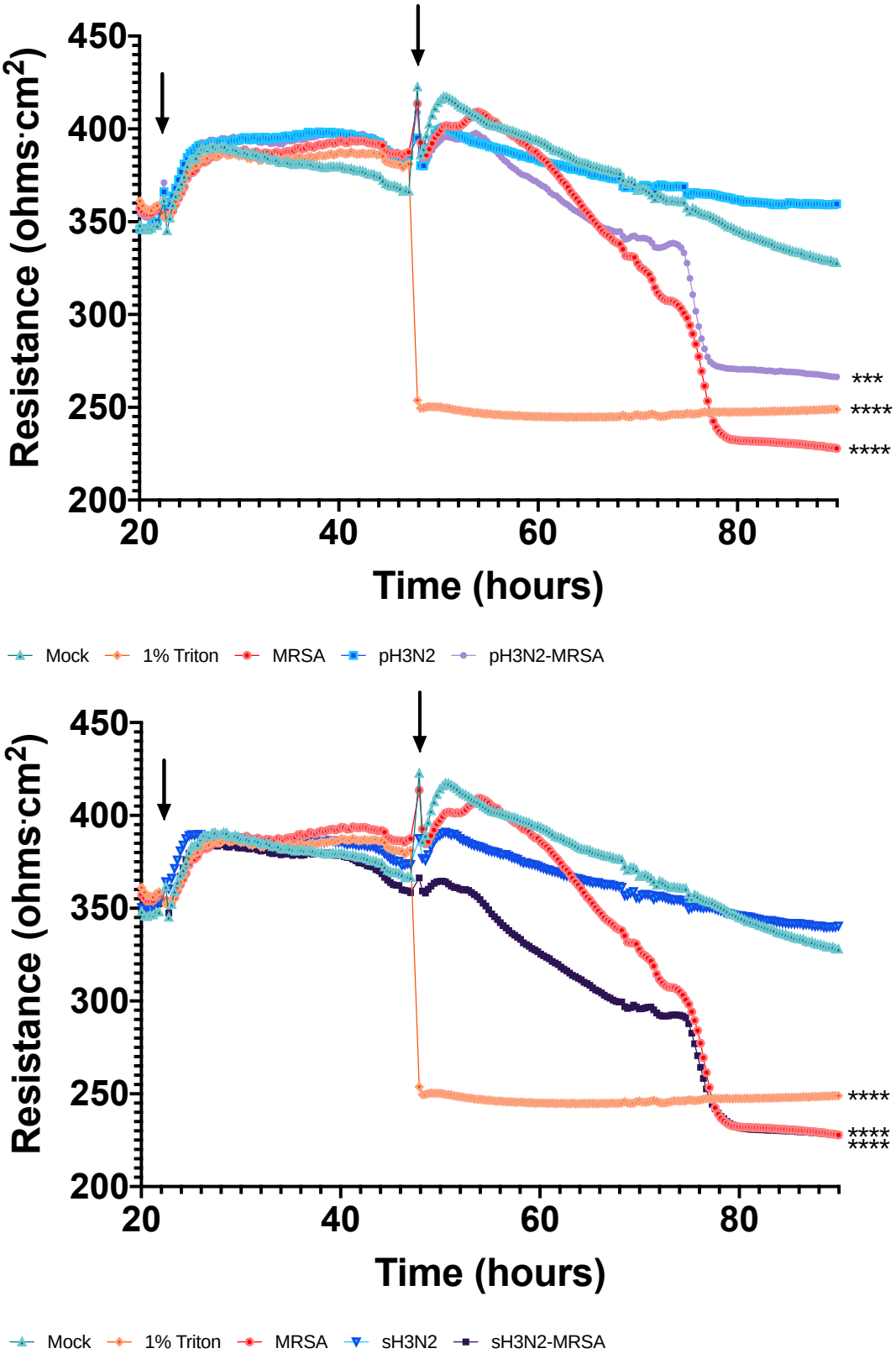

Figure 27: H3N2-MRSA Co-infection Decreases Barrier Function in Alveolar Epithelial Cells.

Figure 27: H3N2-MRSA Co-infection Decreases Barrier Function in Alveolar Epithelial Cells.

Visual summary only. Statistical comparisons and analyses were derived from the direct experimental comparisons (see Figure 25). Resistance values have been plotted for all data point obtained during the experiment. Resistance data represent the median of three biological replicates with eight technical replicates per biological replicate ($n = 3$). Error bars have been removed to allow for clear visualization of all datasets, but were consistent across all biological replicates.

A) Alveolar epithelial A549 cells were plated 24 h prior to mock-infection or infection with pH3N2 at a MOI of 0.1. Cells were infected with MRSA (MOI 0.1) or mock-infected 24 h later. Controls included cells infected with MRSA-alone, pH3N2-alone, 1% triton, and mock-infection. Arrows designate the addition of IAV (first arrow) and MRSA or 1% triton (second arrow) to the cells. Cells infected with 1% triton, MRSA-alone, and pH3N2-MRSA were all significantly downregulated at 90 h compared with mock-infected cells ($P < 0.0001$, $P < 0.0001$, $P = 0.0004$).

B) Alveolar epithelial A549 cells were plated 24 h prior to mock-infection or infection with sH3N2 at a MOI of 0.1. Cells were infected with MRSA (MOI 0.1) or mock-infected 24 h later. Controls included cells infected with MRSA-alone, sH3N2-alone, 1% triton, and mock-infection. Arrows designate the addition of sH1N1 (first arrow) and MRSA or 1% triton (second arrow) to the cells. Cells infected with 1% triton, MRSA-alone, and sH1N1-MRSA were all significantly downregulated at 90 h compared with mock-infected cells ($P < 0.0001$ for all).

27B). Cells infected with 1% triton, MRSA-alone, and sH1N1-MRSA were all significantly downregulated at 90 h compared with mock-infected cells ($P < 0.0001$ for all). When compared with cells co-infected with pH3N2-MRSA, a more severe loss in resistance was observed in sH3N2-MRSA infected cells, similar to when co-infection occurred with pH1N1 or sH1N1. This may suggest that co-infection with sH3N2 leads to greater disruption of alveolar epithelial cell barrier function as compared with co-infection with pH3N2.

As our results suggested that disruption of the alveolar epithelial barrier during IAV-MRSA co-infection strongly resembles the disruption seen during MRSA infection alone, we sought to further expand on these observations by examining the effects of infection using higher and lower MOIs of pH1N1 and MRSA. When cells were infected with MRSA at a MOI of 0.01, a similar loss in resistance was seen as when cells were infected with the higher MOI of 0.1 (Figure 28). In contrast, the trend in resistance measurements differed slightly between the two MOIs of MRSA during co-infection with pH1N1 at a MOI of 0.1. Similarly, co-infection with pH1N1-MRSA (MOI 0.01 and MOI 0.1, respectively) resulted in a similar loss in resistance across the epithelial barrier as infection with MRSA alone. When cells were infected with pH1N1 at a higher MOI of 3.0, resistance measurements began to decrease compared with mock-infected cells at 9 h post-IAV infection. When MRSA at a low MOI of 0.01 was added to cells infected with pH1N1 (MOI 3.0), resistance values began to decrease at the same time as MRSA-alone and MOI 0.1 pH1N1-MRSA infections. However, when cells were infected with pH1N1-MRSA at a MOI of 3.0 and 0.1 respectively, losses in resistance equivalent to those of 1% triton-treated cells were seen. At 70 h, 1% triton, MRSA-alone (MOI 0.01), PH1N1-MRSA (MOI 0.1; 0.01) and pH1N1-MRSA (MOI 3.0; 0.01) ($P < 0.0001$ for all) and pH1N1 (MOI 0.1; $P = 0.05$).

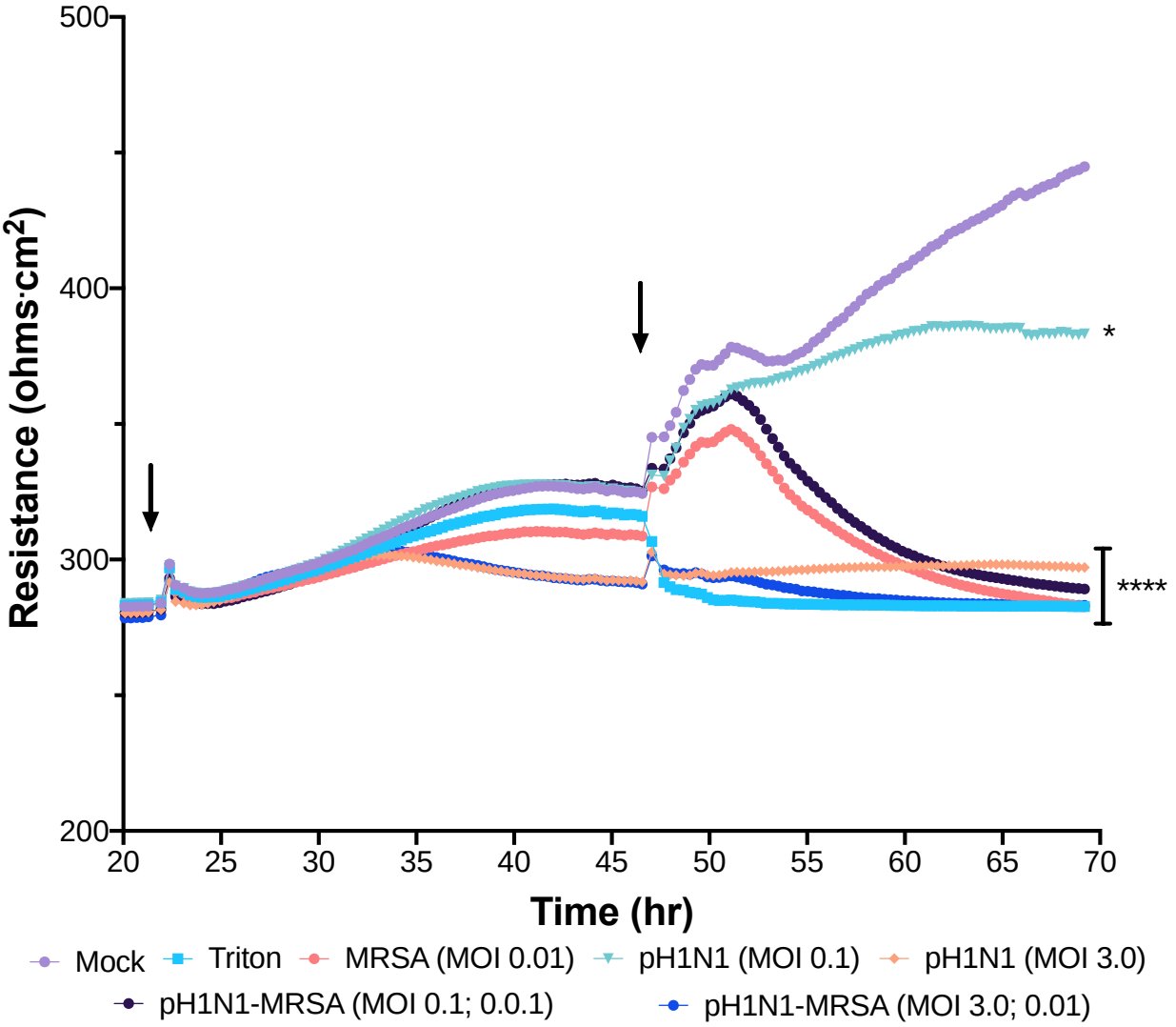

Figure 28: pH1N1-MRSA Co-infection Decreases Barrier Function in Alveolar Epithelial Cells Regardless of the MOI.

Figure 28: pH1N1-MRSA Co-infection Decreases Barrier Function in Alveolar Epithelial Cells Regardless of the MOI.

Median resistance values have been plotted for all data point obtained during the experiment. Alveolar epithelial A549 cells were plated 24 h prior to initial infection. Cells were infected or mock-infected with pH1N1 (MOI 0.1 or 3.0). MRSA (MOI 0.01) was added 24 h later. Controls included cells infected with MRSA-alone, pH1N1-alone, 1% triton, and mock-infection. Arrows designate the addition of pH1N1 (first arrow) and MRSA or 1% triton (second arrow) to the cells. Resistance data represent the median of three biological replicates with eight technical replicates per biological replicate ($n = 3$). Error bars have been removed to allow for clear visualization of all datasets, but were consistent across all biological replicates. Time, the infection condition, and the interaction between the two were each statistically significant ($P < 0.0001$ for all). At 20 h and 45 h (just prior to IAV infection and MRSA infection, respectively), no statistically significant differences were seen between any infection condition as compared with mock-infected cells. At 70 h, 1% triton, MRSA-alone (MOI 0.01), PH1N1-MRSA (MOI 0.1; 0.01) and pH1N1-MRSA (MOI 3.0; 0.01) ($P < 0.0001$ for all) and pH1N1 (MOI 0.1; $P = 0.05$) were all significantly downregulated as compared with mock-infected.

These data further support the hypothesis that the loss in barrier integrity observed during IAV-MRSA co-infection largely resembles the loss found during MRSA infection alone. Moreover, IAV infection alone does not seem to result in a loss of alveolar epithelial barrier integrity, except for when pH1N1-alone infection occurs at a very high MOI.

Finally, to examine the effect of pH1N1-MRSA co-infection in distal regions of the lung, we investigated the effects of co-infection on HBEC-3KT human bronchial epithelial cells (Figure 29). Time, the infection condition, and the interaction between the two were each statistically significant ($P < 0.0001$ for all). At 50 h and 70 h (just prior to IAV infection and MRSA infection, respectively), no statistically significant differences were seen between any infection condition as compared with mock-infected cells. At 110 h, 1% triton, MRSA-alone, and pH1N1-MRSA were each significantly downregulated ($P < 0.0001$ for all) as compared with mock-infected. Virtually no loss in resistance was found in cells infected with pH1N1 (MOI 0.1), while infection with pH1N1-MRSA (MOI 0.1) resulted in a complete loss of resistance comparable to infection with MRSA-alone at a MOI of 0.1. These trends in loss of resistance were similar to pH1N1-MRSA co-infection in A549 alveolar epithelial cells, suggesting that pH1N1-MRSA co-infection results in a similar outcome in anatomically- and physiologically-distinct regions of the lungs.

Collectively, these data suggest that IAV does not play a significant role in the loss of barrier integrity during infection. Instead, these data suggest that the presence of MRSA in alveolar epithelial cells does result in a significant loss in barrier integrity, regardless of whether infection occurs alone or as a secondary co-infection during IAV infection.

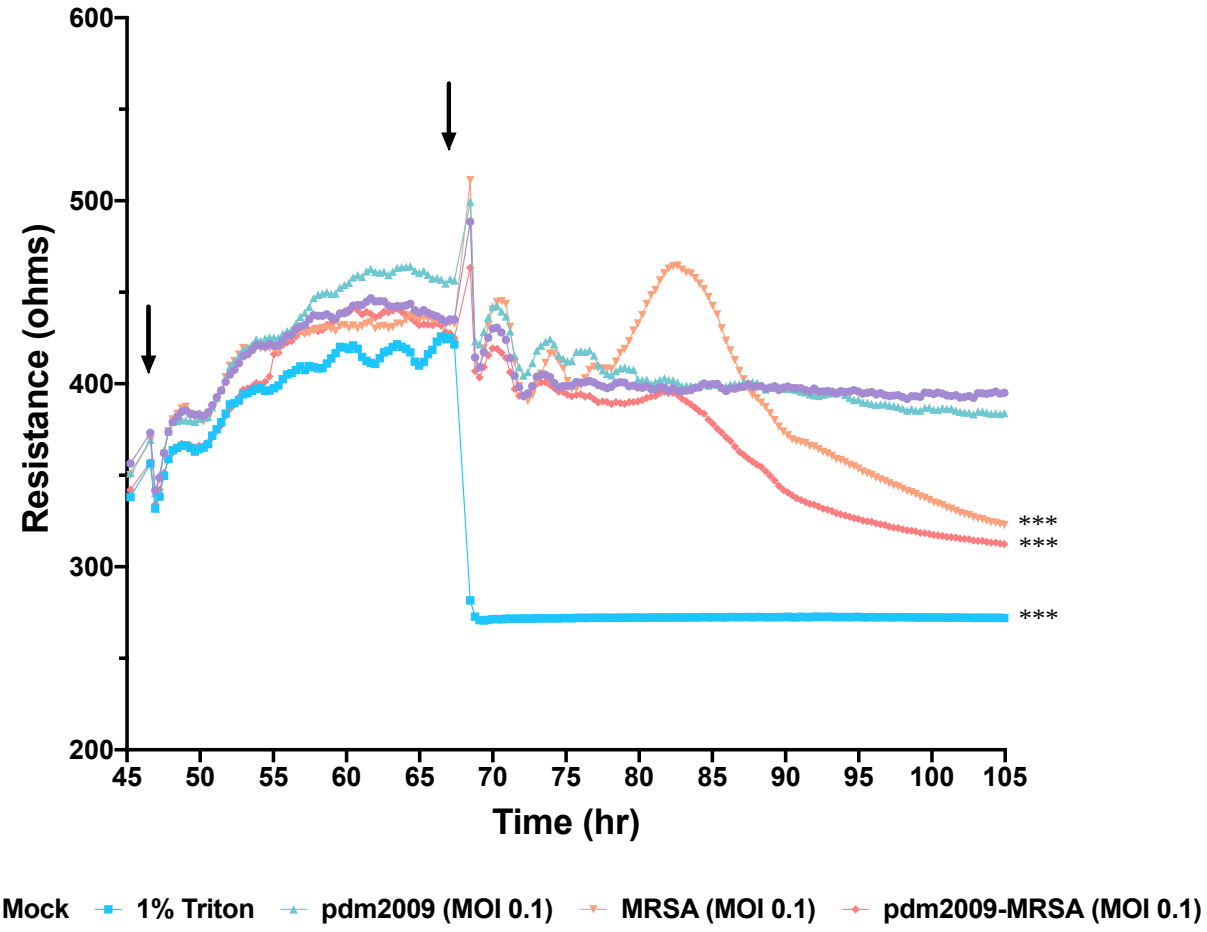

Figure 29: pH1N1-MRSA Co-infection Decreases Barrier Function in HBEC3-KT Cells.

Figure 29: pH1N1-MRSA Co-infection Decreases Barrier Function in HBEC3-KT Cells.

Median resistance values have been plotted for all data points obtained during the experiment. Normal human bronchial HBEC3-KT cells were plated 24 h prior to initial infection. Cells were mock-infected or infected with pH1N1 at a MOI of 0.1; MRSA (MOI 0.1) was added 24 h later. MRSA-alone, pH1N1-alone, 1% triton, and mock-infected cells acted as controls. Resistance data represent the median of three biological replicated with eight technical replicates per biological replicate ($n = 3$). Error bars have been removed to allow for clear visualization of all datasets, but were consistent across all biological replicates. Arrows designate the addition of pH1N1 (first arrow) and MRSA or triton (second arrow). Time, the infection condition, and the interaction between the two were each statistically significant ($P < 0.0001$ for all). At 45 h and 65 h (just prior to IAV infection and MRSA infection, respectively), no statistically significant differences were seen between any infection condition as compared with mock-infected cells. At 110 h, 1% triton, MRSA-alone, and pH1N1-MRSA were each significantly downregulated ($P < 0.0001$ for all) as compared with mock-infected.

Temporal Analysis of Host Kinome Responses During pH1N1-MRSA Infection

As our previous analyses had suggested that IAV does not play a role in the modulation of alveolar epithelial barrier integrity or in the modulation of MRSA's replication kinetics, we next sought to characterize the aberrant cell-mediated immune response which may contribute to the disease pathogenesis observed in our ECIS data. We performed temporal kinome analysis on alveolar epithelial cells when infected with pH1N1-alone, MRSA-alone, or pH1N1-MRSA. Cells were harvested at equivalent time points to those used for the bacterial replication kinetics experiment. Kinome analysis allowed for the characterization of the activation state of host cell signaling responses across our conditions in order to provide insight into differential cellular responses mitigated during co-infection as compared with pathogens alone.

Kinome peptide arrays were used to quantitate the host kinome response by probing cell lysates at each time point across all infection conditions. Kinome analysis provides information regarding the activation state of host kinases by measuring the phosphorylation of specific kinase targets (immobilized peptides) on the arrays by active kinases in a cell lysate [321, 322]. Data from our arrays, comprised of 309 unique kinase recognition sequences related to a broad spectrum of cell signaling pathways and processes was analyzed using PIIKA 2 software [311]. Hierarchical clustering analysis of the kinome data is presented in Figure 30. Each column is indicative of an infection condition at a specific time point. Each line within each column corresponds to a phosphorylation site that is presented on the array. Pixel intensity is representative of the intensity of fluorescence at each possible phosphorylation site on the array, as analyzed by PIIKA 2. Red depicts upregulation, while green depicts downregulation as compared with the background.

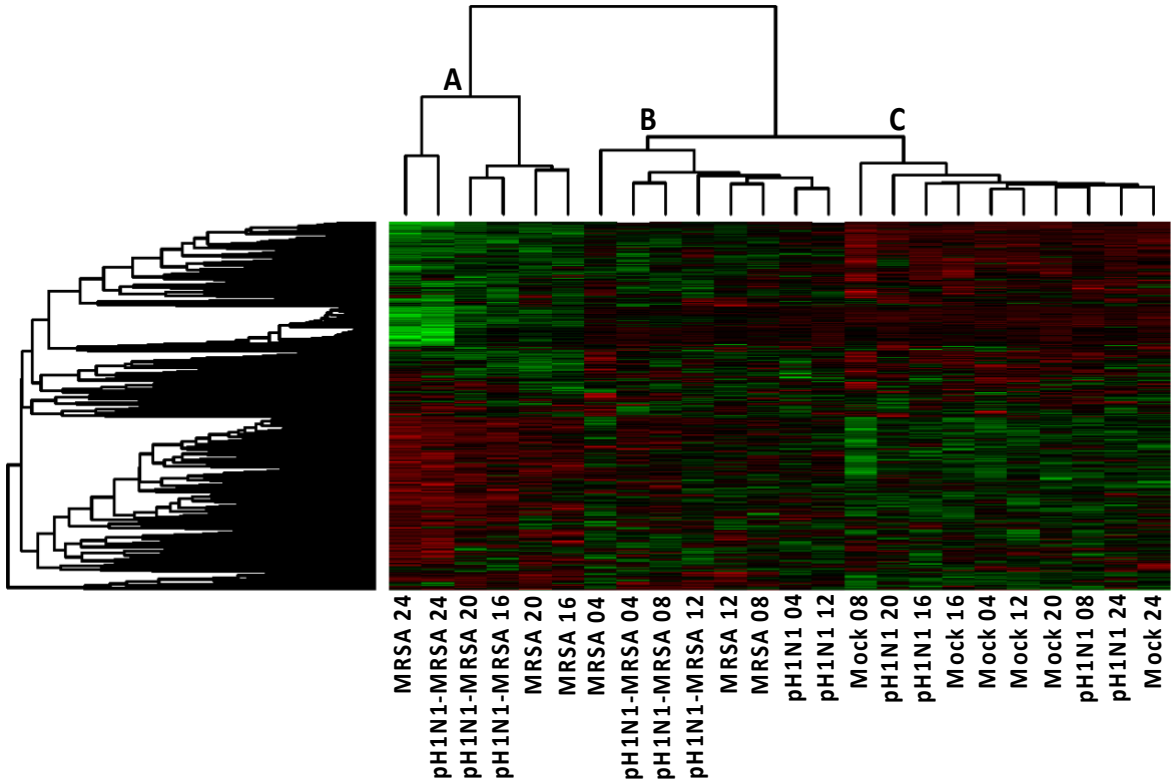

Figure 30: Hierarchical Clustering of Temporal Kinome Responses of pH1N1, MRSA, and pH1N1-MRSA Infection in Alveolar Epithelial Cells.

Figure 30: Hierarchical Clustering of Temporal Kinome Responses of pH1N1, MRSA, and pH1N1-MRSA Infection in Alveolar Epithelial Cells.

Cells were plated 24 h prior to initial infection. Cells were either mock-infected or infected with pH1N1 at a MOI of 0.1; MRSA (MOI 0.1) was added 24 h later. Cells were harvested for kinome analysis at 4, 8, 12, 16, 20, and 24 h. Controls included MRSA-alone, pH1N1-alone, and mock-infected time-matched samples. Cell lysates were probed to quantitate host kinome responses by kinome peptide arrays. Red depicts upregulation, while green depicts downregulation as compared with the background. A-C designate the three major dataset clusters as identified following hierarchical clustering.

The kinome datasets clustered into 3 major clusters. From left to right, the first major cluster consisted of MRSA-alone at 16, 20, and 24 h and pH1N1-MRSA at 16, 20, and 24 h (denoted as A). The second cluster (denoted as B) was comprised of MRSA-alone at 4, 8, and 12 h, pH1N1-alone at 4 and 12 h, and pH1N1-MRSA at 4, 8, and 12 h. The final cluster, denoted as C, consisted of each of the remaining time points and conditions: mock-infected at 4, 8, 12, 16, 20, and 24 h and pH1N1-alone at 8, 16, 20, and 24 h. These data suggested that the host kinome response of MRSA-alone and pH1N1-MRSA at the later time points of 16, 20, and 24 h are highly conserved. Moreover, these host kinome responses differentiated strongly from each of the other infection conditions and time points.

Next, we performed biological subtraction of the time-matched mock-infected kinome datasets from their respective infected counterparts, as previously described, to gain further insight into the similarities and/or differences of the host kinome response during pH1N1-MRSA co-infection [310, 311, 316, 323, 324]. Subsequent hierarchical clustering analysis of the resulting kinome data following mock-infected background subtraction is presented in Figure 31. As seen previously, the MRSA-alone and pH1N1-MRSA datasets at the later time points of 16, 20, and 24 h clustered together independently of the time-matched pH1N1-alone datasets. In contrast, the pH1N1-alone and pH1N1-MRSA at the initial early time point of 4 h post-infection clustered together independently of the MRSA-alone 4 h time point. Most notably, the MRSA-alone, pH1N1-alone, and pH1N1-MRSA datasets at 8 h clustered together, as well as the MRSA-alone, pH1N1-alone, and pH1N1-MRSA datasets at 12 h. These data suggest that the host cellular response switches from a pH1N1-centric response to a MRSA-centric response at 8-12 h post-MRSA infection. To further validate our kinome data, Phospho-kinase Proteome Profiler

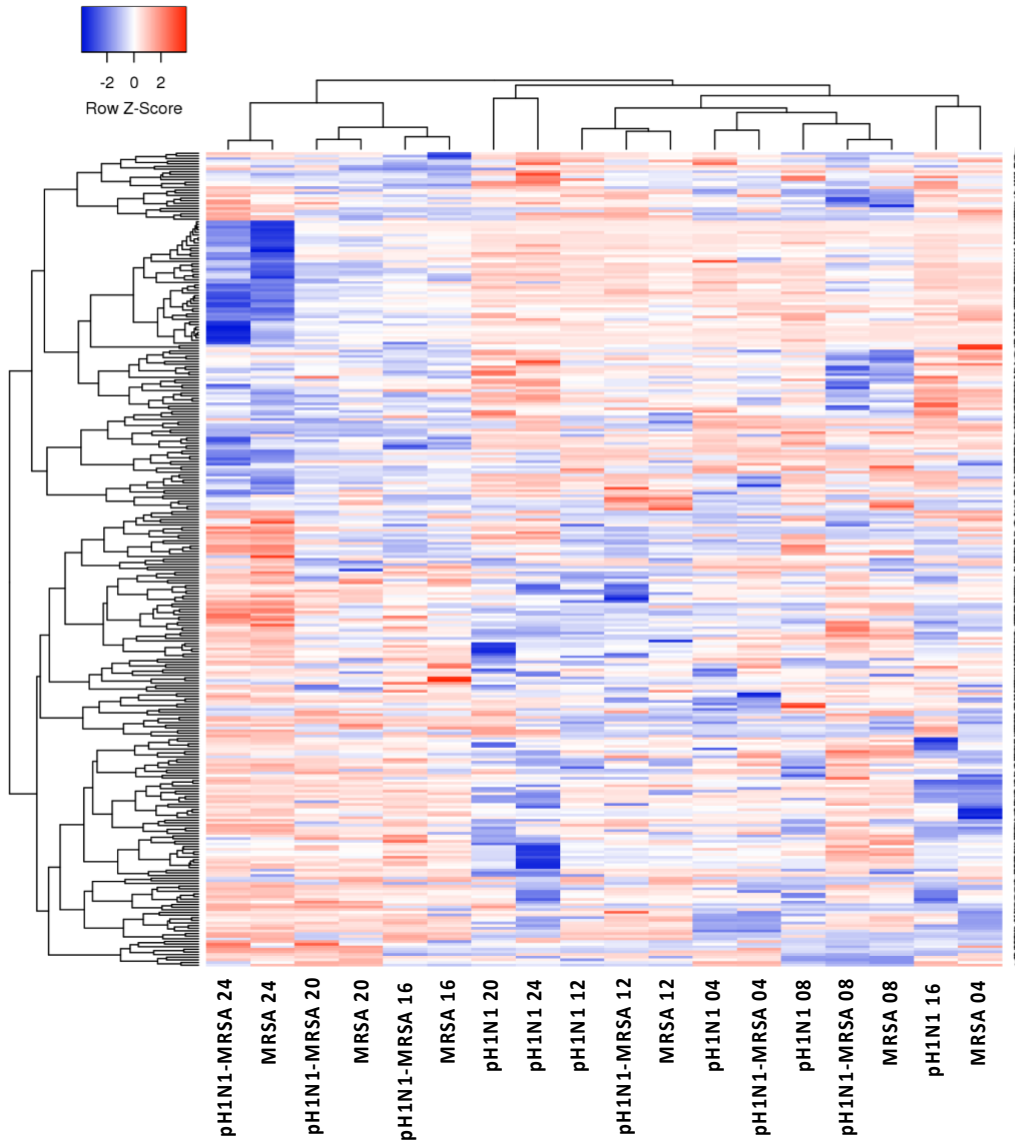

Figure 31: Background-subtracted Temporal Kinome Responses of pH1N1, MRSA, and pH1N1-MRSA Infection in Alveolar Epithelial Cells.

Figure 31: Background-subtracted Temporal Kinome Responses of pH1N1, MRSA, and pH1N1-MRSA Infection in Alveolar Epithelial Cells.

Mock-infected kinome responses were subtracted from time-matched infected samples in Figure 30. Fold change phosphorylation values are plotted for all kinase recognition sequences on the kinome peptide arrays. Clustering analysis was performed with the Heatmapper software suite. Z-score values represent fold change differences in phosphorylation as compared with time-matched mock-infected control cells. Red depicts upregulation, while blue depicts downregulation as compared with the background.

Arrays (R&D Systems) were used to perform phospho-Western blot analysis. Phosphorylation events that were conserved between the upregulated phosphorylation on the arrays (fold change > 1.5; p-value < 0.05) and the phospho-Western blots are presented in Table 4.

As our previous data suggested that the host response undergoes a switch at 8-12 h post-MRSA infection, we next sought to identify host cell signaling responses or biological networks that were selectively modulated in pH1N1-MRSA co-infected cells (Table 5). All data related to pathway overrepresentation and biological processes is presented. However, it is important to note that our assays were conducted in an adenocarcinomic alveolar cell line, and as such pathways related to cancer signaling will be overrepresented.

Pathway over-representation analysis at 8 h post-MRSA addition revealed numerous pathways that were selectively upregulated as compared with mock-infected cells. These pathways were primarily related to apoptosis and the antiviral response. Apoptosis related pathways included p75(NTR)-, NRAGE-, NADE-, Tsp-1, and BH3-mediated signaling events, while pathways related to cell-cell contacts included α6-β4 integrin-, and ephrin-mediated signaling events. Signaling pathways directly related to antiviral response were also identified, including type I IFN and inflammatory response-related events. At 12 h post-MRSA addition, the host response was again dominated by antiviral response-mediated events, including IFN-related response and TRAF6-mediated IRF7 activation, and NOTCH-related signaling events. From 16-24 h post-MRSA addition, there were strong signaling pathways between pH1N1-MRSA infection and MRSA-alone infection, as predicated by our hierarchical clustering analysis. Upregulated pathways were primarily related to pro-apoptotic (e.g. p53- and caspase-mediated responses), cytokine signaling (e.g., TNF; IL-1; NFκB), innate immune responses (e.g.,

Table 4: Conservation of Phosphorylation Status Between Kinome Analysis and Phospho-Western Blots.

Phospho-kinase Proteome Profiler Arrays (R&D Systems) were used to perform phospho-Western blot analysis. Phosphorylation events that were conserved between the upregulated phosphorylation on the arrays (fold change > 1.5; p-value < 0.05) and the phospho-Western blots are summarized below.

Target	Phosphosite	Phospho-Western Blot (Fold Change)	Kinome Analysis (Fold Change)
PDGFRb	Y751	1.81	1.61
Fyn	Y420	11.12	1.54
STAT5b	Y699	9.06	2.25
Lyn	Y397	21.30	2.11
Lck	Y394	14.42	2.03
CREB	S133	2.00	2.54
β-catenin	Y654	8.97	2.39
EGFR	Y1086	2.25	2.24
Akt	S473	9.47	3.39
p38a	T180/Y182	2.65	2.13
ERK1/2	T202/Y204;T185/Y187	29.17	2.62
GSK3a/b	S21/S9	1.75	1.73
HSP60	S70	2.02	1.83
STAT3	S727	1.36	1.87
Pyk2	Y402	1.76	2.53
PLCg1	Y783	1.67	1.31
c-Jun	S63	1.87	2.49
p53	S392	3.04	2.58

Table 5: Pathway Overrepresentation Analysis of Host Kinome Responses in pH1N1-MRSA Infected Samples (8-12 h post-MRSA Infection).

Pathway overrepresentation of pH1N1-MRSA co-infected alveolar epithelial cells at 8 h post-MRSA infection revealed signaling pathways primarily related to apoptosis, cell-cell contacts, and the antiviral response. The host response at 12 h continued to be dominated by the antiviral response.

Time	Signaling Pathway	Uploaded Protein Count	Pathway Upregulated P-Value
8 h	Intrinsic Pathway for Apoptosis	12	0.039
	BH3-only Proteins Associate with and Inactivate Anti-Apoptotic BCL-2 Members	4	0.043
	Apoptotic Signaling in Response to DNA Damage	7	0.058
	Cell-Cell Communication	7	0.058
	Amyotrophic Lateral Sclerosis (ALS)	10	0.061
	p75 NTR Receptor-Mediated Signaling	10	0.061
	α6β4-Integrin	20	0.070
	Cell Death Signaling via NRAGE, NRIF, and NADE	5	0.090
	DEx/H-box Helicases Activate Type I IFN and Inflammatory Cytokine Production	5	0.090
	EPH-Ephrin Signaling	5	0.090
	EPHB-Mediated Forward Signaling	5	0.090
	Metabolism of proteins	5	0.090
	TSP-1 Induced Apoptosis in Microvascular Endothelial Cells	5	0.090
	Validated Targets of C-MYC Transcriptional Activation	5	0.090
	Viral Myocarditis	5	0.090
	Apoptosis	21	0.092
	Activation of BH3-only Proteins	8	0.095
	Calcium Signaling by HBx of Hepatitis B Virus	8	0.095
	Cell Surface Interactions at the Vascular Wall	8	0.095
12 h	Pre-NOTCH Expression and Processing	3	0.049
	Pre-NOTCH Transcription and Translation	3	0.049
	TRAF6 Mediated IRF7 Activation	7	0.054
	Presenilin Action in NOTCH and Wnt Signaling	8	0.078
	Basal Cell Carcinoma	4	0.090
	Regulation of Cell Cycle Progression by Plk3	4	0.090

	Signaling by NOTCH	4	0.090
	TRAF6 Mediated IRF7 Activation in TLR 7/8 or 9 Signaling	4	0.090
	The Information Processing Pathway at the IFN-β Enhancer	4	0.090

Table 6: Pathway Overrepresentation Analysis of Host Kinome Responses in MRSA Infected Samples (8-12 h post-MRSA Infection).

Pathway overrepresentation of alveolar epithelial cells infected with MRSA-alone at 8 h post-infection. Compared with pH1N1-MRSA co-infected cells at 8 h, signaling pathways directly related to cell-cell contacts were markedly absent, while apoptosis related pathways were not overrepresented to the same degree.

Time	Signaling Pathway	Uploaded Protein Count	Pathway Upregulated P-Value
8 h	IL-13 Signaling	5	0.027
	Alzheimer's Disease	6	0.049
	Amyotrophic Lateral Sclerosis	10	0.050
	STING Mediated Induction of Host Immune Responses	3	0.064
	Apoptotic Signaling in Response to DNA Damage	7	0.077
	Oxidative Stress Induced Senescence	12	0.095
12 h	HIF-1α Transcription Factor Network	6	0.002
	Tsp-1 Induced Apoptosis in Microvascular Endothelial Cells	5	0.012
	TRAF6 Mediated IRF7 Activation	7	0.035
	Oxidative Stress Induced Senescence	12	0.036
	Calcium Signaling in the CD4+ TCR Pathway	3	0.036
	Caspase Cascade in Apoptosis	3	0.036
	Negative Regulators of RIG-1/MDA5 Signaling	3	0.036
	Pertussis Toxin-Insensitive CCR5 Signaling in Macrophage	3	0.036
	Pre-NOTCH Expression and Processing	3	0.036
	Pre-NOTCH Transcription and Translation	3	0.036
	Calcineurin-Regulated NFAT-dependent Transcription in Lymphocytes	8	0.052
	Calcium Signaling by HBx of Hepatitis B Virus	8	0.052
	Calcium Signaling Pathway	8	0.052
	Endothelins	8	0.052
	Regulation of Telomerase	8	0.052
	LPA Receptor Mediated Events	14	0.062
	Wnt Signaling Pathway	14	0.062
	FOXA1 Transcription Factor Network	4	0.067
	Hypoxia-Inducible Factor in the Cardiovascular System	4	0.067

	Latent Infection of *Homo sapiens* with *Mycobacterium tuberculosis*	4	0.067
	Oxidative Stress Induced Gene Expression via NRF2	4	0.067
	Phagosomal Maturation (Early Endosomal Stage)	4	0.067
	Platelet Homeostasis	4	0.067
	Regulation of Cell Cycle Progression by Plk3	4	0.067
	Repression of Pain Sensation by the Transcriptional Regulator Dream	4	0.067
	Signaling by NOTCH	4	0.067
	Validated Transcriptional Targets of API Family Members FRA1 and FRA2	4	0.067
	Osteopontin-mediate Events	9	0.072
	Regulation of Nuclear SMAD2/3 Signaling	9	0.089
	Colorectal Cancer	22	0.089

Table 7: Pathway Overrepresentation Analysis of Host Kinome Responses in pH1N1 Infected Samples (8-12 h post-MRSA Infection).

Pathway overrepresentation of alveolar epithelial cells infected with pH1N1-alone at 8 h post-infection. Compared with pH1N1-MRSA co-infected cells at 8 h, signaling pathways directly related to apoptosis and cell-cell contacts were markedly absent. At 12 h, similar NOTCH signaling pathways were overrepresented as in pH1N1-MRSA co-infected cells.

Time	Signaling Pathway	Uploaded Protein Count	Pathway Upregulated P-Value
8 h	TRAF6 Mediated IRF7 Activation	7	0.031
	IL-13 Signaling	5	0.056
	Metabolism of Proteins	5	0.056
	Phagosome	5	0.056
	TRAF3-dependent IRF Activation Pathway	5	0.056
	Validated Targets of C-MYC Transcriptional Activation	5	0.056
12 h	Glucocorticoid Receptor Regulatory Network	13	0.003
	Wnt Signaling Pathway	14	0.004
	METs Effect on Macrophage Differentiation	2	0.008
	Alzheimer's Disease	6	0.010
	ErbB2/ErbB3 Signaling Events	12	0.014
	Oxidative Stress Induced Senescence	12	0.014
	AKT Phosphorylates Targets in the Cytosol	7	0.017
	Apoptotic Signaling in Response to DNA Damage	7	0.017
	Cellular Responses to Stress	20	0.021
	Calcium Signaling in the CD4+ TCR Pathway	3	0.022
	Pertussis Toxin-Insensitive CCR5 Signaling in Macrophages	3	0.022
	Pre-NOTCH Expression and Processing	3	0.022
	Pre-NOTCH Transcription and Translation	3	0.022
	Unfolded Protein Response (UPR)	3	0.022
	Activation of BH3-only Proteins	8	0.026
	Calcineurin-Regulated NFAT-dependent Transcription in Lymphocytes	8	0.026
	Presenilin Action in NOTCH and Wnt Signaling	8	0.026
	Colorectal Cancer	8	0.026
	Regulation of Nuclear SMAD 2/3 Signaling	9	0.037
	BH3-only Proteins Associate with and Inactivate Anti-Apoptotic BCL-2 Members	4	0.042

	Basal Cell Carcinoma	4	0.042
	FOXA1 Transcription Factor Network	4	0.042
	LKB1 Signaling Events	4	0.042
	Oxidative Stress Induced Gene Expression via NRF 2	4	0.042
	Repression of Pain Sensation by the Transcriptional Regulator DREAM	4	0.042
	Signaling by NOTCH	4	0.042
	The Information Processing Pathway at the IFNβ Enhancer	4	0.042
	Amyotrophic Lateral Sclerosis (ALS)	10	0.049
	Direct p52 Effectors	10	0.049
	Cellular Senescence	17	0.051
	T cell Receptor Signaling Pathway	18	0.062
	AP-1 Transcription Factor Network	11	0.064
	Phosphoinositides and their Downstream Targets	11	0064
	Role of Clcineurin-dependent NFAT Signaling in Lymphocytes	11	0.064
	Signaling Mediated by p38-α and p38-β	11	0.064
	Activation of BAD and Translocation to Mitochondria	5	0.066
	ATM Signaling Pathway	5	0.066
	IL12 Signaling Mediated by STAT4	5	0.066
	Metabolism of Proteins	5	0.066
	Regulation of Nuclear β-catenin Signaling and Target Gene Transcription	5	0.066
	S1P2 Pathway	5	0.066
	Tsp-1 Induced Apoptosis in Microvascular Endothelial Cell	5	0.066
	ATF-2 Transcription Factor Network	12	0.081
	Downstream Signaling in Naïve CD8+ T Cells	12	0.081
	Intrinsic Pathway for Apoptosis	12	0.081
	Activation of the AP-1 Family of Transcription Factors	6	0.093
	Aurora A Signaling	6	0.093
	Cadmium Induces DNA Synthesis and Proliferation in Macrophages	6	0.093
	FOXM1 Transcription Factor Network	6	0.093
	HIF-1-α Transcription Factor Network	6	0.093

TLR signaling; IFN), and wound healing (e.g., TGF-mediated signaling). In contrast, pH1N1-alone infected samples were dominated by IFN-, JAK/STAT-, and IL-4-mediated signaling from 16-24 h. At 24 h, p53-mediated signaling pathways were overrepresented in samples infected with pH1N1-alone.

We directly compared the host response of samples infected with pH1N1-MRSA and MRSA-alone to provide additional clarity in the differences in host response during the 8-12 h transition period (Table 8). Apoptosis-related signaling pathways were overrepresented in pH1N1-MRSA infected cells compared with MRSA-alone infected cells at 8 h. Apoptosis-related signaling pathways were also markedly absent in cells infected with pH1N1-alone (Table 7). This suggests that earlier activation of apoptosis occurs when alveolar epithelial cells are co-infected with pH1N1-MRSA. There were fewer differentially-upregulated pathways between pH1N1-MRSA infection and MRSA-alone infection at 12 h. While pathways related to TRAF6-, p73NTR, and apoptosis were upregulated in co-infected samples, no clear over-representation of a particular biological pathway was seen.

Lastly, gene ontology analysis was performed to identify possible overrepresented biological processes in pH1N1-MRSA kinome data during the 8-12 h transition period (Tables 9-11). Identified biological processes largely mirrored those seen in our previous pathway over-representation analysis, such as apoptosis- and IFN-related responses. Other identified processes included cellular damage related responses [e.g., adenosine triphosphate (ATP) catabolism, unfolded protein response, DNA damage] and IL-6- and IL-8-related cellular responses, suggesting a potential role of these immune mediators in the host response to pH1N1-MRSA co-infections. At 24 h post-MRSA addition, a number of signaling pathways were significantly upregulated, including those related to a pro-inflammatory response (i.e., TNF- and IL-1-

Table 8: Pathway Overrepresentation Analysis of Differentially Upregulated Host Kinome Responses in pH1N1-MRSA Infected Cells vs MRSA Infection Alone (8-12 h post-MRSA Infection).

Direct comparison of the host response of cells infected with pH1N1-MRSA as compared with MRSA-alone at 8 and 12 h. Apoptosis-related signaling pathways were overrepresented at 8 h, suggesting that activation of apoptosis is a direct result of co-infection.

Time	Signaling Pathway	Uploaded Protein Count	Pathway Up-regulated P-Value
8 h	Cell Death Signaling via NRAGE, NRIF, and NADE	5	0.005
	Caspase Cascade in Apoptosis	10	0.007
	p75 NTR Receptor-Mediated Signaling	10	0.007
	Intrinsic Pathway for Apoptosis	12	0.014
	Caspase Cascade in Apoptosis	3	0.022
	Apoptosis	14	0.026
	p75(NTR)-Mediated Signaling	14	0.026
	CDC42 Signaling Events	15	0.033
	Toxoplasmosis	31	0.037
	BH3-only Proteins Associate with and Inactivate Anti-Apoptotic BCL-2 Members	4	0.042
	Stress Induction of HSP Regulation	4	0.042
	TRAF6 Mediate IRF7 Activation in TLR 7/8 or 9 Signaling	4	0.042
	p75NTR Recruits Signaling Complexes	4	0.042
12 h	Cell Death Signaling via NRAGE, NRIF, and NADE	5	0.003
	p75 NTR Receptor-Mediate Signaling	10	0.016
	TRAF6 Mediated IRF7 Activation in TLR 7/8 or 9 Signaling	4	0.017
	TRAF6 Mediated IRF7 Activation	7	0.018
	Phagosome	5	0.038

Table 9: Gene Ontology Analysis of Host Kinome Responses in pH1N1-MRSA Infected Samples (8-12 h post-MRSA Infection).

Gene ontology analysis was performed to identify possible overrepresented biological processes in pH1N1-MRSA kinome data during the 8-12 h transition period. Identified biological processes included apoptosis and antiviral responses, similarly to our prior analyses. Other biological processes included cellular damage related responses and IL-related cellular responses.

Time	Signaling Pathway	Uploaded Protein Count	Pathway Upregulated P-Value
8 h	Regulation of Inflammatory Response	6	0.003
	Positive Regulation of Release of Cytochrome C from Mitochondria	5	0.011
	Positive Regulation of IL-6 Production	3	0.013
	Intrinsic Apoptotic Signaling Pathway	12	0.037
	Intrinsic Apoptotic Signaling Pathway in Response to DNA Damage	7	0.055
	Cellular Protein Metabolic Process	5	0.087
	Negative Regulation of Protein Catabolic Process	5	0.087
	Neuron Apoptotic Process	5	0.087
	Positive Regulation of IFNα Production	5	0.087
	Positive Regulation of Peptidyl-Tyrosine Phosphorylation	5	0.087
	Response to Progesterone	5	0.087
	Positive Regulation of Cell Migration	11	0.087
	Extrinic Apoptotic Signaling Pathway in Absence of Ligand	8	0.091
	Release of Cytochrome C from Mitochondria	8	0.091
	Positive Regulation of Neuron Apoptotic Process	10	0.004
	Cellular Response to DNA Damage Stimulus	13	0.017
	Positive Regulation of IFNα Production	5	0.018
	Positive Regulation of TNF Production	6	0.033
	Transforming Growth Factor β Receptor Signaling Pathway	11	0.043
	ATP Catabolic Process	3	0.048
	ER Overload Response	3	0.048
	Ion Transport	3	0.048
	Positive Regulation of IL6 Production	3	0.048

12 h	Positive Regulation of IL8 Production	3	0.048
	Positive Regulation of Type I IFN-Mediated Signaling Pathway	3	0.048
	Protein Localization to Nucleus	3	0.048
	Proteolysis	3	0.048
	Response to Unfolded Protein	3	0.048
	B Cell Homeostasis	7	0.052
	Intrinsic Apoptotic Signaling Pathway in Response to DNA Damage	7	0.052
	Regulation of Apoptotic Process	12	0.059
	Release of Cytochrome C from Mitochondria	8	0.076
	Positive Regulation of Apoptotic Process	24	0.076
	Transcription from RNA Polymerase II Promoter	13	0.077
	B Cell activation	4	0.088
	T Cell Homeostasis	4	0.088
	Erythrocyte Differentiation	4	0.088
	Mammary Gland Development	4	0.088
	Negative Regulation of Protein Phosphorylation	4	0.088
	Positive Regulation of Protein Phosphorylation	4	0.088
	Regulation of Protein Phosphorylation	4	0.088
	Response to UV	4	0.088
	Transport	4	0.088
	Type I IFN Biosynthetic Process	4	0.088

Table 10: Gene Ontology Analysis of Host Kinome Responses in MRSA Infected Samples (8-12 h post-MRSA Infection).

Gene ontology analysis was performed to identify possible overrepresented biological processes in MRSA-alone kinome data during the 8-12 h transition period. Biological processes related to apoptosis were markedly absent at 8 h, while processes related to the immune response and IFN production were overrepresented instead. At 12 h, processes related to the cell cycle were highly overrepresented in infection with MRSA-alone as compared with pH1N1-MRSA co-infection.

Time	Signaling Pathway	Uploaded Protein Count	Pathway Upregulated P-Value
8 h	Positive Regulation of IFN-α Production	5	0.006
	Defense Response to Gram-positive Bacterium	3	0.007
	Negative Regulation of Protein Phosphorylation	4	0.025
	Positive Regulation of IFN-β Production	4	0.025
	Regulation of Immune Response	4	0.025
	Cellular Protein Metabolic Process	5	0.054
	Neuron Apoptotic Process	5	0.054
	Oxidation-Reduction Process	5	0.054
	Positive Regulation of Peptidyl-Tyrosine Phosphorylation	5	0.054
	Positive Regulation of Neuron Projection Development	6	0.093
	Protein Homooligomerization	6	0.093
	Regulation of Inflammatory Response	6	0.093
12 h	ER Overload Response	3	0.001
	Positive Regulation of Mitochondrial Outer Membrane Permeabilization Involved in Apoptotic Signaling Pathway	4	0.002
	Transcription from RNA Polymerase II Promoter	13	0.002
	Wnt Signaling Pathway	8	0.002
	Release of Cytochrome C from Mitochondria	8	0.002
	Negative Regulation of Canonical Wnt Signaling Pathway	5	0.005
	Positive Regulation of Release of Cytochrome C from Mitochondria	5	0.005
	Positive Regulation of Transcription from RNA Polymerase II Promoter	39	0.007
	Positive Regulation of Apoptotic Process	24	0.009

	Positive Regulation of Transcription, DNA-templated	24	0.009
	Activation of Signaling Protein Activity Involved in Unfolded Protein Response	3	0.021
	Cellular Response to Calcium Ion	3	0.021
	Endoplasmic Reticulum Unfolded Protein Response	3	0.021
	Negative Regulation of Glycogen Biosynthetic Process	3	0.021
	Positive Regulation of Protein Catabolic Process	3	0.021
	Positive Regulation of Protein Oligomerization	3	0.021
	Regulation of Mitochondrial Membrane Permeability	3	0.021
	Regulation of Mitochondrial Membrane Permeability Involved in Apoptotic Process	3	0.021
	Regulation of Transcription, DNA-templated	37	0.021
	Extrinsic Apoptotic Signaling Pathway in Absence of Ligand	8	0.025
	Positive Regulation of Intrinsic Apoptotic Signaling Pathway	9	0.035
	Positive Regulation of Protein Insertion into Mitochondrial Membrane Involved in Apoptotic Signaling Pathway	9	0.035
	Epithelial to Mesenchymal Transition	4	0.041
	Glycogen Metabolic Process	4	0.041
	Positive Regulation of Neuron Apoptotic Process	10	0.048
	Sequence-Specific DNA Binding	17	0.049
	Transforming Growth Factor β Receptor Signaling Pathway	11	0.062
	Cellular Protein Metabolic Process	5	0.064
	Cellular Response to UV	5	0.064
	Neuron Apoptotic Process	5	0.064
	Response to Progesterone	5	0.064
	Intrinsic Apoptotic Signaling Pathway	12	0.078
	Regulation of Sequence-Specific DNA Binding Transcription Factor Activity	6	0.091
	Response to cAMP	6	0.091
	Cellular Response to DNA Damage Stimulus	13	0.096
	Negative Regulation of Transcription, DNA-templated	13	0.096

Table 11: Gene Ontology Analysis of Host Kinome Responses in pH1N1 Infected Samples (8-12 h post-MRSA Infection).

Gene ontology analysis was performed to identify possible overrepresented biological processes in pH1N1-alone kinome data. The inflammatory response was strongly overrepresented as compared with pH1N1-MRSA co-infected cells, while biological processes related to TLRs were absent.

Time	Signaling Pathway	Uploaded Protein Count	Pathway Upregulated P-Value
8 h	Neuron Apoptotic Process	5	0.030
	Regulation of Transcription from RNA Polymerase II Promoter	13	0.037
	Defense Response to Gram-positive Bacterium	3	0.067
	Multicellular Organism Growth	3	0.067
	Positive Regulation of IL6 Production	3	0.067
	Positive Regulation of Protein Oligomerization	3	0.067
	Regulation of Mitochondrial Membrane Permeability Involved in Apoptotic Process	3	0.067
	In utero Embryonic Development	15	0.068
	Inflammatory Response	20	0.073
12 h	Positive Regulation of TNF Production	6	0.021
	Response to cAMP	6	0.021
	Transforming Growth Factor β Receptor Signaling Pathway	11	0.025
	Cellular Response to Calcium Ion	3	0.035
	Defense Response to Gram-positive Bacterium	3	0.035
	Negative Regulation of Type I IFN Production	3	0.035
	Nitric Oxide Biosynthetic Process	3	0.035
	Receptor-Mediated Endocytosis	3	0.035
	Response to Immobilization Stress	3	0.035
	Somitogenesis	3	0.035
	Defense Response to Virus	8	0.050
	Release of Cytochrome C from Mitochondria	8	0.050
	Defense Response to Bacterium	4	0.066
	Interaction with Host	4	0.066
	Phagosome Maturation	4	0.066

	Positive Regulation of INF-β Production	4	0.066
	Positive Regulation of Vasodilation	4	0.066
	Response to UV	4	0.066
	Transport	4	0.066
	Regulation of Cell Proliferation	15	0.075
	Negative Regulation of Cell Proliferation	22	0.085
	Positive Regulation of Neuron Apoptotic Process	10	0.093
	Response to Hypoxia	10	0.093

mediated signaling), general innate immune responses (i.e., NFκB-, TLR-, and RIG-1/MDA5-mediated signaling), wound healing (e.g., TGF signaling), cell-cell contacts (e.g., α6β4-integin signaling), and apoptosis.

Taken together, our host kinome response data demonstrated that pH1N1-MRSA co-infection in alveolar epithelial cells resulted in the selective activation of host cell signaling events primarily related to apoptosis, cellular damage, and innate immune responses including the antiviral response and interleukin production. Moreover, signaling pathways in pH1N1-MRSA co-infected cells largely resembled those seen in pH1N1-alone and MRSA-alone infected cells at 8-12 h, while upregulated signaling pathways in pH1N1-MRSA co-infected cells strongly resembled those of MRSA-alone infections from 16 h onwards.

MRSA Replication Kinetics in a Co-culture Model are Similar during MRSA-alone and pH1N1-MRSA Infection

As our previous study had suggested that the presence of pH1N1 does not affect bacterial replication in A549 cells, we sought to determine how these results compared with an *in vitro* tissue culture model of the alveolar-capillary barrier. To create this model, we first seeded primary HMPECs on the basal side of a 0.4 μm transwell insert and HPAEpiCs on the apical side, as seen in Figure 13. Using a 0.4 μm insert ensured that MRSA, which has a diameter of 0.5-1.0 μm, would not be able to cross the barrier and was only able to infect alveolar epithelial cells [325]. This is in line with what was seen in fatal cases of pH1N1-MRSA co-infection [254].

Specifically, we wished to determine if bacterial replication kinetics were similarly unaffected during co-infection in primary human alveolar cells. Temporal enumeration of MRSA was investigated by adding MRSA to our mock-infected or pH1N1-infected tissue culture model 24 h post-infection (n = 3). As our previous findings suggested that MRSA infection

simultaneously with IAV infection or at peak viremia did not affect the growth kinetics, we based our timing on observational data from human patients with influenza-bacterial co-infections during the 2009 H1N1 pandemic, where bacterial co-infection commonly occurred during the peak of viral infection, as well as our previous findings [262, 278]. The number of adherent and internalized bacteria in epithelial cells of the tissue culture model were temporally-enumerated through standard bacterial plating.

MRSA replication within primary human pulmonary alveolar epithelial cells following viral- and bacterial-infection of the tissue culture model revealed a trend towards faster bacterial replication in pH1N1-MRSA co-infection as compared with infection with MRSA-alone at 1 and 4 h post-MRSA infection (Figure 32). When the model was infected with MRSA-alone, MRSA entered the exponential phase at 4 h post-infection, while in the presence of pH1N1, MRSA did not enter the exponential phase until 8 h post-infection. MRSA entered the stationary phase by 16 h post-infection whether the model was infected with MRSA-alone or with pH1N1-MRSA. MRSA growth over time showed statistical significance ($P = 0.0050$). However, no statistically significant differences were observed between either infection condition ($P = 0.3258$) or between either infection condition over time ($P > 0.6000$). This suggests that MRSA fitness within pulmonary respiratory epithelial cells at the alveolar-capillary barrier is not affected by the presence of pH1N1, similar to our observations in A549 cells.

Modulation of Bacterial Virulence Factors in a Co-culture Model of the Alveolar-Capillary Barrier

We next sought to characterize how bacterial virulence factor modulation might influence alveolar-capillary barrier permeability and pathogenesis during co-infection at the alveolar-

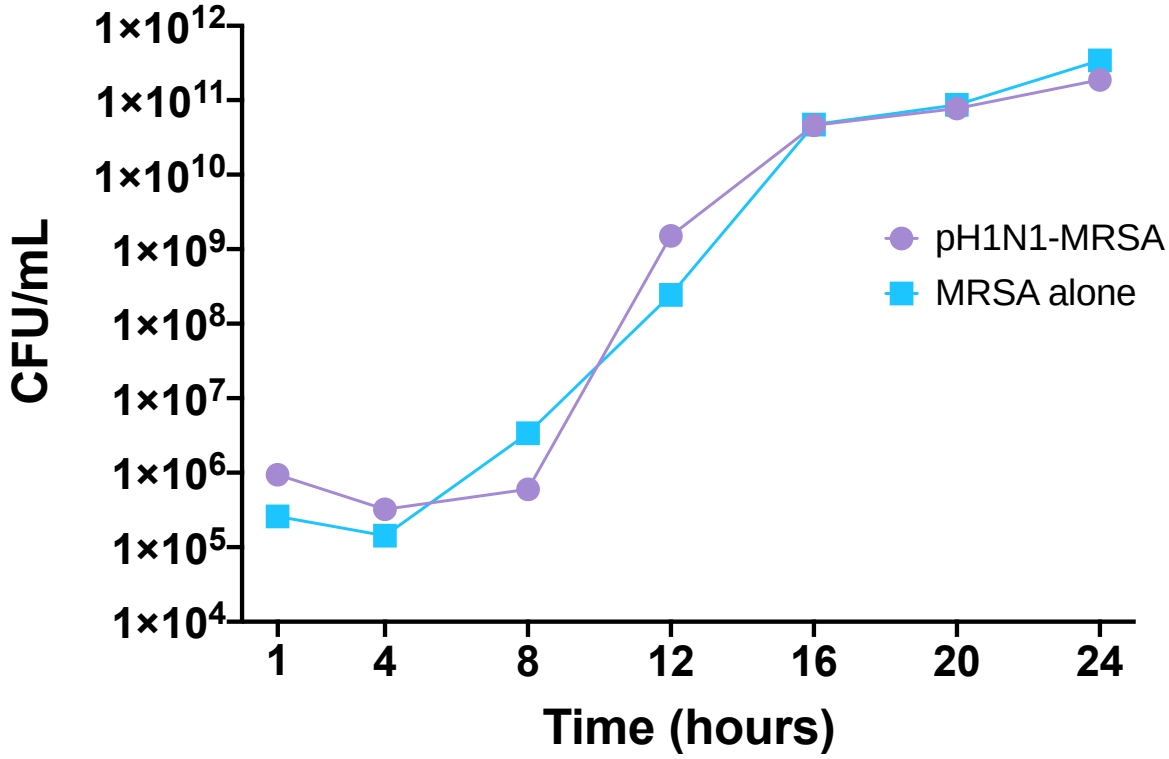

Figure 32: MRSA Replication Kinetics during MRSA Infection and pH1N1-MRSA Co-infection in a Co-culture Model of the Alveolar-Capillary Barrier.

Figure 32: MRSA Replication Kinetics during MRSA Infection and pH1N1-MRSA Co-infection in a Co-culture Model of the Alveolar-Capillary Barrier.

Primary human alveolar epithelial cells of the co-culture model were mock-infected or infected with pH1N1 at a MOI of 0.1. MRSA (MOI 0.1) was added 24 h later. Cells were selectively lysed at each of the indicated time points and CFU were quantified by standard bacterial plating. Error bars represent SEM calculated from three biological replicates (n = 3). Error bars for time points are not visible due to the y-axis. While statistically significant MRSA growth was observed over time (P = 0.0050), no significant differences were found between either infection condition (P = 0.3258) or between either infection condition over time (P > 0.6000).

capillary barrier. We employed RT-qPCR to examine differential modulation of MRSA virulence factor gene expression in the presence or absence of pre-existing influenza virus infection in a co-culture model. The alveolar pulmonary cells of our co-culture model of the alveolar-capillary barrier were infected with pH1N1 (MOI 0.1) or mock-infected and allowed to rest for 24 h prior to MRSA-infection at a MOI of 0.1 (n = 3). Cell lysates for both pulmonary epithelial and endothelial cells were collected at multiple time points post-infection. We once again chose to study 13 virulence factor genes directly related to adhesion and invasion: *coa*, *ebpS, eno, fnbA, fnbB, hla, hlgA, icaA, icaB, sbi, sek, seq*, and *spA*. At 1 h post-bacterial infection, each of the examined genes were upregulated in the presence of pH1N1, as compared with infection with MRSA-alone (Figure 33). However, only *eno* (P = 0.0120), *icaB* (P < 0.0001), *sek* (P = 0.0146), and *seq* (P = 0.0135) were significantly upregulated at 1 h. At 4 h post-MRSA infection, each of the 13 genes were upregulated in the presence of pH1N1 as compared with MRSA infection alone. However, only *coa* (P < 0.0001), *fnbB* (P < 0.0001), *hla* (P = 0.0014), *hlgA* (P < 0.0001), *icaA* (P < 0.0001), *icaB* (P < 0.0001), *sbi* (P < 0.0001), and *sek* (P < 0.0001) were significantly upregulated at 4 h. These data coincide with the initial stages of the exponential phase of MRSA at 4 h, suggesting that adhesion- and invasion-associated virulence factors may play a role in the beginning stages of MRSA infection in primary alveolar cells previously infected with pH1N1. No upregulation of our bacterial virulence factors was observed at any later time point. This mimicked our findings in A549 cells.

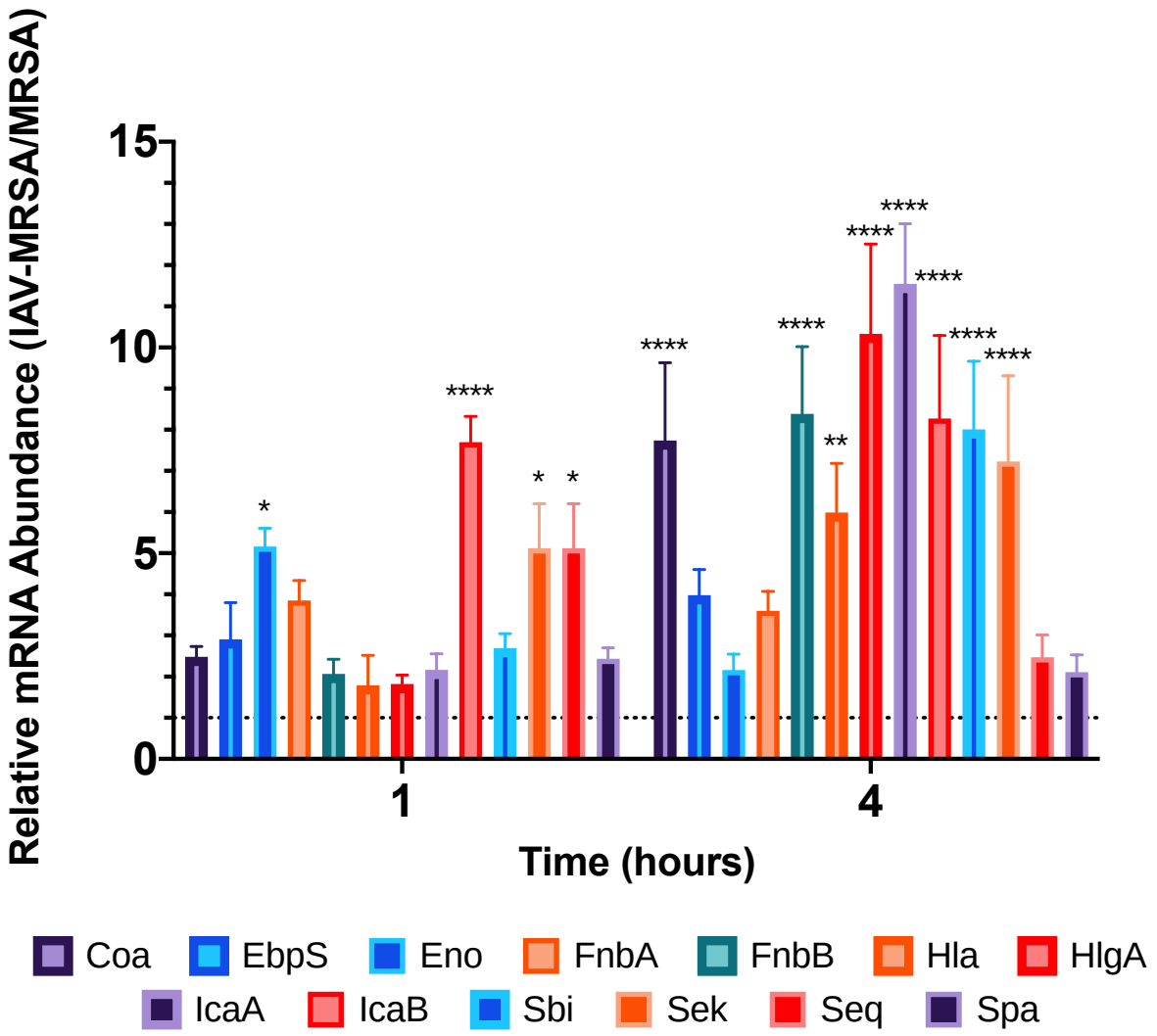

Figure 33: Modulation of MRSA Virulence Factors in a Model of the Alveolar-Capillary Barrier during pH1N1-MRSA Co-infection.

Figure 33: Modulation of MRSA Virulence Factors in a Model of the Alveolar-Capillary Barrier during pH1N1-MRSA Co-infection.

Primary alveolar epithelial cells of the co-culture model were mock-infected or infected with pH1N1 at a MOI of 0.1. MRSA (MOI 0.1) was added 24 h later. Cells were selectively lysed and RT-qPCR was employed to examine differential modulation of relative MRSA virulence factor mRNA abundance at 1 and 4 h. Error bars represent SEM calculated from three biological replicates ($n = 3$). Relative mRNA abundance fold changes represent pH1N1-MRSA vs MRSA infection alone and were calculated by the $2^{-\Delta\Delta CT}$ method. The time point, the virulence factor, and the interaction were each statistically significant ($P < 0.0001$ for all). At 1 h post-MRSA infection, *eno* ($P = 0.0120$), *icaB* ($P < 0.0001$), *sek* ($P = 0.0146$), and *seq* ($P = 0.0135$) were significantly upregulated in pH1N1-MRSA infected cells as compared with MRSA-alone. At 4 h post-MRSA infection, *coa* ($P < 0.0001$), *fnbB* ($P < 0.0001$), *hla* ($P = 0.0014$), *hlgA* ($P < 0.0001$), *icaA* ($P < 0.0001$), *icaB* ($P < 0.0001$), *sbi* ($P < 0.0001$), and *sek* ($P < 0.0001$) were significantly upregulated compared with MRSA-alone.

Barrier Integrity of a Co-culture Model of the Alveolar-Capillary Barrier during pH1N1-MRSA Co-infection

As our previous study in an epithelial alveolar cell line had suggested that MRSA-alone and IAV-MRSA infection resulted in epithelial cell barrier dysfunction, we sought to characterize the effect of pH1N1-MRSA co-infection on barrier integrity in our co-culture model by measuring temporal changes in resistance. The co-culture model was either mock-infected or infected with pH1N1 at a MOI of 0.1 (first arrow; designated as Time 0), allowed to rest for 24 h, and either mock-infected or infected with MRSA at a MOI of 0.1 (second arrow). The resistance values associated with our co-culture model were markedly lower than the values observed in our alveolar epithelial cells. This is likely due to the differences in primary cells as compared with an adenocarcinomic cell line, such as the shape and size of the cells, the structure of the cell membranes, and the intracellular components. Resistance values were determined from the three biological replicates with four technical replicates per biological replicate ($n = 3$). No change in resistance was observed following pH1N1-alone infection as compared with mock-infected cells, with the resistance of each of the observed conditions remaining steadily at 110 ohms (Figure 34). Following bacterial addition, infection with MRSA-alone resulted in no changes in resistance. No significant differences in barrier integrity were observed at any time point between models infected with MRSA-alone and pH1N1-alone. Samples co-infected with pH1N1-MRSA resulted in a steady decrease in resistance beginning at 4 h post-MRSA addition. At 90 h, pH1N1-MRSA was significantly downregulated ($P = 0.0005$) as compared with mock-infected. This decrease in barrier resistance coincided with the significant upregulation of virulence factor genes observed at 4 h post-bacterial infection.

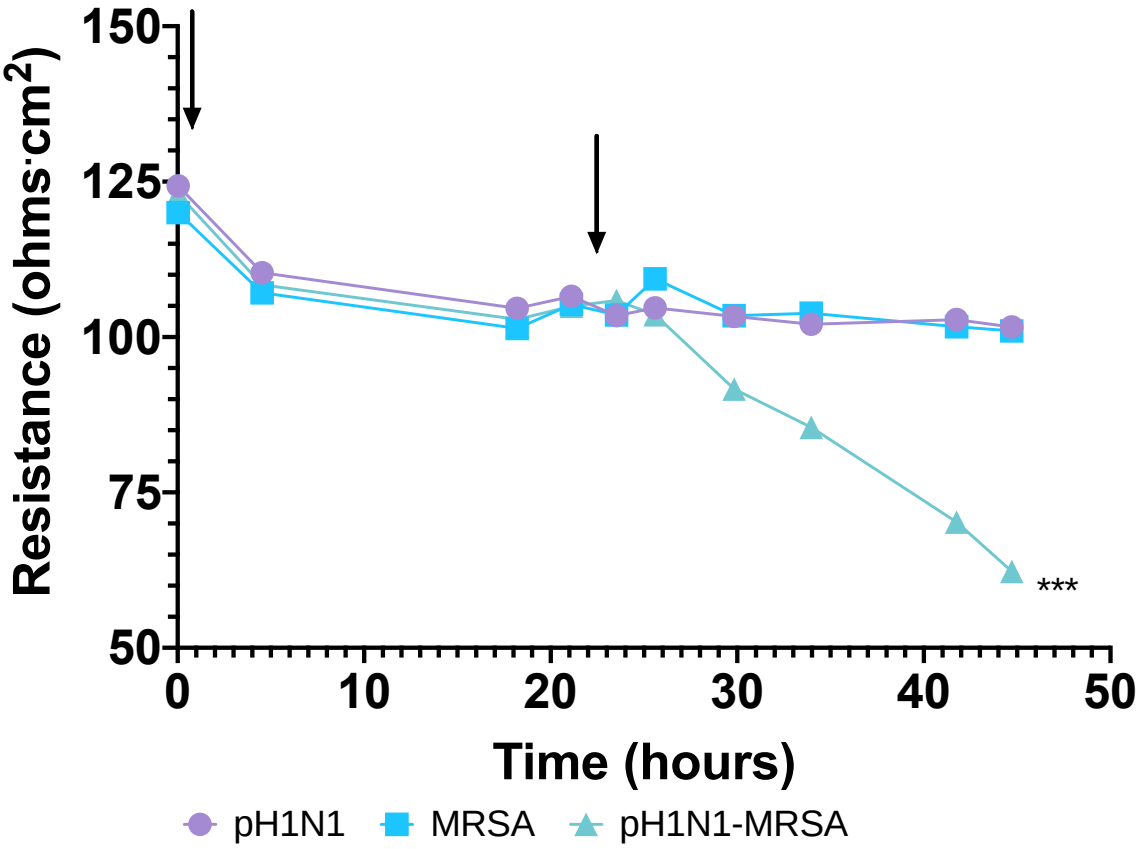

Figure 34: pH1N1-MRSA Co-infection Decreases Barrier Function in a Co-culture Model of the Alveolar-Capillary Barrier.

Figure 34: pH1N1-MRSA Co-infection Decreases Barrier Function in a Co-culture Model of the Alveolar-Capillary Barrier.

Median resistance values have been plotted for all data points obtained during the experiment. Error bars have been removed to allow for clear visualization of all data sets, but were consistent across all biological replicates. Primary human alveolar cells were mock-infected or infected with pH1N1 at a MOI of 0.1. MRSA (MOI 0.1) was added 24 h later. MRSA-alone and pH1N1-alone acted as controls and were also analyzed at the indicated time points. Resistance data represent the median of three biological replicates with three technical replicates per biological replicate ($n = 3$). Arrows designate the addition of pH1N1 (first arrow) and MRSA or triton (second arrow). Time, the infection condition, and the interaction between the two were each statistically significant ($P < 0.0001$ for all). At 0 h and 22 h (just prior to IAV infection and MRSA infection, respectively), no statistically significant differences were seen between any infection condition as compared with mock-infected cells. At 45 h, pH1N1-MRSA was significantly downregulated ($P = 0.0005$) as compared with mock-infected.

pH1N1-MRSA Co-infection May Decrease ZO-1 and ZO-2 Protein Levels in Microvascular Endothelial Cells

As our ECIS data demonstrated that a decrease in barrier integrity was seen when the co-culture model underwent pH1N1-MRSA co-infection, we next sought to characterize the expression of tight junctions in the underlying microvascular endothelial cells. Following co-infection, endothelial cells were collected at 4 and 24 h post-MRSA addition. Mock-, pH1N1-alone-, and MRSA-alone-infected cells were collected as controls. Protein lysates from each infection condition were separated on a 8% SDS-PAGE gel, followed by transfer to a PVDF membrane, and subsequently probed with ZO-1 and ZO-2 antibodies. β-tubulin acted as a loading control.

At 4 h, bands were not present for either ZO-1 or ZO-2 in any infection condition; β-tubulin was present in each of our four infection conditions. At 24 h, ZO-1 was present in pulmonary microvascular endothelial cells when mock-, pH1N1-, and MRSA-infected (Figure 35). As compared with our other infection conditions, ZO-1 levels were decreased in pulmonary endothelial cells co-infected with pH1N1-MRSA. At 24 h, ZO-2 appeared present in pH1N1- and MRSA-alone infected samples. While ZO-2 did not appear in pH1N1-MRSA infection at 24 h, bands were not seen in our mock-infection either. While this may indicate that pH1N1-MRSA co-infection results in a decrease in ZO-1 and ZO-2 as compared to infection with either pathogen alone, these results are inconclusive as protein did not appear in any of our 4 h samples. Further, ZO-2 did not appear in our mock-infected samples at 24 h either.

In an effort to further substantiate claims that the loss of barrier integrity observed in pH1N1-MRSA co-infection is a direct result of tight junction degradation, we attempted to obtain confocal images of ZO-1, ZO-2, and cadherin in both our alveolar epithelial and

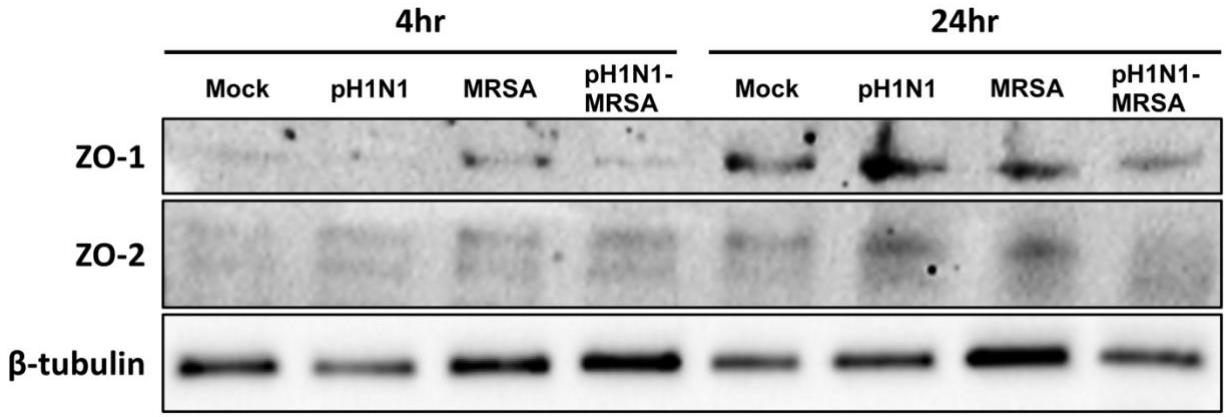

Figure 35: pH1N1-MRSA Co-infection May Decrease Tight Junction Proteins in Endothelial Cells of a Model of the Alveolar-Capillary Barrier.

Figure 35: pH1N1-MRSA Co-infection May Decrease Tight Junction Proteins in Endothelial Cells of a Model of the Alveolar-Capillary Barrier.

Primary human alveolar cells were mock-infected or infected with pH1N1 at a MOI of 0.1. MRSA (MOI 0.1) was added 24 h later. MRSA-alone, pH1N1-alone, and mock-infection acted as controls. Underlying human microvascular cells were collected at 4 and 24 h, resolved by electrophoresis, and transferred to PVDF membranes. Membranes were probed with anti-ZO-1, anti-ZO-2, and anti-β-tubulin. ZO-1 and ZO-2 levels appear to be decreased in pH1N1-MRSA infected samples, as compared with pH1N1-alone and MRSA-alone.

microvascular endothelial cells during co-infection. However, despite our efforts and acquiring assistance from several different avenues, we were not able to obtain images, leaving our results inconclusive.

Temporal Analysis of the Host Kinome Response in a Co-culture Model of the Alveolar-Capillary Barrier during pH1N1-MRSA Co-infection

As our temporal analysis of barrier integrity suggested that pH1N1-MRSA co-infection results in a more severe disease pathogenesis as compared with either pathogen alone, we next sought to address whether aberrant cell-mediated immune responses contribute to pH1N1-MRSA co-infection pathogenesis. We performed temporal kinome analysis of pH1N1-, MRSA-, and pH1N1-MRSA-infected alveolar epithelial and microvascular endothelial cells. We postulated that the activation state of host cell signaling responses or individual cellular kinases could provide insight into differential cellular responses found within co-infected cells as compared with IAV- or MRSA-alone. Time-matched mock-infected controls cells served as controls. Our co-culture model of the alveolar-capillary barrier was initially infected with pH1N1 (MOI 0.1) or mock-infected and rested for 24 h prior to bacterial infection. MRSA addition to MRSA-infected and pH1N1-MRSA co-infected cells was designated as Time 0. Epithelial and endothelial cells were harvested separately at 4, 8, 12, and 24 h post-MRSA infection. Both pH1N1-alone infected cells and mock-infected control cells were treated with MRSA-free infection inoculum at Time 0 to normalize cellular responses that may have been induced through the physical stress of the inoculum addition. Time-matched pH1N1-, MRSA-, and mock-infected control cells were collected throughout the duration of the experiment. Cell lysates were subsequently probed to quantitate host kinome responses by kinome peptide arrays

as described previously. Data from our arrays was analyzed using the PIIKA 2 software tool [311].

Hierarchical clustering analysis of the primary alveolar epithelial kinome data is presented in Figure 36. Datasets clustered into 2 major clusters, with the mock-infected 4 h time point clustering alone. The first cluster (denoted as A) consisted of 4 and 8 h post-bacterial infection of cells infected with MRSA-alone, along with pH1N1-alone infected cells at 4 h, and mock-infected cells at 8 and 12 h. The second major cluster (denoted as B) was comprised of all of the remaining samples, including mock-infected samples at 24 h, IAV-alone infected samples at 8, 12, and 24 h, MRSA-alone infected samples at 12 and 24 h post-bacterial infection, and pH1N1-MRSA co-infected samples at 4, 8, 12, and 24 h.

To gain further insight into the similarities and/or differences in the host kinome response of human pulmonary alveolar cells during pH1N1-MRSA co-infection as compared with infection with either pathogen alone, we performed biological subtraction of the time-matched mock-infected kinome datasets from their respective infected counterparts. Respective hierarchical clustering analysis of the kinome data following mock-infected background subtraction is presented in Figure 37. Notably, each of the time-matched samples from IAV-alone, MRSA-alone, and IAV-MRSA infected samples clustered together, resulting in four major clusters. From left to right, the first cluster (denoted as A) consisted of each of the 4 h time-matched samples, the second cluster (denoted as Cluster B) consisted of each of the 12 h time-matched samples, the third cluster (denoted as Cluster C) consisted of each of the 8 h time-matched samples, and the fourth cluster (denoted as Cluster D) consisted of each of the 24 h time-matched samples. Clusters B and C, consisting of the 8 and 12 h time points, respectively, clustered together more strongly than with the samples from 4 and 24 h post-MRSA infection.

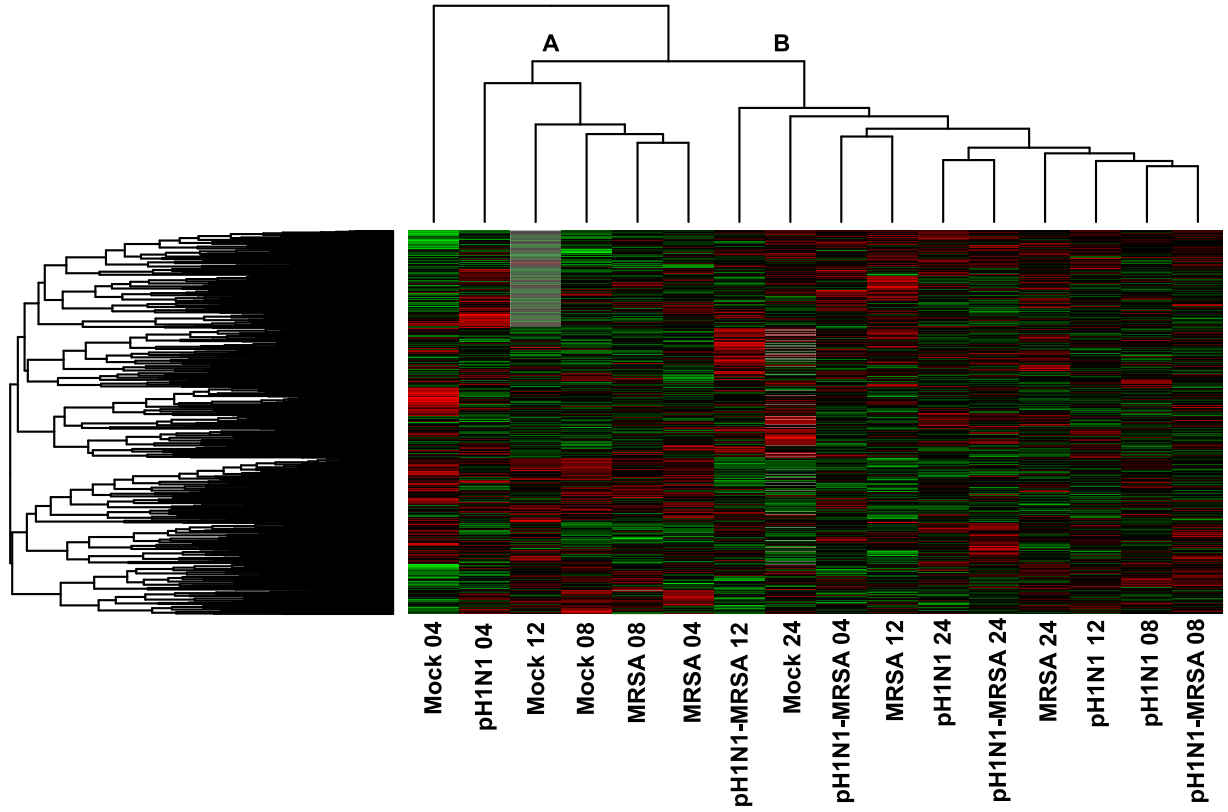

Figure 36: Hierarchical Clustering of Temporal Kinome Responses of pH1N1, MRSA, and pH1N1-MRSA Infection in Epithelial Cells of a Model of the Alveolar-Capillary Barrier.

Figure 36: Hierarchical Clustering of Temporal Kinome Responses of pH1N1, MRSA, and pH1N1-MRSA Infection in Epithelial Cells of a Model of the Alveolar-Capillary Barrier.

Primary human alveolar cells were mock-infected or infected with pH1N1 at a MOI of 0.1. MRSA (MOI 0.1) was added 24 h later. Cells were harvested for kinome analysis at 4, 8, 12, and 24 h. Controls included pH1N1-alone, MRSA-alone, and mock-infected time-matched samples. Cell lysates were probed to quantitate host kinome responses by kinome peptide arrays. Red indicates upregulation, while green indicates downregulation as compared with the background. A and B designate the two major dataset clusters as identified following hierarchical clustering.

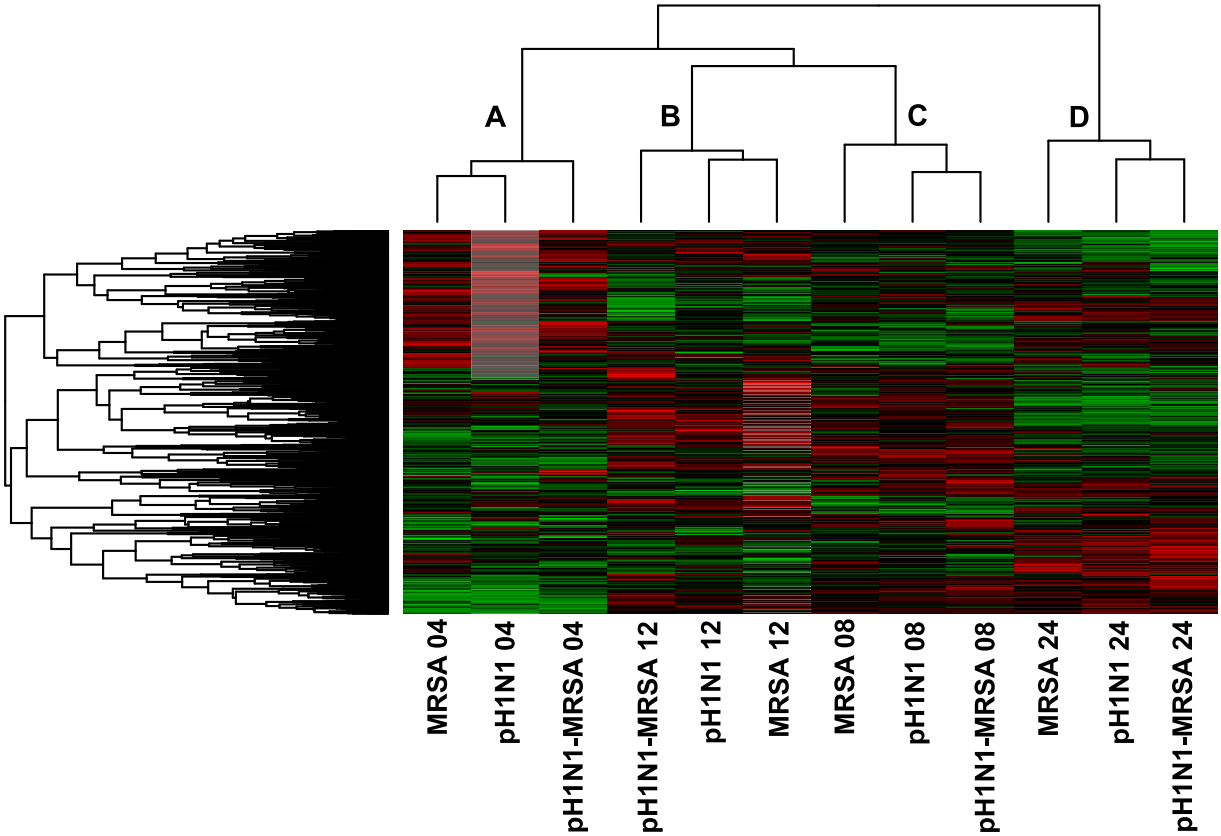

Figure 37: Background-subtracted Temporal Kinome Responses of pH1N1, MRSA, and pH1N1-MRSA Infection in Epithelial Cells of a Co-culture Model of the Alveolar-Capillary Barrier.

Figure 37: Background-subtracted Temporal Kinome Responses of pH1N1, MRSA, and pH1N1-MRSA Infection in Epithelial Cells of a Co-culture Model of the Alveolar-Capillary Barrier.

Mock-infected kinome responses were subtracted from time-matched infected samples in Figure 36. Fold change phosphorylation values are plotted for all kinase recognition sequences on the kinome peptide arrays. Clustering analysis was performed with the Heatmapper software suite. Red depicts upregulation, while green depicts downregulation as compared with the background. A-D designate the four major dataset clusters as identified following hierarchical clustering.

Moreover, the 24 h samples differentiated most strongly from each of the other time points. These data suggest that the modulation of the host kinome response is related strongly to post-infection time points, with intra-time point dependent differences in the host response to the infection conditions.

We next sought to identify host cell signaling responses or biological networks in the pH1N1-MRSA-infected pulmonary alveolar cells that were selectively modulated at 24 h post-MRSA infection. Kinome analysis at 24 h post-MRSA addition demonstrated that pH1N1-MRSA co-infection resulted in the activation of numerous signaling pathways as compared with either pH1N1- or MRSA-infection alone (Table 12). "Cytokine Signaling in Immune System" and "Signaling by Interleukins" had the largest number of associated proteins from our kinome arrays included in the analysis (56 and 44, respectively). Further, TLR pathways were not identified in pH1N1- or MRSA-alone datasets, while there was a unique over-representation of TLR signaling pathways and TLR-associated pathways during co-infection. Significant upregulation of cell cycle-, apoptosis-, and interferon-associated pathways was also associated with pH1N1-MRSA co-infection in alveolar epithelial cells. In contrast, MRSA infection alone resulted in relatively few upregulated pathways as compared with the mock-infected control, namely inflammasome- and NLR-associated signaling pathways (Table 13). Infection with pH1N1-alone resulted in upregulation of innate immune responses, including IFN signaling pathways and interleukin pathways, cell cycle- and apoptosis-associated pathways (Table 14). This data demonstrates that pH1N1-MRSA co-infection results in a unique cell response signature in primary differentiated alveolar epithelial cells grown in close proximity to pulmonary endothelial cells. This contrasts to kinome analysis in A549 cells where co-infection kinome responses largely overlapped with the pH1N1- and MRSA-alone conditions.

Table 12: Pathway Overrepresentation Analysis of Host Kinome Responses in Epithelial Cells of a Model of the Alveolar-Capillary Barrier in pH1N1-MRSA Infection (24 h post-MRSA Infection).

Pathway overrepresentation of primary alveolar epithelial cells co-infected with pH1N1-MRSA at 24 h post- infection. Cytokine Signaling in Immune System and Signaling by Interleukins were both strongly overrepresented. Pathways related to apoptosis, cell cycle, and TLRs were also overrepresented.

Signaling Pathway	**Uploaded Protein Count**	**Pathway Upregulated P-Value**
Estrogen responsive protein efp controls cell cycle and breast tumors growth	4	1.78E-04
Cyclin A/B1 associated events during G2/M transition	5	4.35E-04
G1/S Transition	6	8.50E-04
Cyclins and cell cycle regulation	7	0.001452
Mitotic G1-G1/S phases	8	0.002268
G2/M Checkpoints	3	0.003969
G2/M Transition	10	0.004632
Mitotic G2-G2/M phases	10	0.004632
Cell Cycle Checkpoints	4	0.007759
Cyclin A:Cdk2-associated events at S phase entry	4	0.007759
Cyclin E associated events during G1/S transition	4	0.007759
D4gdi signaling pathway	4	0.007759
ERK1 activation	4	0.007759
G0 and Early G1	4	0.007759
IRAK1 recruits IKK complex	4	0.007759
IRAK1 recruits IKK complex upon TLR7/8 or 9 stimulation	4	0.007759
Internal ribosome entry pathway	4	0.007759
Regulation of cell cycle progression by plk3	4	0.007759
p53 signaling pathway	12	0.008093
Cytokine Signaling in Immune system	56	0.012262
E2F transcription factor network	5	0.012642
Interferon alpha/beta signaling	5	0.012642
S Phase	5	0.012642
Signaling by Interleukins	44	0.018475
Degradation of the extracellular matrix	6	0.018538
ERK activation	6	0.018538
TRAF6 mediated IRF7 activation	6	0.018538

p73 transcription factor network	6	0.018538
Cell cycle	16	0.018709
IFN-gamma pathway	17	0.022178
Caspase cascade in apoptosis	7	0.025372
Cell death signalling via NRAGE, NRIF and NADE	7	0.025372
Amyotrophic lateral sclerosis (ALS)	8	0.033073
FOXM1 transcription factor network	8	0.033073
Retinoic acid receptors-mediated signaling	8	0.033073
MyD88 cascade initiated on plasma membrane	35	0.035765
Toll Like Receptor 10 (TLR10) Cascade	35	0.035765
Toll Like Receptor 5 (TLR5) Cascade	35	0.035765
MyD88 dependent cascade initiated on endosome	36	0.039263
TRAF6 mediated induction of NFkB and MAP kinases upon TLR7/8 or 9 activation	36	0.039263
Toll Like Receptor 7/8 (TLR7/8) Cascade	36	0.039263
Cell cycle: g1/s check point	9	0.041573
RAF/MAP kinase cascade	9	0.041573
AndrogenReceptor	37	0.042958
MyD88:Mal cascade initiated on plasma membrane	37	0.042958
Toll Like Receptor 2 (TLR2) Cascade	37	0.042958
Toll Like Receptor 9 (TLR9) Cascade	37	0.042958
Toll Like Receptor TLR1:TLR2 Cascade	37	0.042958
Toll Like Receptor TLR6:TLR2 Cascade	37	0.042958
Cell Cycle	22	0.044538
Cell Cycle, Mitotic	22	0.044538
Interferon gamma signaling	10	0.050809
NOD1/2 Signaling Pathway	10	0.050809
Signalling to p38 via RIT and RIN	10	0.050809
p75 NTR receptor-mediated signalling	10	0.050809
ARMS-mediated activation	11	0.060718
Factors involved in megakaryocyte development and platelet production	11	0.060718
GRB2 events in EGFR signaling	11	0.060718
GRB2 events in ERBB2 signaling	11	0.060718
SHC1 events in ERBB4 signaling	11	0.060718
SOS-mediated signalling	11	0.060718
p75(NTR)-mediated signaling	11	0.060718
Activated TLR4 signalling	42	0.064408
MAP kinase activation in TLR cascade	26	0.068308
Toll Like Receptor 4 (TLR4) Cascade	43	0.069293
SHC-mediated signalling	12	0.071243
SHC-related events triggered by IGF1R	12	0.071243
SHC1 events in EGFR signaling	12	0.071243
SHC1 events in ERBB2 signaling	12	0.071243
Oncostatin_M	27	0.075024

Extracellular matrix organization	13	0.082329
FRS2-mediated cascade	13	0.082329
Frs2-mediated activation	13	0.082329
Interleukin-1 signaling	13	0.082329
RIG-I/MDA5 mediated induction of IFN-alpha/beta pathways	13	0.082329
Signaling by Leptin	13	0.082329
Interferon Signaling	14	0.093924
NCAM signaling for neurite out-growth	14	0.093924
Nucleotide-binding domain, leucine rich repeat containing receptor (NLR) signaling pathways	14	0.093924
Prolonged ERK activation events	14	0.093924
SHC-related events	14	0.093924
VEGFR2 mediated cell proliferation	14	0.093924

Table 13: Pathway Overrepresentation Analysis of Host Kinome Responses in Epithelial Cells of a Model of the Alveolar-Capillary Barrier in MRSA Infection (24 h post-MRSA Infection).

Pathway overrepresentation of alveolar epithelial cells infected with MRSA at 24 h post-infection. Compared with pH1N1-MRSA co-infected cells, pathways related to apoptosis and cell cycle were markedly absent. Further, the number of overrepresented pathways was significantly lower compared with co-infected cells.

Signaling Pathway	**Uploaded Protein Count**	**Pathway Upregulated P-Value**
Regulation of Insulin-like Growth Factor (IGF) transport and uptake by Insulin-like Growth Factor Binding Proteins (IGFBPs)	4	1.59E-04
Metabolism of proteins	20	0.004914
IGF1 signaling pathway	22	0.005958
Interleukin-1 processing	3	0.018828
PERK regulates gene expression	3	0.018828
D4gdi signaling pathway	4	0.025051
Internal ribosome entry pathway	4	0.025051
Cellular roles of Anthrax toxin	5	0.031248
Inflammasomes	5	0.031248
The NLRP3 inflammasome	5	0.031248
Cytosolic DNA-sensing pathway	6	0.037418
Unfolded Protein Response (UPR)	6	0.037418
Caspase cascade in apoptosis	7	0.043562
FOXA2 and FOXA3 transcription factor networks	7	0.043562
Amyotrophic lateral sclerosis (ALS)	8	0.04968
NOD1/2 Signaling Pathway	10	0.061838
Direct p53 effectors	11	0.067877
Nucleotide-binding domain, leucine rich repeat containing receptor (NLR) signaling pathways	14	0.085841

Table 14: Pathway Overrepresentation Analysis of Host Kinome Responses in Epithelial Cells of a Model of the Alveolar-Capillary Barrier in pH1N1 Infection (24 h post-MRSA Infection).

Pathway overrepresentation of alveolar epithelial cells infected with pH1N1-alone at 24 h. Infection with pH1N1-alone resulted in the overrepresentation of pathways related to the innate immune response. Pathways related to apoptosis and cell cycle were also overrepresented, similar to pH1N1-MRSA co-infection in primary alveolar epithelial cells.

Signaling Pathway	**Uploaded Protein Count**	**Pathway Upregulated P-Value**
IFN-gamma pathway	17	4.66E-04
D4gdi signaling pathway	4	0.003405
Internal ribosome entry pathway	4	0.003405
Cytokine Signaling in Immune system	56	0.007846
Caspase cascade in apoptosis	7	0.011422
Amyotrophic lateral sclerosis (ALS)	8	0.015016
Signaling by FGFR1 mutants	9	0.019035
Oncostatin_M	27	0.025447
Factors involved in megakaryocyte development and platelet production	11	0.02827
Pathways in cancer	77	0.030483
Glucocorticoid receptor regulatory network	12	0.033448
p53 signaling pathway	12	0.033448
Interferon Signaling	14	0.044833
Signaling by FGFR mutants	15	0.051006
EPO signaling pathway	17	0.064226
Inhibition of cellular proliferation by gleevec	17	0.064226
Immune System	161	0.068943
IL2-mediated signaling events	18	0.071243
IL6-mediated signaling events	18	0.071243
Alternative complement pathway	3	0.073891
Apoptotic signaling in response to dna damage	3	0.073891
Caspase-mediated cleavage of cytoskeletal proteins	3	0.073891
Classical complement pathway	3	0.073891
G1/S DNA Damage Checkpoints	3	0.073891
G2/M Checkpoints	3	0.073891
Granzyme a mediated apoptosis pathway	3	0.073891
IFN gamma signaling	3	0.073891

Ifn gamma signaling pathway	3	0.073891
Interleukin-1 processing	3	0.073891
Lectin induced complement pathway	3	0.073891
PERK regulates gene expression	3	0.073891
Regulation of Apoptosis	3	0.073891
Terminal pathway of complement	3	0.073891
The information processing pathway at the ifn beta enhancer	3	0.073891
BCR	70	0.084334
Amoebiasis	20	0.086013
GPCR signaling	20	0.086013
IL2	44	0.0898
Signaling by Interleukins	44	0.0898
Antiviral mechanism by IFN-stimulated genes	4	0.097386
Cell Cycle Checkpoints	4	0.097386
Complement cascade	4	0.097386
Cyclin A:Cdk2-associated events at S phase entry	4	0.097386
Cyclin E associated events during G1/S transition	4	0.097386
Estrogen responsive protein efp controls cell cycle and breast tumors growth	4	0.097386
G0 and Early G1	4	0.097386
IFN alpha signaling	4	0.097386
IRAK1 recruits IKK complex	4	0.097386
ISG15 antiviral mechanism	4	0.097386
Ifn alpha signaling pathway	4	0.097386
P53 signaling pathway	4	0.097386
Pyruvate metabolism	4	0.097386
Regulation of Complement cascade	4	0.097386
Regulation of Insulin-like Growth Factor (IGF) transport and uptake by Insulin-like Growth Factor Binding Proteins (IGFBPs)	4	0.097386
Regulation of cell cycle progression by plk3	4	0.097386
SHC-mediated cascade	4	0.097386
Stress induction of hsp regulation	4	0.097386
Systemic lupus erythematosus	4	0.097386

Primary pulmonary endothelial cells at the alveolar-capillary barrier were also isolated throughout the course of infection for kinome analysis. Hierarchical clustering analysis of the primary pulmonary endothelial data resulted in three major clusters, with samples infected with IAV-alone at 4 h clustering alone (Figure 38). From left to right, the first cluster (denoted as A) consisted of MRSA-alone and IAV-MRSA-infected samples at 24 h. The second cluster (denoted as B) was comprised of mock-infected samples at 4 h, samples infected with IAV-alone at 8 h, samples infected with MRSA-alone at 4, 8, and 24 h, and IAV-MRSA co-infected samples at 4 h post-MRSA infection. The third cluster (denoted as C) consisted of mock-infected samples at 8 and 12 h post-infection, IAV-alone infected samples at 12 and 24 h post-infection, MRSA-alone infected samples at 12 h post-bacterial infection, and IAV-MRSA infected samples at 8 and 12 h post-MRSA infection.

Biological subtraction of time-matched mock-infected kinome datasets from their respective infected counterparts was performed, to gain further insight into the similarities and/or differences in the host kinome response of primary microvascular endothelial cells during pH1N1-MRSA co-infection (Figure 39). Once again, similar to the kinome response of epithelial cells, biological subtraction revealed four major clusters matched by time point. From left to right, the 8 h time points of pH1N1-alone, MRSA-alone, and pH1N1-MRSA infected samples clustered together (denoted as A). The second cluster consisted of pH1N1-alone, MRSA-alone, and pH1N1-MRSA infected samples at 12 h post-bacterial infection (denoted as B). The third cluster was comprised of the 24 h time points of IAV-alone, MRSA-alone, and IAV-MRSA infected samples (denoted as C). Lastly, samples infected with IAV-alone, MRSA-alone, and IAV-MRSA at 4 h post-bacterial infection clustered together (denoted as D). A and B clustered together; C and D also clustered together. These data suggest that the modulation of the host

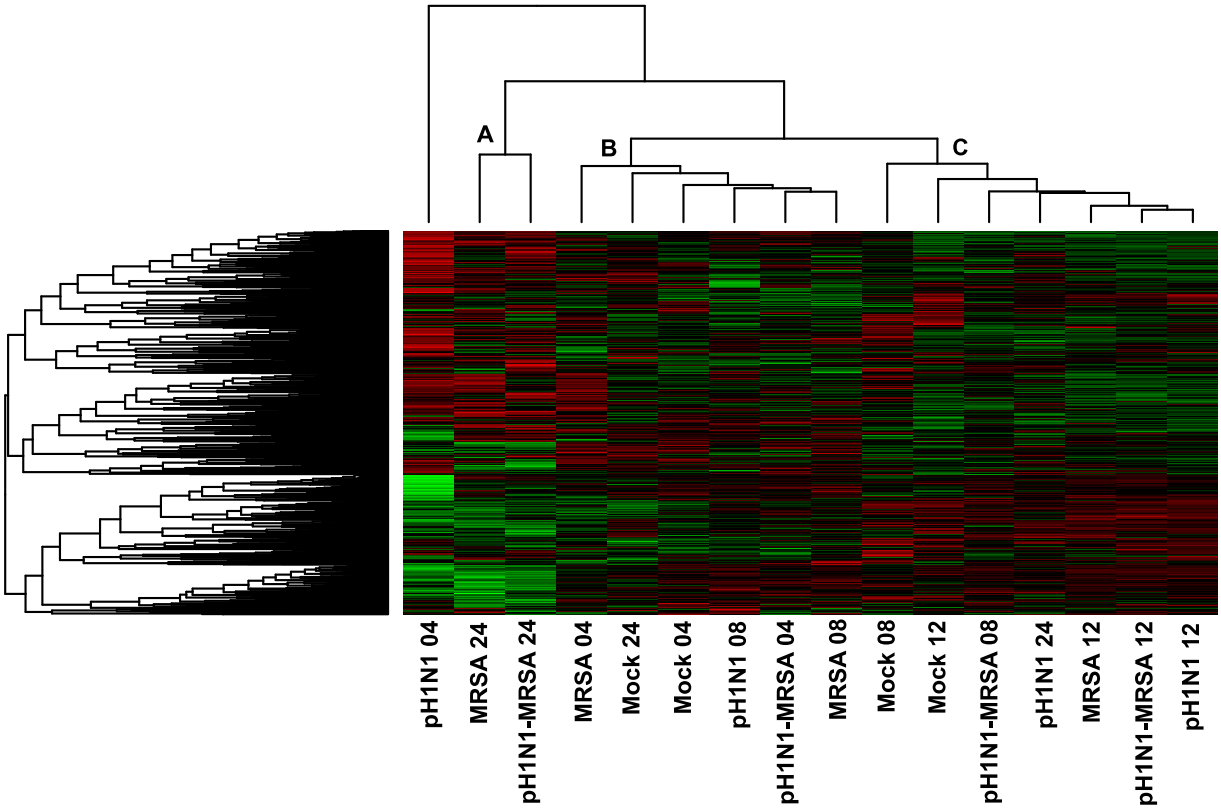

Figure 38: Hierarchical Clustering of Temporal Kinome Responses of pH1N1, MRSA, and pH1N1-MRSA Infection in Endothelial Cells of a Model of the Alveolar-Capillary Barrier.

Figure 38: Hierarchical Clustering of Temporal Kinome Responses of pH1N1, MRSA, and pH1N1-MRSA Infection in Endothelial Cells of a Model of the Alveolar-Capillary Barrier.

Primary human alveolar cells were mock-infected or infected with pH1N1 at a MOI of 0.1. MRSA (MOI 0.1) was added 24 h later. Underlying microvascular endothelial cells were harvested for kinome analysis at 4, 8, 12, and 24 h. Controls included pH1N1-alone, MRSA-alone, and mock-infected time-matched samples. Cell lysates were probed to quantitate host kinome responses by kinome peptide arrays. Red indicates upregulation, while green indicates downregulation as compared with the background. A-C designate the three major dataset clusters as identified following hierarchical clustering.

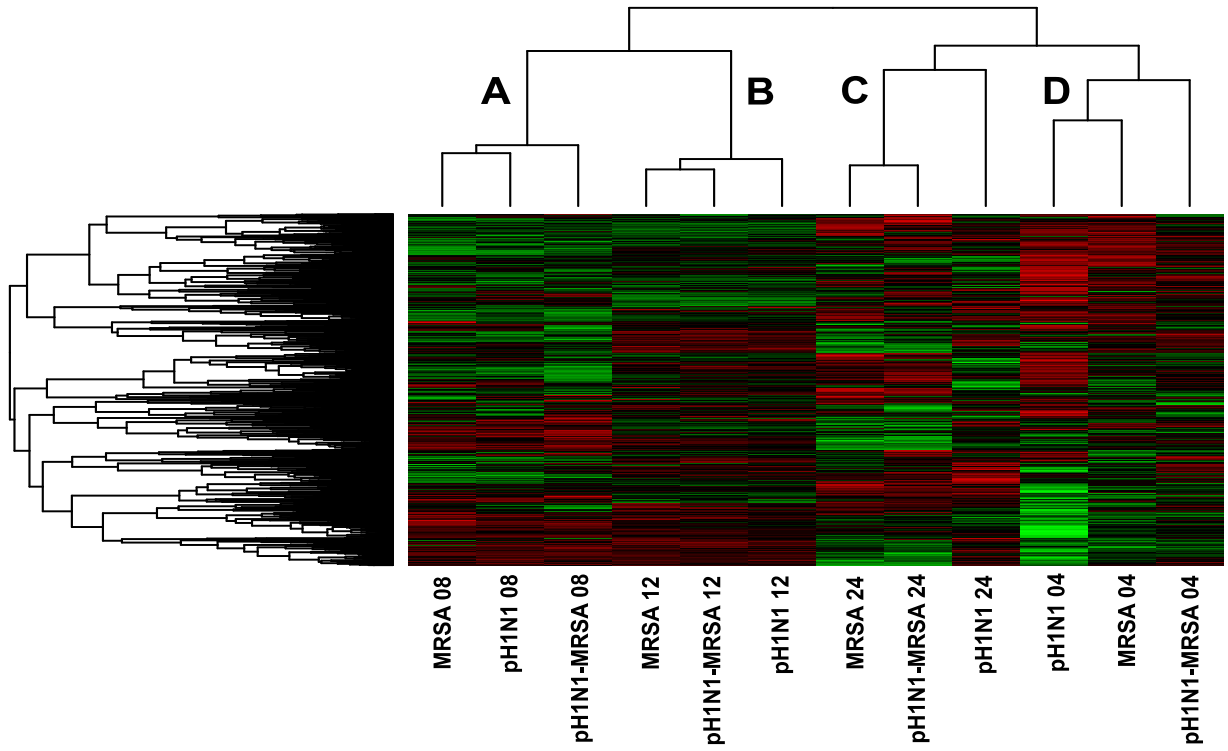

Figure 39: Background-subtracted Temporal Kinome Responses of pH1N1, MRSA, and pH1N1-MRSA Infection in Endothelial Cells of a Model of the Alveolar-Capillary Barrier.

Figure 39: Background-subtracted Temporal Kinome Responses of pH1N1, MRSA, and pH1N1-MRSA Infection in Endothelial Cells of a Model of the Alveolar-Capillary Barrier.

Mock-infected kinome responses were subtracted from time-matched infected samples in Figure 38. Fold change phosphorylation values are plotted for all kinase recognition sequences on the kinome peptide arrays. Clustering analysis was performed with the Heatmapper software suite. Red depicts upregulation, while green depicts downregulation as compared with the background. A-D designate the four major dataset clusters as identified following hierarchical clustering.

kinome response is related strongly to post-infection time, mimicking that seen in the epithelial cells of the co-culture model.

Relatively few signaling pathways were differentially modulated in the endothelial cells during pH1N1-alone infection, JAK/STAT signaling being the most noteworthy pathway identified at 24 h (Table 15). MRSA-alone infection showed notable upregulation of hedgehog- and Wnt/β-catenin-associated signaling pathways as compared with time-matched mock-infected controls (Table 16). In contrast, signaling pathways related to cellular stress responses, TLR signaling, mitogen-activated protein kinase (MAPK) responses, and vascular endothelial growth factor (VEGF)-3 were upregulated in pH1N1-MRSA co-infection (Table 17). This data suggests that co-infection results in the differential modulation of host responses within alveolar epithelial cells which then results in downstream modulation of associated pulmonary endothelial cells at the alveolar-capillary barrier. Given that our TEER data demonstrated that co-infection of our model of the alveolar-capillary barrier resulted in increased permeability, our kinome data provides the identities of specific signaling pathways and cellular responses (e.g. interferons, interleukins) that are selectively modulated during pH1N1-MRSA co-infection and modulate barrier permeability.

Cytokine Expression is Modulated during pH1N1-MRSA Co-infection in a Co-culture Model of the Alveolar-Capillary Barrier

As our kinome data had revealed that host cell signaling in pH1N1-MRSA co-infection is highly distinct as compared with that seen in pH1N1-alone or MRSA-alone infection, we next sought to characterize the expression of pro-inflammatory cytokines by pH1N1-, MRSA-, and pH1N1-MRSA infected cells. Supernatants were collected at 4, 8, 12, and 24 h post-MRSA addition

Table 15: Pathway Overrepresentation Analysis of Host Kinome Responses in Endothelial Cells of a Model of the Alveolar-Capillary Barrier in pH1N1 Infection (24 h post-MRSA Infection).

Pathway overrepresentation of microvascular endothelial cells infected with pH1N1-alone at 24 h. Few pathways were overrepresented with JAK/STAT signaling being the most noteworthy.

Signaling Pathway	**Uploaded Protein Count**	**Pathway Upregulated P-Value**
Pyruvate metabolism	4	0.007759
IL23-mediated signaling events	11	0.060718
Pyruvate metabolism and Citric Acid (TCA) cycle	11	0.060718
JAK/STAT signaling pathway	27	0.075024
The citric acid (TCA) cycle and respiratory electron transport	13	0.082329

Table 16: Pathway Overrepresentation Analysis of Host Kinome Responses in Endothelial Cells of a Model of the Alveolar-Capillary Barrier in MRSA Infection (24 h post-MRSA Infection).

Pathway overrepresentation of primary microvascular endothelial cells infected with MRSA-alone at 24 h. The most notable pathways included those related to the Hedgehog and Wnt/ β-catenin signaling pathways.

Signaling Pathway	**Uploaded Protein Count**	**Pathway Upregulated P-Value**
Hedgehog signaling pathway	6	1.78E-04
Hedgehog 'off' state	4	8.70E-04
Signaling by Hedgehog	4	8.70E-04
Degradation of GLI2 by the proteasome	3	0.011089
GLI3 is processed to GLI3R by the proteasome	3	0.011089
Metabolism of lipids and lipoproteins	3	0.011089
PKA-mediated phosphorylation of CREB	3	0.011089
Transcription regulation by methyltransferase of carm1	3	0.011089
Beta-catenin phosphorylation cascade	4	0.021308
CREB phosphorylation through the activation of CaMKII	4	0.021308
CRMPs in Sema3A signaling	4	0.021308
GPCR Dopamine D1like receptor signaling pathway	4	0.021308
Metabolism	4	0.021308
Presenilin action in Notch and Wnt signaling	12	0.033806
Repression of pain sensation by the transcriptional regulator dream	5	0.034124
Vasopressin-regulated water reabsorption	5	0.034124
AMER1 mutants destabilize the destruction complex	6	0.049193
APC truncation mutants are not K63 polyubiquitinated	6	0.049193
APC truncation mutants have impaired AXIN binding	6	0.049193
AXIN missense mutants destabilize the destruction complex	6	0.049193
AXIN mutants destabilize the destruction complex, activating WNT signaling	6	0.049193
Ca-calmodulin-dependent protein kinase activation	6	0.049193
Degradation of beta-catenin by the destruction complex	6	0.049193
S33 mutants of beta-catenin aren't phosphorylated	6	0.049193
S37 mutants of beta-catenin aren't phosphorylated	6	0.049193

S45 mutants of beta-catenin aren't phosphorylated	6	0.049193
Stathmin and breast cancer resistance to antimicrotubule agents	6	0.049193
T41 mutants of beta-catenin aren't phosphorylated	6	0.049193
TCF7L2 mutants don't bind CTBP	6	0.049193
Deletions in the AMER1 gene destabilize the destruction complex	6	0.049193
Deletions in the AXIN genes in hepatocellular carcinoma result in elevated WNT signaling	6	0.049193
Misspliced GSK3beta mutants stabilize beta-catenin	6	0.049193
Phosphorylation site mutants of CTNNB1 are not targeted to the proteasome by the destruction complex	6	0.049193
Truncated APC mutants destabilize the destruction complex	6	0.049193
Truncations of AMER1 destabilize the destruction complex	6	0.049193
RNF mutants show enhanced WNT signaling and proliferation	14	0.051314
Signaling by WNT in cancer	14	0.051314
TCF dependent signaling in response to WNT	14	0.051314
XAV939 inhibits tankyrase, stabilizing AXIN	14	0.051314
Misspliced LRP5 mutants have enhanced beta-catenin-dependent signaling	14	0.051314
Disassembly of the destruction complex and recruitment of AXIN to the membrane	7	0.066198
Wnt signaling pathway	26	0.072268
Noncanonical Wnt signaling pathway	8	0.084852
Wnt signaling pathway	8	0.084852

Table 17: Pathway Overrepresentation Analysis of Host Kinome Responses in Endothelial Cells of a Model of the Alveolar-Capillary Barrier in pH1N1-MRSA Infection (24 h post-MRSA Infection).

Pathway overrepresentation of primary microvascular endothelial cells co-infected with pH1N1-MRSA at 24 h. Many pathways overlapped with those seen in pH1N1-alone, including those related to Hedgehog and Wnt/β-catenin signaling. Pathways related to MAPK and VEGF-3 signaling were overrepresented only in co-infected cells.

Signaling Pathway	**Uploaded Protein Count**	**Pathway Upregulated P-Value**
Hedgehog 'off' state	4	7.05E-04
Signaling by Hedgehog	4	7.05E-04
Hedgehog signaling pathway	6	0.003249
Class I MHC mediated antigen processing & presentation	8	0.008394
Degradation of GLI2 by the proteasome	3	0.009664
GLI3 is processed to GLI3R by the proteasome	3	0.009664
Transcription factor creb and its extracellular signals	17	0.013452
Cellular responses to stress	36	0.013505
VEGFR3 signaling in lymphatic endothelium	10	0.016598
Antigen processing-Cross presentation	4	0.018624
Beta-catenin phosphorylation cascade	4	0.018624
Circadian Clock	11	0.021926
Factors involved in megakaryocyte development and platelet production	11	0.021926
CREB phosphorylation	5	0.029912
Tnfr1 signaling pathway	5	0.029912
Role of Calcineurin-dependent NFAT signaling in lymphocytes	13	0.035082
Signaling by Wnt	23	0.039044
MAPK targets/ Nuclear events mediated by MAP kinases	14	0.042903
P38 mapk signaling pathway	14	0.042903
RNF mutants show enhanced WNT signaling and proliferation	14	0.042903
Signaling by WNT in cancer	14	0.042903
TCF dependent signaling in response to WNT	14	0.042903
XAV939 inhibits tankyrase, stabilizing AXIN	14	0.042903
Misspliced LRP5 mutants have enhanced beta-catenin-dependent signaling	14	0.042903
AMER1 mutants destabilize the destruction complex	6	0.043243

APC truncation mutants are not K63 polyubiquitinated	6	0.043243
APC truncation mutants have impaired AXIN binding	6	0.043243
AXIN missense mutants destabilize the destruction complex	6	0.043243
AXIN mutants destabilize the destruction complex, activating WNT signaling	6	0.043243
Degradation of beta-catenin by the destruction complex	6	0.043243
Degradation of the extracellular matrix	6	0.043243
S33 mutants of beta-catenin aren't phosphorylated	6	0.043243
S37 mutants of beta-catenin aren't phosphorylated	6	0.043243
S45 mutants of beta-catenin aren't phosphorylated	6	0.043243
Stathmin and breast cancer resistance to antimicrotubule agents	6	0.043243
T41 mutants of beta-catenin aren't phosphorylated	6	0.043243
TCF7L2 mutants don't bind CTBP	6	0.043243
Deletions in the AMER1 gene destabilize the destruction complex	6	0.043243
Deletions in the AXIN genes in hepatocellular carcinoma result in elevated WNT signaling	6	0.043243
Misspliced GSK3beta mutants stabilize beta-catenin	6	
Phosphorylation site mutants of CTNNB1 are not targeted to the proteasome by the destruction complex	6	
Truncated APC mutants destabilize the destruction complex	6	0.043243
Truncations of AMER1 destabilize the destruction complex	6	0.043243
Signaling mediated by p38-alpha and p38-beta	15	0.051533
MAP kinase activation in TLR cascade	26	0.05824
Wnt signaling pathway	26	0.05824
Fas signaling pathway	7	0.058356
Disassembly of the destruction complex and recruitment of AXIN to the membrane	7	0.058356
RAC1 signaling pathway	17	0.071129
Amyotrophic lateral sclerosis (ALS)	8	0.075009
ERK/MAPK targets	8	0.075009
Fas signaling pathway (cd95)	8	0.075009
Noncanonical Wnt signaling pathway	8	0.075009
Recycling pathway of L1	8	0.075009
ErbB signaling pathway	42	0.089179
Antigen processing and presentation	9	0.092985
Regulation of Androgen receptor activity	9	0.092985
RhoA signaling pathway	9	0.092985
MAPK signaling pathway	69	0.09367

and cytokine concentration measured using a MilliPlex Human Cytokine/Chemokine Magnetic Bead Panel MAP kit for each condition at 4, 8, 12, and 24 h. We screened for 15 cytokines based on previous observations from the literature, though measurable responses were only observed for 7: epidermal growth factor (EGF), fibroblast growth factor 2 (FGF-2), IL-6, IL-8, interferon gamma-induced protein 10 (IP-10/CXCL10), monocyte chemoattractant protein-1 (MCP-1/CCL2), and VEGF.

As seen in Figure 40A, time ($P = 0.0039$) and the infection condition ($P < 0.0001$) were each statistically significant when measuring EGF secretion; however the interaction between the two was not ($P = 0.5492$). There was a trend towards EGF repression in pH1N1-alone and pH1N1-MRSA infection at 4, 8, 12, and 24 h as compared with mock-infected samples. Nevertheless, significant downregulation was only observed at 12 h in pH1N1-alone ($P = 0.0003$) and pH1N1-MRSA ($P = 0.0002$) infection and was resolved by 24 h. Conversely, EGF expression in MRSA-alone infection was similar to expression in mock-infected samples at 4, 8, and 24 h; however, EGF was repressed at 12 h in MRSA-alone infection as compared with mock-infection. This suggests that while the presence of pH1N1 affects EGF expression, the presence of MRSA-alone does not result in modulation.

When measuring FGF-2 expression (Figure 40B), time ($P < 0.0001$), the infection condition ($P < 0.0001$), and the interaction between the two ($P = 0.0009$) were each statistically significant. At 4 h, significant upregulation was observed in pH1N1- alone infection ($P = 0.0053$). At 8 h, MRSA-alone was significantly repressed ($P = 0.0001$). At 12 h, pH1N1-alone ($P = 0.0035$) and pH1N1-MRSA ($P = 0.0140$) were both significantly upregulated. At 24 h, pH1N1-alone ($P = 0.0008$) and pH1N1-MRSA ($P = 0.0002$) were both upregulated as compared with mock-infection.

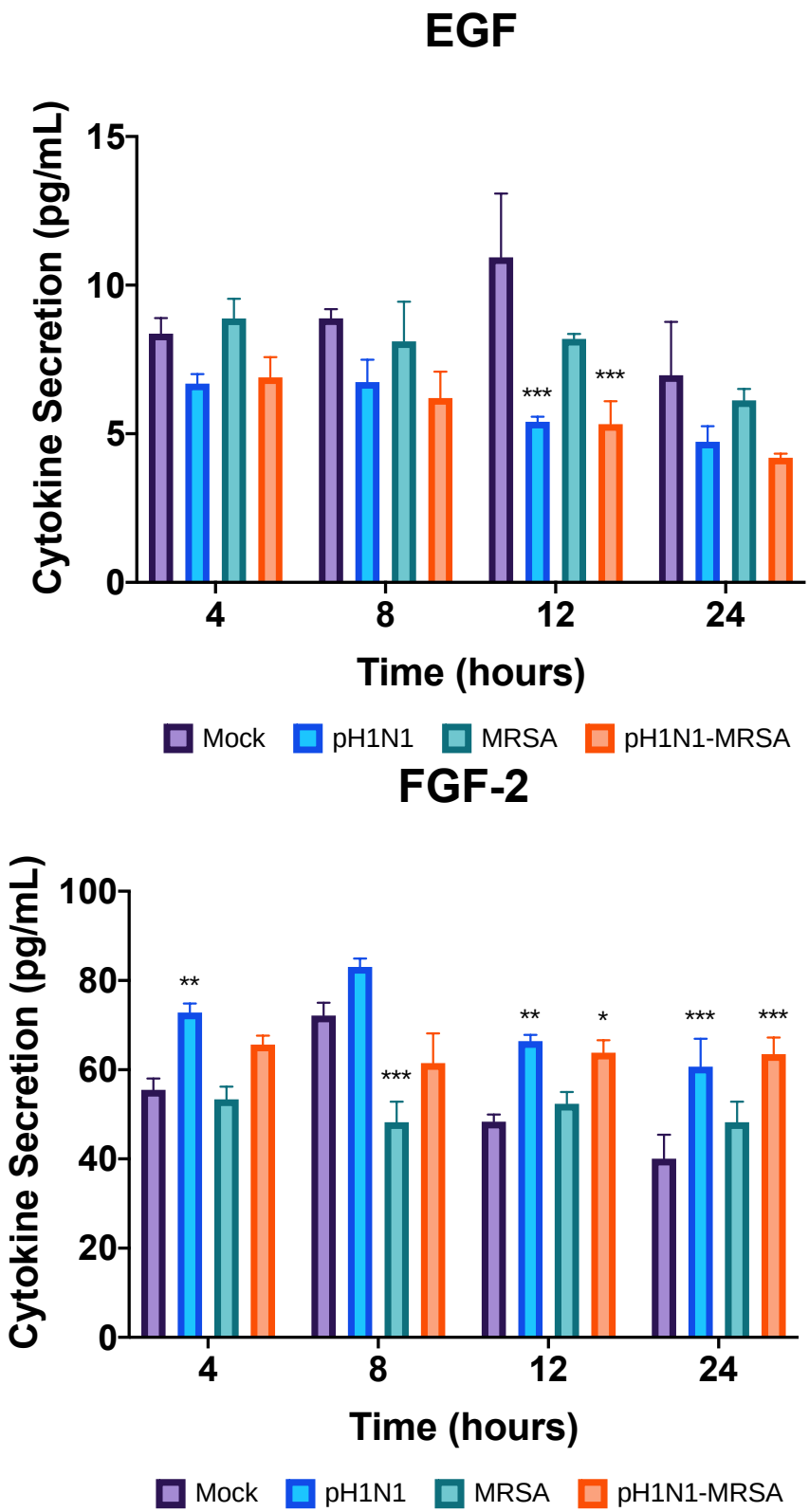

Figure 40: EGF and FGF-2 Secretion in pH1N1, MRSA, and pH1N1-MRSA Infection in a Model of the Alveolar-Capillary Barrier.

Figure 40: EGF and FGF-2 Secretion in pH1N1, MRSA, and pH1N1-MRSA Infection in a Model of the Alveolar-Capillary Barrier.

Primary human alveolar cells were mock-infected or infected with pH1N1 at a MOI of 0.1. MRSA (MOI 0.1) was added 24 h later. Supernatants were harvested at 4, 8, 12, and 24 h and cytokine levels determined using the Milliplex MAP multiplex kit. Error bars represent SEM calculated from three biological replicates ($n = 3$).

A) When measuring EGF secretion, time ($P = 0.0039$) and the infection condition ($P < 0.0001$) were each statistically significant; however the interaction between the two was not ($P = 0.5492$). At 12 h, pH1N1-alone ($P = 0.0003$) and pH1N1-MRSA ($P = 0.0002$) were both significantly downregulated.

B) When measuring FGF-2 secretion, time ($P < 0.0001$), the infection condition ($P < 0.0001$), and the interaction between the two ($P = 0.0009$) were each statistically significant. At 4 h, pH1N1-alone was significantly upregulated ($P = 0.0053$). At 8 h, MRSA-alone was significantly downregulated ($P < 0.0001$). At 12 h, pH1N1-alone ($P = 0.0035$) and pH1N1-MRSA ($P = 0.0140$) were both significantly upregulated. This upregulation continued at 24 h in pH1N1-alone ($P = 0.0008$) and pH1N1-MRSA ($P = 0.0002$).

When measuring IL-6 secretion, time, the infection condition, and the interaction between the two were each statistically significant ($P < 0.0001$ for each; Figure 41A). A trend towards IL-6 upregulation is observed in pH1N1-alone infection and pH1N1-MRSA co-infection at each time point, with statistical significance at 8 and 24 h in pH1N1-MRSA infection ($P = 0.0303$ and $P < 0.0001$, respectively) and 24 h in pH1N1-alone infection ($P < 0.0001$). Alternatively in our MRSA-alone infections, expression of IL-6 was similar to mock-infection at 4, 8, and 12 h, with upregulation seen only at 24 h. This suggests that the presence of MRSA does not affect IL-6 expression, while IL-6 may play a role in cytokine signaling in the presence of pH1N1.

When measuring IL-8 secretion, time ($P < 0.0001$), the infection condition ($P < 0.0001$), and the interaction between the two ($P = 0.0050$) were each statistically significant. There was a trend towards IL-8 upregulation in each infection condition at every time point (Figure 41B). Statistically significant upregulation was seen at 4, 8, 12, and 24 h in pH1N1-alone infection ($P = 0.0059$, $P = 0.0056$, $P = 0.0280$, and $P < 0.0001$, respectively). IL-8 was also significantly upregulated at 4, 8, and 24 h in pH1N1-MRSA co-infection ($P = 0.0002$, $P < 0.0001$, and $P < 0.0001$). In cells infected with MRSA-alone, IL-8 was significantly upregulated at 24 h ($P = 0.0016$). This suggests that IL-8 may play an important role in cytokine signaling in the presence of each pathogen, but especially in pH1N1-alone infection.

As seen in Figure 42A, when measuring IP-10, time, the infection condition, and the interaction between the two were each statistically significant ($P < 0.0001$ for all). Upregulation of IP-10 was observed at every time point in each condition as compared with our mock-infected samples. Highly significant upregulation was seen at 4, 8, 12 and 24 h in pH1N1-alone infection ($P < 0.0001$ for each time point) and at 4, 8, 12, and 24 h in pH1N1-MRSA infection ($P <$

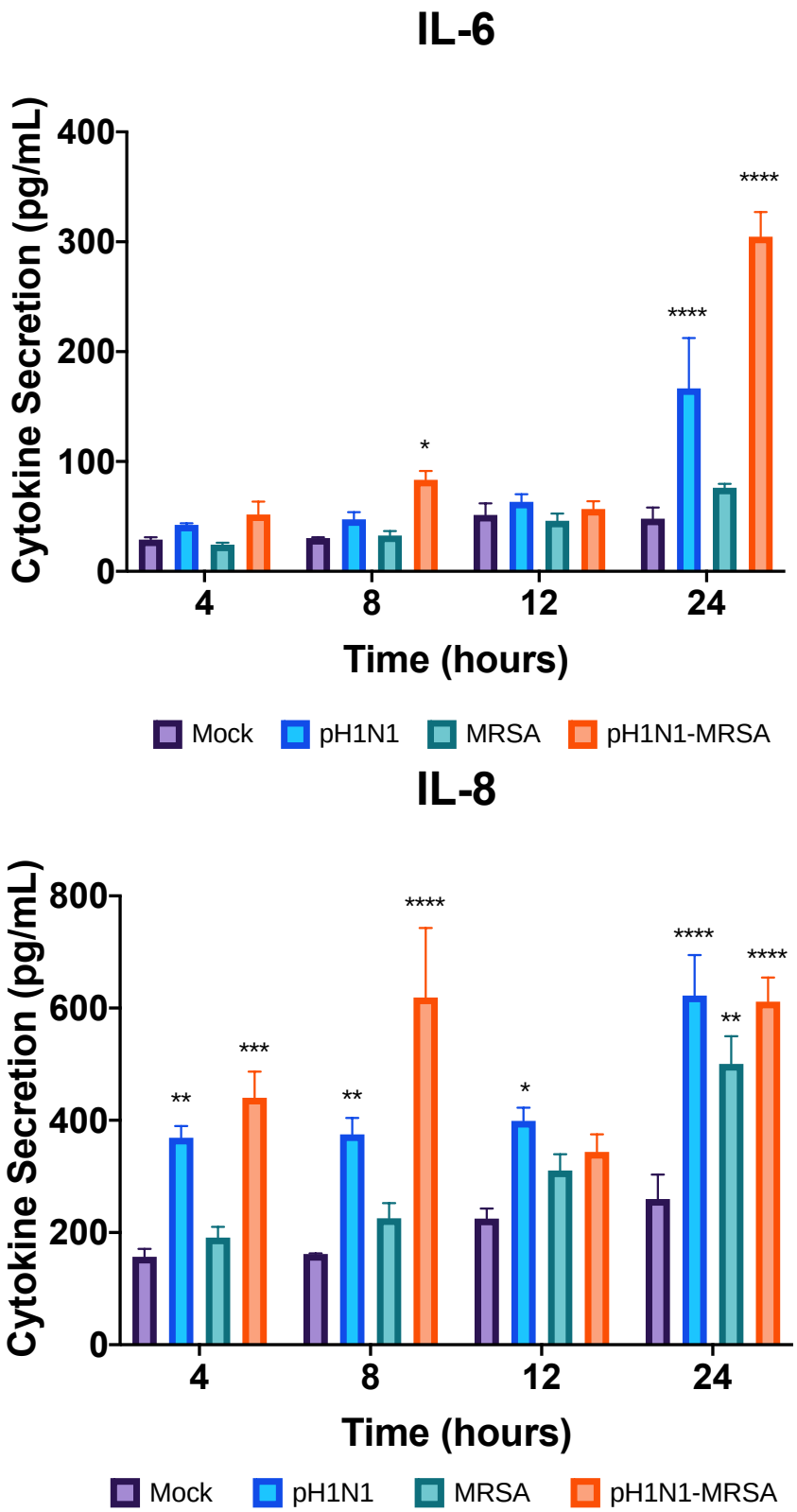

Figure 41: IL-6 and IL-8 Secretion in pH1N1, MRSA, and pH1N1-MRSA Infection in a Model of the Alveolar-Capillary Barrier.

Figure 41: IL-6 and IL-8 Secretion in pH1N1, MRSA, and pH1N1-MRSA Infection in a Model of the Alveolar-Capillary Barrier.

Primary human alveolar cells were mock-infected or infected with pH1N1 at a MOI of 0.1. MRSA (MOI 0.1) was added 24 h later. Supernatants were harvested at 4, 8, 12, and 24 h and cytokine levels determined using the Milliplex MAP multiplex kit. Error bars represent SEM calculated from three biological replicates ($n = 3$).

A) When measuring IL-6 secretion, time, the infection condition, and the interaction between the two were each statistically significant ($P < 0.0001$ for each). At 8 h, pH1N1-MRSA was significantly upregulated ($P = 0.0303$). At 24 h, pH1N1-alone and pH1N1-MRSA were significantly upregulated ($P < 0.0001$ for both).

B) When measuring IL-8 secretion, time ($P < 0.0001$), the infection condition ($P < 0.0001$), and the interaction between the two ($P = 0.0050$) were each statistically significant. At 4 h, pH1N1-alone ($P = 0.0059$) and pH1N1-MRSA ($P = 0.0002$) were significantly upregulated. At 8 h, pH1N1-alone ($P = 0.0056$) and pH1N1-MRSA ($P < 0.0001$) were again significantly upregulated. At 12 h, pH1N1-alone was significantly upregulated ($P = 0.0280$). At 24 h, pH1N1-alone, MRSA-alone, and pH1N1-MRSA were each significantly upregulated ($P < 0.0001$, $P = 0.0016$, $P < 0.0001$, respectively).

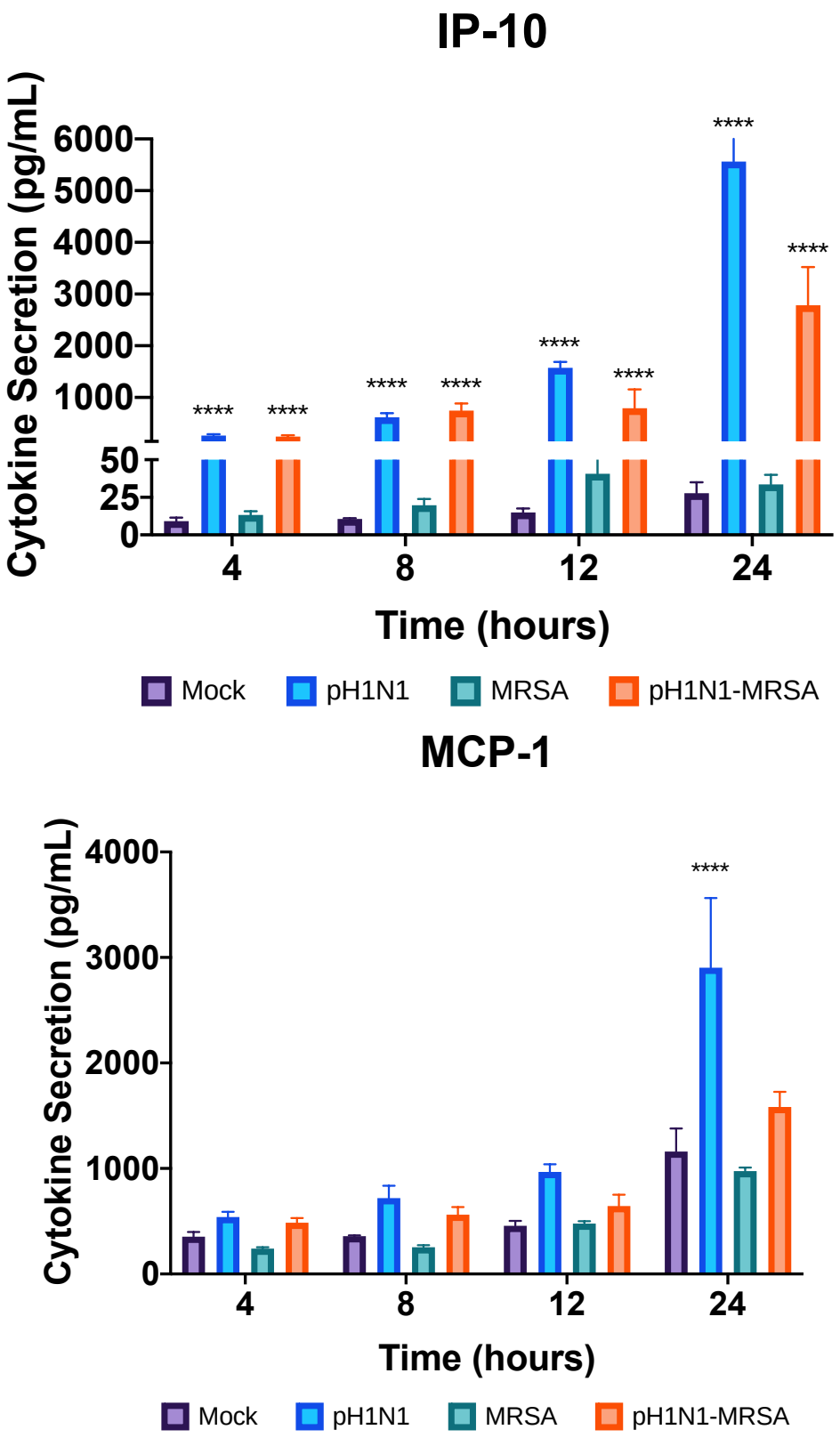

Figure 42: IP-10 and MCP-1 Secretion in pH1N1, MRSA, and pH1N1-MRSA Infection in a Model of the Alveolar-Capillary Barrier.

Figure 42: IP-10 and MCP-1 Secretion in pH1N1, MRSA, and pH1N1-MRSA Infection in a Model of the Alveolar-Capillary Barrier.

Primary human alveolar cells were mock-infected or infected with pH1N1 at a MOI of 0.1. MRSA (MOI 0.1) was added 24 h later. Supernatants were harvested at 4, 8, 12, and 24 h and cytokine levels determined using the Milliplex MAP multiplex kit. Error bars represent SEM calculated from three biological replicates ($n = 3$).

A) When measuring IP-10, time, the infection condition, and the interaction between the two were each statistically significant ($P < 0.0001$ for all). At 12 h, pH1N1-alone is significantly upregulated ($P = 0.0043$). At 24 h, both pH1N1-alone and pH1N1-MRSA are significantly upregulated ($P < 0.001$ for both).

B) When measuring MCP-1, time ($P < 0.0001$), the infection condition ($P < 0.0001$), and the interaction between the two ($P = 0.0018$) were each statistically significant. At 24 h, pH1N1-alone was significantly upregulated ($P < 0.0001$).

0.0001). This suggests that IP-10 is highly upregulated in the presence of pH1N1, and that this trend proceeds throughout pH1N1 infection.

When measuring MCP-1, time ($P < 0.0001$), the infection condition ($P < 0.0001$), and the interaction between the two ($P = 0.0018$) were each statistically significant. Expression of MCP-1 was upregulated in pH1N1-alone and pH1N1-MRSA infection at each time point, while expression was repressed in MRSA-alone infection at each time point (Figure 42B). Significant upregulation of MCP-1 was observed at 24 h post in pH1N1-alone infection ($P < 0.0001$). This suggests that while pH1N1 infection results in upregulation of MCP-1, the addition of MRSA does not result in a further increase of MCP-1 release beyond that found for pH1N1-alone infection.

When measuring VEGF, time ($P < 0.0001$), the infection condition ($P < 0.0001$), and the interaction between the two ($P = 0.0005$) were statistically significant. VEGF was significantly repressed at 4 h in each infection condition as compared with our mock-infected samples ($P < 0.0001$ for all three conditions; Figure 43). This repression was also observed at 8, 12, and 24 h post-MRSA infection in pH1N1-alone infection and pH1N1-MRSA co-infection, with significant repression occurring at 8 h in pH1N1-MRSA infection ($P = 0.0019$). In contrast, similar expression of VEGF in mock-infected and MRSA-alone infected samples was observed at 8 and 12 h. This suggests that infection with a pathogen, whether viral or bacterial, may result in repression of the cytokine VEGF.

Taken together, these data suggest that cytokine expression by our co-culture model may play an important role in barrier disruption. Downregulation of our growth factors, EGF and VEGF, may play an important role in IAV-bacterial co-infection at the alveolar-capillary barrier,

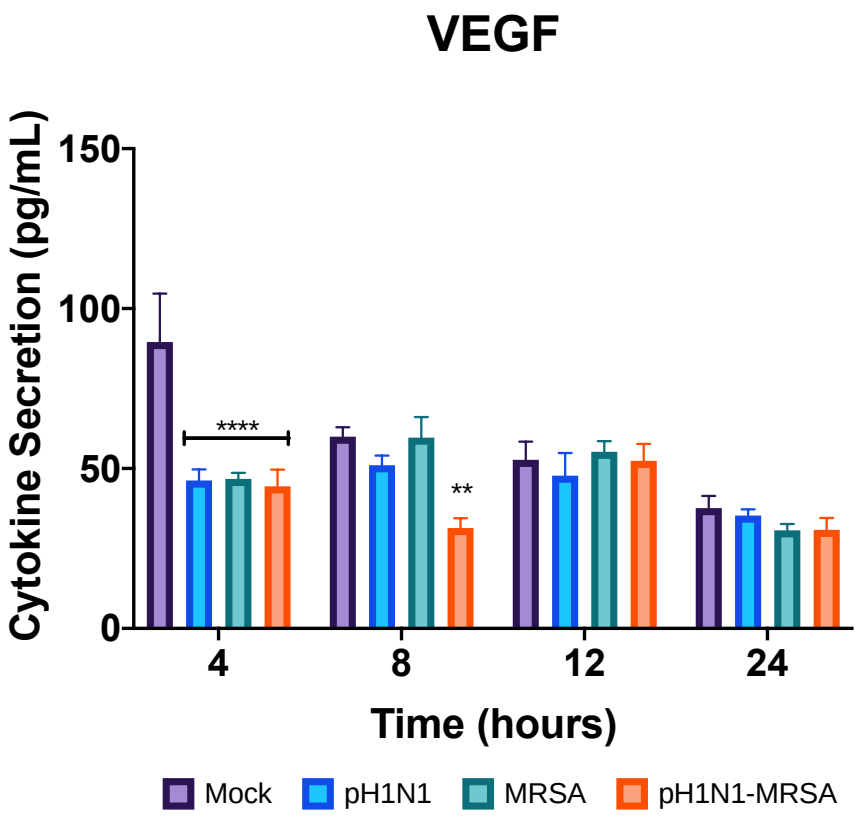

Figure 43: VEGF Secretion in pH1N1, MRSA, and pH1N1-MRSA Infection in a Model of the Alveolar-Capillary Barrier.

Figure 43: VEGF Secretion in pH1N1, MRSA, and pH1N1-MRSA Infection in a Model of the Alveolar-Capillary Barrier.

Primary human alveolar cells were mock-infected or infected with pH1N1 at a MOI of 0.1. MRSA (MOI 0.1) was added 24 h later. Supernatants were harvested at 4, 8, 12, and 24 h and chemokine levels determined using the Milliplex MAP multiplex kit. Error bars represent SEM calculated from three biological replicates ($n = 3$). When measuring VEGF, time ($P < 0.0001$), the infection condition ($P < 0.0001$), and the interaction between the two ($P = 0.0005$) were statistically significant. At 4 h, pH1N1-alone, MRSA-alone, and pH1N1-MRSA were each significantly repressed ($P < 0.0001$). At 8 h, pH1N1-MRSA continued to be significantly repressed ($P = 0.0019$).

while significant upregulation of other chemokines may imply that inflammation plays an important role in pH1N1-MRSA disease pathogenesis in our co-culture model.

Discussion

Secondary bacterial infections complicate both seasonal and pandemic IAV infections, resulting in increased morbidity and mortality [49]. Most notably, ~95% of lethal cases during the 1918 Spanish flu were complicated by a secondary bacterial infection [49, 260, 261]. More recently, up to 44% of fatal cases from the 1968 H3N2 Hong Kong flu pandemic and 55% of fatal cases from the 2009 H1N1 swine flu pandemic were complicated by secondary bacterial infections, including *S. aureus* [49, 262]. Bacteria have the ability to sense and adapt to their surrounding environment, including during infection. This includes the modulation of replication kinetics and the synthesis of virulence factors or toxins, which can enhance both adhesive and invasive properties [326]. As such, we first sought to assess the role of bacterial factors in influenza-bacterial co-infection-mediated alveolar epithelial cell barrier dysfunction, followed by the role the host response plays in dysfunction. Pathophysiology associated with co-infection is thought to occur mainly in the lower respiratory tract [262]. Thus, we began by utilizing the well-characterized alveolar epithelial adenocarcinoma A549 cells for our investigation. While it is appreciated that the potential biological implications of immortalized cell host response data must be interpreted cautiously, A549 cells provide the opportunity to assess alveolar epithelial cell responses directly in a well-characterized cell line. We also demonstrated that bacterial replication kinetic trends were nearly identical in the presence or absence of pH1N1-MRSA co-infection in both A549 cells and HBEC3-KT cells, a normal human bronchial cell line. Further, barrier dysfunction analysis by ECIS demonstrated similar trends in loss of barrier integrity during MRSA infection alone or in conjunction with pH1N1 in both A549 and HBEC3-KT cells.

Despite previous studies hypothesizing that pre-existing IAV infection may enhance MRSA replication in a monolayer of alveolar epithelial cells due to the exposure of additional

bacterial binding sites on infected cells, this was not observed in human alveolar cells [327]. Virtually identical bacterial replication kinetics were observed regardless of the IAV strain used to infect A549 cells prior to MRSA addition; no significant difference was seen at any time point between any infection condition. We also demonstrated that whether bacterial infection occurs simultaneously with pH1N1 infection or at peak viremia has no bearing on bacterial replication. Together, this would suggest that cellular damage induced by pre-existing IAV infections does not affect MRSA fitness in respiratory alveolar cells, as previously postulated. This is further supported by the similar trend observed when MRSA replication kinetics were studied in HBEC3-KT cells, a normal human bronchial cell line, co-infected with pH1N1.

When MRSA was co-infected with IAV in A549 cells, the expression of virulence factors directly related to adhesion and invasion were selectively upregulated at 1 and 4 h, but not at any later time points. This upregulation of gene expression corresponded with the beginning of the exponential phase of MRSA in our replication data, suggesting that adhesion and invasion play a critical role in the initial stages of MRSA replication and infection. At 1 h post-MRSA infection, upregulation was observed in a number of virulence factor genes. However, significant upregulation occurred only in *hla*, *hlgA*, and *spA* in the presence of specific IAVs. Both *hla* and *hlgA* act as MRSA toxins. The *hla* genes codes for α-hemolysin, which forms pores in the cytoplasmic membrane of infected cells, resulting in lysis [328]. Similarly, *hlgA* is part of the γ-hemolysin locus and is also involved in hemolysis by forming pores in the cytoplasmic membrane of infected cells [329-332]. The product of *spA*, SpA, mediates binding and adhesion to airway epithelial cells, while also being able to repress innate and adaptive immune responses [333]. Multiple mouse models have demonstrated that SpA plays an important role in pneumonia

[334-336]. Besides mediating binding and adhesion to cells, SpA is able to bind to the Fcγ domain of IgG, thus preventing IgG from binding to host receptors [337].

Both *hla* and *hlgA* were significantly upregulated in pH1N1-MRSA infected cells; *hla* was also significantly upregulated in the case of pH1N1+MRSA co-infection. This may suggest a critical role for the bacterial toxins *hla* and *hlgA* in the immediate stages of MRSA infection which may contribute to secondary bacterial co-infection pathogenesis in the presence of pH1N1. Additionally, this may suggest that hemolysis of MRSA-infected cells plays an important role in the initial stages of MRSA infection in the presence of pH1N1, and that this hemolysis may occur via a number of pathways. Moreover, α-hemolysin is known to play a role in clinical pneumonia [177]. Lastly, *spA* was significantly upregulated in sH3N2-MRSA co-infections. Upregulation of *spA* at 1 h post-MRSA addition suggests that IAV infection of alveolar epithelial cells results in cellular damage and exposure of host molecules in the extracellular matrix and plasma membrane.

At 4 h post-MRSA addition, significant upregulation was observed in *hlgA*, *sbi* and *spA*. As mentioned previously, hlgA is involved in hemolysis and plays a role in clinical pneumonia [177]. Sbi, the product of *sbi*, is involved in the binding of the Fc domain of immunoglobulin, as well as binding complement protein C3 and promoting C3-C3b conversion [106, 338, 339]. The binding of Sbi to IgG and C3 may result in the recruitment of plasmin to degrade the bound complement components, a novel immune evasion approach [337]. As previously mentioned, SpA is also able to bind IgG [337]. The expression of *sbi* was significantly upregulated at 4 h in sH1N1-MRSA co-infections. Alternately, *spA* was significantly upregulated in sH3N2-MRSA co-infections. This upregulation occurred only in the seasonal IAVs studied, and corresponds with mid-exponential phase for both sH1N1 and sH3N2. Significant upregulation of virulence

factors able to bind IgG, and thus inhibit antibody responses and the development of protective antibody-mediated immunity suggests that sH1N1 and sH3N2 may aid in eliciting a stronger immune evasion response in MRSA.

The modulation of nine other bacterial virulence factors associated with bacterial adhesion and invasion were also studied via RT-qPCR. Coagulase, the product of *coa*, triggers the cleavage of fibrinogen to fibrin, as well as binding and activation of prothrombin, making it an important virulence factor in MRSA adhesion to epithelial cells [114, 330, 340]. The *ebpS* gene codes for a cell-wall associated protein which facilitates the initial attachment of MRSA to host cells by binding elastin in injured tissues ,while *eno* binds to laminin, a fibrous protein present in the basal lamina of the epithelia [108, 331]. The fnb locus codes for both *fnbA* and *fnbB* which bind to fibronectin, fibrinogen, and elastin to mediate adhesion to cells for internalization [216, 330, 331, 341-343]. The *icaA* and *icaB* genes are coded for by the ica locus, and are involved in intracellular adhesion and biofilm formation. Specifically, *icaA* encodes N-acetylglucosaminyltransferase while the product of *icaB* is the deacetylase responsible for deacetylation of poly-N-acetylglucosamine, both of which are essential for biofilm formation [86, 344-346]. Lastly, *sek* and *seq* are secreted exotoxins known as Staphylococcal enterotoxin K and Q, respectively, which are able to alter the permeability of the cell membrane, resulting in the lysis of infected cells [347, 348]. Staphylococcal enterotoxin K is known to play a role in sepsis induced by MRSA USA300 [347].

Taken together, our data suggest that IAV infection of alveolar epithelial cells results in cellular damage and subsequent exposure of host molecules (i.e., fibrinogen, elastin, and fibronectin) in the extracellular matrix and plasma membrane, resulting in the upregulation of MRSA binding factors. Moreover, specific bacterial adhesion and invasion factors may provide

an advantage for bacterial entry into influenza-infected cells. Further investigations of the relation between targeted inhibition of upregulated genes, such as *hla*, *hlgA*, *spA*, and *sbi*, and IAV-MRSA co-infection pathogenesis in alveolar epithelial cells are warranted and may provide important information regarding novel antimicrobial therapeutic targets. Specifically, investigation into the role of *spA*, which was significantly upregulated in the presence of pH1N1 and sH3N2 IAVs, may result in a further understanding of the severe pathogenesis seen in IAV-MRSA co-infection, and a possible therapeutic target. Likewise, investigation of toxins significantly upregulated by MRSA in the presence of IAVs, such as *hla* and *hlgA*, may further our understanding of the severe pathogenesis seen in IAV-MRSA co-infection at the alveolar-capillary barrier. Additionally, these toxins are often involved in tissue penetration and enable MRSA to invade the host cells, and as such may provide important information regarding novel antimicrobial therapeutic targets [332]. However, our data also suggest that there is likely no competitive advantage for expression of adherence and invasion-related bacterial virulence factors post-entry between IAV-MRSA infection and MRSA-alone infection. Further analyses of additional bacterial toxins and virulence factors may provide evidence for bacterial molecules that are related to post-bacterial adhesion/invasion co-infection pathogenesis.

As our analyses of the modulation of bacterial factors in IAV-MRSA co-infections did not reveal why secondary bacterial infections result in a severe disease pathogenesis, we next chose to examine the host response. We first began by studying the dysfunction of alveolar epithelial cells when infected with IAV-MRSA, using ECIS. The addition of any IAV-alone to the alveolar epithelial cells at a low MOI of 0.1 did not result in a significant decrease in resistance, nor any negative repercussions in regards to barrier integrity. This reflects the majority of influenza infections in healthy adults, which do not generally result in severe disease

[33, 349]. However, the addition of high MOI (3.0) pH1N1 resulted in significantly decreased barrier integrity and may reflect a relation between exacerbated disease and infectious titer of the exposure.

In contrast, the addition of MRSA resulted in significant decrease in resistance and eventual loss of alveolar epithelial barrier integrity across all tested MOIs. Clinically, MRSA colonization is known to occur in healthy, young adults and may lead to overt infections, such as pneumonia [195, 350]. Additionally, the development of bacterial pneumonia is known to result in inflammation of the lungs and hypoxemia, a direct result of cell barrier failure [351]. Resistance measurement trends were nearly identical between the MRSA-alone and IAV-MRSA infections following the addition of MRSA. These data suggest that while influenza infection may provide for increased adhesion and/or attachment of bacteria to the surfaces of infected epithelial cells, disruption of alveolar epithelial cell barrier function appears highly dependent on the induction of bacterial- or host cell-mediated cytotoxicity. However, the role of these differentially expressed virulence factors in additional post-infection processes in the lung remain to be determined.

Our ECIS data suggested that disruption of the alveolar monolayer was not a result of IAV infection, as barrier integrity remained similar regardless of the IAV strain used to infect alveolar epithelial cells However, loss of barrier integrity was observed upon infection with MRSA, whether on its own or in conjunction with IAV. As such, we hypothesized that the severe disease pathogenesis observed in IAV-MRSA co-infection may be a result of a dysregulated host response. Our characterization of the temporal host kinome response of alveolar epithelial cells in response to pH1N1-MRSA co-infection supported this idea that host response dysregulation plays an integral role in co-infection pathogenesis. Interestingly, the host

kinome response of pH1N1-MRSA co-infected alveolar epithelial cells clustered most strongly with that of cells infected with pH1N1-alone. This was perhaps surprising, as significant upregulation of bacterial virulence factors was observed at these time points, including those with immunomodulatory activities.

For example, *spA* was significantly upregulated in pH1N1+MRSA and sH3N2-MRSA co-infected samples at 1 h post-MRSA addition. A previous investigation by Kumar *et al.* demonstrated that stimulation of epithelial cells with SpA resulted in the induction of TNF and IL-8 secretion and activation of NFκB signaling [352]. Gene ontology analysis demonstrated that IL-6-, IL-8-, TNF-, and NFκB-mediated signaling events were overrepresented in pH1N1-MRSA co-infected epithelial cells, while absent in our MRSA-alone and pH1N1-alone infected samples. Upregulation of these signaling events corresponds with the upregulation of *spA* expression in the co-infected samples as compared with MRSA infection alone. This suggests that while the early host response during co-infection is largely dominated by the induction of antiviral responses, the upregulation of bacterial virulence factors might have an underlying influence on the induction of antiviral responses and host cell cytotoxic responses. Additionally, a study by Gonzalez *et al.* demonstrated that Sbi also induces production of IL-6 and CXCL1 in mice [353]. As the expression of *sbi* was significantly upregulated in sH1N1-MRSA infected cells at 4 h, further analysis of the host kinome response during MRSA co-infection with other IAVs should be done to fully understand the effect of bacterial virulence factors on the host response.

Direct comparison of host kinome responses during pH1N1-MRSA infection and MRSA-alone infection suggests that a stronger apoptosis response is seen in co-infected samples during the 8-12 h transition phase. This supports our hypothesis that IAV-MRSA co-infections

specifically alter host cellular responses as compared with either pathogen alone. Focused *in vitro* and *in vivo* investigations of the contributions of host response dysregulation, and in particular modulation of alveolar epithelial cell apoptosis, may provide important clues to the molecular mechanisms underlying the pathophysiology of influenza-bacterial co-infections.

In contrast, the kinome data for pH1N1-MRSA co-infection and MRSA-alone infection clustered together from 16 h onwards. This was reflected in strong upregulation of cell death responses, such as apoptosis-related pathways, in both infection conditions. From 8-12 h post-MRSA infection, host kinome data from the three different infection conditions clustered together. Taken together, our clustering data suggest that the host response transitions from an influenza- to bacterial-centric response during infection. Importantly, this transition phase in the host response corresponded with mid- to late-exponential MRSA growth in the presence of pH1N1.

Our investigations of IAV-MRSA co-infections in an alveolar epithelial monolayer suggested that severe disease pathogenesis is a result of dysregulation of the host response. As such, further studies concerning IAV-MRSA co-infections in an *in vitro* model which more closely mimicked the alveolar-capillary barrier were warranted. We developed a co-culture model of the alveolar-capillary barrier using primary human pulmonary alveolar epithelial cells and primary human pulmonary microvascular endothelial cells. This model allowed us to study the host response of differentiated primary alveolar cells and the downstream response of primary microvascular endothelial cells.

As our previous investigations had revealed that the presence of IAV did not affect the growth kinetics of MRSA in A549s, an adenocarcinoma alveolar cell line, we next sought to clarify these observations in a physiologically-relevant model of the lower respiratory tract. For

this, we constructed a primary co-culture model of the alveolar-capillary barrier. No significant differences were found for MRSA replication kinetics at any time point across our different infection conditions. This further supports our previous conclusion that pre-existing IAV infections do not affect MRSA fitness in alveolar epithelial cells. Specifically, this suggests that MRSA fitness is not altered by cellular damage or host molecule secretion resulting from pre-existing pH1N1 influenza infection at the alveolar-capillary barrier. This also suggests that the increased disease severity associated with influenza bacterial co-infections is not simply due to increased bacterial burden within the lungs during co-infection.

Similar to our previous findings in A549 cells, the expression of virulence factors related to adhesion and invasion were selectively upregulated only at 1 and 4 h in the model. This upregulation of gene expression corresponded with the lag phase of MRSA at 1 and 4 h post-addition. At 1 h post-MRSA infection, upregulation was observed in each of the 13 virulence factors studied; however, significant upregulation was only seen in *eno*, *icaB*, *sek*, and *seq*. As mentioned previously, the *eno* protein binds to laminin in the basal lamina of the epithelia, while *seq* and *sek* code for secreted exotoxins able to alter the permeability of the cell membrane, resulting in lysis [331, 347, 348]. This is interesting as upregulation of each of these three genes was not observed in A549 cells, regardless of the IAV strain used to infect cells.

Increased concentration of enolase has been shown to be an important biomarker of disease severity in non-malignant inflammatory lung disorders, hemophagocytic lymphohistiocytosis, and tuberculosis [354-357]. The significant upregulation of enolase early in MRSA infection could act as a biomarker in disease severity. Further, studies have shown that the high prevalence of *eno* could play an important role in future MRSA vaccine designation [358, 359]. The ica locus, which codes for *icaB*, is involved in intracellular adhesion and biofilm

formation. Upregulation of *icaB* early in infection may be indicative of the increased lag phase of MRSA in primary alveolar cells as compared with our A549 cell line. This may be due to the fact that epithelial cells within our co-culture model had been allowed to differentiate for two weeks prior to infection. As differentiated pulmonary alveolar epithelial cells produce surfactant, this may help protect cells from MRSA adhesion and invasion [262]. Further, studies in mice and sheep have shown that the deactylase activity of the *icaB* gene plays an important role in retaining poly-N-acetylglucosamine (PNAG) on the cell surface of MRSA, such that deacylated PNAG is considered a promising candidate for vaccine development [360-364]. The superantigen properties of *sek* and *seq* are known to directly contribute to MRSA virulence as a pulmonary pathogen [365-367]. Studies have shown that lysis of neutrophils by *S. aureus* exotoxins, such as *sek* and *seq*, results in the release of reactive oxygen species, resulting in damage and inflammation to surrounding lung tissue [366, 367]. Lastly, a study in mice suggested that the *sek* and *seq* superantigens present in MRSA play a role in T-cell signaling responsible for much of the early lung damage seen in *S. aureus* infection [365].

At 4 h post-MRSA addition, upregulation was again observed in each of the virulence factors studied. While *eno* and *seq* were no longer significantly upregulated, *icaB* and *sek* did remain significantly upregulated. Additionally, *coa, fnbB, hla, hlgA, icaA, sbi,* and *sek* were all significantly upregulated at 4 h post-bacterial infection in our model of the alveolar-capillary barrier. The product of *coa,* coagulase, plays an important role in initial adhesion to epithelial cells by cleaving fibrinogen and activating prothrombin [114, 330, 340]. Both *hla* and *hlgA* result in the lysis of infected cells, and were upregulated at 1 h in pH1N1-MRSA infected A549 cells, which corresponded with the lag phase. This may further underline the idea that bacterial toxins play a critical role in secondary bacterial pathogenesis early in infection of alveolar epithelial

cells. In contrast to the upregulation of *icaB* observed at 1 h post-MRSA infection, *icaA* was upregulated at 4 h. As *icaA* is similarly involved in adhesion to cells and biofilm formation, upregulation may also be indicative of the challenges present in intracellular adhesion of MRSA in differentiated alveolar cells. Lastly, *sbi* was also upregulated at 4 h. This may suggest that the presence of pH1N1 in primary differentiated human alveolar epithelial cells may aid in eliciting a strong immune evasion response in MRSA, by inhibiting antibody responses [337].

As a whole, our investigation of MRSA in secondary bacterial infections presented a number of novel vaccine candidates against MRSA infection. Proper vaccinations against *S. aureus*, and MRSA in particular, would help relieve the burden of disease during influenza pandemics, as well as during seasonal epidemics. Additionally, revealing that *eno* is significantly upregulated early in MRSA infection during the lag phase, may provide a candidate for detection of MRSA as a secondary pathogen in high-risk patients admitted to hospitals with severe influenza infections. Measuring of *eno* levels as a biomarker for disease severity early in infection may allow for healthcare providers to provide preventative care early in infection.

As our study of the modulation of MRSA in the presence of pH1N1 in an alveolar-capillary barrier largely mirrored that seen in A549 cells, we next sought to characterize the host response to pH1N1-MRSA co-infection. We first sought to examine the dysfunction of our co-culture model of the alveolar-capillary barrier when infected with pH1N1-alone, MRSA-alone, and pH1N1-MRSA. As our previous studies of A549 cells revealed that infection with IAV-alone at a MOI of 0.1 did not result in any negative repercussions in regards to barrier integrity and cell morphology, we wished to determine whether this is also reflected in our co-culture model. When our model of the alveolar-capillary barrier was infected with either pH1N1-alone or MRSA-alone, there was virtually no change in resistance values. This differed from the results

observed when our alveolar epithelial cell monolayer was co-infected with various IAV strains and MRSA, where the presence of MRSA in A549 cells resulted in cellular dysfunction regardless of prior IAV infection. However, when our model underwent pH1N1-MRSA co-infection, resistance steadily decreased throughout the course of the experiment, beginning at 8 h post-MRSA addition, which correlated well with the beginning of the exponential phase of MRSA. These differences may further support the hypothesis that surfactant present on differentiated alveolar epithelial cells may help protect cells from MRSA adhesion and invasion [238, 247, 262, 368]. As such, the presence of MRSA alone does not result in a severe disease pathogenesis. Our data suggest that this virus-induced disruption to the epithelial cells of the alveolar-capillary barrier is necessary for the dysfunction observed in secondary bacterial co-infections, as healthy cells are able to refute either pathogen on its own. This may not be surprising as pH1N1-alone infection in healthy adults rarely results in severe disease [33, 349]. Likewise, *S. aureus* is infrequently associated with community-acquired pneumonia, with severe illness and death in otherwise healthy adults often associated with prior influenza infection [167, 196, 369-371]. Moreover, the decrease in resistance in our pH1N1-MRSA infected model was not as pronounced as the decrease in resistance observed in our co-infected A549 cells (P = 0.0005 compared with $P < 0.0001$). As our prior studies had revealed that pH1N1 does not migrate from the alveolar epithelial cells to the microvascular endothelial cells below, this milder drop in resistance may be indicative of dysfunction only in the alveolar epithelial cells.

As our TEER data demonstrated that pH1N1-MRSA co-infection resulted in increased alveolar-capillary barrier permeability, we next investigated whether this was a by-product of decreased levels of tight junction proteins. While ZO-1 protein levels in our pH1N1-MRSA co-infected endothelial cells appeared to be decreased at 24 h as compared with our pH1N1- and

MRSA-alone time-matched samples, these results were inconclusive. Further investigation is warranted, especially as recent investigations have suggested that severe cases of IAV have an abortive effect on endothelial cells, despite never becoming infected [372]. As secondary MRSA infections are known to further exacerbate IAV infections in the lower respiratory tract, this may further compound the abortive effect on endothelial cells. Further, a recent study by Becker *et al.* revealed a marked downregulation of ZO-1 and ZO-2 in endothelial cells treated with α-hemolysin of *S. aureus* [373]. We observed significant upregulation of the α-hemolysin gene, *hla*, at 4 h in pH1N1-MRSA infection ($P = 0.0014$). Additionally, *hlgA*, a secondary MRSA exotoxin involved in hemolysis, was significantly upregulated at 4 h when our model had been infected with pH1N1 prior to MRSA addition ($P < 0.0001$). Further investigations should be done regarding the possibility that the upregulation of *hlgA* and *hla* which we observed may play a role in the degradation of ZO-1 and ZO-2 in endothelial cells during co-infection. As degradation of tight junctions is believed to play an important role in the vascular permeability observed in severe co-infection pathogenesis, understanding this important key during co-infection of our *in vitro* model may further reveal the molecular mechanisms of tight junction degradation.

We next sought to identify specific pathways and cellular responses which are selectively modulated during severe co-infection at the alveolar-capillary barrier. We wished to determine the host kinome response of both our epithelial and endothelial cells in the presence of pH1N1-alone, MRSA-alone, and pH1N1-MRSA at 24 h. Our latest iteration of human kinome peptide arrays had a greater breadth of 1294 targets, as compared to the 309 targets found on the arrays utilized in our A549 assay. In A549 cells, similar clustering of pH1N1-alone and pH1N1-MRSA infection at early time points was observed, while the host response when infected with MRSA-

alone and pH1N1-MRSA clustered most strongly late in infection. Moreover, a transition phase from an IAV-mediated immune response to a MRSA-mediated immune response occurred from 8-12 h. However, this was not observed in our primary alveolar epithelial cells. Instead, clustering between time points, regardless of the infection condition, was seen. This is perhaps surprising, as recent whole-blood transcription analysis in IAV-bacterial infected patients showed a shift in gene signatures from viral response to bacterial response [374]. However, the authors cautioned that the stage and severity of disease must be taken into account when interpreting the host response [374]. The differences observed between the kinome response of primary alveolar epithelial cells and the immortalized A549 cells may simply be due to the differences between immortalized and primary cells, such as differences in cell cycle or apoptotic events, or could be due to intercellular interactions between the epithelial and endothelial cells. Interestingly, in our primary epithelial cells, the 8 and 12 h time points still clustered together more strongly than with the 4 and 24 h time points. A number of pathways were overrepresented in pH1N1-MRSA infected alveolar epithelial cells as compared with pH1N1-alone or MRSA-alone, including those related to TLR signaling, cell cycle/ apoptosis regulation, and cytokine signaling. Taken together, our gene ontology analysis of differentiated alveolar epithelial cells further supports our postulate that IAV-bacterial co-infections are able to specifically modulate host cellular responses independently of infection with pH1N1- or MRSA-alone. Moreover, as MRSA is not able to cross the alveolar-capillary barrier to infect the endothelial cells of the capillaries, any pathway overrepresentation seen within the endothelial cells likely results from perturbation of the alveolar epithelial cells.

Most notably, pathways related to TLRs, including TLR-2, -4, -5, -7/8, -9, and -10 were overrepresented only in IAV-MRSA co-infected cells. TLRs are pattern recognition receptors able to recognize pathogen-associated molecular patterns (PAMPs) leading to the activation of signaling cascades and thus an inflammatory response, an important aspect of severe IAV-MRSA co-infections [259, 375]. The TLR pathway is primarily mediated through MyD88, which is also strongly overrepresented in our co-infected epithelial cells, resulting in the activation of NF-κB [376-378]. Interestingly, *S. aureus* on its own is known to dampen TLR-2 activation, thus downregulating NK-κB activation [378]. TLR-7/8 is able to recognize IAV's single-stranded RNA, and signal through pathways similar to TLR-2 and -4 [379]. The activation of these pathways results in the production of proinflammatory cytokines and chemokines such as IL-1, IL-6, and MIP-1, as well as the anti-inflammatory cytokine IL-10 [380, 381]. Overrepresentation of TLR-9 signaling cascade in pH1N1-MRSA infections, but not in pH1N1-alone and MRSA-alone may not be surprising, as a study in mice showed that TLR-9 signaling plays a role in MRSA clearance which only manifests post-IAV infection [382]. A second study showed that TLR-2 agonist stimulation improved disease outcome, and clearance of both virus and bacteria during co-infection [383]. Taken together, our data supports the hypothesis that further understanding of the TLR response to pH1N1-MRSA co-infection may provide new opportunities for targeted drug therapies which are able to manipulate the host immune response, ameliorating disease progression.

A number of other signaling pathways, such as those related to apoptosis and regulation of the cell cycle were overrepresented in pH1N1-MRSA co-infected epithelial cells. Overrepresentation of these pathways was not observed in MRSA-alone infection and only modestly observed in pH1N1-alone infection, suggesting that the presence of both pathogens is

responsible for this dysregulation. Many of these overrepresented pathways were involved in the G1 and G2 phases, and the transition between these two phases. Previous gene-expression analysis in patients infected with pH1N1 has shown that progression towards severe IAV infection is often characterized by abnormal deviations in cell cycle and apoptosis signaling pathways [384]. Specifically, progression to severe infection was characterized by increased aberrant DNA replication in the G1/S phase but delayed exit from the G2/M phase [384]. Other overrepresented pathways were related to G2/M transition and apoptosis related to p53 signaling. Multiple studies have reported conflicting information regarding the role of apoptosis in lung inflammation observed during severe disease [50, 385, 386]. However, our data seems to support the hypothesis that the relationship between cell cycle perturbations and apoptosis via the p53-dependent pathways may influence the outcome of disease in pH1N1-MRSA infected alveolar cells.

Lastly, cytokine signaling was severely overrepresented at 24 h in the presence of pH1N1, whether MRSA was present or not. “Cytokine Signaling in Immune System” was highly upregulated (56 associated proteins from our kinome arrays) in both pH1N1-MRSA and pH1N1-alone infection conditions in alveolar epithelial cells. Infection with pH1N1-alone also resulted in upregulation in “Signaling by Interleukins”, with 44 associated proteins from our kinome arrays, in addition to upregulation of IL-1, IL-2, and IL-6. Various studies have suggested that severe lung inflammation seen in highly pathogenic influenza strains may be due to increased levels of proinflammatory cytokines [50, 385-387]. The role of pro-inflammatory cytokines in severe pH1N1 and pH1N1-MRSA co-infections was further investigated below.

In comparison to pH1N1-MRSA and pH1N1-alone infection, relatively few pathways were upregulated in alveolar epithelial cells infected with MRSA-alone. Notably, upregulation of

pathways related to NOD1/2 and NLR signaling was observed. Similar to TLRs, NLRs are able to recognize PAMPs and activate downstream signaling pathways leading to expression of inflammatory cytokines [259, 375, 378]. However, NLRs are cytoplasmic while TLRs are localized to the cell surface or intracellular compartments [378]. NOD2 has been specifically implicated in the recognition of muramyl dipeptide (MDP) of Gram-positive bacteria [388-391].

Determination of the kinome response of our endothelial cells within the co-culture model in the presence of pH1N1-alone, MRSA-alone, and pH1N1-MRSA at 24 h revealed upregulation of few pathways as compared with our epithelial cells. Overrepresentation of pathways was most commonly seen in pH1N1-MRSA infection, followed by MRSA-alone infection, and pH1N1-alone infection. This is in contrast to our epithelial cells, which had the lowest number of pathways in cells infected with MRSA-alone. Only 5 pathways were overrepresented in cells infected with pH1N1-alone, with 27 associated proteins from our kinome arrays associated with the JAK/STAT signaling pathway. The JAK/STAT signaling pathway acts as a signaling pathway for a number of cytokines and growth factors, stimulating cell proliferation, cell migration, and apoptosis [392]. Failure to regulate JAK/STAT signaling is known to result in inflammation, and may contribute to severe influenza disease pathogenesis [392].

Pathways related to Wnt/β-catenin signaling were most commonly overrepresented in endothelial cells in both our MRSA-alone and pH1N1-MRSA infection conditions. The Wnt signaling pathway regulates a number genes involved in cell growth, differentiation, survival, and immune functions [393]. However, recent studies have revealed both a pro- and anti-inflammatory response from Wnt/β-catenin signaling, suggesting that the role of Wnt may be dependent on the stimulus, cell type, and crosstalk with other signaling pathways [393-397]. The

majority of evidence notes that activation of the Wnt pathway is able to reduce inflammatory processes triggered by bacterial pathogens [393]. As MRSA is not present in the endothelial cells of the co-culture model, overrepresentation of pathways related to Wnt signaling may be indicative of the ability of the alveolar epithelial cells to communicate with the underlying endothelial cells of the capillary.

As our kinome data revealed that cytokine signaling was upregulated in primary alveolar epithelial cells infected with pH1N1-alone or pH1N1-MRSA, we next wished to characterize the expression of 15 cytokines and chemokines which had previously been implicated in severe pH1N1-MRSA infections. The pro-inflammatory response may be an important factor in disease outcome from secondary bacterial pneumonia, as various studies have suggested that severe lung inflammation seen in highly pathogenic influenza strains may be due to increased levels of proinflammatory cytokines and thus a massive influx of neutrophils into the lung [50, 385-387]. Severe influenza infections have been associated with a dysregulated proinflammatory cytokine response in the lungs, referred to as a cytokine storm [269, 398-402]. Specifically, pH1N1 is known to induce expression of a number of interleukins in both the respiratory tract and central nervous system [269]. However, there is a paucity of information concerning cytokine expression at the alveolar-capillary barrier during pH1N1-MRSA co-infection. To address this, supernatant was collected at 4, 8, 12, and 24 h post-MRSA infection of our co-culture model. Samples were processed using the Luminex Bio-Plex Immunoassay Multiplex Platform. A difference in concentration was observed in 7 of the cytokines studied: EGF, FGF-2, IL-6, IL-8, IP-10, MCP-1, and VEGF.

Significant downregulation of EGF was observed at 12 h in both pH1N1-alone and pH1N1-MRSA infection, as compared with mock-infection. EGF is a growth factor capable of

stimulating proliferation of epithelial cells by activating cellular signaling through engagement of the EGF receptor [403]. A previous study in human patients infected with pH1N1 reported that EGF was significantly higher in healthy patients, as compared with those infected with pH1N1 infection [404]. The authors suggested that EGF was actively suppressed, in an effort to protect the lung from host or virus mediated damage [404]. This may explain the significant downregulation of EGF observed in our pH1N1-alone and pH1N1-MRSA infected cells.

Significant upregulation of FGF-2, a member of the fibroblast growth factor family, was observed in pH1N1-alone infection at 4, 12, and 24 h. Significant upregulation was also observed at 12 and 24 h in pH1N1-MRSA co-infection. Conversely, FGF-2 was significantly downregulated at 8 h in cells infected with MRSA-alone. FGF-2 plays an important role in epithelial repair in the lung and in wound healing [405-407]. Mice lacking the FGF-2 gene have reduced vascular tone and defects in response to pulmonary and cardiac injury [407]. FGF-2 dysregulation is implicated in many inflammatory diseases, and a study in mice suggested that FGF-2 plays a vital role in IAV-induced lung injury [408]. Interestingly, FGF-2 was significantly downregulated in MRSA-alone infection at 8 h. Prior studies have suggested that FGF-2 expression was significantly downregulated in wounds infected with MRSA [409]. While our data seems to suggest that pH1N1 infection results in a significant increase in FGF-2 expression regardless of the presence of MRSA, further investigation will need to be done to fully understand the role of FGF-2 in severe pH1N1-MRSA infections.

IL-6 is significantly upregulated at 8 and 24 h in pH1N1-MRSA infections, and at 24 h in pH1N1-alone infections. IL-6 acts as both a pro- and anti-inflammatory cytokine [410]. IL-6 levels have been shown to be significantly elevated in the presence of a clinically-relevant secondary bacterial infection, which may make its upregulation in pH1N1-MRSA co-infection

unsurprising [259, 374]. The significant upregulation of IL-6 observed may have played a role in the decrease in TEER measurements of our alveolar-capillary barrier model when co-infected with pH1N1-MRSA, as high levels of IL-6 are known to directly damage endothelial cells [411]. Further, elevated serum IL-6 levels have been implicated as a potential biomarker for disease severity in pH1N1-alone infections [412]. Our data suggests that IL-6 could act as a novel disease biomarker for secondary MRSA co-infections, as elevated IL-6 expression is first observed at 8 h in pH1N1-MRSA infection which coincides with the beginning of the exponential phase of MRSA in the presence of pH1N1.

IL-8 is significantly upregulated in pH1N1-alone and pH1N1-MRSA infections at 4 h and 8 h, pH1N1-alone at 12 h, and in each infection condition at 24 h. IL-8 shows distinct target specificity for attracting and activating neutrophils to inflammatory regions [413]. The significant upregulation of IL-8 at 24 h in MRSA-alone infection supports previous studies which have shown that IL-8 is significantly increased at the transcriptional level in humans [414]. Further, IL-8 levels in pH1N1-MRSA infected mice have been shown to be significantly upregulated earlier in co-infection as compared with IL-6 in co-infected mice, which may allow it to be used as a disease biomarker in the future [411].

IP-10 is significantly upregulated at each of our selected time points in pH1N1-MRSA and pH1N1-alone infection. This is perhaps unsurprising as previous studies have reported that interferon-related signaling, such as IP-10, were more abundant in cases of severe disease [374]. IP-10 is able to directly influence apoptosis in disease, which may explain the significant upregulation of apoptosis pathways in our kinome data of primary alveolar epithelial cells infected by pH1N1-MRSA and pH1N1-alone [415].

Significant upregulation of MCP-1, also known as CCL2, was only seen in pH1N1-alone infection at 24 h. Interestingly, this upregulation was not observed when secondary infection with MRSA occurred. MCP-1 is a key chemokine involved in regulation of migration and infiltration of monocytes and macrophages [416]. As the presence of monocytes and macrophages in the lungs during IAV infection is directly associated with the development of lung injury, regulating the expression of MCP-1 may be an important key in mitigating severe lung damage [417]. In fact, mice deficient in the MCP-1 receptor, CCR2, show a decrease in monocyte and macrophage accumulation, lung damage, and mortality [417, 418].

Lastly, VEGF was significantly downregulated at 4 h post-MRSA addition in pH1N1-alone, MRSA-alone, and pH1N1-MRSA infection, as compared with mock-infection. VEGF is a regulator of cell growth, and is most abundant in the lung; transcripts are primarily localized in ATII cells in the alveoli [419-421]. The downregulation observed in our model is perhaps surprising, as previous studies have reported that hypoxia, commonly seen in severe pH1N1-MRSA infection, results in increased induction of VEGF from ATII cells [421]. Additionally, high levels of VEGF have been reported in the pulmonary edema fluid of patients with hypoxemic respiratory fluid [421]. Further investigations in a more advanced *in vitro* model of severe pH1N1-MRSA and/or a longer course of infection may be necessary to fully understand the role VEGF plays at the alveolar-capillary barrier.

Overall, significant upregulation of cytokine expression is often observed in pH1N1-MRSA co-infection. Further understanding of how elevation of specific cytokines impact pH1N1-MRSA disease severity may reveal potential therapeutic targets to reduce the generation of a cytokine storm in infected patients. This strategy has previously shown promise, as inhibition of certain cytokines, such as IL-10, have shown improved survival from bacterial

pneumonia late after influenza infection [422, 423]. As neutrophils and macrophages have been implicated as the primary cause of lung damage in most cases of ALI and ARDS, drug therapies which specifically target IL-8 and MCP-1 may improve disease outcome in pH1N1-MRSA infection [417].

Our investigations into IAV-bacterial co-infections in a primary co-culture model of the alveolar-capillary barrier suggest that infection with both pH1N1 and MRSA appears to have a synergistic effect, as infection with either pathogen on its own did not result in the loss of barrier integrity and dysregulated host response observed during co-infection. However, dysregulation of the host response seems to be driven primarily by the response of alveolar epithelial cells to both pathogens. This is contrary to what was observed in an alveolar cell line, which suggested that MRSA-alone infection resulted in a similar dysregulation as IAV-MRSA co-infection. This disparity could be due to a number of reasons. Primarily, there are a multitude of differences between the behaviour of primary differentiated cells and a cell line, indicating that the host response of HPAEpiCs may more closely reflect that found physiologically, though further investigations are needed to confirm this. Additionally, our co-culture model is able to reflect the crosstalk that is able to occur between the alveolar epithelial and microvascular endothelial cells at the alveolar-epithelial barrier.

Conclusion

Although bacteria can exacerbate influenza virus infections and result in increased morbidity and/or mortality, there is a paucity of information regarding the molecular mechanisms underlying the pathogenesis of co-infections. We hypothesize that secondary bacterial co-infections result in severe dysfunction of the alveolar-capillary barrier due to the modulation of bacterial virulence factor expression in the presence of IAV, thus leading to dysregulated host cell signaling responses. Our studies in A549s, an adenocarcinoma alveolar cell line, demonstrated that bacterial replication kinetics were similar in MRSA- and IAV-MRSA-infected cells. This similarity was independent of IAV strain, as demonstrated with H1N1 and H3N2 viruses, or type (i.e. pandemic or seasonal IAV). Further, the timing of bacterial infection in relation to IAV infection had no bearing on bacterial replication kinetics as no significant differences were found when MRSA infection occurred simultaneously with IAV infection or at peak viral replication. Despite this, we found that the expression of bacterial virulence factors specifically related to adhesion and invasion were significantly upregulated during the early course of co-infection. However, this upregulation quickly subsided during the exponential and stationary phase of MRSA infection. Our study of cell barrier integrity by ECIS using A549 cells cultured as a monolayer demonstrated loss of alveolar epithelial barrier function and integrity during MRSA-, and IAV-MRSA-infections. However, no loss of barrier function and integrity was observed when cells were infected alone with any of the four IAV strains we investigated. To further assess the dysregulation of A549 cells in the presence of IAV-MRSA, we analyzed the temporal host kinome response when pH1N1-MRSA co-infection occurs. We demonstrated that host cell signaling responses shifted from viral- to bacterial-centric throughout the course of co-infection with a transition phase in the response from 8-12 h post-

MRSA addition to pH1N1 infected cells. This related well to the loss of alveolar epithelial barrier function and integrity seen in our ECIS data.

As our prior investigations revealed that the severe disease pathogenesis observed in IAV-MRSA co-infections was mediated by the dysregulation of the host response, we next sought to investigate this in a co-culture model of the alveolar-capillary barrier. Further analysis of the bacterial response during co-infection in the co-culture model revealed similar findings as compared with co-infection in A549 cells. Bacterial replication kinetics were similar during MRSA- and IAV-MRSA-infection, and bacterial virulence factors were only significantly upregulated early in bacterial infection. However, investigation into the host response by kinome analysis revealed different results than those observed in our A549 cells. Barrier integrity and loss of function only occurred in the presence of both IAV and MRSA; no dysfunction was observed during infection with MRSA-alone or IAV-alone. This aligned with our analysis of the host kinome response of both alveolar epithelial cells and microvascular endothelial cells. Overrepresentation of a multitude of pathways, including those involved in TLR signaling, cell cycle, and cytokine signaling was seen when our epithelial cells underwent co-infection. However, few pathways were overrepresented in our epithelial cells when infected with IAV- or MRSA-alone , or in the underlying endothelial cells of the co-cultures regardless of their infection status. Lastly, investigation of cytokine expression in our co-culture model revealed the highest similarity of expression of cytokines in pH1N1- or pH1N1-MRSA-infection.

As a whole, our investigations revealed that the severe disease pathogenesis observed in IAV-MRSA co-infections is likely not due to the sustained modulation of MRSA in the presence of IAV. However, our kinome analysis suggests that pathogenesis likely correlates with dysregulated host responses specifically related to apoptosis and the cell cycle signaling in the

co-infected cells of the alveolar-capillary barrier, especially the response of the alveolar epithelial cells to co-infection.

Implications

This research presents a number of statistically significant upregulated bacterial virulence factors, which may be used as biomarkers of IAV-MRSA disease. Testing patient samples for these specific virulence factors may provide healthcare providers with an earlier disease biomarker, while also allowing healthcare providers a clue as to where in disease progression the patients is. For example, at 1 h post-MRSA infection, *eno, icaB, sek, and seq* are each significantly upregulated, whereas at 4 h post-infection, *hla, hlgA, icaA icaB* and *sek* are each significantly upregulated. This is especially important as co-infections present similarly to IAV infection alone, and early antibiotic treatment is directly correlated with survival [262]. Further, antibiotics which target these virulence factors specifically involved in the severe disease pathogenesis seen in IAV-MRSA co-infections could be developed. Further, as these antibiotics are not bactericidal, development should help combat the growing problem of antimicrobial resistance.

In the same vein, pathogen targeting approaches have inherent limitations, such as the growing problem of antimicrobial resistance and the constant evolution of influenza strains. This research has revealed a number of host pathways involved in cell maintenance during IAV-MRSA co-infection, which may provide a new therapeutic avenue instead of using antivirals or antibiotics. Targeting host pathways involved in maintenance of pulmonary host tolerance during infection could help mitigate any damage or changes caused by infection at the alveolar-capillary barrier. Further, alterations to homeostasis which occur during a disease state, such as tissue damage, inflammation, metabolic changes, and changes in respiration, are independent from pathogen burden. As such, targeting these host pathways may provide future directions for therapeutics aimed at a number of different infections, instead of only IAV-MRSA co-infections.

Future Directions

The development of our co-culture model of the alveolar-capillary barrier provides a physiologically-relevant model to study severe disease progression in the lower respiratory tract during IAV-bacterial infection. Further investigations of IAV-MRSA co-infections, using additional IAV strains or additional bacterial species associated with IAV co-infection, would help expand our understanding of infection-mediated pathogenesis observed at the alveolar-capillary barrier. Specifically, this model could be used to study how the relationship between MRSA and the 1918 H1N1 pandemic IAV strain affects the host response. Future studies concerning prior infection with the 1918 H1N1 IAV would expand our comprehension of the synergism between highly pathogenic IAV strains and secondary bacterial co-infections. Additionally, this may provide insight into why secondary bacterial co-infections occurred in 95% of fatal influenza cases during this pandemic [49, 260, 261]. Moreover, as the 1918 H1N1 strain is known to have played a part in each of the pandemics over the past century, a better understanding of this IAV strain may help prepare us for dealing with secondary bacterial co-infections in future pandemics [51].

In a similar respect, characterizing the differences in host response during secondary bacterial infection with additional bacterial strains may provide vital information concerning broad similarities in the mechanisms of co-infection pathogenesis. Further, this information could provide important information regarding novel host targets that could be targeted therapeutically to help reduce the pathology associated with secondary bacterial co-infections. In particular, the presence of *S. pneumoniae*, *S. pyogenes*, and *H. influenzae* have also been reported in fatal IAV cases [49, 260, 261]. Ultimately, these host response studies would allow for a better

understanding of how host response dysregulation occurs at a cellular level in a tissue- specific manner.

Lastly, introducing immune cells to this model, such as macrophages, neutrophils, and leukocytes may reveal key information in how IAV-bacterial co-infections are addressed at the alveolar-capillary barrier *in vivo*. For example, it is already known that leukocyte proliferation plays an important role in the host immune response and is critical for the clearance of influenza infection [424]. It is also known that the presence of macrophages and neutrophils at the site of lung injury generally results in a greater burden of disease [417]. Prior studies have shown that alveolar macrophages and neutrophils produce proteases and miRNAs directly involved in degradation of tight junctions, pulmonary inflammation, and tissue damage [300, 301, 304]. ZO-1 degradation by macrophages has specifically has been implicated in a loss of alveolar-capillary barrier integrity [301]. As our study of tight junction degradation was inconclusive, the addition of these cells may further clarify how tight junction degradation occurs in IAV-MRSA co-infection, as reported by other studies [280]. Introduction of these immune cells to our model would allow us to further discern the mechanism of action in severe disease pathogenesis.

References

1. Kash JC, Taubenberger JK: **The Role of Viral, Host, and Secondary Bacterial Factors in Influenza Pathogenesis**. *Am J Pathol* 2015, **185**(6).
2. Saunders-Hastings PR, Krewski D: **Reviewing the History of Pandemic Influenza: Understanding Patterns of Emergence and Transmission**. *Pathogens* 2016, **5**(66).
3. Krammer F, Smith GJD, Fouchier RAM, Peiris M, Kedzierska K, Doherty PC, Palese P, Shaw ML, Treanor J, Webster RG *et al*: **Influenza**. *Nat Rev* 2018, **4**(3).
4. Horimoto T, Kawaoka Y: **Influenza: Lessons from Past Pandemics, Warnings From Current Incidents**. *Nat Rev Microbiol* 2005, **3**.
5. Su S, Fu X, Li G, Kerlin F, Veit M: **Novel Influenza D virus: Epidemiology, pathology, evolution and biological characteristics**. *Virulence* 2017, **8**(8).
6. Breen M, Nogales A, Baker SF, Martinez-Sobrido L: **Replication-Competent Influenza A Viruses Expressing Reporter Genes**. *Viruses* 2016, **8**(7).
7. Kash JC, Goodman AG, Korth MJ, Katze MG: **Hijacking of the host-cell response and translational control during influenza virus infection**. *Virus Res* 2006, **119**(1).
8. Shapira SD, Gat-Viks I, Shum BOV, Dricot A, Degrace MM, Liguo W, Gupta PB, Hao T, Silver SJ, Root DE *et al*: **A physical and regulatory map of host-influenza interactions reveals pathways in H1N1 infection**. *Cell* 2009, **139**(7).
9. Taubenberger JK, Morens DM: **The Pathology of Influenza Virus Infections**. *Annu Rev Pathol* 2008, **3**.
10. Mehle A: **Unusual Influenza A Viruses in Bats**. *Viruses* 2014, **6**(9).

11. Atkin-Smith GK, Duan M, Chen W, Poon IKH: **The induction and consequences of Influenza A virus-induced cell death**. *Cell Death Dis* 2018, **9**(10).

12. te Velthuis AJW, Fodor E: **Influenza virus RNA polymerase: insights into the mechanisms of viral RNA synthesis**. *Nature Reviews Microbiology* 2016, **14**.

13. van Dijk JGB, Verhagen JH, Wille M, Waldenström J: **Host and virus ecology as determinants of influenza A virus transmission in wild birds**. *Curr Opin Virol* 2018, **28**.

14. Monne I, Fusaro A, Nelson MI, Bonfanti L, Mulatti P, Hughes J, Murcia PR, Schivo A, Valastro V, Moreno A *et al*: **Emergence of a highly pathogenic avian influenza virus from a low-pathogenic progenitor**. *J Virol* 2014, **88**(8).

15. Röhm C, Horimoto T, Kawaoka Y, Süss J, Webster RG: **Do hemagglutinin genes of highly pathogenic avian influenza viruses constitute unique phylogenetic lineages?** *Virology* 1995, **209**(2).

16. Banks J, Speidel ES, Moore E, Plowright L, Piccirillo A, Capua I, Cordiolo P, Fioretti A, Alexander DJ: **Changes in the haemagglutinin and the neuraminidase genes prior to the emergence of highly pathogenic H7N1 avian influenza viruses in Italy**. *Arch Virol* 2001, **146**(5).

17. Banks J, Speidel ES, McCauley JW, Alexander DJ: **Phylogenetic analysis of H7 haemagglutinin subtype influenza A viruses**. *Arch Virol* 2000, **145**.

18. Horimoto T, Rivera E, Pearson J, Seene D, Krauss S, Kawaoka Y, Webster RG: **Origin and molecular changes associated with emergence of a highly pathogenic H5N2 influenza virus in Mexico**. *Virology* 1995, **213**.

19. Garcia M, Crawford JM, Latimer JW, Rivera-Cruz E, Perdue ML: **Heterogeneity in the haemagglutinin gene and emergence of the highly pathogenic phenotype among recent H5N2 avian influenza viruses from Mexico**. *J Gen Virol* 1996, **77**.

20. Spackman E, Senne DA, Davison S, Suarez DL: **Sequence analysis of recent H7 influenza viruses associated with three different outbreaks in commercial poultry in the United States**. *J Virol* 2003, **77**.

21. Suarez DL, Senne DA, Banks J, Brown IH, Essen SC, Lee CW, Manvell RJ, Mathieu-Benson C, Moreno V, Pedersen JC *et al*: **Recombination resulting in virulence shift in avian influenza outbreak, Chile**. *Emerg Infect Dis* 2004, **10**.

22. Pasick J, Handel K, Robinson J, Copps J, Ridd D, Hills K, Kehler H, Cottam-Birt C, Neufeld J, Berhane Y *et al*: **Intersegmental recombination between the haemagglutinin and matrix genes was responsible for the emergence of a highly pathogenic H7N3 avian influenza virus in British Columbia**. *J Gen Virol* 2005, **86**.

23. Maurer-Stroh S, Lee RT, Gunalan V, Eisenhaber F: **The highy pathogenic H7N3 avian influenza strain from July 2012 in Mexico acquired an extended cleavage site through recombination with host 28S rRNA**. *Virol J* 2013, **10**.

24. **Highly Pathogenic Avian Influenza**. In. http://www.cfsph.iastate.edu/DiseaseInfo/disease.php?name=avian-influenza&lang=en.

25. **What Will The Next Influenza Pandemic Look Like?** . In. https://www.scientificamerican.com/article/next-influenza-pandemic/.

26. **Centers for Disease Control and Prevention. Asian Lineage Avian Influenza A (H7N9) Virus** In. https://www.cdc.gov/flu/avianflu/h7n9-virus.htm.

27. Horimoto T, Kawaoka Y: **Pandemic threat posed by avian influenza A viruses**. *Clin Microbiol Rev* 2001, **14**(1).

28. Richard M, Fouchier RAM: **Influenza A virus transmission via respiratory aerosols or droplets as it relates to pandemic potential**. *FEMS Microbiol Rev* 2015, **40**(1).

29. Neumann G, Kawaoka Y: **Transmission of Influenza A Viruses**. *Virology* 2015, **0**.

30. England PH: **Chapter 19: Influenza**. In: *Immunisation Against Infectious Disease.* edn.; 2013.

31. Honce R, Schultz-Cherry S: **Impact of Obesity on Influenza A Virus Pathogenesis, Immune Response, and Evolution**. *Front Immunol* 2019, **10**(1071).

32. Sellers SA, Hagan RS, Hayden FG, Fischer WA: **The hidden burdern of influenza: A review of the extra-pulmonary complications of influenza infection**. *Influenza Other Respir Viruses* 2017, **11**(5).

33. Ghebrehewet S, MacPherson P, Ho A: **Influenza**. *BMJ* 2016, **355**(i6258).

34. Ampomah PB, Kong WT, Zharkova O, Chua SCJH, Samy RP, Lim LHK: **Annexins in Influenza Virus Replication and Pathogenesis**. *Front Pharmacol* 2018.

35. Wareing MD, Lyon AB, Lu B, Gerard C, Sarawar SR: **Chemokine expression during the development and resolution of a pulmonary leukocyte response to influenza A virus infection in mice**. *Journal of Leukocyte Biology* 2004, **76**(4).

36. Hayden FG, Fritz RS, Lobo MC, Alvord WG, Strober W, Straus SE: **Local and systemic cytokine responses during experimental human influenza A virus infection. Relation to Symptom Formation and Host Defense**. *J Clin Invest* 1998, **101**(3).

37. Salihefendic N, SZildzic M, Ahmetagic S: **Acute Respiratory Distress Syndrome (ARDS) from Endemic Influenza A/H1N1: Prehospital Management**. *Med Arch* 2015, **69**(1).

38. Ragaller M, Richter T: **Acute lung injury and acute respiratory distress syndrome**. *J Emerg Trauma Shock* 2010, **3**(1).

39. Homsi S, Milojkovic N, Homsi Y: **Clinical Pathological Characteristics and Management of Acute Respiratory Distress Syndrome Resulting from Influenza (H1N1) Virus**. *South Med J* 2010, **103**(8).

40. **Influenza**

41. **Canadian Immunization Guide Chapter on Influenza and Statement on Seasonal Influenza Vaccine for 2018-2019** [https://www.canada.ca/en/public-health/services/publications/healthy-living/canadian-immunization-guide-statement-seasonal-influenza-vaccine-2018-2019.html#4]

42. Public Health Agency of Canada: **Seasonal Influenza Vaccine Coverage in Canada, 2017-2018**. In.; 2017.

43. Pielak RM, Chou JJ: **Influenza M2 proton channels.** *Biochim Biophys Acta* 2011, **1808**(2).

44. Pielak RM, Schnell JR, Chou JJ: **Mechanism of drug inhibition and drug resistance of influenza A M2 channel.** *Proc Natl Acad Sci U S A* 2009, **106**(18).

45. McKimm-Breschkin JL: **Influenza meuraminidase inhibitors: antiviral action and mechanisms of resistance**. *Influenza Other Respir Viruses* 2013, **7**.

46. Nickol ME, Kindrachuk J: **A year of terror and a century of reflection: perspectives on the great influenza pandemic of 1918-1919**. *BMC Infect Dis* 2019, **19**(117).

47. Kempińska-Mirosławska B, Woźniak-Kosek A: **The influenza epidemic of 1889-90 in selected European cities - a picture based on the reports of two Poznań daily newspapers from the second half of the nineteenth century**. *Medical Science Monitor* 2013, **19**.

48. Valleron AJ, Cori A, Valtat S, Meurisse S, Carrat F, Boëlle PY: **Transmissibility and geographic spread of the 1889 influenza pandemic**. *Proc Natl Acad Sci U S A* 2010, **107**(19).

49. McCullers JA: **The co-pathogenesis of influenza viruses with bacteria in the lung.** *Nat Rev Microbiol* 2014, **12**(4).

50. Tumpey TM, Basier CF, Aguilar PV, Zeng H, Solórzano A, Swayne DE, Cox NJ, Katz JM, Taubenberger JK, Palese P *et al*: **Characterization of the reconstructed 1918 Spanish influenza pandemic virus**. *Science* 2005, **310**(5745).

51. Taubenberger JK, Morens DM: **1918 Influenza: the mother of all pandemics**. *Emerg Infect Dis* 2006, **12**(1):15-22.

52. Radusin M: **The Spanish flu—part II: the second and third wave**. *Vojnosanit Pregl* 2012, **69**(10).

53. Humphries MO: **Paths of Infection: The First World War and the Origins of the 1918 Influenza Pandemic**. *War Hist* 2013, **21**.

54. Barry JM: **The site of origin of the 1918 influenza pandemic and its public health implications**. *J Transl Med* 2004, **2**(1).

55. Radusin M: **The Spanish flu—part I: the first wave**. *Vojnosanit Pregl* 2012, **69**(9).

56. Henderson DA, Courtney B, Inglesby TV, Toner E, Nuzzo JB: **Public health and medical responses to the 1957-58 influenza pandemic**. *Biosecur Bioterror* 2009, **7**(3).

57. Viboud C, Simonsen L, Fuentes R, Flores J, Miller MA, Chowell G: **Global Mortality Impact of the 1957-1959 Influenza Pandemic**. *J Infect Dis* 2015, **213**.

58. Pyle GF: **The diffusion of influenza: patterns and paradigms**. New Jersey: Rowan & Littlefield; 1986.

59. Stryjewski ME, Corey GR: **Methicillin-Resistant *Staphyloccocus aureus*: An Evolving Pathogen**. *Clin Infect Dis* 2014, **58**.

60. Gajdacs M: **The Continuing Threat of Methicillin-Resistant *Staphylococcus aureus***. *Antibiotics* 2019, **8**(2).

61. Shaddix G, Patel K, Simmons M, Burner K: **Successful Clearance of Persistent Methicillin-Resistant *Staphylococcus aureus* Bacteremia with Daptomycin, Linezolid, and Meropenem Salvage Therapy**. *Case Rep Infect Dis* 2019, **2019**.

62. Kong E, Johnson JK, Jabra-Rizk MA: **Community-Associated Methicillin-Resistant Staphylococcus aureus: An Enemy amidst Us**. *PLoS Pathog* 2016, **12**(10).

63. Yilmaz ES, Aslantas O: **Antimicrobial resistance and underlying mechanisms in *Staphylococcus aureus* isolates**. *Asian Pacific Journal of Tropical Medicine* 2017, **10**(11).

64. Peacock SJ, Paterson GK: **Mechanisms of Methicillin Resistance in *Staphyloccocus aureus***. *Annu Rev Biochem* 2015, **84**.

65. Stapleton PD, Taylor PW: **Methicillin resistance in *Staphylococcus aureus***. *Sci Prog* 2002, **85**.

66. Labischinski H: **Consequences of the interaction of beta-lactam antibiotics with penicillin binding proteins from sensitive and resistant Staphylococcus aureus strains**. *Med Microbiol Immunol* 1992, **181**(5).

67. Chambers HF: **Methicillin resistance in staphylococci: molecular and biochemical basis and clinical implications**. *Clin Microbiol Rev* 1997, **10**(4).

68. Baddiley J: **Bacterial cell walls and membranes. Discovery of the teichoic acids**. *Bioessays* 1989, **10**(6).

69. Mistretta N, Brossaud M, Telles F, Sanchez V, Talaga P, Rokbi B: **Glycosylation of *Staphylococcus aureus* cell wall teichoic acid is influenced by environmental conditions**. *Sci Rep* 2019, **9**.

70. Baur S, Rautenberg M, Faulstich M, Grau T, Severin Y, Unger C, Hoffmann WH, Rudel T, Autenrieth IB, Weidenmaier C: **A nasal epithelial receptor for Staphylococcus aureus WTA governs adhesion to epithelial cells and modulates nasal colonization**. *PLoS Pathog* 2014, **10**(5).

71. Misawa Y, Kelley KA, Wang X, Wang L, Park WB, Birtel J, Saslowsky D, Lee JC: **Staphylococcus aureus Colonzation of the Mouse Gastrointestinal Tract Is Modulated by Wall Teichoic Acid, Capsule, and Surface Proteins**. *PLoS Pathog* 2015, **11**(7).

72. Atilano ML, Pereira PM, Yates J, Reed P, Veiga H, Pinho MG, Filipe SR: **Teichoic acids are temporal and spatial regulators of peptidoglycan cross-linking in *Staphylococcus aureus***. *PNAS* 2010, **107**(44).

73. Wanner S, Schade J, Keinhörster D, Weller N, George SE, Kull L, Bauer J, Grau T, Winstel V, Stoy H *et al*: **Wall teichoic acids mediate increased virulence in Staphylococcus aureus**. *Nat Microbiol* 2017, **23**.

74. Mazmanian SK, Ton-That H, Schneewind O: **Sortase-catalysed anchoring of surface proteins to the cell wall of Staphylococcus aureus**. *Mol Microbiol* 2001, **40**(5).

75. Perry AM, Ton-That H, Mazmanian SK, Schneewind O: **Anchoring of Surface Proteins to the Cell Wall of *Staphylococcus aureus***. *J Biol Chem* 2002, **277**.

76. Becker S, Frankel MB, Schneewind O, Missiakas D: **Release of protein A from the cell wall of *Staphylococcus aureus***. *Proc Natl Acad Sci U S A* 2014, **111**(4).

77. Kuipers A, Stapels DAC, Weerwind LT, Ko YP, Ruyken M, Lee JC, van Kessel KPM, Rooijakkers SHM: **The *Staphylococcus aureus* polysaccharide capsule and Efb-dependent fibrinogen shield act in concert to protect against phegocytosis**. *Microbiol* 2016, **162**(7).

78. van Kessel KP, Bestebroer J, van Strijp JA: **Neutrophil-Mediated Phagocytosis of Staphylococcus aureus**. *Front Immunol* 2014, **5**(467).

79. Chan YG, Kim HK, Schneewind O, Missiakas D: **The Capsular Polysccharide of *Staphylococcus aureus* Is Attached to Peptidoglycan by the LytR-CpsA-Psr (LCP) Family of Enzymes**. *J Biol Chem* 2014, **289**.

80. Arbeit RD, Karakawa WW, Vann WF, Robbins JB: **Predominance of two newly described capsular polysaccharide types among clinical isolates of *Staphylococcus aureus***. *Diagn Microbiol Infect Dis* 1984, **2**(2).

81. von Eiff C, Taylor KL, Mellmann A, Fattom AI, Friedrich AW, Peters G, Becker K: **Distribution of capsular and surface polysaccharide serotypes of *Staphylococcus aureus***. *Diagn Microbiol Infect Dis* 2007, **58**(3).

82. Labandeira-Rey M, Couzon F, Boisset S, Brown EL, Bes M, Benito Y, Barbu EM, Vazquez V, Höök M, Etienne J *et al*: **Staphylococcus aureus Panton-Valentine leukocidin causes necrotizing pneumonia**. *Science* 2007, **315**(5815).

83. Montgomery CP, Boyle-Vavra S, Adem PV, Lee JC, Husain AN, Clasen J, Daum RS: **Comparison of virulence in community-associated methicillin-resistant Staphylococcus aureus pulsotypes USA300 and USA400 in a rat model of pneumonia**. *J Infect Dis* 2008, **198**(4).

84. Vandenesch F, Lina G, Henry T: ***Staphylococcus aureus* Hemolysins, bi-component Leukocidins, and Cytolytic Peptides: A Redundant Arsenal of Membrane-Damging Virulence Factors?** *Front Cell Infect Microbiol* 2012, **2**(12).

85. Venkatasubramaniam A, Kanipakala T, Ganjbaksh N, Mehr R, Mukherjee I, Krishnan S, Bae T, Aman MJ, Adhikari RP: **A Critical Role for HlgA in *Staphylococcus aureus* Pathogenesis Revealed by A Switch in the SaeRS Two-component Regulatory System**. *Toxins* 2018, **10**(9).

86. Jenkins A, Diep BA, Mai TT, Vo NH, Warrener P, Zuzich J, Stover CK, Sellman BR: **Differential Expression and Roles of *Staphylococcus aureus* Virulence Determinants during Colonization and Disease**. *mBio* 2015, **6**(1).

87. Date SV, Modrusan Z, Lawrence M, Morisaki JH, Toy K, Shah IM, Kim J, Park S, Xu M, Basuino L *et al*: **Global gene expression of methicillin-resistant Staphylococcus aureus USA300 during human and mouse infection**. *J Infect Dis* 2014, **209**(10).

88. Spaan AN, Vrieling M, Wallet P, Badiou C, Reyes-Robles T, Ohneck EA, Benito Y, de Haas CJC, Day CJ, Jennings MP *et al*: **The staphylococcal toxins γ-haemolysin AB and CB differentially target phagocytes by employing specific chemokine receptors**. *Nat Commun* 2014, **5**.

89. Alonzo III F, Torres VJ: **The bicomponent pore-forming leucocidins of Staphylococcus aureus**. *Microbiol Mol Biol Rev* 2014, **78**(2).

90. Spaan AN, van Strijp JA, Torres VJ: **Leukocidins: staphylococcal bi-component pore-forming toxins find their receptors**. *Nat Rev Microbiol* 2017, **15**(7).

91. Spaan AN, Reyes-Robles T, Badiou C, Cochet S, Bogulawski KM, Yoong P, Day CJ, de Haas CJ, van Kessel KP, Vandenesch F *et al*: **Staphylococcus aureus Targets the Duffy Antigen Receptor for Chemokines (DARC) to Lyse Erythrocytes**. *Cell Host Microbe* 2015, **18**(3).

92. Kong C, Chee CF, Richter K, Thomas N, Rahman NA, Nathan S: **Suppression of *Staphylococcus aureus* biofilm formation and virulence by a benzimidazole derivative, UM-C162**. *Sci Rep* 2018, **8**.

93. Kumar S, Ménoret A, Ngoi SM, Vella AT: **The Systemic and Pulmonary Immune Response to Staphylococcal Enterotoxins**. *Toxins* 2010, **2**(7).

94. Pinchuk IV, Beswick EJ, Reyes VE: **Staphylococcal Enterotoxins**. *Toxins* 2010, **2**(8).

95. Cue D, Lei MG, Lee CY: **Genetic regulation of the intercellular adhesion locus in staphylococci**. *Front Cell Infect Microbiol* 2012.

96. Heilmann C, Schweitzer O, Gerke C, Vanittanakom N, Mack D, Götz F: **Molecular basis of intercellular adhesion in the biofilm-forming Staphylococcus epidermis**. *Mol Microbiol* 1996, **20**(5).

97. Cramton SE, Gerke C, Schnell NF, Nichols WW, Götz F: **The Intercellular Adhesion (*ica*) Locus Is Present in *Staphylococcus aureus* and Is Required for Biofilm Formation**. *Infect Immun* 1999, **67**(10).

98. Merino N, Toledo-Arana A, Vergara-Irigaray M, Valle J, Salona C, Calvo E, Lopez JA, Foster TJ, Penadés JR, Lasa I: **Protein A-mediated multicellular behavior in Staphylococcus aureus**. *J Bacteriol* 2009, **191**(3).

99. O'Neill E, Pozzi C, Houston P, Humphreys H, Robinson DA, Loughman A, Foster TJ, O'Gara JP: **A novel Staphylococcus aureus biofilm phenotype mediated by the fibronectin-binding proteins, FnBPA and FnBPB**. *J Bacteriol* 2008, **190**(11).

100. Sinha B, François PP, Nüsse O, Foti M, Hartford OM, Vaudaux P, Foster TJ, Lew DP, Hermann M, Krause KH: **Fibronectin-binding protein acts as Staphylococcus aureus invasin via fibronectin bridging to integrin alpha5beta1**. *Cell Microbiol* 1999, **1**(2).

101. Sinha B, Francois P, Que YA, Hussain M, Heilmann C, Moreillon P, Lew DP, Krause KH, Peters G, Herrmann M: **Heterologously expressed Staphylococcus aureus fibronectin-binding proteins are sufficient for invasion of host cells**. *Infect Immun* 2000, **68**(12).

102. Fowler T, Wann ER, Joh D, Johansson S, Foster TJ, Höök M: **Cellular invasion by Staphylococcus aureus involves a fibronectin bridge between the bacterial fibronectin-binding MSCRAMMs and host cell beta1 integrins**. *Eur J Cell Biol* 2000, **79**(10).

103. Massey RC, Kantzanou MN, Fowler T, Day NP, Schofield K, Wann ER, Berendt AR, Höök M, Peacock SJ: **Fibronectin-binding protein A of Staphylococcus aureus has multiple, substituting, binding regions that mediate adherence to fibronectin and invasion of endothelial cells**. *Cell Microbiol* 2001, **3**(12).

104. Josse J, Laurent F, Diot A: **Staphylococcal Adhesion and Host Cell Invasion: Fibronectin-Binding and Other Mechanisms**. *Front Microbiol* 2017, **8**.

105. Wertheim HF, Walsh E, Choudhurry R, Melles DC, Boelens HA, Miajlovic H, Verbrugh HA, Foster T, van Belkum A: **Key role for clumping factor B in Staphylococcus aureus nasal colonization of humans**. *PLoS Med* 2008, **5**(1).

106. Smith EJ, Corrigan RM, van der Sluis T, Gruendling A, Speziale P, Geoghegan JA, Foster TJ: **The immune evasion protein Sbi of *Staphylococcus aureus* occurs both extracellulary and anchored to the cell envelope by binding lipoteichoic acid**. *Mol Microbiol* 2012, **83**.

107. Weidenmaier C, Goerke C, Wolz C: **Staphylococcus aureus determinants for nasal colonzation**. *Trends Microbiol* 2012, **20**(5).

108. Downer R, Roche F, Park PW, Mecham RP, Foster TJ: **The elastin-binding protein of Staphyloccocus aureus (EbpS) is expressed at the cell surface as an integral membrane protein and not as a cell wall-associated protein**. *J Biol Chem* 2002, **277**(1).

109. Lähteenmäki K, Edelman S, Korhonen TK: **Bacterial metastasis: the host plasminogen system in bacterial invasion**. *Trends Microbiol* 2005, **13**(2).

110. Bergmann S, Rohde M, Chhatwal GS, Hammerschmidt S: **alpha-Enolase of *Streptococcus pneumoniae* is a plasmin(ogen)-binding protein displayed on the bacterial cell surface**. *Mol Microbiol* 2001, **40**.

111. Carneiro CR, Postol E, Nomizo R, Reis LF, Brentani RR: **Identification of enolase as a laminin-binding protein on the surface of *Staphylococcus aureus***. *Microbes Infect* 2004, **6**.

112. Pancholi V, Chhatwal GS: **Housekeeping enzymes as virulence factors for pathogens**. *Int J Med Microbiol* 2003, **293**.

113. Ko YP, Kuipers A, Freitag CM, Jongerius I, Medina E, van Rooijen WJ, Spaan AN, van Kessel KP, Höök M, Rooijakkers SH: **Phagocytosis escape by a Staphylococcus aureus**

protein that connects complement and coagulation proteins at the bacterial surface. *PLoS Pathog* 2013, **9**(12).

114. Cheng AG, McAdow M, Kim HK, Bae T, Missiakas DM, Schneewind O: **Contribution of Coagulases towards *Staphylococcus aureus* Disease and Protective Immunity**. *PLoS Pathog* 2010.

115. Ko YP, Kang M, Ganesh VK, Ravirajan D, Li B, Höök M: **Coagulase and Efb of *Staphylococcus aureus* Have a Common Fibrinogen Binding Motif**. *MBio* 2016, **7**(1).

116. Smith EJ, Visai L, Kerrigan SW, Speziale P, Foster TJ: **The Sbi protein is a multifunctional immune evasion factor of Staphylococcus aureus**. *Infect Immun* 2011, **79**(9).

117. Zhang L, Jacobsson K, Vasi J, Lindberg M, Frykberg L: **A second IgG-binding protein in Staphylococcus aureus** *Microbiol* 1998, **144**.

118. Atkins KL, Burman JD, Chamberlain ES, Cooper JE, Poutrel B, Bagby S, Jenkins AT, Feil EJ, van den Elsen JM: **S. aureus IgG-binding proteins SpA and Sbi: host specificity and mechanisms of immune complex formation**. *Mol Immunol* 2008, **45**(6).

119. Peterson PK, Verhoef J, Sabath LD, Quie PG: **Effect of protein A on staphylococcal opsonization**. *Infect Immun* 1977, **15**(3).

120. Spratt BG: **Resistance to antibiotics mediated by target alterations**. *Science* 1994, **264**(5157).

121. McDermott PF, Walker RD, White DG: **Antimicrobials: modes of action and mechanisms of resistance**. *Int J Toxicol* 2003, **22**(2).

122. Magnet S, Blanchard JS: **Molecular insights into aminoglycoside action and resistance**. *Chem Rev* 2005, **105**(2).

123. Wright GD: **Bacterial resistance to antibiotics: enzymatic degradation and modification**. *Adv Drug Deliv Rev* 2005, **57**(10).

124. **Trends and Changes in Drug Research and Development**: Springer Science & Business Media; 2012.

125. Jevons MP: **"Celbenin"-resistant Staphylococci**. *Br Med J* 1961, **1**(5219).

126. Jevons MP, Coe AW, Parker MT: **Methicillin Resistance in Staphylococci**. *Lancet* 1963, **281**(7287).

127. Barber M: **Methicillin-resistant Staphylococci**. *J Clin Pathol* 1961, **14**.

128. Giesbrecht P, Kersten T, Maidhof H, Wecke J: **Staphylococcal cell wall: morphogenesis and fatal variations in the presence of penicillin**. *Microbiol Mol Biol Rev* 1998, **62**(4).

129. Walsh C: **Where will new antibiotics come from?** *Nat Rev Microbiol* 2003, **1**(1).

130. Walsh C: **Molecular mechanisms that confer antibacterial drug resistance**. *Nature* 2000, **406**(6797).

131. Wu SW, de Lencastre H, Tomasz A: **Recruitment of the mecA gene homologue of Staphylococcus sciuri into a resistance determinant and expression of the resistant phenotype in Staphylococcus aureus**. *J Bacteriol* 2001, **183**(8).

132. Katayama Y, Ito T, Hiramatsu K: **A new class of genetic element, staphylococcus cassette chromosome mec, encodes methicillin resistance in Staphylococcus aureus**. *Antimicrob Agents Chemother* 2000, **44**(6).

133. Rodvold KA, McConeghy KW: **Methicillin-resistant *Staphylococcus aureus* therapy: past, present, and future**. *Clin Infect Dis* 2014, **58**.

134. Stryjewski ME, Corey GR: **Methicillin-resistant *Staphylococcus aureus*: an evolving pathogen**. *Clin Infect Dis* 2014, **58**.

135. Kos VN, Desjardins CA, Griggs A, Cerqueira G, Van Tonder A, Holden MTG, Godfrey P, Palmer KL, Bodi K, Mongodin EF *et al*: **Comparative genomics of vancomycin-resistant *Staphylococcus aureus* strains and their positions within the clade most commonly associated with methicillin-resistant *S. aureus* hospital-acquired infection in the United States**. *MBio* 2012, **3**.

136. Gould IM, David MZ, Esposito S, Garau J, Lina G, Mazzei T, Peters G: **New insights into methicillin-resistant *Staphylococcus aureus* (MRSA) pathogenesis, treatment, and resistance**. *Int J Antimicrob Agents* 2012, **39**.

137. Yu Z, Xheng L, Junshu Y, Ting L, Yinduo J: **Characterization of essential enolase in Staphylococcus aureus**. *World J Microbiol Biotchenol* 2011, **27**(4).

138. Carrel M, Perencevich EN, David MZ: **USA300 Methicillin-Resistant *Staphylococcus aureus*, United States, 2000-2013**. *Emerg Infect Dis* 2015, **21**(11).

139. Centers for Disease Control and Prevention: **Methicillin-resistant staphylococcus aureus infections among competitive sports-participants—Colorado, Indiana, Pennsylvania, and Los Angeles County, 2000-2003**. *MMWR Morb Mortal Wkly Rep* 2003, **52**(33).

140. Tenover FC, Goering RV: **Methicillin-resistant *Staphylococcus aureus* strain USA300: origin and epidemiology**. *J Antimicrob Chemother* 2009, **64**(3).

141. Kwong JC, Chua K, Charles PG: **Managing Severe Community-Acquired Pneumonia Due to Community Methicillin-Resistant Staphylococcus aureus (MRSA)**. *Curr Infect Dis Rep* 2012, **14**(3).

142. McDougal LK, Fosheim GE, Nicholson A, Bulens SN, Limbago BM, Shearer JES, Summers AO, Patel JB: **Emergence of resistance among USA300 MRSA isolates causing invasive disease in the United States**. *Antimicrob Agents Chemother* 2010, **54**.

143. Moran GJ, Krishnadasan A, Gorwitz RJ, Fosheim GE, McDougal LK, Carey RB, Talan DA: **Methicillin-Resistant *S. aureus* Infections among Patients in the Emergency Department**. *N Engl J Med* 2006, **355**.

144. Diekema DJ, Richter SS, Heilmann KP, Dohm CL, Riahi F, Tendolkar S, McDanel JS, Doern GV: **Continued Emergence of USA300 Methicillin-Resistant *Staphylococcus aureus* in the United States: Results from a Nationwide Surveillance Study**. *Infect Control Hosp Epidemiol* 2014, **35**(3).

145. Bartlett JG: **Methicillin-Resistant *Staphylococcus aureus* Infections**. *Top HIV Med* 2008, **16**(5).

146. Boakes E, Kearns AM, Ganner M, Perry C, Hill RL, Ellington MJ: **Distinct Bacteriophages Encoding Panton-Valentine Leukocidin (PVL) among International Methicillin-Resistant *Staphylococcus aureus* Clones Harboring PVL**. *J Clin Microbiol* 2011, **49**(2).

147. Brown ML, O'Hara FP, Close NM, Mera RM, Miller LA, Suaya JA, Amrine-Madsen H: **Prevalence and Sequence Variation of Panton-Valentine Leukocidin in Methicillin-Resistant and Methicillin-Susceptible *Staphylococcus aureus* Strains in the United States**. *J Clin Microbiol* 2012, **50**(1).

148. Olsen RJ, Kobayashi SD, Ayeras AA, Ashraf M, Graves SF, Ragasa W, Humbird T, Greaver JL, Cantu C, Swain JL *et al*: **Lack of a major role of Staphylococcus aureus**

Panton-Valentine leukocidin in lower respiratory tract infection in nonhuman primates. *Am J Pathol* 2010, **176**(3).

149. Chua T, Moore CL, Perri MB, Donabedian SM, Masch W, Vager D, Davis SL, Lulek K, Zimnicki B, Zervos MJ: **Molecular epidemiology of methicillin-resistant Staphylococcus aureus bloodstream isolates in urban Detroit**. *J Clin Microbiol* 2008, **46**(7).

150. David MZ, Daum RS: **Community-associated methicillin-resistant Staphylococcus aureus: epidemiology and clinical consequences of an emerging epidemic**. *Clin Microbiol Rev* 2010, **23**(6).

151. Genestier AL, Michallet MC, Prévost G, Bellot G, Chalabreysse L, Peyrol S, Thivolet F, Etienne J, Lina G, Vallette FM *et al*: **Staphylococcus aureus Panton-Valentine leukocidin directly targets mitochondria and induces Bax-independent apoptosis of human neutrophils**. *J Clin Invest* 2005, **115**(11).

152. Voyich JM, Otto M, Mathema B, Braughton KR, Whitney AR, Welty D, Long RD, Dorward DW, Gardner DJ, Lina G *et al*: **Is Panton-Valentine leukocidin the major virulence determinant in community-associated methicillin-resistant Staphylococcus aureus disease?** *J Infect Dis* 2006, **194**(12).

153. Tenover FC, McDougal LK, Goering RV, Kiligore G, Projan SJ, Patel JB, Dunman PM: **Characterization of a strain of community-associated methicillin-resistant Staphylococcus aureus widely disseminated in the United States**. *J Clin Microbiol* 2006, **44**(1).

154. Han LL, McDougal LK, Gorwitz RJ, Mayer KH, Patel JB, Sennott JM, Fontana JL: **High frequencies of clindamycin and tetracycline resistance in methicillin-resistant**

Staphylococcus aureus pulsed-field type USA300 isolates collected at a Boston ambulatory health center. *J Clin Microbiol* 2007, **45**(4).

155. Shore AC, Coleman DC: **Staphylococcal cassette chromosome mec: recent advances and new insights**. *Int J Med Microbiol* 2013, **303**(6-7).

156. Reichmann NT, Pinho MG: **Role of SCC*mec* type in resistance to the synergistic activty of oxacillin and cefoxitin**. *Sci Rep* 2017, **7**.

157. Rubinstein E, Kollef MH, Nathwani D: **Pneumonia Caused by Methicillin-Resistant *Staphylococcus aureus***. *Clin Infect Dis* 2008, **46**.

158. DeRyke CA, Lodise Jr TP, Rybak MJ, McKinnon PS: **Epidemiology, treatment, and outcomes of nosocomial bacteremic Staphylococcus aureus pnuemonia**. *Chest* 2005, **128**(3).

159. Nichol KA, Adam HJ, Roscoe DL, Golding GR, Lagacé-Wiens PR, Hoban DJ, Zhanel GG: **Changing epidemiology of methicillin-resistant Staphylococcus aureus in Canada**. *J Antimicrob Chemother* 2013, **68**.

160. Achiam CC, Fernandes CM, McLeod SL, Salvadori MI, John M, Seabrook JA, Theakston KD, Milburn S, Hussain Z: **Methicillin-resistant Staphylococcus aureus in skin and soft tissue infections presenting to the Emergency Department of a Canadian Academic Health Care Center**. *Eur J Emerg Med* 2011, **18**(1).

161. Harrison B, Ben-Amotz O, Sammer DM: **Methicillin-resistant Staphylococcus aureus infection in the hand**. *Plast Reconstr Surg* 2015, **135**(3).

162. Nichol KA, Adam HJ, Hussain Z, Mulvey MR, McCracken M, Mataseje LF, Thompson K, Kost S, Lagacé-Wiens PR, Hoban DJ *et al*: **Comparison of community-associated**

and health care-associated methicillin-resistant Staphylococcus aureus in Canada: results of the CANWARD 2007-2009 study. *Diagn Microbiol Infect Dis* 2011, **69**(3).

163. **Environmental management of Staph and MRSA in community settings** [http://www.djj.state.fl.us/docs/health- services/environmental-management-of-mrsa.pdf?sfvrsn=0]

164. **Methicillin-resistant *Staphylococcus aureus* (MRSA): General Information** [https://www.cdc.gov/mrsa/community/index.html]

165. Pham J, Asif T, Hamarshi MS: **Community-acquired Pneumonia with Methicillin-resistant Staphylococcus Aureus in a Patient Admitted to the Intensive Care Unit: A Therapeutic Challenge**. *Cureus* 2018, **10**(1).

166. Gillet Y, Issartel B, Vanhems P, Fournet JC, Lina G, Bes M, Vandenesch F, Piémont Y, Brousse N, Floret D *et al*: **Association between Staphylococcus aureus strains carrying gene for Panton-Valentine leukocidin and highly lethal necrotising pneumonia in young immunocompetent patients**. *Lancet* 2002, **359**(9308).

167. Hageman JC, Uyeki TM, Francis JS, Jernigan DB, Wheeler JG, Bridges CB, Barenkamp SJ, Sievert DM, Srinivasan A, Doherty MC *et al*: **Severe Community-acquired Pneumonia Due to *Staphylococcus aureus*, 2003-04 Influenza Season**. *Emerg Infect Dis* 2006, **12**(6).

168. Monaco M, Antonucci R, Palange P, Venditti M, Pantosti A: **Methicillin-resistant Staphylococcus aureus necrotizing pneumonia**. *Emerg Infect Dis* 2005, **11**(10).

169. Peleg AY, Munckhof WJ: **Fatal necrotising pneumonia due to community-acquired methicillin-resistant Staphylococcus aureus (MRSA)**. *Med J Aust* 2004, **181**(4).

170. Groom AV, Wolsey DH, Naimi TS, Smith K, Johnson S, Boxrud D, moore KA, Cheek JE: **Community-acquired methicillin-resistant Staphylococcus aureus in a rural American Indian community**. *JAMA* 2001, **286**(10).

171. Dietrich DW, Auld DB, Mermel LA: **Community-acquired methicillin-resistant Staphylococcus aureus in southern New England children**. *Pediatrics* 2004, **113**(4).

172. Saravolatz LD, Markowitz N, Arking L, Pohlod D, Fisher E: **Methicillin-resistant Staphylococcus aureus. Epidemiologic observations during a community-acquired outbreak**. *Ann Intern Med* 1982, **96**(1).

173. Huang H, Flynn NM, King JH, Monchaud C, Morita M, Cohen SH: **Comparisons of Community-Associated Methicillin-Resistant *Staphylococcus aureus* (MRSA) and Hospital-Associated MRSA Infections in Sacramento, California**. *J Clin Microbiol* 2006, **44**(7).

174. Vysakh PR, Jeya M: **A Comparative Analysis of Community Acquired and Hospital Acquired Methicillin Resistant *Staphylococcus Aureus***. *J Clin Diagn Res* 2013, **7**(7).

175. Al-Rawahi GN, Reynolds S, Porter SD, Forrester L, Kishi L, Chong T, Bowie WR, Doyle PW: **Community-associated CMRSA-10 (USA-300) is the predominant strain among methicillin-resistant Staphylococcus aureus strains causing skin and soft tissue infections in patients pressenting to the emergency department of a Canadian tertiary care hospital**. *J Emerg Med* 2010, **38**(1).

176. Irvine J: **Community-associated methicillin-resistant Staphylococcus aureus in Indigenous communities in Canada**. *Paediatr Child Health* 2012, **17**(7).

177. Tong SYC, Davis J, S., Eichenberger E, Holland TL, Fowler Jr. VG: ***Staphylococcus aureus*** **Infections: Epidemiology, Pathophysiology, Clinical Manifestations, and Management**. *Clin Microbiol Rev* 2015.

178. Wertheim HFL, Melles DC, Vos MC, van Leeuwen W, van Belkum A, Verbrugh HA: **The role of nasal carriage in *Staphylococcus aureus* infections**. *Lancet Infect Dis* 2005, **5**(12).

179. Laupland KB, Ross T, Gregson DB: ***Staphylococcus aureus*** **Bloddstream Infections: Risk Factors, Outcomes, and the Influenza of Methicillin Resistance in Calgary, Canada, 2000-2006**. *J Infect Dis* 2008, **198**(3).

180. American Thoarcic Society, Infectious Diseases Society of America: **Guidelines for the management of adults with hospital-acquired, ventilator-associated, and healthcare-associated pneumonia**. *Am J Respir Crit Care Med* 2005, **171**(4).

181. Nakou A, Woodhead M, Torres A: **MRSA as a cause of community-acquired pneumonia**. *Eur Respir J* 2009, **34**(5).

182. Cunha BA: **Methicillin-resistant *Staphylococcus aureus*: clinical manifestations and antimicrobial therapy**. *Eur J Clin Microbiol* 2005, **11**.

183. Cimolai N: **Methicillin-resistant Staphylococcus aureus in Canada: a historical perspective and lessons learned**. *Can J Microbiol* 2010, **56**(2).

184. Ofner-Agostini M, Simor AE, Bryce E, McGreer A, Paton S: **Methicillin-Resistant *Staphylococcus aureus* in Canadian Aboriginal People**. *Infect Control Hosp Epidemiol* 2006, **27**(2).

185. Leman R, Alvarado-Ramy F, Pocock S: **Nasal carriage of methicillin-resistant *Staphylococcus aureus* in an American Indian population**. *Infect Control Hosp Epidemiol* 2004, **25**.

186. Meddles-Torres C, Hu S, Jurgens C: **Changes in prespective practices in skin and soft tissue infections associated with the increased occurrence of community acquired methicillin resistant Staphylococcus aureus**. *J Infect Public Health* 2013, **6**(6).

187. Vayalumki JV, Suh KN, Toye B, Saginur R, Roth VR: **Skin and soft tissue infections caused by methicillin-resistant Staphylococcus aureus (MRSA): an affliction of the underclass**. *CJEM* 2012, **14**(6).

188. Hennessy TW, Ritter T, Holman RC, Bruden DL, Bulkow L, Cheek JE, Singleton RJ, Smith J: **The relationship between in-home water service and the risk of respiratory tract, skin, and gastrointestinal tract infections among rural Alaska natives**. *Am J Public Health* 2008, **98**(11).

189. Larcombe L, J. W, Schellenberg J, Ormond M: **Rapid emergence of methicillin-resistant Staphylococcus aureus (MRSA) among children and adolescents in northern Manitoba, 2003-2006**. *Can Commun Dis Rep* 2007, **33**(2).

190. R. GG, Levett PN, McDonald RR: **High rates of Staphylococcus aureus USA400 infection, Northern Canada**. *Emerg Infect Dis* 2011, **17**(4).

191. Dalloo A, Sobol I, Palacios C, Mulvey M, Gravel D, Panaro L: **Investigation of community-associated methicillin-resistant Staphylococcus aureus in a remote northern community, Nunavut, Canada**. *Can Commun Dis Rep* 2008, **34**(5).

192. Rutledge-Taylor K: **Methicillin-resistant Staphylococcus aureus (MRSA) activity in the NWT**. *EpiNorth* 2012, **22**(1).

193. Tong SY, van Hal SJ, Einsiedel L, Currie BJ, Turnidge JD: **Impact of ethnicity and socio-economic status on Staphylococcus aureus bacteremia incidence and mortality: a heavy burden in Indigenous Australians**. *BMC Infect Dis* 2012, **12**(249).

194. Kollef MH, Shorr A, Tabak YP, Gupta V, Liu LZ, Johannes RS: **Epidemiology and outcomes of health-care-associated pneumonia: results from a large US database of culture-positive pneumonia**. *Chest* 2005, **128**(6).

195. Defres S, Marwick C, Nathwani D: **MRSA as a cause of lung infection including airway infection, community-acquired pneumonia and hospital-acquired pneumonia**. *Eur Respir J* 2009, **34**.

196. Chickering HT, Park JH: ***Staphylococcus aureus* pneumonia**. *JAMA* 1919, **72**.

197. Wallace HJ: **Specimen from a case of staphylococcal pneumonia**. *Proc R Soc Med* 1937, **30**.

198. Johnson A: **Report on a case of staphylococcal pneumonia with staphylococcal septicaemia: treated with penicillin**. *Ulster Med J* 1944, **13**.

199. American Thoracic Society, Infectious Diseases Society of America: **Guidelines for the management of adults with hospital-acquired, ventilator-associated, and healthcare-associated pneumonia**. *Am J Respir Crit Care Med* 2005, **171**(4).

200. Barton-Forbes M, Hawkes M, Moore D, Conly J, Nicolle L, Allen U, Boyd N, Embree J, Van Horne L, Le Sauz N *et al*: **Guidelines for the prevention and management of community-associated methicillin-resistant *Staphylococcus aureus*: A perspective for Canadian health care practitioners**. *Can J Infect Dis Med Microbiol* 2006, **17**.

201. Centers for Disease Control and Prevention: **Severe methicillin-resistant *Staphylococcus aureus* community-acquired pneumonia associated with influenza -**

Louisiana and Georgia, December 2006-January 2007. *MMWR Morb Mortal Wkly Rep* 2007, **56**.

202. Self WH, Wunderink RG, Williams DJ, Zhu Y, Anderson EJ, Balk RA, Fakhran SS, Chappell JD, Casimir G, Courtney DM *et al*: ***Staphylococcus aureus*** **Community-acquired Pneumonia: Prevalence, Clinical Characterisitics, and Outcomes**. *Clin Infect Dis* 2016, **63**(3).

203. Vardakas KZ, Matthaiou DK, Falagas ME: **Incidence, characteristics and outcomes of patients with severe community-acquired MRSA pneumonia**. *Eur Respir J* 2009, **34**.

204. Ede S, Davis GM, Holmes FH: **Staphylococcic pneumonia**. *J Am Med Assoc* 1959, **170**(6).

205. Heimann HA: **Primary staphylococcal pnuemonia**. *JAMA* 1933, **101**.

206. DeLeo FR, Diep BA, Otto M: **Host Defense and Pathogenesis in *Staphylococcus aureus* Infections**. *Infect Dis Clin North Am* 2009, **23**(1).

207. Soell M, Diab M, Haan-Archipoff G, Beretz A, Herbelin C, Poutrel B, Klein JP: **Capsular polysaccharide types 5 and 8 of Staphylococcus aureus bind specifically to human epithelial (KB) cells, endothelial cells, and monocytes and induce release of cytokines**. *Infect Immun* 1995, **63**(4).

208. Yao L, Lowy FD, Berman JW: **Interleukin-8 gene expression in Staphylococcus aureus-infected endothelial cells**. *Infect Immun* 1996, **64**(8).

209. McLoughlin RM, Solinga RM, Rich J, Zaleski KJ, Cocchiaro JL, Risley A, Tzianabos AO, Lee JC: **CD4+ T cells and CXC chemokines modulate the pathogenesis of Staphylococcus aureus wound infections**. *Proc Natl Acad Sci U S A* 2006, **103**(27).

210. Tzianabos AO, Wang JY, Lee JC: **Structural rationale for the modulation of abscess formation by Staphylococcus aureus capsular polysaccharides**. *Proc Natl Acad Sci U S A* 2001, **98**(16).

211. Schmeling DJ, Peterson PK, Hammerschmidt DE, Kim Y, Verhoef J, Wilkinson BJ, Quie PG: **Chemotaxigenesis by cell surface components of Staphylococcus aureus**. *Infect Immun* 1979, **26**(1).

212. Voyich JM, Braughton KR, Sturdevant DE, Whitney AR, Saïd-Salim B, Porcella SF, Long RD, Dorward DW, Gardner DJ, Kreiswirth BN *et al*: **Insights into mechanisms used by Staphylococcus aureus to avoid destruction by human neutrophils**. *J Immunol* 2005, **175**(6).

213. Akira S, Takeda K: **Toll-like receptor signalling**. *Nat Rev Immunol* 2004, **4**(7).

214. Sabroe I, Prince LR, Jones EC, Horsburgh MJ, Foster SJ, Vogel SN, Dower SK, Whyte MK: **Selective roles for Toll-like receptor (TLR)2 and TLR4 in the regulation of neutrophil activation and life span**. *J Immunol* 2003, **170**(10).

215. Hayashi F, Means TK, Luster AD: **Toll-like receptors stimulate human neutrophil function**. *Blood* 2003, **102**(7).

216. Wardenburg JB, Bae T, Otto M, DeLeo FR, Schneewind O: **Poring over pores: α-hemolysin and Panton-Valentine leukocidin in *Staphylococcus aureus* pneumonia**. *Nat Med* 2007, **13**.

217. Kebaier C, Chamberland RR, Allen IC, Gao X, Broglie PM, Hall JD, Jania C, Doerschuk CM, Tilley SL, Duncan JA: **Staphylococcus aureus α-hemolysin mediates virulence in a murine model of severe pneumonia through activation of the NLRP3 inflammasome**. *J Infect Dis* 2012, **205**(5).

218. Parimon T, Li Z, Bolz DD, McIndoo ER, Bayer CR, Stevens DL, Bryant AE: **Staphylococcus aureus α-hemolysin promotes platelet-neutrophil aggregate formation**. *J Infect Dis* 2013, **208**(5).

219. DeLeo FR, Otto M: **An antidote for *Staphylococcus aureus* pneumonia?** *J Exp Med* 2008, **205**(2).

220. Hua L, Hilliard JJ, Shi Y, Tkaczyk C, Cheng LI, Yu X, Datta V, Ren S, Feng H, Zinsou R *et al*: **Assessment of an anti-alpha-toxin monoclonal antibody for prevention and treatment of *Staphylococcus aureus*-induced pneumonia**. *Antimicrob Agents Chemother* 2014, **58**.

221. Skinner D, Keefre CS: **Significance of bacteremia caused by *Staphylococcus aureus***. *Arch Intern Med* 1941, **68**(5).

222. van Hal SJ, Jensen SO, Vaska VL, Espedido BA, Paterson DL, Gosbell IB: **Predictors of mortality in Staphylococcus aureus Bacteremia**. *Clin Microbiol Rev* 2012, **25**(2).

223. Torok E, Moran E, Cooke F: **Oxford Handbook of Infectious Diseses and Microbiology**, 2 edn: Oxford University Press; 2009.

224. Kim SH, Park WB, Lee KD, Kang CI, Kim HB, Oh MD, Kim EC, Choe KW: **Outcome of Staphylococcus aureus bacteremia in patients with eradicable foci versus noneradicable foci**. *Clin Infect Dis* 2003, **37**(6).

225. Kalil AC, Metersky ML, Klompas M, Muscedere J, Sweeney DA, Palmer LB, Napolitano LM, O'Grady NP, Bartlett JG, Carratalà J *et al*: **Management of Adults With Hospital-acquired and Ventilator-associated Pneumonia: 2016 Clinical Practice Guidelines by the Infectious Diseases Society of America and the American Thoracic Society**. *Clin Infect Dis* 2016, **63**(5).

226. Monteiro JF, Hahn SR, Gonçalves J, Fresco P: **Vancoymycin therapeutic drug monitoring and population pharmacokinetic models in special patient subpopulations**. *Pharmacol Res Perspect* 2018, **6**(4).

227. Ishii H, Hirai K, Sugiyama K, Nakatani E, Kimura M, Itoh K: **Validation of a Nomogram for Achieving Target Trough Concentration of Vancomycin: Accuracy in Patients With Augmented Renal Function**. *Ther Drug Monit* 2018, **40**(6).

228. Patanwala AE, Norris CJ, Nix DEK, B. J., Erstad BL: **Vancomycin dosing for pneumonia in critically ill trauma patients**. *Chest* 2009, **67**(4).

229. Lee T, Pang S, Abraham S, Coombs GW: **Antimicrobial-resistant CC17 Enterococcus faecium: The past, the present, and the future**. *J Glob Antimicrob Resist* 2019, **16**.

230. Bartoletti M, Giannella M, Tedeschi S, Viale P: **Mutlidrug-Resistant Bacterial Infections in Solid Organ Transplant Candidates and Recipients**. *Infect Dis Clin North Am* 2018, **32**(3).

231. Singh M, Chang J, Coffman L, Kim SJ: **A Hidden Mode of Action of Glycopeptide Antibiotics: Inhibition of Teichoic Acid Biosynthesis**. *J Phys Chem B* 2017, **121**(16).

232. Wunderink RG, Niederman MS, Kollef MH, Shorr AF, Kunkel MJ, Baruch A, McGee WT, Reisman A, Chastre J: **Linezolid in methicillin-resistant Staphylococcus aureus nosocomial pneumonia: a randomized, controlled study**. *Clin Infect Dis* 2012, **54**(5).

233. Conte Jr JE, Golden JA, Kipps J, Zurlinden E: **Intrapulmonary pharmacokinetics of linezolid**. *Antimicrob Agents Chemother* 2002, **46**.

234. Arias CA, Murray BE: **Antibiotic-resistant bugs in the 21st century—a clinical super-challenge**. *N Engl J Med* 2009, **360**(5).

235. Hsia CCW, Hyde DM, Weibel ER: **Lung Structure and the Intrinsic Challenges of Gas Exchange**. *Compr Physiol* 2016, **6**(2).

236. **Human Anatomy and Physiology**. In., edn.: OpenStax.

237. Hashim AAA, El-Ahmady O, Khaled HM, Elmazar MM, Hassen Z: **Serum VEGF and HGF in Egyptian Patients with Lung and Pleural Cancers**. *International Journal of Avances in Pharmacy, Biology, and Chemistry* 2014, **3**(4).

238. Knudsen L, Ochs M: **The micromechanics of lung alveoli: structure and function of surfactant and tissue components**. *Histochem Cell Biol* 2018, **150**:661-676.

239. Herrero R, Sanchez G, Lorente JA: **New insights into the mechanisms of pulmonary edema in acute lung injury**. *Ann Tranls Med* 2018, **6**(2):32.

240. Audesirk G, Audesirk T, Byers BE: **Biology: Life on Earth**, 8 edn: Benjamin Cummings; 2007.

241. Maina JN, West JB: **Thin and strong! The bioengineering dilemma in the structural and functional design of the blood-gas barrier**. *Physiol Rev* 2005, **85**(3).

242. Schneeberger EE, Karnovsky MJ: **Substructure of Intercellular Junctions in Freeze-Fractured Alveolar-Capillary Membranes of Mouse Lung**. *Circ Res* 1976, **38**(5).

243. Wittekindt OH: **Tight junctions in pulmonary epithelia during lung inflammation**. *Pfugers Arch* 2017, **469**(1).

244. Crane MJ, Lee KM, FitzGerald ES, Jamieson AM: **Surviving Deadly Lung Infections: Innate Host Tolerance Mechanisms in the Pulmonary System**. *Front Immunol* 2018.

245. Peter A, Fatykhova D, Kershaw O, Gruber AD, Rueckert J, Neudecker J, Toennies M, Bauer TT, Schneider P, Schimek M *et al*: **Localization and pneumococcal alteration of**

junction proteins in the human alveolar-capillary compartment. *Histochem Cell Biol* 2017, **147**.

246. Bhattacharya J, Matthay MA: **Regulation and repair of the alveolar-capillary barrier in acute lung injury**. *Annu Rev Physiol* 2013, **75**.

247. Olmeda B, Martinez-Calle M, Pérez-Gil J: **Pulmonary surfactant metabolism in the alveolar airspace: Biogenesis, extracellular conversions, recycling**. *Ann Anal* 2017, **209**.

248. Pastva AM, Wright JR, Williams KL: **Immunomodulatory Roles of Surfactant Proteins A and D**. *Proc Am Thorac Soc* 2007, **4**(3).

249. De Rose V, Molloy K, Gohy S, Pilette C, Greene CM: **Airway Epithelium Dysfunction in Cystic Fibrosis and COPD**. *Mediators Inflamm* 2018, **2018**.

250. Ganesan S, Comstock AT, Sajjan US: **Barrier function of airway tract epithelium**. *Tissue Barriers* 2013, **1**(4).

251. Mei M, Xiang RL, Cong X, Zhang Y, Li J, Yi X, Park K, Han JY, Wu LL, Yu GY: **Claudin-3 is required for modulation of paracellular permeability by TNF-α through ERK1/2/slug signaling axis in submandibular gland**. *Cell Signal* 2015, **27**(10).

252. Ward C, Schlingmann B, Stencenko AA, Guidot DM, Koval M: **NF-κB inhibitors impair lung epithelial tight junctions in the absence of inflammation**. *Tissue Barriers* 2015, **3**.

253. Weibel ER: **What makes a good lung?** *Swiss Med Wkly* 2009, **139**.

254. Short KR, Veldhuis Kroeze EJ, Reperant LA, Richard M, Kuiken T: **Influenza virus and endothelial cells: a species specific relationship**. *Front Microbiol* 2014, **5**.

255. Gehr P, Bachofen M, Weibel ER: **The normal human lung: ultrastructure and morphometric estimation of diffusion capacity**. *Respir Physiol* 1978, **32**(2).

256. Aman J, Weijers EM, van Nieuw Amerongen GP, Malik AB, van Hinsbergh VWM: **Using cultured endothelial cells to study endothelial barrier dysfunction: Challenges and opportunities**. *Am J Physiol Lung Cell Mol Pysiol* 2016, **311**(2).

257. Hough RF, Bhattacharya S, Bhattacharya J: **Crosstalk signaling between alveoli and capillaries**. *Pulm Circ* 2018, **8**(3).

258. Kuebler WM, Parthasarthi K, Wang PM, Bhattacharya J: **A novel signaling mechanism between gas and blood compartments of the lung**. *J Clin Invest* 2000, **105**(7).

259. McCullers JA: **Insights into the Interaction between Influenza Virus and Pneumococcus**. *Clin Microbiol Rev* 2006, **19**(3).

260. Bellinghausen C, Rohde GGU, Savelkoul PHM, Wouters EFM, Stassen FRM: **Viral-bacterial interactions in the respiratory tract**. *J Gen Virol* 2016, **97**.

261. Rudd JM, Ashar HK, Chow VTK, Teluguakula N: **Lethal Synergism between Influenza and *Streptococcus pneumoniae***. *J Infect Pulm Dis* 2016, **2**(2).

262. Chertow DS, Memoli MJ: **Bacterial Coinfection in Influenza: A Grand Rounds Review**. *JAMA* 2013, **309**.

263. Belser JA, Szretter KJ, Katz JM, Tumpey TM: **Use of animal models to understand the pandemic potential of highly pathogenic avian influenza viruses**. *Adv Virus Res* 2009, **73**.

264. Chertow DS, Kindrachuk J, Sheng ZM, Pujanauski LM, Cooper K, Nogee D, Claire MS, Colomon J, Perry D, Sayre P *et al*: **Influenza A and methicillin-resistant**

Staphylococcus aureus co-infection in rhesus macaques - A model of severe pneumonia. *Antiviral Res* 2016, **129**.

265. Berendt RF: **Simian model for the evaluation of immunity to influenza**. *Infect Immun* 1974, **9**(1).

266. Berendt RF, Long GG, Walker JS: **Influenza alone and in sequence with pneumonia due to Streptococcus pneumoniae in the squirrel monkey**. *J Infect Dis* 1975, **132**(6).

267. Kobayashi SD, Olsen RJ, LaCasse RA, Safronetz D, Ashraf M, Porter AR, Braughton KR, Feldmann F, Clifton DR, Kash JC *et al*: **Seasonal H3N2 influenza A virus fails to enhance Staphylococcus aureus co-infection in a non-human primate respiratory tract infection model**. *Virulence* 2013, **4**(8).

268. Miyake T, Soda K, Itoh Y, Sakoda Y, Ishigaki H, Nagata T, Ishida H, Nakayama M, Ozaki H, Tsuchiya H *et al*: **Amelioration of pneumonia with Streptococcus pneumoniae infection by inoculation with a vaccine against highly pathogenic avian influenza virus in a non-human primate mixed infection model**. *J Med Primatol* 2010, **39**.

269. Short KR, Veeris R, Leijten LM, van den Brand JM, Jong VL, Stittelaar K, Osterhaus ADME, Andeweg A, van Riel D: **Proinflammatory Cytokine Responses in Extra-Respiratory Tissues During Severe Influenza**. *J Infect Dis* 2017, **216**(7).

270. Hermanns MI, Kasper J, Dubruel P, Pohl C, Uboldi C, Vermeersch V, Fuchs S, Unger RE, Kirkpatrick CJ: **An impaired alveolar-capillary barrier *in vitro*: effect of proinflammatory cytokines and consequences on nanocarrier interaction**. *J R Soc Interface* 2010, **7**.

271. Walters KA, D'Agnillo F, Sheng ZM, Kindrachuk J, Schwartzman LM, Keustner RE, Chertow DS, Golding BT, Taubenberger JK, Kash JC: **1918 pandemic influenza virus and *Streptococcus pneumoniae* coinfection results in activation of coagulation and widespread pulmonary thrombosis in mice and humans**. *J Pathol* 2015, **238**(1).

272. Gill JR, Sheng ZM, Ely SF, Guinee Jr. DG, Beasley MB, Suh J, Deshpande C, Mollura DJ, Morens DM, Bray M *et al*: **Pulmonary Pathologic Findings of Fatal 2009 Pandemic Influenza A/H1N1 Viral Infections**. *Arch Pathol Lab Med* 2010, **134**(2).

273. Hers JFP, Masurel N, Mulder J: **Bacteriology and Histopathology of the Respiratory Tract and Lungs in Fatal Asian Influenza**. *Lancet* 1958, **2**(7057).

274. Guamer J, Paddock CD, Shieh WJ, Packard MM, Montague JL, Uyeki TM, Bhat N, Balish A, Lindstrom S, Limov A *et al*: **Histopathologic and immunohistochemical features of fatal influenza virus infection in children uring the 2003-2004 season**. *Clin Infect Dis* 2006, **43**(2).

275. Guamer J, Shieh WJ, Dawson J, Subbarao K, Shaw M, Ferebee T, Morken T, Nolte KB, Freifeld A, Cox NJ *et al*: **Immunohistochemical and in situ hybridization studies of influenza A virus infection in human lungs**. *Am J Clin Pathol* 2000, **114**(2).

276. Kumar A, Zarychanski R, Pinto R, Cook DJ, Marshall J, Lacroix J, Stelfox T, Bagshaw S, Choong K, Lamontagne F *et al*: **Critically Ill Patients with 2009 Influenza A(H1N1) Infection in Canada**. *JAMA* 2009, **302**(17).

277. Mauad T, Hajjar LA, Callegari GD, da Silva LF, Schout D, Galas FRBG, Alves VAF, Malheiros DMAC, Auler Jr. JOC, Ferreira AF *et al*: **Lung Pathology in Fatal Novel Human Influenza A (H1N1) Infection**. *Am J Respir Crit Care Med* 2010, **181**(1).

278. Nickol ME, Ciric J, Falcinelli S, Chertow DS, Kindrachuk J: **Characterization of Host and Bacterial Contributions to Lung Barrier Dysfunction Following Co-infection with 2009 Pandemic Influenza and Methicillin Resistant *Staphylococcus aureus***. *Viruses* 2019, **11**(2).

279. Short KR, Veldhuis Kroeze EJ, Fouchier RA, Kuiken T: **Pathogenesis of influenza-induced acute respiratory distress syndrome**. *The Lancet Infectious Diseases* 2014, **14**(1).

280. Short KR, Kasper J, van der Aa S, Andeweg AC, Zaaraoui-Boutahar F, Goeijenbier M, Richard M, Herold S, Becker C, Scott DP *et al*: **Influenza virus damages the alveolar barrier by disrupting epithelial cell tight junctions**. *Eur Respir J* 2015, **47**.

281. Rynda-Apple A, Robinson KM, Alcorn JF: **Influenza and bacterial superinfection: illuminating the immunologic mechanisms of disease**. *Infect Immun* 2015, **83**.

282. Ivanov S, Renneson J, Fontaine J, Barthelemy A, Paget C, Fernandez EM, Blanc F, De Trez C, Van Maele L, Dumoutier L *et al*: **Interleukin-22 reduces lung inflammation during influenza A virus infection and protects against secondary bacterial infection**. *J Virol* 2013, **87**(12).

283. Damjanovic D, Small C-L, Jeyanathan M, McCormick S, Xing Z: **Immunopathology in influenza virus infection: uncoupling the friend from foe**. *Clin Immunol* 2012, **144**.

284. Yoo J-K, Kim TS, Hufford MM, Braciale TJ: **Viral infection of the lung: host response and sequelae**. *J Allergy Clin Immunol* 2013, **132**.

285. Braciale TJ, Hahn YS: **Immunity to viruses**. *Immunol Rev* 2013, **255**.

286. Iwasaki A, Pillai PS: **Innate immunity to influenza virus infection**. *Nat Rev Immunol* 2014, **14**.

287. Numata M, Kandasamy M, Nagashima Y, Fikes R, Murphy RC, Voelker DR: **Phosphatidylinositol inhibits respiratory syncytial virus infection**. *J Lipid Res* 2015, **56**.

288. Shirey KA, Lai W, Scott AJ, Lipsky M, Mistry P, Pletneva LM, Karp CL, McAlees J, Gioannini TL, Weiss J *et al*: **The TLR4 antagonist Eritoran protects mice from lethal influenza infection**. *Nature* 2013, **497**(7450).

289. Huang L-Y, Stuart C, Takeda K, D'Agnillo F, Golding B: **Poly(I:C) induces human lung endothelial barrier dysfunction by disrupting tight junction expression of claudin-5**. *PLoS One* 2016, **11**.

290. Miettinen M, Sareneva T, Julkunen I, Matikainen S: **IFNs activate toll-like receptor gene expression in viral infections**. *Genes Immun* 2001, **2**.

291. Teijaro JR, Walsh KB, Cahalan S, Fremgen DM, Roberts E, Scott F, Martinborough E, Peach R, Oldstone MB, Rosen H: **Endothelial cells are central orchestrators of cytokine amplification during influenza virus infection**. *Cell* 2011, **146**(6).

292. Tundup S, Kandasamy M, Perez JT, Mena N, Steel J, Nagy T, Albrecht RA, Manicassamy B: **Endothelial cell tropism is a determinant of H5N1 pathogenesis in mammalian species**. *PLoS Pathog* 2017, **13**(3).

293. Vidaña B, Martínez J, Martorell J, Montoya M, Córdoba L, Pérez M, Natàlia M: **Involvement of the different lung compartments in the pathogenesis of pH1N1 influenza virus infection in ferrets**. *Vet Res* 2016, **47**.

294. Robinson KM, K. R, Clay ME, McHugh KJ, Pilewski MJ, Nickolich KL, Corey C, Shiva S, Wang J, Muzumdar R *et al*: **The inflammasome potentiates influenza/Staphylococcus aureus superinfection in mice**. *JCI Insight* 2018, **3**(7).

295. Johnston LK, Rims CR, Gill SE, McGuire JK, Manicone AM: **Pulmonary macrophage subpopulations in the induction and resolution of acute lung injury**. *Am J Respir Cell Mol Bio* 2012, **47**.

296. Purnama C, Ng SL, Tetlak P, Setiagana YA, Kandasamy M, Baalasubramanian S, Karjalainen K, Ruedi C: **Transient ablation of alveolar machrophages leads to massive pathology of influenza infection without affecting cellular adaptive immunity**. *Eur J Immunol* 2014, **44**(7).

297. Gamradt P, Xu Y, Gratz N, Duncan K, Kobzik L, Högler S, Kovarik P, Decker T, Jamieson AM: **The Influenza of Programmed Cell Death in Myeloid Cells on Host Resilience to Infection with Legionella pneumophila or Straptococcus pyogenes**. *PLoS Pathog* 2016, **12**(12).

298. Araya J, Hara H, Kuwano K: **Autophagy in the pathogenesis of pulmonary disease**. *Intern Med* 2013, **52**.

299. Chow SH, Deo P, Naderer T: **Macrophage cell death in microbial infections**. *Cell Microbiol* 2016, **18**.

300. Ishii T, Abboud RT, Wallace AM, English JC, Coxson HO, Finley RJ, Shumansky K, Paré PD, Sandford AJ: **Alveolar macrophage proteinase/antiproteinase expression in lung function and emphysema**. *Eur Respir J* 2014, **43**(1).

301. Yuan Z, Petree JR, Lee EHF, Fan Z, Salaita K, Guidot DM, Sadikot RT: **Macrophages exposed to HIV viral protein disrupt lung epithelial cell integrity and mitochondrial bioenergetics via exosomal microRNA shuttling**. *Cell Death Dis* 2019, **580**.

302. Narasaraju T, Yang E, Samy RP, Ng HH, Poh WP, Liew A-A, Phoon MC, van Rooijen N, Chow VT: **Excessive neutrophils and neutrophil extracellular traps contribute to acute lung injury of influenza pneumonitis**. *Am J Pathol* 2011, **179**(1).

303. Haick AK, Rzepka JP, Brandon E, Balemba OB, Miura TA: **Neutrophils are needed for an effective immune response against pulmonary rat coronavirus infection, but also contribute to pathology**. *J Gen Virol* 2014, **95**.

304. Hermant B, Bibert S, Concord E, Dublet B, Weidenhaupt M, Vernet T, Gulino-Debrac D: **Identification of Proteases Involved in the Proteolysis of Vascular Endothelium Cadherin during Neutrophil Transmigration**. *J Biol Chem* 2003, **278**.

305. Qi L, Kash JC, Dugan VG, Wang R, Jin G, Cunningham RE, Taubenberger JK: **Role of Sialic Acid Binding Specificity of the 1918 Influenza Virus Hemagglutinin Protein in Virulence and Pathogenesis for Mice**. *J Virol* 2009, **83**.

306. Sanders ER: **Aseptic Laboratory Techniques: Plating Methods**. *J Vis Exp* 2012, **63**.

307. Rowe HM, Meliopoulos VA, Iverson A, Bomme P, Schultz-Cherry S, Rosch JW: **Direct interactions with influenza promote bacterial adherence during respiratory infections**. *Nat Microbiol* 2019, **4**:1328-1336.

308. Atshan SS, Shamsudin MN, Karunandihi A, van Belkum A, Lung LT, Sekawi Z, Nathan JJ, Ling KH, Seng JS, Ali AM *et al*: **Quantitative PCR analysis of genes expressed during biofilm development of methicllin resistant *Staphylococcus aureus* (MRSA)**. *Infect Genet Evol* 2013, **18**:106-112.

309. Kindrachuk J, Wahl-Jensen V, Safronetz D, Trost B, Hoenen T, Arsenault R, Feldmann F, Traynor D, Postnikova E, Kusalik A *et al*: **Ebola virus modulates transforming**

growth factor β signaling and cellular markers of mesenchyme-like transition in hepatocytes. *J Virol* 2014, **88**(17).

310. Kindrachuk J, Ork B, Hart BJ, Mazur S, Holbrook MR, Frieman MB, Traynor D, Johnson RF, Dyall J, Kuhn JH *et al*: **Antiviral Potential of ERK/MAPK and PI3K/AKT/mTOR Signaling Modulation for Middle East Respiratory Syndrom Coronavirus Infection as Identified by Temporal Kinome Analysis**. *Antimicrob Agents Chemother* 2014, **59**.

311. Trost B, Kindrachuk J, Maattanen P, Napper S, Kusalik A: **PIIKA 2: an expanded, web-based platform for analysis of kinome microarray data**. *PLoS One* 2013, **8**(11).

312. Huber W, von Heydebreck A, Sültmann H, Poutska A, Vingron M: **Variance stabilization applied to microarray data calibration and to the quantification of differential expression**. *Bioinformatics* 2002, **18**.

313. Kindrachuk J, Arsenault R, Kusalik A, Kindrachuk KN, Trost B, Napper S, Jahrling PB, Blaney JE: **Systems Kinomics Demonstrates Congo Basin Monkeypox Virus Infection Selectively Modulates Host Cell Signaling Responses as Compared to West African Monkeypox Virus**. *Mol Cell Proteomics* 2012, **11**(6).

314. Babicki S, Amdt D, Marcu A, Liang Y, Grant JR, Maciejewski A, Wishart DS: **Heatmapper: web-enabled heat mapping for all**. *Nucleic Acids Res* 2016, **44**(W1).

315. Lynn DJ, Winsor GL, Chan C, Richard N, Laird MR, Barsky A, Gardy JL, Roche FM, Chan THW, Shah N *et al*: **InnateDB: facilitating systems-level analyses of the mammalian innate immune response**. *Mol Syst Biol* 2008, **4**(218).

316. Li Y, Arsenault RJ, Trost B, Slind J, Griebel PJ, Napper S, Kusalik A: **A Systemic Approach for Analysis of Peptide Array Kinome Data**. *Sci Signal* 2012, **5**(220).

317. Goni R, García P, Foissac S: **The qPCR data statistical analysis**. In. Madrid Science Park, Spain: Integromics SL; 2009.

318. Rieu I, Powers SJ: **Real-time quantitative RT-PCR: design, calculations, and statisitics**. *Plant Cell* 2009, **21**(4).

319. Smith AM, McCullers JA: **Secondary bacterial infections in influenza virus infection pathogenesis**. *Curr Top Microbiol Immunol* 2014, **385**.

320. Stolwijk JA, Matrougui K, Renken CW, Trebak M: **Impedance analysis of GPCR-mediated changes in endothelial barrier function: overview and fundamental considerations for stable and reproducible measurements**. *Pflugers Arch* 2015, **467**(10).

321. Kindrachuk J, Falcinelli S, Wada J, Kuhn JH, Hensley LE, Jahrling PB: **Systems kinomics for characterizing host responses to high consequence pathogensat the NIH/NIAID Integrate Research Facility-Frederick**. *Pathogens and Disease* 2014, **71**(2).

322. Arsenault R, Griebel P, Napper S: **Peptide arrays for kinome analysis: new opportunities and remaining challenges**. *Proteomics* 2011, **11**(24):4595-4609.

323. Määttänen P, Trost B, Scruten E, Potter A, Kusalik A, Griebel P, Napper S: **Divergent Immune Responses to *Mycobacterium avium* subsp. *paratuberculosis* Infection Correlate with Kinome Responses at the Site of Intestinal Infection**. *Infect Immun* 2013, **81**(8).

324. Arsenault R, Li Y, Bell K, Doig K, Potter A, Griebel P, Kusalik A, Napper S: ***Mycobacterium avium* subsp. *paratuberculosis* Inhibits Gamma Interferon-Induced**

Signaling in Bovine Monocytes: Insights into the Cellular Mechanisms of Johne's Disease. *Infect Immun* 2012, **80**(9).

325. Foster T: **Medical Microbiology**, 4th edn. Galveston, Texas: University of Texas Medical Branch at Galveston; 1996.

326. Powers ME, Bubeck Wardenburg J: **Igniting the fire: Staphylococcus aureus virulence factors in the pathogenesis of sepsis**. *PLoS Pathog* 2014, **12**(2).

327. Walters KA, D'Agnillo F, Sheng ZM, Kindrachuk J, Schwarzman LM, Keutsner RE, Chertow DS, Golding BT, Taubenberger JK, Kash JC: **1918 pandemic influenza virus and *Streptococcus pneumoniae* coinfection results in activation of coagulation and widespread pulmonary thrombosis in mice and humans**. *J Pathol* 2016, **283**(1).

328. Gouaux E, Hobaugh M, Song L: **alpha-Hemolysin, gama-hemolysin, and leukocidin from Staphylococcus aureus: distant in sequence but similar in structure.** *Protein Sci* 1997, **6**(12):263-265.

329. Cooney J, Kienle Z, Foster TJ, O'Toole PW: **The gamma-hemolysin locus of Staphylococcus aureus comprises three linked genes, two of which are identical to the genes for the F and S components of leukocidin**. *Infect Immun* 1993, **61**(2).

330. Peacock SJ, Moore CE, Justice A, Kantzanou M, Story L, Mackie K, O'Neill G, Day NPJ: **Virulent combinations of adhesin and toxin genes in natural populations of *Staphylococcus aureus*** *Infect Immun* 2002, **70**.

331. Chavakis T, Preissner KT, Hermann M: **The anti-inflammatory activities of *Staphylococcus aureus***. *Trends Immunol* 2007, **28**.

332. Kong C, Neoh H, Nathan S: **Targeting *Staphylococcus aureus* Toxins: A Potential form of Anti-Virulence Therapy**. *Toxins* 2016, **8**(3).

333. Kim HK, Cheng AG, Kim H, Missiakas DM, Schneewind O: **Nontoxigenic protein A vaccine for methicillin-resistant *Staphyloccocus aureus* infections in mice**. *J Exp Med* 2010, **207**(9).

334. Gómez MI, Lee A, Reddy B, Muir A, Soong G, Pitt A, Cheung A, Prince A: **Staphylococcus aureus protein A induces airway epithelial inflammatory responses by activating TNFR1**. *Nat Med* 2004, **10**(8).

335. Bubeck Wardenburg J, Patel RJ, Schneewind O: **Surface proteins and exotoxins are required for the pathogenesis of Staphylococcus aureus pneumonia**. *Infect Immun* 2007, **75**(2).

336. Cheng AG, Kim HK, Burts ML, Krausz T, Schneewind O, Missiakas DM: **Genetic requirements for Staphylococcus aureus abscess formation and persistence in host tissues**. *FASEB J* 2009, **23**(10).

337. Zhao F, Chong AS, Montgomery CP: **Importance of B Lymphocytes and the IgG-Binding Protein Sbi in *Staphylococcus aureus* Skin Infection**. *Pathogens* 2016, **5**(1).

338. Koch TK, Reuter M, Barthel D, Böhm S, van den Elsen J, Kraiczy P, Zipfel PF, Skerka C: **Staphylococcus aureus Proteins Sbi and Efb Recruit Human Plasmin to Degrade Complement C3 and C3b**. *PloS One 2012*, **7**.

339. Thammavongsa V, Kim HK, Missiakas D, Schneewind O: **Staphylococcal manipulation of host immune responses**. *Nat Rev Microbiol* 2015, **13**(9).

340. McAdow M, Missiakas DM, Schneewind O: ***Staphylococcus aureus* secretes coagulase and von Willebrand factor binding protein to modify the coagulation cascade and establish host infections**. *J Innate Immun* 2012, **4**.

341. Speziale P, Pietrocola G, Rindi S, Provenzano G, Di Poto A, Visai L, Arciola CR: **Structural and functional role of *Staphylococcus aureus* surface components recognizing adhesive matrix molecules of the host**. *Future Microbiol* 2009, **4**(10).

342. Clarke SR, Foster SJ: **Surface adhesins of *Staphylococcus aureus***. *Adv Microb Physiol* 2006, **51**.

343. Shinji H, Yosizawa Y, Tajima A, Iwase T, Sugimoto S, Seki K, Mizunoe Y: **Role of fibronectin-binding proteins A and B in in vitro cellular infections and in vivo septic infections by Staphylococcus aureus**. *Infect Immun* 2011, **79**(6).

344. Basanisi MG, La Bella G, Nobili G, Franconieri I, La Salandra G: **Genotyping of methicillin-resistant Staphyloccous aureus (MRSA) isolated from milk and dairy products in South Italy**. *Food Microbiol* 2017, **62**.

345. Ocal DN, Dolapci I, Karahan ZC, Tekeli A: **Investigation of biofilm formation properties of staphylococcus isolates**. *Mikrobiyoloji Bulteni* 2017, **51**.

346. Piechota M, Kot B, Frankowska-Maciejewska A, Gruźewska A, Woźniak-Kosek A: **Biofilm formation by Methicillin-Resistant and Methicillin-Sensitive *Staphylococcus aureus* Strains from Hospitalized Patients in Poland**. *BioMed Res Int* 2018, **2018**.

347. Aguilar JL, Varshney AK, Pechuan X, Dutta K, Nosanchuk JD, Fries BC: **Monoclonal antibodies protect from Staphylococcal Enterotoxin K (SEK) induced toxic shock and sepsis by USA300 *Staphylococcus aureus***. *Virulence* 2017, **8**(6).

348. Yarwood JM, McCormick JK, Paustian ML, Orwin PM, Kapur V, Schlievert PM: **Characterization and expression analysis of Staphylococcus aureus pathogenicity island 3. Implications for the evolution of staphylococcal pathogenicity islands**. *J Biol Chem* 2002, **277**(15).

349. Moghadami M: **A Narrative Review of Influenza: A Seasonal and Pandemic Disease**. *Iran J Med Sci* 2017, **42**(1).

350. Davis KA, Stewart JJ, Crouch HK, Florez CE, Hospenthal DR: **Methicillin-Resistant *Staphylococcus aureus* (MRSA) Nares Colonization at Hospital Admission and Its Effect on Subsequent MRSA Infection**. *Clin Infect Dis* 2004, **39**(6).

351. Sarkar M, Niranjan N, Banyal PK: **Mechanisms of hypoxemia**. *Lung India* 2017, **34**(1).

352. Kumar A, Tassopoulos AM, Li Q, Yu FS: **Staphylococcus aureus protein A induced inflammatory response in human corneal epithelial cells**. *Biochem Biophys Res Commun* 2007, **354**(4).

353. Guerra FE, Borgogna TR, Patel DM, Sward EW, Voyich J: **Epic Immune Battles of History: Neutrophils vs. *Staphylococcus aureus***. *Front Cell Infect Microbiol* 2017.

354. Collazos J, Esteban C, Fernández A, Genoliá J: **Measurement of the serum tumor marker neuron-specific enolase in patients with benign pulmonary diseases**. *Am J Respir Crit Care Med* 1994, **150**(1).

355. Song TJ, Choi YC, Lee KY, Kim WJ: **Serum and cerebrospinal fluid neuron-specific enolase for diagnosis of tuberculous meningitis**. *Yonsei Med J* 2012, **53**(6).

356. Honda K, Ohga S, Takada H, Nomura A, Ohshima K, Kinukawa N, Mizuno Y, Hara T: **Neuron-specific enolase in hemophagocytic lymphohistiocytosis: a potential indicator for macrophage activation?** *Int J Hematol* 2000, **72**(1).

357. Nam SJ, Jeong JY, Jang TW, Jung MH, Chun BK, Cha HJ, Oak CH: **Neuron-specific enolase as a novel biomarker reflecting tuberculosis activity and treatment response**. *Korean J Intern Med* 2016, **31**(4).

358. Ghasemian A, Peerayeh SN, Bakhshi B, Mirzaee M: **The Microbial Surface Components Recognizing Adhesive Matrix Molecules (MSCRAMMs) Genes among Clinical Isolates of *Staphylococcus aureus* from Hospitalized Childre**. *Iran J Pathol* 2015, **10**(4).

359. Spellberg B, Daum R: **Development of a vaccine against *Staphylococcus aureus***. *Semin Immunopathol* 2012, **34**(2).

360. McKenney D, Hübner J, Muller E, Wang Y, Goldmann DA, Pier GB: **The ica locus of Staphylococcus epidermis encode production of the capsular polysaccharide/adhesin**. *Infect Immun* 1998, **66**(10).

361. McKenney D, Pouliot KL, Wang Y, Murthy V, Ulrich M, Döring G, Lee JC, Goldmann DA, Pier GB: **Broadly protective vaccine for Staphylococcus aureus based on an in vivo-expressed antigen**. *Science* 1999, **284**(5419).

362. Pérez MM, Prenafeta A, Valle J, Penadés J, Rota C, Solano C, Marco J, Grilló MJ, Lasa I, Irache JM *et al*: **Protection from Staphylococcus aureus mastitis associated with poly-N-acetyl beta-1,6 glucoasmine specific antibody production using biofilm-embedded bacteria**. *Vaccine* 2009, **27**(17).

363. Vuong C, Kocianova S, Voyich JM, Yao Y, Fischer ER, DeLeo FR, Otto M: **A crucial role for exopolysaccharide modification in bacterial biofilm formation, immune evasion, and virulence**. *J Biol Chem* 2004, **279**(52).

364. Gening ML, Maira-Litrán T, Kropec A, Skumik D, Grout M, Tsvetkov YE, Nifantiev NE, Pier GB: **Synthetic {beta}-(1->6)-linked N-acetylated and nonacetylated oligoglucosamines used to produce conjugate vaccines for bacterial pathogens**. *Infect Immun* 2010, **78**(2).

365. Parker D, Ryan CL, Alonzo III F, Torres VJ, Planet PJ, Prince AS: **CD4+ T cells Promote the Pathogenesis of *Staphylococcus aureus* Pneumonia**. *J Infect Dis* 2015, **211**(5).

366. Bloes DA, Haasbach E, Hartmayer C, Hertlein T, Kingel K, Kretschmer D, Planz O, Peschel A: **Phenol-Soluble Modulin Peptides Contribute to Influenza A Virus-Associated *Staphylococcus aureus* Pneumonia**. *Infect Immun* 2017, **85**(12).

367. Sibille Y, Marchandise FX: **Pulmonary immune cells in health and disease: polymorphonuclear neutrophils**. *Eur Respir J* 1993, **6**(10).

368. Loosli CG, Stinson SF, Ryan DP, Hertweck MS, Hardy JD, Serebrin R: **The destruction of type 2 pneumocytes by airborne influenza PR8-A virus; its effect on surfactant and lecithin content of the pneumonic lesions of mice**. *Chest* 1975, **67**.

369. Martin CM, Kunin CM, Gottlieb LS, Finland M: **Asian influenza A in Boston, 1957-1958. II. Severe staphylococcal pneumonia complicating influenza**. *AMA Arch Intern Med* 1959, **103**(4).

370. Schwarzmann SW, Adler JL, Sullivan RJJ, Marine WM: **Bacterial pneumonia during the Hong Kong influenza epidemic of 1968-1969**. *Arch Intern Med* 1971, **127**(6).

371. Fine MJ, Smith MA, Carson CA, Mutha SS, Sankey SS, Weissfeld LA, Kapoor WN: **Prognosis and outcomes of patients with community-acquired pneumonia. A meta-analysis**. *JAMA* 1996, **275**.

372. Short KR, Kuiken T, van Riel D: **Role of Endothelial Cells in the Pathogenesis of Influenza in Humans**. *J Infect Dis* 2019.

373. Becker KA, Fahsel B, Kemper H, Mayeres J, Li C, Wilker B, Keitsch S, Soddemann M, Sehl C, Kohnen M *et al*: ***Staphylococcus aureus* Alpha-Toxin Disrupts Endothelial-**

Cell Tight Junctions via Acid Sphingomyelinase and Ceramide. *Infect Immun* 2018, **86**(1).

374. Dunning J, Blankley S, Hoang LT, Cox M, Graham CM, James PL, Bloom CI, Chaussabel D, Banchereau J, Brett SJ *et al*: **Progression of whole-blood transcriptional signatures from interferon-induced to neutrophil-associated patterns in severe influenza**. *Nat Immunol* 2018, **19**.

375. Kadioglu A, Andrew PW: **The innate immune response to pneumococcal lung infection: the untold story**. *Trends Immunol* 2004, **25**(3).

376. Koedel U, Rupprecht T, Angele B, Heesemann J, Wagner H, Pfister HW, Krischning CJ: **MyD88 is required for mounting a robust host immune response to Streptococcus pneumoniae in the CNS**. *Brain* 2004, **127**.

377. Yoshimura A, Lien E, Ingalis RR, Tuomanen E, Dziarski R, Golenbock D: **Cutting edge: recognition of Gram-positive bacterial cell wall components by the innate immune system occurs via Toll-like receptor 2**. *J Immunol* 1999, **163**(1).

378. Askarian F, Wagner T, Johannessen M, Nizet V: ***Staphylococcus aureus* modulation of innate immune responses through Toll-like (TLR), (NOD)-like (NLR) and C-type lectin (CLR) receptors**. *FEMS Microbiol Rev* 2018, **42**(5).

379. Beutler B: **Inferences, questions and possibilities in Toll-like receptor signalling**. *Nature* 2004, **430**(6996).

380. Bergeron Y, Ouellet N, Deslauriers AM, Simard M, Olivier M, Bergeron MG: **Cytokine kinetics and other host factors in response to pneumococcal pulmonary infection in mice**. *Infect Immun* 1998, **66**(3).

381. Dallaire F, Ouellet N, Bergeron Y, Turmel V, Gauthier MC, Simard M, Bergeron MG: **Microbiological and inflammatory factors associated with the development of pneumococcal pneumonia**. *J Infect Dis* 2001, **184**(3).

382. Martinez-Colón GJ, Warheit-Niemi H, Gurczynski SJ, Taylor QM, Wilke CA, Podsiad AB, Crespo J, Bhan U, Moore BB: **Influenza-induced immune suppression to methicillin-resistant *Staphylococcus aureus* is mediated by TLR9**. *PLoS Pathog* 2019.

383. Mifsud EJ, Tan AC, Short KR, Brown LE, Chua BY, Jackson DC: **Reducing the impact of influenza-associated secondary pneumococcal infections**. *Immunol Cell Biol* 2016, **94**(1).

384. Parnell G, McLean A, Booth D, Huang S, Nalos M, Tang B: **Aberrant Cell Cycle and Apoptotic Changes Characterise Severe Influenza A Infection - A Meta-Analysis of Genomic Signatures in Circulating Leukocytes**. *PLoS One* 2011.

385. Tumpey TM, Garcia-Sastre A, Taubenberger JK, Palese P, Swayne DE, Pantin-Jackwood MJ, Schultz-Cherry S, Solórzano A, Van Rooijen N, Katz JM *et al*: **Pathogenicity of influenza viruses with genes from the 1918 pandemic virus: functional roles of alveolar macrophages and neutrophils in limiting virus replication and mortality in mice**. *J Virol* 2005, **79**(23).

386. Beigel JH, Farrar J, Han AM, Hayden FG, Hyer R, de Jong MD, Lochindarat S, Nguyen TK, Nguyen TH, Tran TH *et al*: **Avian influenza A (H5N1) infection in humans**. *N Engl J Med* 2005, **353**(13).

387. Cheung CY, Poon LL, Lau AS, Luk W, Lau YL, Shortridge KF, Gordon S, Guan Y, Peiris JS: **Induction of proinflammatory cytokines in human macrophages by**

influenza A (H5N1) viruses: a mechanism for the unusal severity of human disease? *Lancet* 2002, **360**(9348).

388. Volz T, Nega M, Buschmann J, Kaesler S, Guenova E, Peschel A, Röcken M, Götz F, Biedermann T: **Natural Staphylococcus aureus-derived peptidoglycan fragments activate NOD2 and act as potent costimulators of the innate immune system exclusively in the presence of TLR signals**. *FASEB J* 2010, **24**(10).

389. Strober W, Murray PJ, Kitani A, Watanabe T: **Signalling pathways and molecular interactions of NOD1 and NOD2**. *Nat Rev Immunol* 2006, **6**(1).

390. Moreira LO, Zamboni DS: **NOD1 and NOD2 Signaling in Infection and Inflammation**. *Front Immunol* 2012, **3**(328).

391. Oviedo-Boyso J, Bravo-Patiño A, Baizabal-Aguirre V: **Collaborative Action of Toll-Like and Nod-Like Receptors as Modulators of the Inflammatory Response to Pathogenic Bacteria**. *Mediators Inflamm* 2014, **2014**.

392. Rawlings JS, Rosler KM, Harrison DA: **The JAK/STAT signaling pathway**. *J Cell Sci* 2004, **117**.

393. Silva-García O, Valdez-Alarcón JJ, Baizabal-Aguirre VM: **The Wnt/ B-Catenin Signaling Pathway Controls the Inflammatory Response in Infections Caused by Pathogenic Bacteria**. *Mediators Inflamm* 2014, **2014**.

394. Gustafson B, Smith U: **Cytokines Promote Wnt SIgnaling and Inflammation and Impair the Normal Differentiation and Lipid Accumulation in 3T3-L1 Preadipocytes**. *J Biol Chem* 2006, **281**.

395. Halleskog C, Mulder J, Dahlström J, Mackie K, Hortobágyi T, Tanila H, Kumar Puli L, Färber K, Harkany T, Schulte G: **WNT signaling in activated microglia is proinflammatory**. *Glia* 2011, **59**(1).

396. Liu X, Lu R, Wu S, Sun J: **Salmonella regulation of intestinal stem cells through the Wnt/beta-catenin pathway**. *FEBS Letters* 2010, **584**(5).

397. Neumann J, Schaale K, Farhat K, Endermann T, Ulmer AJ, Ehlers S, Reiling N: **Frizzled1 is a marker of inflammatory macrophages, and its ligand Wnt3a is involved in reprogramming Mycobacterium tuberculosis-infected macrophages**. *FASEB J* 2010, **24**(11).

398. Neumann G, Kawaoka Y: **Host range restriction and pathogenicity in the context of influenza pandemic**. *Emerg Infect Dis* 2006, **12**(6).

399. Doherty PC, Turner SJ, Webby RG, Thomas PG: **Influenza and the challenge for immunology**. *Nat Immunol* 2006, **7**(5).

400. de Jong MD, Simmons CP, Thanh TT, Hien VM, Smith GJ, Chau TN, Hoang DM, Chau NV, Khanh TH, Dong VC *et al*: **Fatal outcome of human influenza A (H5N1) is associated with high viral load and hypercytokinemia**. *Nat Med* 2006, **12**(10).

401. Uiprasertkul M, Pithavathana P, Sangsiriwut K, Pooruk P, Srisook K, Peiris M, Nicholls JM, Chokephaibulkit K, Vanprapar N, Auewarakul P: **Influenza A H5N1 replication sites in humans**. *Emerg Infect Dis* 2005, **11**(7).

402. Peiris JS, Yu WC, Leung CW, Cheung CY, Ng WF, Nicholls JM, Ng TK, Chan KH, Lai ST, Lim WL *et al*: **Re-emergence of fatal human influenza A subtype H5N1 disease**. *Lancet* 2004, **363**(9409).

403. Federspiel CK, Liu KD: **Critical Care Nephrology**, 3 edn; 2019.

404. Bradley-Stewart A, Jolly L, Adamson W, Gunson R, Frew-Gillespie C, Templeton K, Aitken C, Carman W, Cameron S, McSharry C: **Cytokine responses in patients with mild or severe influenza A(H1N1)pdm09**. *J Clin Virol* 2013, **58**(1).

405. Braun S, auf dem Keller U, Steiling H, Werner S: **Fibroblast growth factors in epithelial repair and cytoprotection**. *Philos Trans R Soc Lond B Biol Sci* 2004, **359**(1445).

406. Meyer M, Müller AK, Yang J, Moik D, Ponzio G, Grose R, Werner S: **FGF receptors 1 and 2 are key regulators of keratinocyte migration in vitro and in wounded skin**. *J Cell Sci* 2012, **125**.

407. Guzy RD, Stoilov I, Elton TJ, Mecham RP, Omitz DM: **Firboblast growth factor 2 is required for epithelial recovery, but not for pulmonary fibrosis, in response to bleomycin**. *Am J Respir Cell Mol Bio* 2015, **52**(1).

408. Wang K, Lai C, Li T, Wang C, Wang W, Ni B, Bai C, Zhang S, Han L, Gu H *et al*: **Basic fibroblast growth factor protects against influenza A virus-induced acute lung injury by recruiting neutrophils**. *J Mol Cell Biol* 2018, **10**(6).

409. Simonetti O, Lucarini G, Orlando F, Pierpaoli E, Ghiselli R, Provinciali M, Castelli P, Guerrieri M, Di Primio R, Offidani A *et al*: **Role of Daptomycin on Burn Wound Healing in an Animal Methicillin-Resistant *Staphylococcus aureus* Infection Model**. *Antimicrob Agents Chemother* 2017, **61**(9).

410. Xin Z, Gauldie J, Cox G, Baumann H, Jordana M, Achong MK: **IL-6 is an antiinflammatory cytokine required for controlling local or systemic acute inflammatory responses**. *J Clin Invest* 1998, **101**(2).

411. Jia L, Zhao J, Yang C, Liang Y, Long P, Liu X, Qiu S, Wang L, Xie J, Li H *et al*: **Severe Pneumonia Caused by Coinfection with Influenza Virus Followed by Methicillin-Resistant *Staphylococcus aureus* Induces Higher Mortality in Mice**. *Front Immunol* 2019.

412. Paquette SG, Banner D, Zhao Z, Fang Y, Huang SS, León AJ, Ng DC, Almansa R, Martin-Loaches I, Ramirez P *et al*: **Interleukin-6 is a potential biomarker for severe pandemic H1N1 influenza A infection**. *PLoS One* 2012, **7**(6).

413. Bickel M: **The role of interleukin-8 in inflammation and mechanisms of regulation**. *J Periodontol* 1993, **64**.

414. Maiti A, Jiranek WA: **Inhibition of Methicillin-resistant *Staphylococcus aureus*-induced cytokines mRNA production in human bone marrow derived mesenchymal stem cells by 1,25-dihydroxyvitamin D3**. *BMC Cell Biol* 2014, **15**.

415. Liu M, Guo S, Hibbert JM, Jain V, Singh N, Wilson NO, Stiles JK: **CXCL10/IP-10 in Infectious Diseases Pathogenesis and Potential Therapeutic Implications**. *Cytokine Growth Factor Rev* 2011.

416. Deshmane SL, Kremlev S, Amini S, Sawaya BE: **Monocyte Chemoattractant Protein-1 (MCP-1): An Overview**. *J Interferon Cytokine Res* 2009, **29**(6).

417. Lin KL, Suzuki Y, Nakano H, Ramsburg E, Gunn MD: **CCR2+ Monocyte-Derived Dendritic Cells and Exudate Macrophages Produce Influenza-Induced Pulmonary Immune Pathology and Mortality**. *J Immunol* 2008, **180**(4).

418. Gurczynski SJ, Nathani N, Warheit-Niemi HI, Hult EM, Podsiad A, Deng J, Zemans RL, Bhan U, Moore BB: **CCR2 mediates increased susceptibility to post-H1N1 bacterial**

pneumonia by limiting dendritic cell induction of IL-17. *Mucosal Immunol* 2019, **12**(2).

419. Marti HH, Risau W: **Systemic hypoxia changes the organ-specific distribution of vascular endothelial growth factor and its receptors**. *Proc Natl Acad Sci U S A* 1998, **95**(26).

420. Monacci W, Merrill M, Oldfield E: **Expression of vascular permeability factor/vascular endothelial growth factor in normal rat tissues**. *Am J Physiol Cell Physiol* 1993, **264**.

421. Tuder RM, Flook BE, Voelkel NF: **Increased gene expression for VEGF and the VEGF receptors KDR/Flk and Flt in lungs exposed to acute or to chronic hypoxia. Modulation of gene expression by nitric oxide**. *J Clin Invest* 1995, **95**(4).

422. van der Poll T, Marchant A, Keogh CV, Goldman M, Lowry SF: **Interleukin-10 impairs host defense in murine pneumococcal pneumonia**. *J Infect Dis* 1996, **174**(5).

423. van der Sluijs KF, van Elden LJ, Nijhuis M, Schuurman R, Pater JM, Florquin S, Goldman M, Jansen HM, Lutter R, van der Poll T: **IL-1- is an important mediator of the enhanced susceptibility to pneumococcal pneumonia after influenza infection**. *J Immunol* 2004, **172**(12).

424. Thomas P, Keating R, Hulse-Post D, Doherty P: **Cell-mediated protection in influenza infection**. *Emerg Infect Dis* 2006, **12**(1).